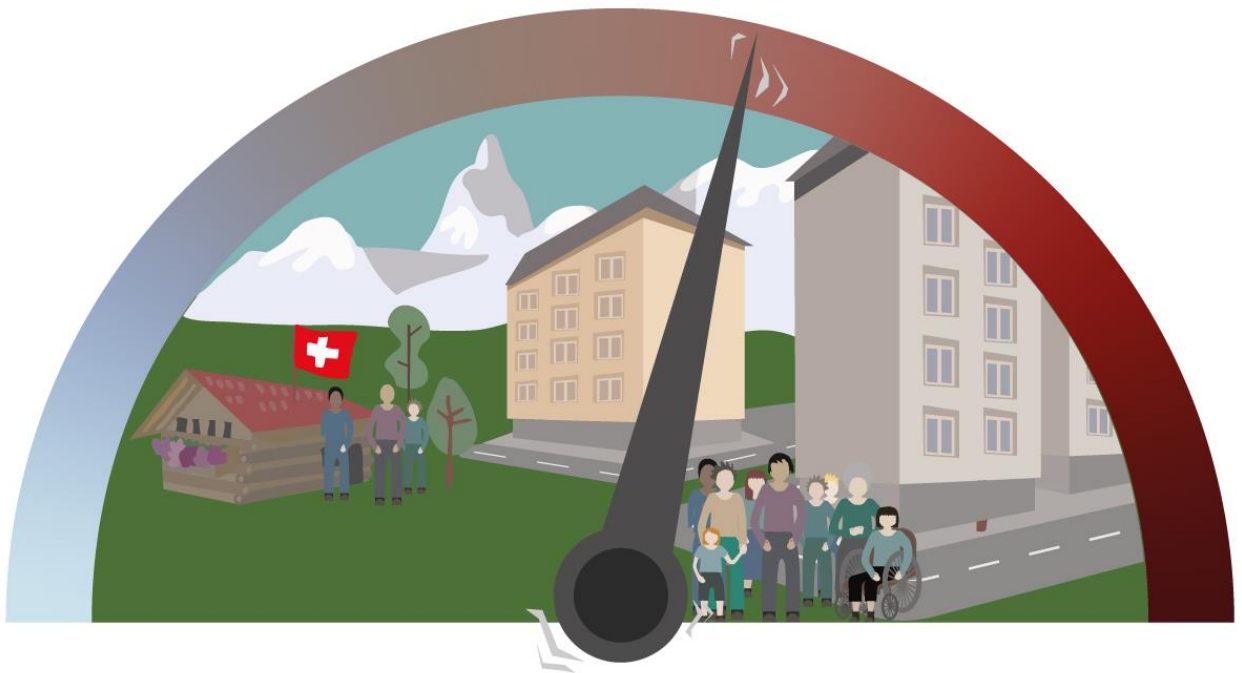# Earthquake Risk Model of Switzerland ERM-CH23

March 2023

Imprint

Publisher

Swiss Seismological Service (SED)

Authors

Stefan Wiemer (SED), Paolo Bazzurro (RED), Paolo Bergamo (SED), Carlo Cauzzi (SED), Irina Dallo (SED), Laurentiu Danciu (SED), Blaise Duvernay (BAFU), Ettore Fagà (RED), Donat Fäh (SED), Conny Hammer (SED), Florian Haslinger (SED), Philipp Kästli (SED), Alireza Khodaverdian (EPFL), Pierino Lestuzzi (EPFL), Michèle Marti (SED), Ömer Odabaşı (RED), Francesco Panzera (SED), Athanasios Papadopoulos (SED), Vincent Perron (SED), Philippe Roth (SED), Nicolas Schmid (SED), Nadja Valenzuela (SED), Simone Zaugg (SED)

Compilation and Layout

Swiss Seismological Service (SED)

Cover picture

Risk indicator

Disclaimer

How to cite

Wiemer S., Papadopoulos A., Roth P., Danciu L., Bergamo P., Fäh D., Duvernay B., Khodaverdian A., Lestuzzi P., Odabaşi Ö., Fagà E., Bazzuro P., Cauzzi C., Hammer C., Panzera F., Perron V., Marti M., Valenzuela N., Dallo I., Zaugg S., Fulda D., Kästli P., Schmid N., Haslinger F. (2023) Earthquake Risk Model of Switzerland (ERM-CH23), Swiss Seismological Service, ETH Zurich, Doi: https://doi.org/10.12686/a20

Version 4.1 (March 2023)

Content

1.   Introduction

1.1   Motivation and context

Switzerland is an earthquake country with an average of 1'200 earthquakes recorded each year by the Swiss Seismological Service at ETH Zurich (SED, www.seismo.ethz.ch). Switzerland has a rich earthquake history that includes numerous damaging earthquakes recorded in the historical reports of the past 800 years and including the strongest earthquake ever documented north of the Alps in Basel in 1356 (magnitude 6.6, see **Figure 1.1**). The SED has been periodically assessing the seismic hazard at a national level since the late 1970s. The result of the latest such effort was published in 2016, the SUIhaz2015 model (Wiemer et al., 2016).

Unbeknown to most citizens, of all natural hazards in Switzerland, earthquakes have the greatest damage potential. Large-scale earthquakes are fortunately quite rare, but if they strike, they can cause far-reaching and very costly damage and lead, potentially, to hundreds or even thousands of fatalities. While devastating events might only occur every 1,000 or 2,000 years (that is, with an annual probability of 0.05 to 0.1%), slightly smaller events of around magnitude 6 could also be catastrophic were they to occur beneath urbanised zones. From historical records we know that since the 13th century 12 earthquakes have occurred which caused substantial damage, meaning that every 50 to 150 years (in statistical terms, a 1% chance annually) such a disaster might strike Switzerland or its neighbouring regions.
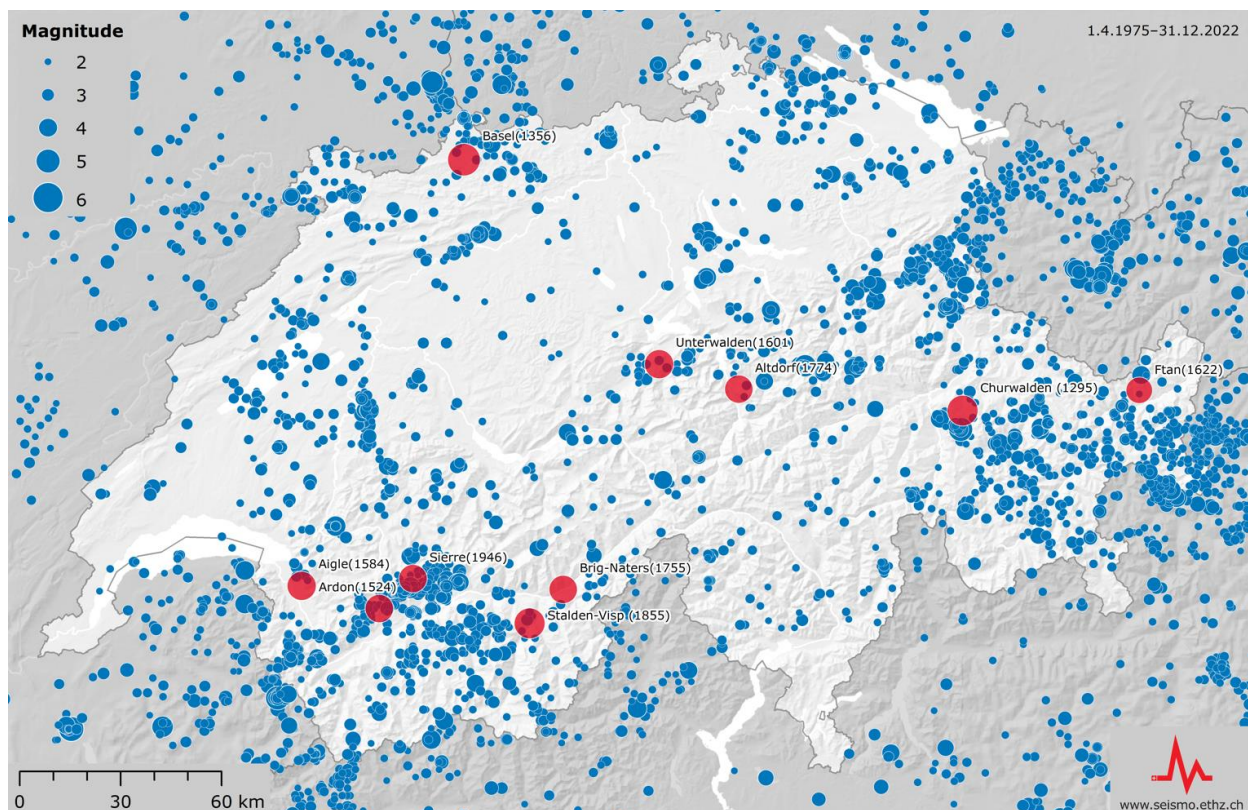
Figure 1.1. Map of the instrumentally recorded earthquakes between 1975 and 1922 (in blue), together with the location of the 10 strongest historical earthquakes (in red).

Seismic risk refers to the probability of damage to a building, system, or other entity from earthquakes and the resulting economic, social and environmental losses that may occur in a specified period of time. From a societal perspective and compared to seismic hazard, seismic risk (also referred to as earthquake risk) is a figure that is both easier to understand and more useful when it comes to earthquake awareness, preparedness and event mitigation. However, until now, and outside of insurance vendor models that are not openly available, seismic risk had never been assessed at a national level in Switzerland. The main reasons are on the one hand the multidisci-

plinary character of seismic risk studies, which requires specialisation beyond the field of seismology, and on the other hand the need for unified, country-wide datasets that until recently were not available.

While the SED – thanks to its continual seismic monitoring and advanced hazard studies – has a pretty good picture of where and with what magnitude and frequency earthquakes may occur in the country, our understanding of what the consequences of such events may be on buildings, people, infrastructure and society in general is rather limited. Thus, seismic risk, despite being regarded as the most prominent natural risk, was until now poorly known.

1.2   Mandate and role of the different actors

Mindful of the lack of knowledge on seismic risk, in 2013 the Federal Council mandated the Federal Department of the Environment, Transport, Energy and Communications (DETEC) and its Federal Office for the Environment (FOEN) to launch and coordinate, in collaboration with the SED and other relevant partners, a project to create and operate a model and IT application to quantify seismic risk in Switzerland. In 2017, it accepted a detailed implementation proposal. The project, the Earthquake Risk Model of Switzerland, or ERM-CH23, aims to determine the financial and human risks associated with building damage, which is thought to be the primary component of seismic risk.

Switzerland being an official founder of the Global Earthquake Model (GEM) initiative, it was planned from the beginning to implement ERM-CH23 with GEM's open-source software platform OpenQuake. The project started in autumn 2017 and is jointly funded by the SED and ETH Zurich, the FOEN, and the Federal Office for Civil Protection (FOCP), with a budget of 4.5 million Swiss Francs.

The SED is the federal agency responsible for monitoring earthquakes in Switzerland and its neighbouring regions and for assessing Switzerland's seismic hazard. Since 2017, it has also been tasked with assessing seismic risk at a national level. In Switzerland, the cantons, municipalities (also known as communes), private individuals and institutions are responsible for implementing earthquake mitigation measures. The Confederation (i.e. Switzerland's federal government) is only responsible for its own buildings and infrastructure systems. Additionally, the cantons are responsible for the building code legislation and, consequently, for the formulation of earthquake-specific requirements. They also lead post-earthquake management, with the support of the federal authorities.

The primary users of the ERM-CH23 model are thus expected to be cantonal and, to a lesser extent, federal and municipal authorities as well as the general public. However, engineering companies, building insurers, banks, reinsurers and infrastructure owners are also expected to be possible stakeholders. In Switzerland, earthquake damage is not covered by mandatory insurance and the Swiss Pool for Earthquake Insurance offers limited insurance coverage of up to CHF 2 billion in 18 cantons. Property owners can also decide for themselves whether or not they would like to be insured against earthquake damage.

Under the direction of Prof. S. Wiemer, the director of SED, ERM-CH23 is organised in seven subprojects (Figure 1.2): two supporting subprojects, coordination and IT, as well as five subprojects representing the components of risk: rock hazard and model implementation, site amplification, exposure, building typology and fragility, and consequence models. The subprojects are supported and challenged by a participatory review team, the Technical Committee, led by Prof. D. Fäh. The Technical Committee consists of experienced representatives from different private and public insurance companies and from a few cantons. The Technical Committee has been following the model-building process from the beginning, with regular opportunities to comment on its development. A Steering Committee, in which the funding bodies are represented, takes the most important managerial decisions.
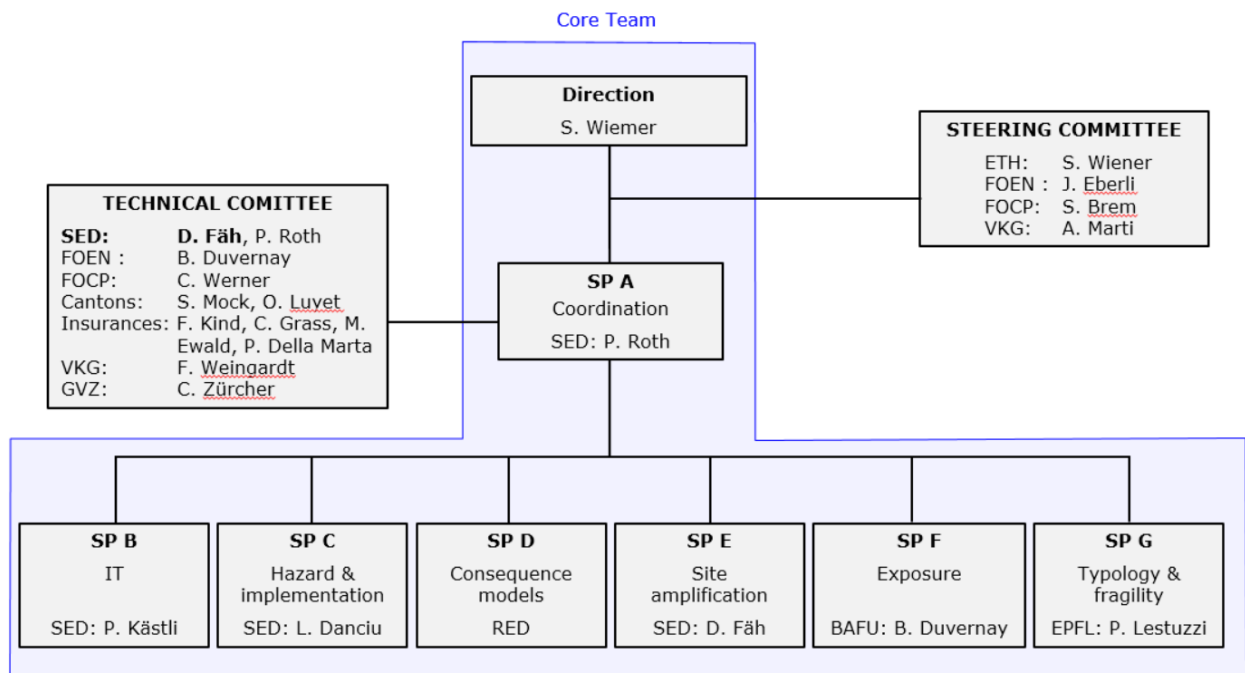
Figure 1.2 Organigram of the ERM-CH23 project

1.3 History of seismic risk assessment in Switzerland

Until recently, there was no state of the r tans openly available model in Switzerland to investigate earthquake risk or to quantify the damage from possible earthquake scenarios. So far, seismic risk in Switzerland had been estimated with the purpose of defining possible variants of a mandatory earthquake insurance. These analyses were based on existing private, in part simplistic and not generally accessible models, developed or used by reinsurers and brokers. For exercises or first-order comparative studies of loss potentials from different natural hazards, the effects for different earthquake scenarios were estimated based on simple and poorly supported models.

The Confederation's strategy for integrated risk management in the area of natural hazards stipulates that their risks are to be transparently quantified and periodically updated and communicated according to the latest available knowledge. The objective is to ensure that all responsible parties are aware of and account for their respective damage potentials and risks.

In the academic field, earthquake risk had primarily been confined to either very local or broader but oversimplified works in the framework of Master'a or PhD theses (e.g. Schwarz, 2015).

1.4 Possible benefits of a national seismic risk model

The potential benefits of an earthquake risk model are manifold, including assistance with earthquake preparedness, mitigation, event management and recovery as well as strengthening seismic resilience. More specifically, such a seismic risk model can help in:

- rapidly assessing the extent of damage and impacts after earthquakes;
- getting information on damage potential and risks at the federal, cantonal and municipal levels (magnitude, uncertainties, geographic distribution, distribution between cost units);
- assessing recurrences of historical earthquakes and worst-case damage estimates (including their probability);
- providing loss scenarios for precautionary planning;
- contributing to continuing education and teaching;

- developing risk-based consideration of seismic safety requirements (e.g., for seismic design standards and recommendations);
- performing cost-benefit analyses of preventive measures and investigating and optimising coverage and financing models;
- enabling scientific research in the field of earthquake risk;
- providing advanced products, e.g. in the field of estimation of anthropogenic earthquake risk in geothermal projects or determination of time-dependent earthquake risk in swarm sequences.

1.5   Elements and data requirement for earthquake risk assessment

Assembling the ingredients of a national seismic risk assessment is a complex task. Each risk study begins with a seismic hazard assessment. Early on in ERM-CH23, the managerial decision was taken to rely on the latest update of the national hazard assessment (Wiemer et al., 2016). The SED updates the national seismic hazard about every 10 years and there was no good reason to develop something new at the beginning of the project (2018). The seismogenic source model and the ground motion models from SuiHaz2015 were retained and used. Additionally, the macroseismic data and information describes the ground motion models. For the latter, a set of Intensity Prediction Equations (IPEs) was assessed (see Chapter 2).

In national risk studies (e.g. Silva et al., 2014; Goda, 2019), the correlation of geological or structural proxies with the superficial shear-wave velocity (Vs30) is typically used to assess the local site effects. This was deemed too simplistic for ERM-CH23, and relying on a dense network of strong-motion stations with well-characterised sites, a country-wide, spectral period-dependent amplification model (including uncertainty) was developed by cross-referencing the empirically observed site response at a set of approximately 250 free-field seismic stations with a lithological classification, a national model of the thickness of quaternary sediments, and topographical slope evaluated at different spatial scales (see Chapter 3).

The exposure model of ERM-CH23 is the result of a collaborative effort at the federal level. Different datasets used in different offices and departments could be linked through the introduction of a common building identifier and complemented with specific missing elements, either through the acquisition of additional data or through the modelling of additional building attributes. The result is a database of nearly 3,000,000 georeferenced buildings (see Chapter 4). Among the attributes considered in the building database, the year of construction, the number of storeys and, partly, the roof inclination, were used specifically to assign individual buildings to the set of building classes representing the Swiss taxonomy.

This 'Swissness' of the building stock is the reason for the organisational separation introduced between the assessment of building vulnerability (performed at EPFL in Lausanne, see Chapter 5) and of consequence models (performed in Pavia by the company RED, see Chapter 6). For the former, a set of fragility curves were obtained for the different building types characteristic of the Swiss construction practice, both for macroseismic intensity and for spectral accelerations, representing the two approaches used to compute seismic risk in ERM-CH23. The consequence models that relate damage to losses were developed based on international models and adapted as much as possible to Swiss practice. As Switzerland has not experienced any devastating earthquake in recent decades, this is only possible to a limited extent.
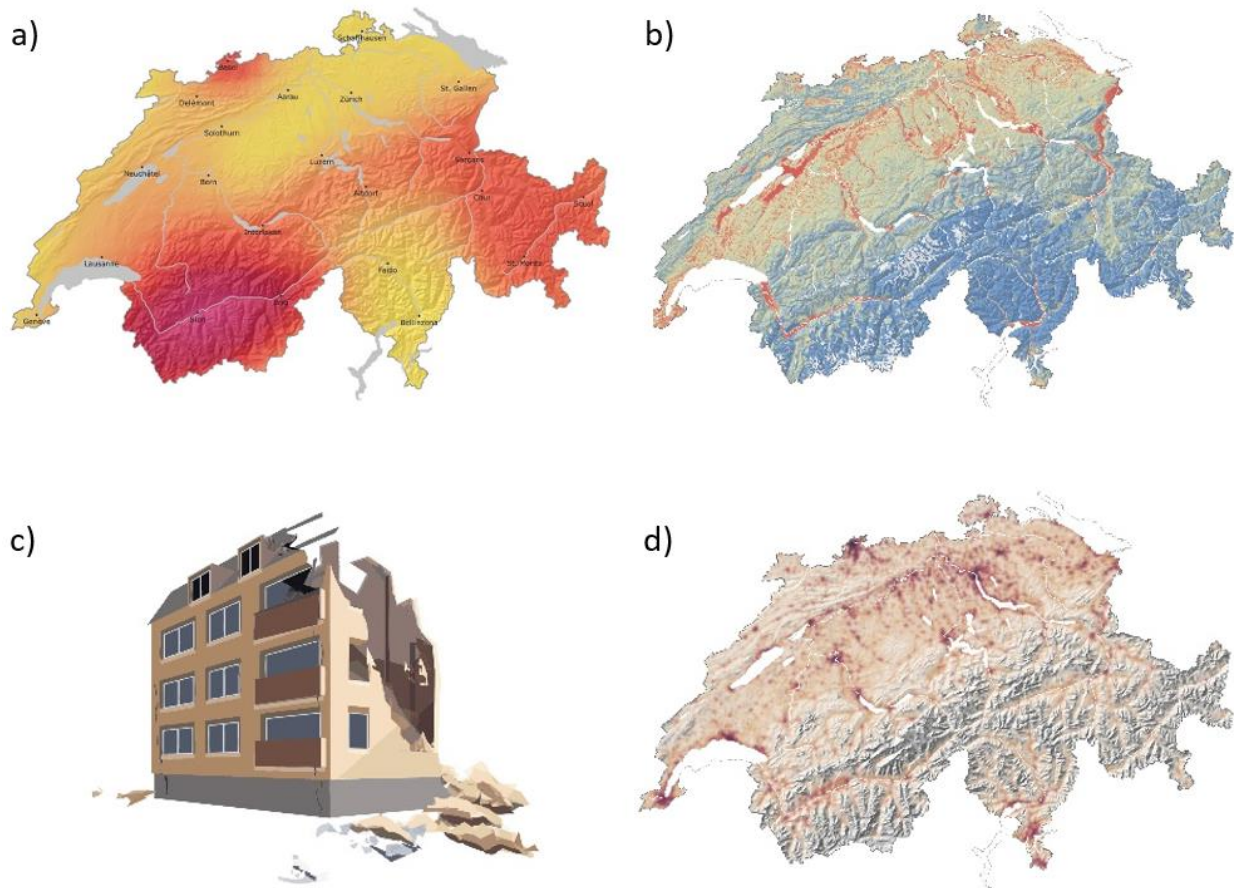
Figure 1.3. The components of risk in ERM-CH23: a) hazard on rock, b) site amplification, c) vulnerability and d) exposure (here as number of buildings per km^2).

Figure 1.3 shows the four major components of the ERM-CH23 seismic risk: seismic hazard on rock (reference V_{S30} velocity of 1,100 m/s), site amplification (for PGV), vulnerability (as the average vulnerability index used for the macroseismic approach, averaged in 1 x 1 km cells) and exposure (as the sum of the replacement values for the buildings in the same raster).

1.6   Logic tree approach

For decades, it has been standard practice in seismic hazard studies to use logic trees to capture the epistemic uncertainty associated with all the components of a model. For site-specific PSHA studies for critical facilities, this arborescence can be very large (10^{24} branches, before trimming, in the case of the hazard studies for Swiss nuclear power plants, PEGASOS[1]). Because they make use of large numbers of ground motion fields and numerous stochastic catalogues, seismic risk calculations are more demanding in terms of computational resources than hazard calculations, and seismic risk studies typically consider far simpler logic trees, if any.

Indeed, to be able to consider the logic tree developed during the course of the ERM-CH23 project, the SED had to ask the GEM foundation to extend OpenQuake's functionality to include the ability to consider alternative submodels for fragility, exposure or consequence.

In the project logic tree (Figure 7.2), we consider, as mentioned in the previous section, two different approaches to obtain the input ground motion. These approaches condition the selection of specific alternative ground motion predictive models (Intensity and Ground Motion Prediction Equations, IPEs and GMPEs). The uncertainty related to site amplification is dependent on the ground motion approach while the two methods used to attribute a building type to individual buildings are independent of the approach (Figure 7.2). In total, the ERM-CH23 logic tree consists

---

[1] E.g https://inis.iaea.org/search/search.aspx?orig_q=RN:39091004

of at least 424 branches, the larger part stemming from the ground motion models. This is partly a consequence of the early managerial decision not to change the components of the national seismic hazard model.

Considering the common practice of capturing epistemic uncertainty in risk studies and considering that ERM-CH23 is a country-wide study (with >10,000 composite 'sites' or 2 x 2 km cells, see Chapter 8), the ERM-CH23 logic tree can be regarded in our opinion as an ambitious attempt to model that type of uncertainty. Chapter 7 specifically focuses on epistemic and aleatory uncertainty and goes into more details of the rationale behind the choice of the final logic variables, including the associated weights. Chapter 8 describes the actual implementation of the logic tree in the computational framework.

1.7   Quality control

The model components having been developed in different, geographically distant entities and partly in different fields of expertise with their specific language, the potential for misunderstanding and therefore errors is real in such a project. Several measures were taken to minimise this threat. First, a series of bilateral, minuted meetings between subprojects were held throughout the project whenever a potential misunderstanding, an information gap or the danger or double-counting had been identified. Often, subproject A, which was responsible for cross-cutting issues, convened these meetings.

Another important measure is the so-called Risk Input Document (RID). This document, written by the risk analyst in charge of the transformation of subproject deliverables – reports and datasets – into risk input files, contains all intermediate steps along this transformation. This may be a simple reformatting of data, a processing step not performed by the subproject but following its instructions or even simplifications. The RID needs to be endorsed by the subproject owner, who confirms that their submodel has not been distorted or misunderstood, that the possible simplifications are acceptable and in general that the described implementation can be released. The risk analysts confirm that they have received all the information they need to create a set of risk input files that faithfully reflect the submodel. Chapter 8 of this report is in essence identical to that RID.

As for OpenQuake (Pagani et al., 2014), although if the software has not received a QA certification from an official independent institution, software development and implementation are fully compatible with the Test-Driven Development (TDD) and Software Quality Assurance (SQA) frameworks of GEM and we therefore assume that it is error proof.

Besides the quality control performed within and across the subprojects, the ERM-CH23 model benefited from two types of technical challenges by two different entities. The first was a participatory review by the Technical Committee (see Figure 1.2): this body, consisting of reinsurance, cantonal civil protection, hazard prevention and building insurance representatives, received the yearly reports and met once a year with the project core team to discuss the project status, the approaches chosen, the possible verification measures, and – towards the end of the project – to think about the provisional results. The second body is a panel of external experts that the project established in 2022. The four international experts in the field of seismic risk, from both academia and industry, received a preliminary version of this report and met for a two-day workshop in July 2022 to discuss all model components. Already there and in the follow-up, the panel made a number of comments and suggestions, to which the project responded in autumn 2022 in the form of a model revision, with new results and a revised report. Both review bodies then issued a document, stating that ERM-CH23 was a best-practice, state-of-the-art probabilistic seismic risk model (see Appendix 1). These statements helped the Steering Committee to approve the model release in October 2022.

1.8   What ERM-CH23 is not

ERM-CH23 is the first national earthquake risk model to be developed and the expectations for its products are understandably high. It is therefore important to emphasise what the model does not yet cover.

The first country-wide database of buildings developed within the project is a collaborative effort by different federal offices aimed at serving various projects. The database is primarily a database of residential and commercial buildings. Buildings with other functions (industrial production buildings, hospitals, etc.) are also included but their fragility could not be modelled specifically. Therefore, the estimated losses associated with them are more uncertain.

Critical infrastructures and lifelines (railway, power grid and other networks, bridges, dams, etc.) are not part of ERM-CH23. Damage to lifelines and its consequences are a considerable source of risk that is not addressed here. An extended and updated Swiss risk model is set to address this aspect in the years to come. The same is true for risk caused by secondary hazards like landslides, rock falls, soil liquefaction, lake tsunamis, fire after earthquakes or falling debris. These secondary effects account for a significant proportion of the total global loss caused by earthquakes (Nowicki Jessee et al., 2020).

With regard to earthquake scenarios and rapid loss assessment, the time of day is roughly taken into account (see Section 7.4). A more precise representation of population movement (weekend vs. weekday, holidays, seasonal variations in tourist areas, movement of border workers) will be addressed later. A new project at the federal level to map population in real time may deliver an important opportunity to make progress in this area. Another temporal factor not yet considered is the weakening of structures (time-dependent vulnerability) after a first, main earthquake. In ERM-CH23, aftershocks are modelled, for possible scenarios, as independent earthquakes.

Uncertainty characterisation of all model components is an important goal of ERM-CH23; however, it is also a difficult task in such complex, multi-layer models. Especially at the interfaces of models there may be double-counting of uncertainties; in other places we may not capture enough of the alternative interpretations. In addition, validation of the model is especially difficult in Switzerland because there have been no major and destructive earthquakes in the last 50 years. Therefore, while we address uncertainties using the state-of-the-art techniques, we feel that in future model updates this uncertainty quantification could be improved.

Finally, losses due to business interruption as a consequence of downtime (inspection, repair, demand surge, etc.) are modeled but only used, on demand, for scenario computations.

References

Goda, K. (2019). Nationwide Earthquake Risk Model for Wood-Frame Houses in Canada. Front. Built Environ. **5**, 128. doi: 10.3389/fbuil.2019.00128

Nowicki Jessee, M.A., Hamburger, M.W., Ferrara, M.R., McLean, A., Fitzgerald, C. (2020), A global dataset and model of earthquake-induced landslide fatalities. Landslides **17**(6), 1363–1376, doi:10.1007/s10346-020-01356-z.

Pagani, M., Monelli, D., Weatherill, G., Danciu, L., Crowley, H., Silva, V., Henshaw, P., Butler, L., Nastasi, M., Panzeri, L., Simionato, M., Vigano, D. (2014). OpenQuake Engine: An Open Hazard (and Risk) Software for the Global Earthquake Model. Seismological Research Letters **85**, 692–702.

Schwarz C. (2015). Towards a Swiss national Earthquake risk model – Sensitivity and gap analysis. Ms Thesis, Delft Univ., ETH Zurich and RWTH Aachen Univ., 68 p.

Silva, V., Crowley, H., Varum, H. Pinho, R. (2014). Seismic risk assessment for mainland Portugal. Bull. Earthq. Eng. **13**, 429–457. doi: 10.1007/s10518-014-9630-0

Wiemer, S., Danciu, L., Edwards, B., Marti, M., Fäh, D., Hiemer, S., Wössner, J, Cauzzi, C., Kästli, P., Kremer, K. (2016). Seismic Hazard Model 2015 for Switzerland (SUIhaz2015). Report Swiss Seismological Service (SED) Zurich.

2.   Seismic hazard for reference rock conditions

2.1   Introduction

The 2015 Seismic Hazard Model (SUIhaz2015, Wiemer et al., 2016) is the authoritative national seismic hazard model and serves as the basis for country-level seismic risk model development. SUIhaz2015 is based on a probabilistic framework and includes two critical components: the seismogenic source model and the ground motion model. The former depicts the earthquakes' spatial and temporal variability across the entire region, while the latter describes the ground shaking properties, such as source, path and site.

In the probabilistic framework for seismic risk analysis, these two seismic hazard model subcomponents are utilised differently than in the traditional seismic hazard assessment. Consequently, they are used to generate stochastic earthquake catalogues that represent potential earthquake rupture locations, followed by ground motion fields corresponding to each rupture. Similarly, for scenario risk analysis, the main event is represented as a single rupture, and the corresponding ground motion fields are generated accordingly.

Further, it was decided to use two ground motion models: an intensity-based model and an acceleration-based model. The former seeks to describe ground shaking properties through the use of macroseismic data and information, whereas the latter is based on the same ground motion model as SUIhaz2015.

This chapter focuses on key aspects of the seismic hazard model as an input and component of the seismic risk model and assessment. Wiemer et al. (2016) provide a comprehensive description of the two subcomponents, the seismogenic source model and the ground motion models, so only important aspects will be summarised in this chapter. However, we intend to discuss and document those aspects that are relevant for seismic risk calculation in the following sections.

2.2   Seismogenic source models: short summary

The SUIhaz2015 seismogenic source model incorporates potential sources of earthquake location, size and faulting style into a seismotectonic framework. Revised tectonic domains and new data on Earth's crust deformation, faults and paleo-earthquakes were incorporated into multiple seismogenic source definitions and representations, including zone-based and smooth seismicity models.

Hierarchical and multi-layered procedures (Woessner et al., 2015) were used to develop the source model and capture the centre, body and range of technical knowledge (Danciu and Giardini, 2015).

A weighted logic tree approach was used to capture inherent uncertainty in the seismic source modelling approach, recurrence rate parameter estimates, and maximum magnitude. Four seismogenic source models were combined in a mutually exclusive but cumulatively exhaustive sense, although models and data spatially overlapped.

Two seismogenic source models were newly developed within the SUIhaz2015 i.e. the SEIS-15 area source model and the CH14 smoothed seismicity model, while two other source models were based on the ECOS-02-based area source model SEIS04 (Fäh et al., 2003; Wiemer et al., 2009) and the area source model of the 2013 European Seismic Hazard Model (ESHM13, SHARE Project, Woessner et al., 2015). Details of each individual seismogenic source model are given in Chapter 4 of Wiemer et al. (2016). Magnitude-dependent weights were used and a spatially distributed ensemble earthquake rate model was built (see Figure 2.1). The ensemble earthquake rate model is defined by its centre or median (50th) and four ranges (2.5th, 16th, 84th, 97.5 th) with weights chosen to represent the area of a normal distribution. The median (50th) earthquake rate model received 68% weighting, the 16th and 84th quantiles received 13.5%, and the 2.5th and 97.5th quantiles received 2.5%.

The seismogenic source model is implemented as individual point sources, with the main parameters describing the seismogenic layers, the depth distribution and the style-of-faulting. The location of seismicity with depth as well as the predominant style-of-faulting is regionally variable.

In Switzerland, seismicity extends deeper beneath the Foreland than the Alps, and instrumental earthquakes are used to ascertain the hypocentres distribution as given in Table 2.1 (Wiemer et al., 2016).

For shallow seismicity in the Alps and Foreland, the upper and lower seismogenic depths have been set at 0 and 9 kilometres, respectively. The average hypocentral depth for shallow earthquake sources is 4.5 km. For sources of deep seismicity, the upper seismogenic depth is set at 9 km, the lower seismogenic depth at 18 km, and the average hypocentral depth at 13.5 km. The final layer of the Foreland sources is defined between 18 and 36 km, with a reported average hypocentre depth of 22.5 km.

Table 2.1. Depth distribution for Foreland and Alpine sources as defined in Wiemer et al. (2016)

Upper Seismogenic Depth	Lower Seismogenic Depth	Hypocentral Depth	Weights	Number of Events
0	9	4.5	0.72	227
9	18	13.5	0.17	55
18	36	22.5	0.11	34
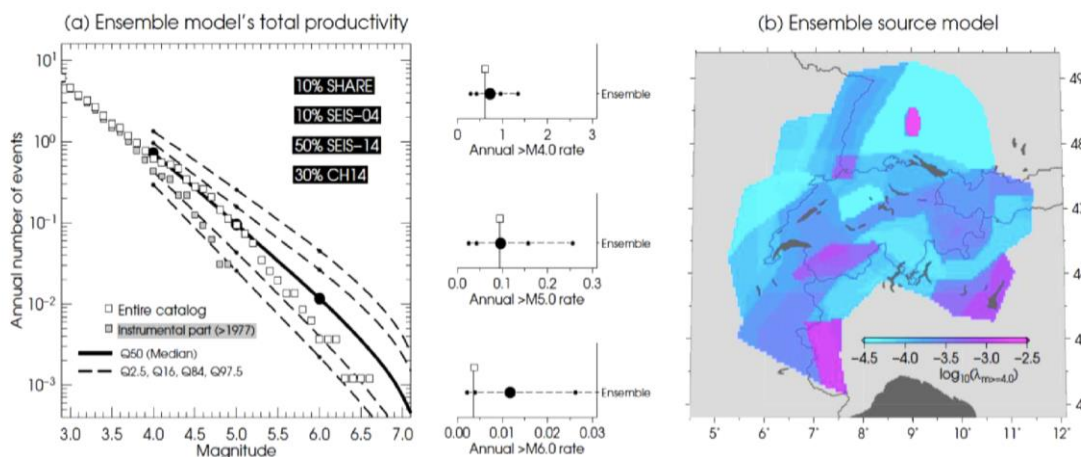
Figure 2.1. (a) Magnitude rate and (b) spatial rate distribution for the ensemble source model using the weighting scheme given in the inset. Map shows median values and the model's building polygon stems from the SEIS models (from Wiemer et al., 2016).

The SUIhaz2015 seismogenic source models are available as input to OpenQuake Engine (Pagani et al., 2014) as equally spaced gridded sources. Point sources, as featured in OpenQuake, can nucleate finite ruptures as extended surfaces. These finite ruptures depend on magnitude-scaling relationships and rupture aspect ratio and their shape is limited to a lower and upper seismogenic depth, preventing uncontrolled surface extension. In the SUIhaz2015 model, it is assumed that seismogenic sources are capable of generating extensive ruptures above Mw5.5; otherwise, earthquake ruptures are approximated as point sources. The lower magnitude bound of the source model is 4.0, whereas the upper magnitude bound is spatially variable and in the range of 6.5 to 7.3 (Chapter 4, Wiemer et al., 2016). For risk calculations, the minimum considered magnitude was set at 4.5, on the assumption that smaller events are not of engineering significance.

2.3   Ground motion models: spectral acceleration

The ground motion model from SUIhaz2015 was also used within the risk framework, as decided in the project's work plan. The ground motion characteristic model is composed of various ground motion predictive equations (GMPEs) that are grouped into an empirical and a stochastic set.

The empirical ground motion models were selected based on their statistical performance with datasets in Europe and worldwide, namely those of Zhao et al. (2006), Chiou and Youngs (2008), Cauzzi and Faccioli (2008), and Akkar and Bommer (2010). These models were further adjusted to match the amplification and attenuation levels typical of the Swiss reference rock, and making them suitable for predictions at moderate-to-low magnitudes (Edwards et al., 2016).

The stochastic models of Edwards and Fäh (2013) are a Swiss-specific prediction, obtained by simulating ground shaking for various source, path and site-specific parametrisations. The development of the unified generic reference-rock definition for hazard estimations is a core component of the SUIhaz2015 ground motion characteristic model. Poggi et al. (2011) developed a Swiss generic reference rock model based on shear-wave velocity as a function of depth from the characterisation of 27 Swiss permanent seismic network sites.

The technique used spectral modelling to connect quarter-wavelength average velocity at these network sites with empirical frequency-dependent amplification functions (Edwards et al., 2008) The resulting Swiss reference rock has a Vs30 = 1,100 m/s velocity and a high-frequency site attenuation parameter (*kappa*) of 0.016 s (Edwards and Fäh, 2013).

The empirical ground motion models were calibrated to this reference rock definition using a host-to-target approach (Al Atik et al., 2014). Unlike other methods for determining kappa from response spectra, this method does not require any assumptions about the background seismological model.

Considering the fact that the selected predictive ground motion models only provide response spectra and peak ground motions, the Fourier Amplitude Spectra (FAS) compatible with response spectra were derived using inverse random vibration theory (iRVT). The V_{s30}-kappa adjustments are finally achieved through a series of iterative steps outlined by Edwards et al. (2015). Eight V_{s30}-kappa adjustments (based on two amplification functions and four kappa values) were obtained for each empirical GMPE. To avoid too many logic-tree branches, however, only three adjustments, representing the mean, lower-bound and upper-bound adjustments were retained for the final implementation of the ground motion logic tree as in SUIhaz2015.

It is important to emphasise that the current methodology for obtaining the V_{s30}-kappa adjustments for empirical ground motion models represents the state of practice in Switzerland with application in site-specific hazard for critical infrastructures (i.e. PEGASOS and PRP). According to Bard et al. (2020), the host-to-target approach is sensitive to epistemic and aleatory uncertainties, resulting in overprediction of ground motion at high frequency. The main limitations are related to how host kappa values are estimated and the robustness of target kappa measurements. Further development will require additional measurements and/or enhanced data and quality site metadata. In this light, the current implementation of the V_{s30}-kappa adjustments is still valid and robust for our model, given that it was obtained through a series of studies that rely on Swiss Seismological Service station data.

Furthermore, Danciu and Fäh (2017) provide a step-by-step procedure for obtaining adjustment ratios between the reference rock (Vs30 1,100m/s, kappa=0.016 s) and other Vs30s values (i.e. 500 to 2,500 m/s).

These modification factors can be used when comparing with other Swiss seismic hazard models, such as SwisHaz 2004 (Giardini et al., 2004), Pegasos Refinement Project 2013 (Renault et al., 2014), or European Seismic Hazard Models (Woessner et al., 2013; Danciu et al., 2021). These adjustment factors also facilitate comparisons with the Swiss seismic design code (SIA261, 2014).

The stochastic ground motion models are combined with the empirical ones in a logic tree to handle the epistemic uncertainties of the ground motion characteristic model as described in Chapter 5 of Wiemer et al. (2016).

Figure 2.2 shows the median values of spectral acceleration at 0.3 s and at 0.6 s, of the empirical models (yellow) and stochastically simulated models (green) for two moment magnitudes (Mw=6.0 and Mw=6.6) – rupture distances ($R_{rup} \sim$ 10 to 200 km) and hypocentral depth (10 km) scenarios.

The different curves corresponding to the stochastic models correspond to the different values of the stress parameter, and for the two different tectonic regimes Alpine and Foreland, while for the empirical models, the curves correspond to the adjusted models. It should be noted that these median estimates span about one order of magnitude in spectral acceleration values over the entire range of distances.

The lower bound is given by the stochastic models with low stress drop (i.e. 10 to 30 bars) whereas the upper bound is given by the empirical models. Although some of the stochastic models forecast relatively low amplitudes compared to empirical models, their inclusion was justified due to their consistency with both small-magnitude weak-motion data and large-magnitude macroseismic data in the context of the shallow (6 km depth) crust.

This observation supports the higher weight (i.e. 0.7) assigned to the lowest three stochastic models (3 MPa) while giving 0.3 weight to the higher stress-drop stochastic models. A combination of stochastic ground motion models with high stress drops (5 MPa to 12 MPa) and empirical models is used to model the ground motion caused by deep seismicity. The inclusion of low stress-drop ground shaking models to describe the ground shaking of moderate to high magnitude scenarios (5.5 to 7.3) and the inclusion of high-stress stochastic ground motion models to forecast the ground shaking due to low-magnitude (4.0 to 5.5) earthquakes are the main reasons for this logic tree's adopted level of conservatism.
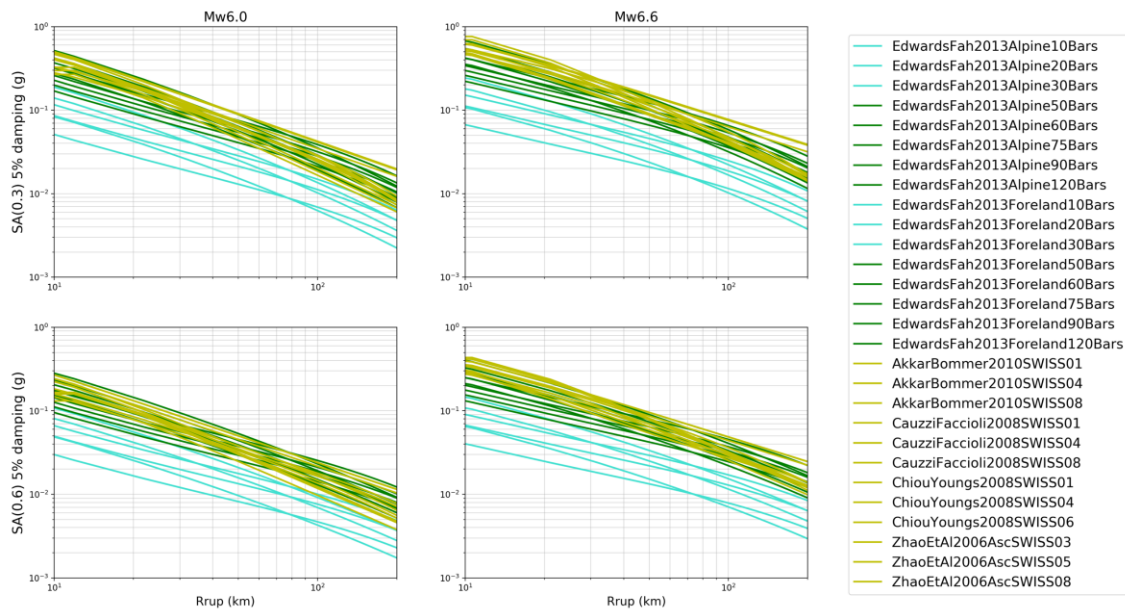
Figure 2.2. Median values of empirical and stochastic ground motion models at 0.3 s and 0.6 s, as a function of hypocentral distance and moment magnitude. For each empirical model, three VS-kappa curves are plotted.

2.4   Ground motion models: macroseismic intensity

The Swiss Seismological Service (SED) has collected, curated and updated a comprehensive macroseismic intensity dataset combining studies, earthquake catalogues and macroseismic databases from Switzerland and neighbouring countries. As part of the update of the ECOS-09 (Fäh et al., 2011) earthquake catalogue, all significant earthquakes in Switzerland and its surroundings were reevaluated and their macroseismic intensity data were determined.

Macroseismic intensity is standardised by the European Macroseismic Scale EMS-98 (Grünthal, 1998) as a classification of the severity and effects of the ground shaking on specific regions. Macroseismic intensity provides insights into the effects of large-magnitude events that have not been observed in recent years, provides a link to structural damage, and aids in the reconstruction of earthquake scenarios from the past.

In addition, the macroseismic data may also provide an alternate perspective on the spatial attenuation of the ground shaking based on the regional pattern of the intensity fields, as well as an indication regarding the possible local site effects. As a result of these applications, the macroseismic intensity is a parameter that can be used to predict ground shaking, and is often incorporated in Intensity Prediction Equations (IPEs).

The intensity-based ground motion model is proposed as an alternative to the acceleration-based ground motion model following the same strategy adopted by the SUIhaz2015's acceleration-based model (Edwards et al., 2016).

The intensity-based model was developed using the following steps:

1)   compile candidate IPEs;

2)   perform software implementation and sanity check of the candidate IPEs;

3)   compile a macroseismic intensity dataset for the region;

4)   assess and rank the performance of the candidate IPEs based on residual analysis;

5)   select the IPEs to represent the body, centre and range of intensity data; and finally

6)   assemble the logic tree with the corresponding weights.

Several IPEs were examined and chosen as potential candidates based on a few criteria such as proximity to the Swiss seismotectonic context, validity range of magnitudes ranging from 4.0 to 7.5 Mw, and local intensity levels ranging from III to XII. No distinction is made for the type of intensity scale used in the IPEs. Although there are obvious differences in the definition of intensity levels in various intensity scales (Musson et al., 2010), conversion between different scales is not easy, as the original datasets of each IPE are not available.

EMS-98 is considered to be the reference for our intensity-based model and this reference is used for deriving the vulnerability models. The candidate IPEs are listed in Table 2.2 and they are implemented in the OpenQuake (Pagani et al., 2014) hazard library.

A subset of ECOS-09 (Fäh et al., 2011; Álvarez-Rubio et al., 2012), consisting of approximately 2,000 intensity samples from 23 earthquakes in Switzerland, is used to evaluate the performance of the candidate IPEs. The dataset depicts shallow and deep seismicity in the Alpine and Foreland regions, with moment magnitudes (Mw) ranging from 4.7 to 6.6 and epicentral distances ranging from 1 to 200 km (see Figure 2.3).

The performance of candidate IPEs is evaluated using mean residual analyses for various macroseismic subsets filtered by various parameters: magnitude, distance, tectonic context (Alpine, Foreland) and hypocentral depths (shallow, deep).

The informational log-likelihood index (LLH) of Scherbaum et al. (2009) is used to rank the candidate IPEs as given in Table 2.2. The LLH index is sensitive to the dataset filters such as the magnitude, distance and intensity threshold. For this investigation we used the minimum magnitude of

Mw=4 and a low intensity threshold of IV. The residuals were weighted with the quadratic weight distance decay within 200 km, i.e. w= (200 − distance)/200)^2 as used in ECOS-09.

The LLH score summarised in Table 2.2 indicates as top performers the ECOS-09-derived IPEs, with both fixed and variable depth IPEs ranking highest. The Faccioli and Cauzzi (2006) model is the next highest performing IPE followed by three IPEs of Baumont et al. (2018), then Bindi et al. (2011) and Allen et al. (2012) (both for R_{hypo}), followed by a few other IPE versions of Baumont et al. (2018), Bindi et al. (2011) for fixed depth, Pasolini et al. (2008) and Musson (2013, 2005).

From Table 2.2, we further selected four IPEs based on their LLH score, namely ECOS-09 variable hypocentral depth (hereinafter *ECOS-09variableDepth*), ECOS-09 – fixed hypocentral depth (here-inafter *ECOS-09fixedDepth*), Baumont et al. (2018) (hereinafter *BaumontEtAl2018High2210IAVGDC30n7*), and Bindi et al. (2011) R_{hypo} (hereinafter *Bindi2011RHypo*).

The two models (*ECOS-09variableDepth*, *ECOS-09fixedDepth*) among the ECOS-09, Swiss-specific IPEs aim to leverage seismogenic depth and its uncertain effects on macroseismic intensity. These models were used in the development of the Swiss ECOS-09 earthquake catalogue and stochastic ground motion models. Both IPEs exhibit a low distance-dependent attenuation of macroseismic intensity.

Bindi2011RHypo, on the other hand, depicts a moderate decay of intensity with distance. This IPE was selected due to its relatively robust performance in describing Swiss data and, more im-portantly, because it is the only IPE based on intensity observations of Mw > 7.0 earthquakes. This IPE necessitates a conversion from local to moment magnitude (Bormann et al., 2013); this magnitude conversion was incorporated in the OpenQuake implementation of the IPE.

Last but not least, *BaumontEtAl2018High2210IAVGDC30n7* is a model that depicts a rapid intensi-ty decay with a distance R_{hypo} > 50 km; this IPE is the best performer among this suite of IPEs proposed by Baumont et al. (2018) for describing the Swiss macroseismic dataset. In particular, this model displays greater intensity values over short distances, particularly for shallow-depth earthquakes. In addition, this IPE includes an aleatory error term, namely the within- and be-tween-event terms, as a component of the IPE's total sigma, which is essential for calculating seismic risk.

The selected IPEs are compared and illustrated in Figure 2.4. These trellis plots depict the median values of macroseismic intensity of the four IPEs for various magnitude values, i.e. M4.5, 5.5, 6.5 and 7.0, as well as two hypocentral depths (5.0 and 10 km) as a function of hypocentral distance.

In general, median intensity values decrease with distance, and three groups of curves can be distinguished: the slow attenuating curves with distance, i.e. *ECOS-09variableDepth*, and *ECOS-09fixedDepth*, the moderately attenuating curves of *Bindi2011RHypo* and in the middle, the model of Baumont et al. (2018). This trend applies to R_{hypo} > 30 km.

Within the near-field range (R_{hypo} < 30 km), the higher intensity values in the near-field are given by *BaumontEtAl2018High2210IAVGDC30n7*, which asymptotically increases towards the higher intensity values, whereas *Bindi2011RHypo* forecasts the lowest intensity.

The shallower scenarios, i.e. those at a depth of 5 km, have median values of intensity that are roughly half a unit higher than those at a depth of 10 km.

In all scenarios, the intensity range among the median intensity values decreases with distance, ranging from one intensity unit at 50 km to more than two intensity units at R_{hypo} 200 km.
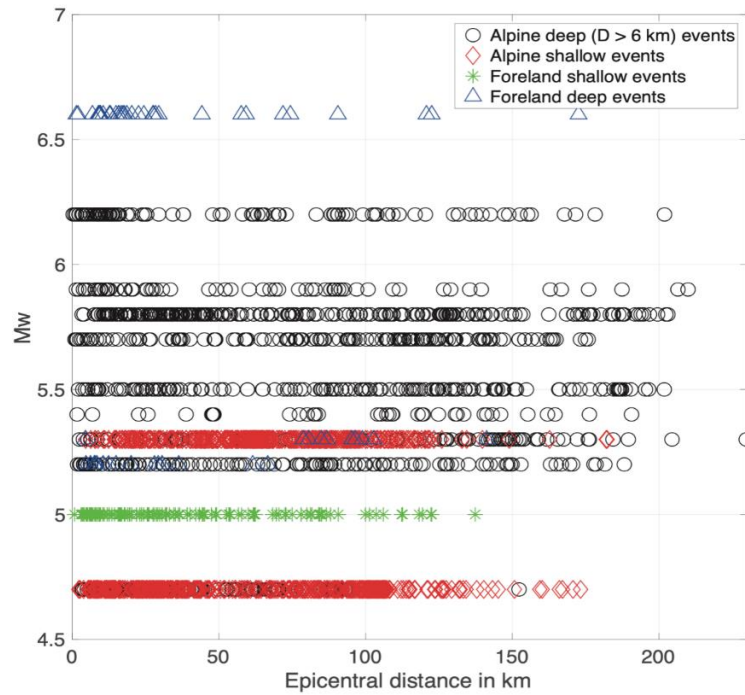
Figure 2.3. ECOS-09 - subset of macroseismic intensity data used for testing the compatibility and the performance of candidate IPEs.

Table 2.2. Ranking of the candidate IPEs based on the informational log-likelihood index (LLH) of Scherbaum et al. (2009).

IPEs	LLH
ECOS-09FixedDepth	1.4700
FaccioliCauzzi2006	1.4700
ECOS-09VariableDepth	1.4850
BaumontEtAl2018High2210IAVGDC30n7	1.4960
BaumontEtAl2018Main2110IAVGDC30n7	1.4960
BindiEtAl2011RHypo	1.4980
AllenEtAl2012Rhypo	1.4980
BaumontEtAl2018Low2210IAVGDC30n7	1.4980
BindiEtAl2011RepiFixedH	1.5240
PasoliniEtAl2008OLS	1.5290
BaumontEtAl2018Main2120IAVGDC50n7	1.5480
BaumontEtAl2018Low2220IAVGDC50n7	1.5550
BaumontEtAl2018Main2120IAVGDC30n7	1.5560
BaumontEtAl2018Low2220IAVGDC30n7	1.5640
PasoliniEtAl2008GOR	1.5710
AllenEtAl2012	1.6110
BindiEtAl2011Repi	1.6350
Musson2005	1.6390
Musson2013	1.7910
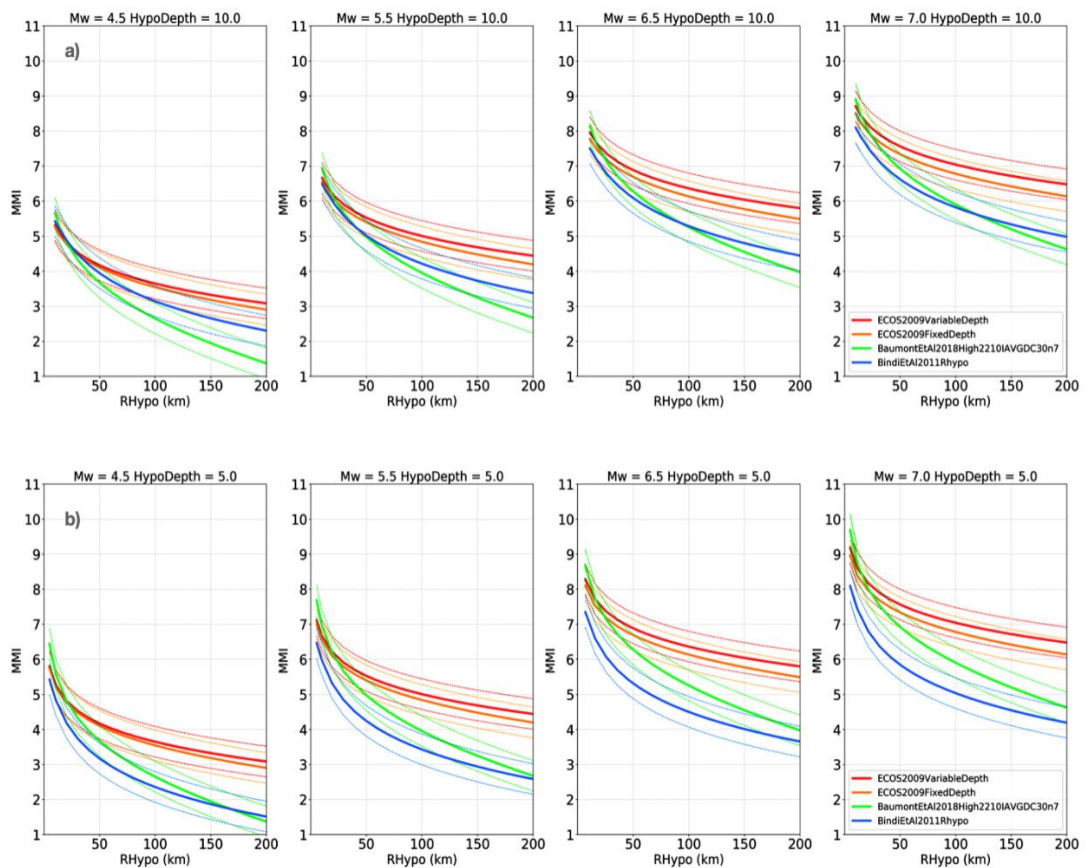
Figure 2.4. Median intensity values of the four selected IPEs as a function of hypocentral depth for different magnitude scenarios (Mw = 4.5, 5.5, 6.5, 7.0) for 10 km (top) and 5 km (bottom) hypocentral depths. The uncertainty range (dash lines) corresponds to the median +/- standard deviation of each IPE.

2.5   Treatment of uncertainty

SUIhaz2015 is a probabilistic hazard model that captures both epistemic and aleatory uncertainties of combined earthquake rate forecast and ground motion models as a function of seismogenic depth in regional seismotectonic settings, i.e. Foreland and Alpine. For each of the following seismotectonic region combinations, a logic tree is produced: Alpine Shallow, Alpine Deep, Foreland Shallow and Foreland Deep. The shallow logic tree characterises the modelling uncertainties of shallow seismicity down to 9 km, whereas the deep logic tree models the observed deep seismicity above 9 km. The resulting overall logic tree has more than 500,000 end branches, and 100,000 end branches were sampled to calculate the SUIhaz2015 hazard.

The seismic hazard updates augment the current ground motion models, namely the acceleration-based model with the intensity-based model. The latter uses macroseismic data and information to describe ground shaking properties, while the former is based on the same ground motion model as SUIhaz2015.

The logic tree of the seismogenic source model is identical with that of SUIhaz2015, with one branching level depicting the five earthquake rate models 2.5th, 16th, 50th, 84th and 97.5th. The assigned weights follow the area under a normal distribution, i.e. 68% for the 50th earthquake rate model, 13.5% for the 16th and 84th, and 2.5% for the 2.5th and 97.5th.

In general, these earthquake rate models are considered correlated in the implementation for calculation of the seismic hazard, as it is impossible to generate a completely uncorrelated source model for very complex and large-scale regional computations; however, uncorrelated uncertainties are routinely used in the implementation of source models for site-specific hazard analyses.

Alternately, one could generate random source models from uncorrelated logic tree branches, which would result in tens of thousands of input models that are similarly challenging to manage.

The use of a collapsed or weighted mean of the earthquake rate forecast is a pragmatic method for reducing computational demand, but it also reduces the influence of the extreme upper and lower values, which can have a significant impact on the regional seismic risk calculation (Crowley et al., 2021). Further sensitivity analyses have confirmed this observation, and it was ascertained by consensus that the synchronous assignment of improbable rates in all sources (e.g. in the 2.5th or 97.5th quantile rate branches) across the nation introduces bias that should be avoided. As a result, a single 'collapsed' source model branch is used, derived by obtaining a weighted average of the rates of the five original branches.

The aleatory uncertainty of the SUIhaz2015 ground motion model aims at reducing the total sigma of the original predictive equation by removing the ergodic assumption (Rodriguez-Marek et al., 2013).

This reduction of the total sigma is based on single-station sigma values obtained using two different approaches: using a regionally independent model for within-event ground motion variability (i.e. *phi_s2s*, Rodriguez-Marek et al., 2013), and using Swiss-specific within-event ground motion variability (i.e. *phi_ss*, Edwards and Fäh, 2013), as illustrated in Figure 2.5.

Within the ERM-CH23 framework, substantial effort was directed towards the development of the national and local site amplification model.
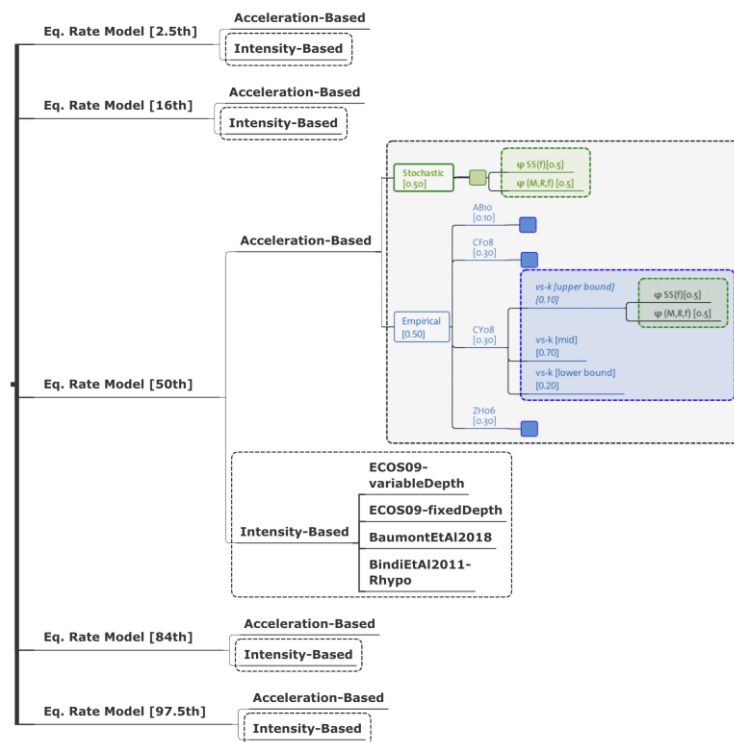
Figure 2.5. Updated SUIhaz2015 logic tree with the intensity-based ground motion models in addition to the earthquake rate branches and the acceleration-based ground motion models. The alternative branches of the single-station sigma are also shown for the empirical and stochastic ground motion models.

Four national amplification maps for PGV and spectral acceleration at 0.3, 0.6, and 1 s are provided by the newly developed amplification model (Bergamo et al., 2022; Panzera et al., 2021). In addition, the spatial variability of site-to-site variability (phi s2s) and single-site within-event variability (phi ss) is mapped with a relatively high resolution, 50 x 50 m.

Models of amplification with a higher resolution are provided for Sion, Visp and Lucerne, which are then used to validate the independently derived national model. The log10 units of the amplifica-

tion factors are converted to natural logarithms and added to the logarithmic spectral accelerations predicted by the relevant GMPEs. In addition, the aleatory component of the GMPEs was updated to account for the updated site-to-site and single-station variability provided by the amplification model. The latter two are given in the form of raster maps and a site-specific definition of uncertainty is embedded in the model.

For the intensity-based model, Baumont et al. (2018) is the only selected IPE that separates the total sigma in between- and within-event terms and it was decided to transfer this aleatory model to all IPEs. The values are 0.373 for the between-event term and 0.227 for the within-event term. Combining these two terms yields 0.436 units of intensity as a total sigma of the IPEs, which is lower than the 0.710 value for Bindi et al. (2011) but almost the same as the sigma for ECOS-09 i.e. 0.4073.

2.6   Verification and sanity checks

Earthquake rate forecast

Validating the earthquake rate forecast is barely possible because of lack of moderate to strong seismicity within the region but also within the time horizon of interest. The earthquake catalogue spans about 1,000 years of seismicity, which might not be enough to capture the recurrence cycle of moderate to large earthquakes. Sanity checks and recurrence rate comparison were performed during the development of the SUIhaz2015 seismogenic source model (section 4.13, Wiemer et al., 2016). These sanity checks were the re-aggregation of the regional b-value evaluation of the recurrence time intervals for various magnitudes.

The average mean recurrence (in years) of very large events Mw>6.5 is depicted in Figure 2.6. As shown, these large events are expected to occur once every 1,500 years in the Valais, which is consistent with historical data – the largest event recorded so far was an M6.2 near Visp in 1852. Furthermore, Figure 2.6 suggests that an earthquake occurs every 3,000 to 4,000 years in the Basel area, which is consistent with paleoseismic data.
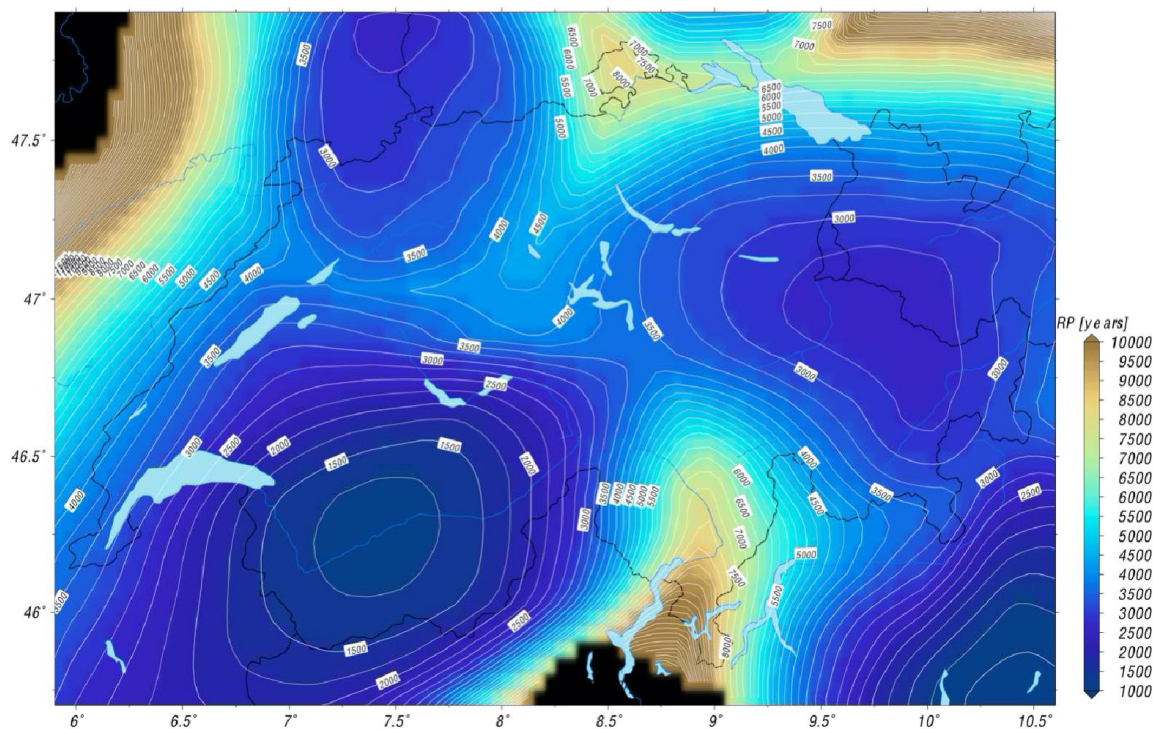
Figure 2.6. Average recurrence period (in years) of a magnitude 6.5 or larger earthquake within a 50 km radius for any point in Switzerland. In the Basel area, this value is around 3,000 years (from Wiemer et al., 2016).

Acceleration-based vs. intensity-based models

The ground motion intensity conversion equations (GMICEs) of Faenza and Michellini (2010, 2011) combined with the SUIhaz2015 GMPEs were used to convert the acceleration to intensity and then compare it with the selected IPEs. The median intensity estimates of GMICEs/GMPEs and IPEs for various scenarios Mw=4.5, 5.5, 6.5 as a function of hypocentral distance are given in Figure 2.7. A hypocentral depth of 10 km is used and the spectral acceleration SA at 1 s is used as the proxy for macroseismic intensity conversion.

Generally, the intensity decays with distance are adequately consistent for all ground motion models. It is interesting to note that the intensity range of the GMICE/GMPEs is lower for the low magnitudes i.e, Mw4.5 and 5.5, than for the moderate to large magnitudes, i.e. Mw6.5 to 7.3. As expected, the lower bounds of the converted intensity are due to the stochastic GMPEs with low stress drop (10, 20, 30 bars), whereas the upper bounds are given by intensity converted from the empirical GMPEs. Overall, there is consistency between the two types of ground motion models, i.e. acceleration- and intensity-based, and the discrepancies are seen as part of the epistemic uncertainty.

The GMICEs could theoretically be used as an alternative intensity-based model, but there are various concerns that using GMICEs will not contribute any additional knowledge to key ground shaking properties such as source path and site, but rather increase the uncertainties due to conversion of ground shaking parameters to intensity.

Indeed, the aleatory uncertainties of the GMICE/GMPE pair cause the model sigma to increase due to the convolution of the GMPE and GMICE standard errors. The inflated aleatory term of the GMICE/GMPE pair will result in extreme intensity field values, which will have a substantial effect on risk calculation and is therefore not preferred. In other words, the macroseismic intensity's randomness is not determined by observations, but rather by a statistical convolution of conversion equations.
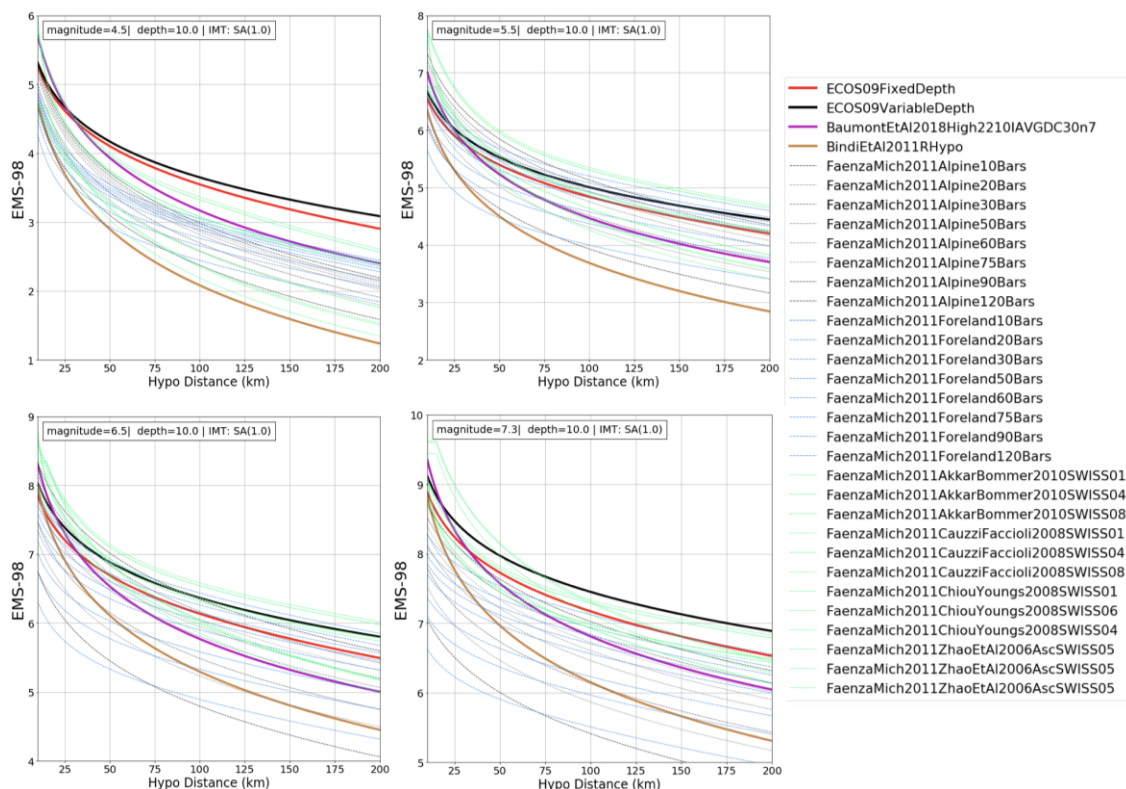
Figure 2.7. Median intensity values of the four selected IPEs together with the median intensity estimates using the GMICEs of Faenza and Michellini (2011) and the SUIhaz2015 GMPEs. The median estimates are given for different magnitude scenarios (Mw = 4.5, 5.5, 6.5, 7.3) as a function of hypocentral distance (R_{hypo}). The hypocentral depth is 10 km.

Intensity-based models vs. observations

The selected IPEs are compared to the intensity data observations available in the ECOS-09 macroseismic database for various magnitude scenarios. The following historical earthquakes are compared here: Ftan (Graubünden) on 03.08.1622, M5.3, Brig-Naters (Valais) 09.12.1755, M5.7, Churwalden (Graubünden) on 03.09.1295, M6.2, and Basel 18.10.1356, M6.6. Macroseismic intensity data points are plotted together with the median and one standard deviation of the four selected IPEs in Figure 2.8. Overall, for all distance ranges, the intensity range of the four selected IPEs adequately covers the intensity data observations for these historical scenarios. Neither the IPEs nor the macroseismic data are corrected to a rock reference for this comparison.
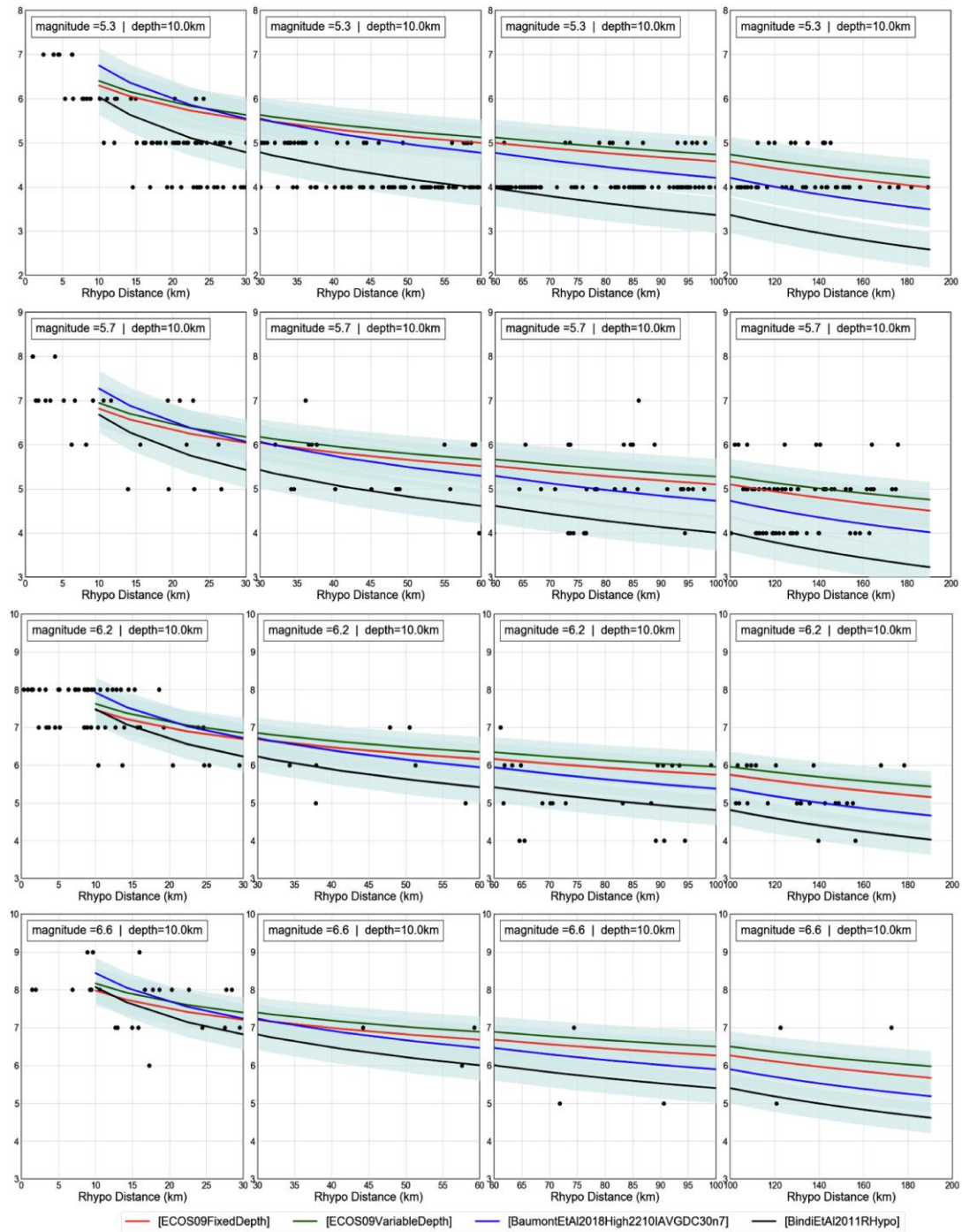
Figure 2.8. Median intensity estimates of the selected IPEs and the intensity data points for four historical earthquakes in the ECOS-09 macroseismic dataset.

These comparisons, which are supported by various sensitivity analyses performed within the seismic risk calculation, indicate that IPEs are a viable alternative to acceleration-based models. Although not as robust as the recent GMPEs, IPEs do provide access to earthquake datasets and information that can be viewed independently of the recorded ground shaking. However, the uncertainties in macroseismic data and information are rather large, particularly for historical events, and this may be viewed as a limitation of intensity-based models that should be considered when deciding on model weights.

References

Al Atik, L., Kottke, A., Abrahamson, N. Hollenback, J. (2014). Kappa (Kappa) Scaling of Ground-Motion Prediction Equations Using an Inverse Random Vibration Theory Approach, Bulletin of the Seismological Society of America **104**, 336–346.

Allen, T.I., Wald, D.J., Worden, C.B. (2012). Intensity attenuation for active crustal regions. Journal of Seismology **16**, 409–433. https://doi.org/10.1007/s10950-012-9278-7

Álvarez-Rubio, S., Kästli, P., Fäh, D., Sellami, S., Giardini, D. (2012). Parameterization of historical earthquakes in Switzerland. Journal of Seismology **16**, 1–24. https://doi.org/10.1007/s10950-011-9245-8

Akkar, S. and J. J. Bommer (2010). Empirical Equations for the Prediction of Pga, Pgv, and Spectral Accelerations in Europe, the Medi- terranean Region, and the Middle East, Seismologocal Research Letters **81**, 195–206.

Bard, P.-Y., Bora, S.S., Hollender, F., Laurendeau, A., Traversa, P. (2020). Are the Standard V$_S$-Kappa Host-to-Target Adjustments the Only Way to Get Consistent Hard-Rock Ground Motion Prediction?. Pure and Applied Geophysics **177**, 2049–2068. https://doi.org/10.1007/s00024-019-02173-9

Baumont, D., Manchuel, K., Traversa, P., Durouchoux, C., Nayman, E., Ameri, G. (2018). Intensity predictive attenuation models calibrated in Mw for metropolitan France. Bulletin of Earthquake Engineering **16**, 2285–2310. https://doi.org/10.1007/s10518-018-0344-6

Bergamo P. et al., 2022. SPE – Deliverable AM3 - Provisional amplification maps for integration in the current implementation of the risk model. ERM-CH report, SPG-SPD-0009.

Bindi, D., Parolai, S., Oth, A., Abdrakhmatov, K., Muraliev, A., Zschau, J., 2011. Intensity prediction equations for Central Asia. Geophysical Journal International **187**, 327–337. https://doi.org/10.1111/j.1365-246X.2011.05142.x

Bormann, P., Wendt, S.,DiGiacomo, D 2013). Seismic Sources and Source Parameters. - In: Bormann, P. (Ed.), New Manual of Seismological Observatory Practice 2 (NMSOP2), Potsdam:Deutsches GeoForschungsZentrum GFZ, 1–259. https://doi.org/10.2312/GFZ.NMSOP-2_ch3

Cauzzi, C. and E. Faccioli (2008). Broadband (0.05 to 20 S) Prediction of Displacement Response Spectra Based on Worldwide Digital Records, Journal of Seismology **12**, 453–475

Chiou, B. S. J. and R. R. Youngs (2008). An Nga Model for the Average Horizontal Component of Peak Ground Motion and Response Spectra, Earthquake Spectra **24**, 173–215

Crowley, H., Dabbeek, J., Despotaki, V., Rodrigues, D., Martins, L., Silva, V., Romão, X., Pereira, N., Weatherill, G., Danciu, L. (2021). European Seismic Risk Model (ESRM20).

Danciu, L. and Giardini, D., (2015). Global Seismic Hazard Assessment Program - GSHAP legacy. Annals of Geophysics **58**. https://doi.org/10.4401/ag-6734

Danciu, L., Fäh, D. (2017). Adjustments Of The 2015 Updates Of The Swiss Hazard Model To Different Rock Conditions (Vs-Kappa Adjustment), Technical Report SED 2017/06, Swiss Seismological Service, ETH Zurich, Switzerland, doi:10.12686/a4

Danciu, L., Nandan, S., Reyes, C., Basili, R., Weatherill, G., Beauval, C., Rovida, A., Vilanova, S., Sesetyan, K., Bard, P-Y., Cotton, F., Wiemer, S., Giardini, D. (2021). The 2020 update of the European Seismic Hazard Model: Model Overview. EFEHR Technical Report 001, v1.0.0, https://doi.org/10.12686/a15

Edwards, B., Cauzzi, C., Danciu, L., Fäh, D. (2016). Region-Specific Assessment, Adjustment, and Weighting of Ground-Motion Prediction Models: Application to the 2015 Swiss Seismic-Hazard Maps. Bulletin of the Seismological Society of America **106**, 1840–1857. https://doi.org/10.1785/0120150367

Edwards, B., Fäh, D. (2013). A Stochastic Ground-Motion Model for Switzerland. Bulletin of the Seismological Society of America **103**, 78–98. https://doi.org/10.1785/0120110331

Edwards, B., Ktenidou, O.-J., Cotton, F., Abrahamson, N., Houtte, C.V., Fäh D. (2015). Epistemic Uncertainty and Limitations of the Kappa0 Model for near-Surface Attenuation at Hard Rock Sites. Geophysical Journal International **202**(3), 1627–1645.

Faccioli, E. and Cauzzi, C., Macroseismic Intensities For Seismic Scenarios, Estimated From Instrumentally Based Correlations (2006) First European Conference On Earthquake Engineering And Seismology, Geneva, Switzerland, 3–8 September 2006 Paper Number: 569.

Fäh, D., Giardini, D., Bay, F., Bernardi, F., Braunmiller, J., Deichmann, N., Furrer, M., Gantner, L., Gisler, M., Isenegger, D., Jimenez, M.-J., Kästli, P., Koglin, R., Masciadri, V., Rutz, M., Scheidegger, C., Schibler, R., Schorlemmer, D., Schwarz-Zanetti, G., Steimen, S., Sellami, S., Wiemer, S., Wössner, J. (2003). Earthquake Catalogue of Switzerland (ECOS) and the related macroseismic database. Eclogae geol. Helv. – Swiss Journal of Geosciences **96**, 219–236.

Fäh, D., Giardini, D., Kästli, P., Deichmann, N., Gisler, M., Schwarz-Zanetti, G., Alvarez- Rubio, S., Sellami, S., Edwards, B., Allmann, B., Bethmann, F., Wössner, J., Gassner-Stamm, G., Fritsche, S., Eberhard, D. (2011). ECOS-09 Earthquake Catalogue of Switzerland Release 2011 Report and Database. Public catalogue, 17.4.2011. Swiss Seismological Service ETH Zurich, Report SED/RISK/R/001/20110417.PDF

Giardini, D., Wiemer, S., Fäh, D. (2004). Seismic Hazard Assessment of Switzerland, 2004, Swiss Seismological Service Report, ver 1.1, Nov 25th, Swiss Federal Institute of Technology (ETH) Zürich.

Musson, R.M.W. (2005). Intensity attenuation in the U.K. Journal of Seismology **9**, 73–86. https://doi.org/10.1007/s10950-005-2979-4

Musson, R.M.W. (2013). Updated intensity attenuation for the UK [WWW Document]. URL https://nora.nerc.ac.uk/id/eprint/503214/ (accessed 6.12.22).

Musson, R.M.W., Grünthal, G., Stucchi, M. (2010). The comparison of macroseismic intensity scales. Journal of Seismology **14**, 413–428. https://doi.org/10.1007/s10950-009-9172-0

Pagani, M., Monelli, D., Weatherill, G., Danciu, L., Crowley, H., Silva, V., Henshaw, P., Butler, L., Nastasi, M., Panzeri, L., Simionato, M., Vigano, D. (2014). OpenQuake Engine: An Open Hazard (and Risk) Software for the Global Earthquake Model. Seismological Research Letters **85**, 692–702. https://doi.org/10.1785/0220130087

Panzera, F., Bergamo, P. Fäh, D. (2021). Reference soil condition for intensity prediction equations derived from seismological and geophysical data at seismic stations. Journal of Seismology **25**, 163–179. https://doi.org/10.1007/s10950-020-09962-z

Pasolini, C., et al. (2008), The attenuation of seismic intensity in Italy, Part II: Modeling and validation. Bulletin of the Seismological Society of America **98**(2), 692–708.

Poggi, V., Edwards, B., Fäh, D. (2011). Derivation of a Reference Shear-Wave Velocity Model from Empirical Site Amplification. Bulletin of the Seismological Society of America **101**, 258–274. https://doi.org/10.1785/0120100060

Renault, P. (2014). Approach and Challenges for the Seismic Hazard Assessment of Nuclear Power Plants: The Swiss Experience. *Bollettino* di Geofisica Teorica ed Applicata **55**, 149–164.

Rodriguez-Marek, A., Cotton, F., Abrahamson, N.A., Akkar, S., Al Atik, L., Edwards, B., Montalva, G.A., Dawood, H.M. (2013). A Model for Single-Station Standard Deviation Using Data from Various Tectonic Regions, Bulletin of the Seismological Society of America **103**, 3149–3163.

Scherbaum, F., Delavaud, E., Riggelsen, C. (2009) Model selection in seismic hazard analysis: an information- theoretic perspective. Bulletin of the Seismological Society of America **99**, 3234–3247.

Wiemer, S., Giardini, D., Fäh, D., Deichmann, N., Sellami, S. (2009). Probabilistic seismic hazard assessment of Switzerland: best estimates and uncertainties. Journal of Seismology, **13**(4), 449–478.

Wiemer, S., Danciu, L., Edwards, B., Marti, M., Fäh, D., Hiemer, S., Wössner, J., Cauzzi, C., Kästli, P., Kremer, K. (2016). Seismic Hazard Model 2015 for Switzerland (SUIhaz2015). https://doi.org/10.12686/A2

Woessner, J., Laurentiu, D., Giardini, D., Crowley, H., Cotton, F., Grünthal, G., Valensise, G., Arvidsson, R., Basili, R., Demircioglu, M.B., Hiemer, S., Meletti, C., Musson, R.W., Rovida, A.N., Sesetyan, K., Stucchi, M., The SHARE Consortium, 2015. The 2013 European Seismic Hazard Model: key components and results. Bulletin of Earthquake Engineering **13**, 3553–3596. https://doi.org/10.1007/s10518-015-9795-1

Zhao, J. X., Zhang, J., Asano, A., Ohno, Y., Oouchi, T., Takahashi, T., Ogawa, H., Irikura, K., Thio, H.K., Somerville, P.G., Fukushima, Y., Fukushima, Y. (2006). Attenuation Relations of Strong Ground Motion in Japan Using Site Classification Based on Predominant Period, Bulletin of the Seismological Society of America **96**, 898–913.

3. Soil amplification

3.1 Introduction

Subproject E was undertaken by the Engineering Seismology group of the Swiss Seismological Service (SED) at ETH Zurich. The scope of the subproject was to develop the site-response layer for the risk model. The work was performed by mapping the local amplification at two different scales, national and local.

At the *national level*, a global site-response model was finalised, covering homogeneously the whole of Switzerland. Consistent with the global architecture of ERM-CH23, the national model is composed of four maps portraying the soil amplification for each of the following ground-motion parameters: peak ground velocity (PGV), pseudo-spectral acceleration (PSA) at periods of 1.0 s, 0.6 s and 0.3 s. The choice was driven by the requirement of consistency with the ground-motion parameters and specific periods selected by modules C ('Seismic hazard for reference rock condition' and 'Risk implementation') and G ('Building taxonomy and fragility models'). Furthermore, Panzera et al. (2016, 2020) showed that PGV and spectral acceleration at 0.3 s are the instrumental quantities that best correlate with macroseismic intensity and hence, by extension, with damage. The produced ground-motion amplification maps are accompanied by corresponding layers mapping their uncertainties. The PGV, PSA(1.0s) and PSA(0.3s) soil amplification maps were also translated to macroseismic intensity aggravation layers, consistently with the two parallel approaches (intensity- and ground-motion-based) followed throughout ERM-CH23.

At the *local scale*, areas with a high level of hazard and/or exposure were targeted for the preparation of specific site response models, achieving higher accuracy and finer spatial resolution than the national model. The zones covered by local models are the areas of Visp and Sion in SW Switzerland, and the sedimentary basin of Lucerne-Horw in Central Switzerland (study undertaken in cooperation with the H2020-EU project URBASIS - New challenges for Urban Engineering Seismology). The local models map the site response in ground motion at the periods of 1.0 s, 0.6 s and 0.3 s as well as their corresponding uncertainties.

3.2 National soil amplification model

Mapping the site response of strong ground motion is one of the key steps in earthquake risk assessment studies. Local, accurate site amplification models are generally obtained in the framework of microzonation studies (e.g. Lachet et al., 1996). On the other hand, at a larger (e.g. national) scale, the approach is generally more approximate, and can consist of mapping proxies for site amplification (e.g. average shear-wave velocity in the upper 30 m V_{S30}), using topographical and/or geological indicators (e.g. Vilanova et al., 2018). More recently, works such as Weatherill et al. (2020) have illustrated the possibility of directly mapping the local amplification at a large spatial scale from indirect site condition parameters. Similarly, we derived a national soil amplification layer for Switzerland by extrapolating the local site amplification measured at seismic stations, and using site condition indicators as predictor variables (cf. our preparatory studies: Bergamo et al. 2019, 2021a, 2022a). The site response measurements at instrumented sites are directly incorporated into the amplification model by means of regression-kriging (RK, Hengl et al., 2007), locally increasing the accuracy of the maps and decreasing their uncertainty.

3.2.1 Dataset of site response measurements from instrumented sites

The local earthquake response was estimated at Swiss instrumented sites by means of the empirical spectral modelling technique (ESM, Edwards et al., 2013). ESM combines physical modelling and a statistical approach for the interpretation of the acceleration spectra recorded by seismic stations after each event; the interpretation is based on the separation of source, path and site terms, modelled according to Edwards and Fäh (2013). The method is routinely applied at the

Swiss Seismological Service to determine the magnitude of events as well as for the reconstruction of local effects at instrumented sites. Processed regional earthquakes must produce – at least at three stations – recordings with S/N ratio > 3 on both horizontal components over at least one order of magnitude on the frequency axis. The experimental spectra are fitted with those expected from a Brune (1970, 1971) ω^2 source model, accounting for geometrical decay and path attenuation. The spectral matching allows the determination of moment magnitude and stress drop (Edwards et al., 2010), and the residuals at each station are then inverted to estimate the local Fourier amplification function, relative to the Swiss standard rock model (having Vs30 = 1,105 m/s, Poggi et al., 2011). The amplification function representative for each instrumented site is therefore obtained by averaging the site-term estimates from several events.

The reliability of ESM-derived local response functions has been assessed by means of comparison with site-to-reference spectral ratios (Edwards et al., 2013), SH-transfer functions from measured V_S profiles (Michel et al., 2014; Hobiger et al. 2021; Bergamo et al. 2022a), measured site-condition parameters (Bergamo et al. 2021a) and surface-to-borehole ratios in its application to Japanese data (Bergamo et al., 2021a). Recently, the reliability of ESM has been assessed in a benchmark study alongside other Generalised Inversion Technique methods (Shible et al., 2022). It is worth specifying that the ESM implementation we use applies the stochastic model of Edwards and Fäh (2013), developed specifically for Switzerland; hence, the other ground-motion models used in ERM-CH23 (Section 2.3) are not considered in this specific step. However, the collation between Edwards and Fäh (2013) with worldwide real and synthetic ground-motion data shows a good reciprocal agreement (Panzera et al., 2021a), i.e. Edwards and Fäh (2013) is affected by neither a systematic overprediction nor underprediction of ground motion.

Processing with ESM all regional earthquakes from the period 2001-2021, we were able to attribute an inelastic Fourier amplification function, constrained by at least five events in the band 0.5-10 Hz, to about 250 (urban) free-field stations (Figure 3.1, top left and bottom panels).

Finally, for compatibility with the other modules of ERM-CH23 (SPC, SPG), the Fourier amplifications are translated to PSA amplifications resorting to random vibration theory (RVT, Boore 2003, see Figure 3.1, top right panel). For the selection of the earthquake scenario for the RVT conversion, we relied on the results of the disaggregation (Bergamo et al., 2022b) of the hazard model for Switzerland with a return period of 475 years (Wiemer et al., 2016). At long periods (disaggregation available for SA(1.0s)), the most common dominant scenario to exceedance is magnitude (M_W) = 5.8 and Joyner-Boore distance (R_{JB}) = 15 km. This scenario has the highest contribution to a SA(1.0s) exceedance at 55% of the nodes of the disaggregation spatial grid covering Switzerland. Sensitivity analyses carried out by varying the magnitude and distance (e.g. Figure 3.2) show – at the periods of interest – a small dependence of the obtained PGV and PSA amplifications on the selected scenario, largely comprised within the within-event variability of local response observed at the stations (consistently with the findings of Poggi and Fäh, 2015).
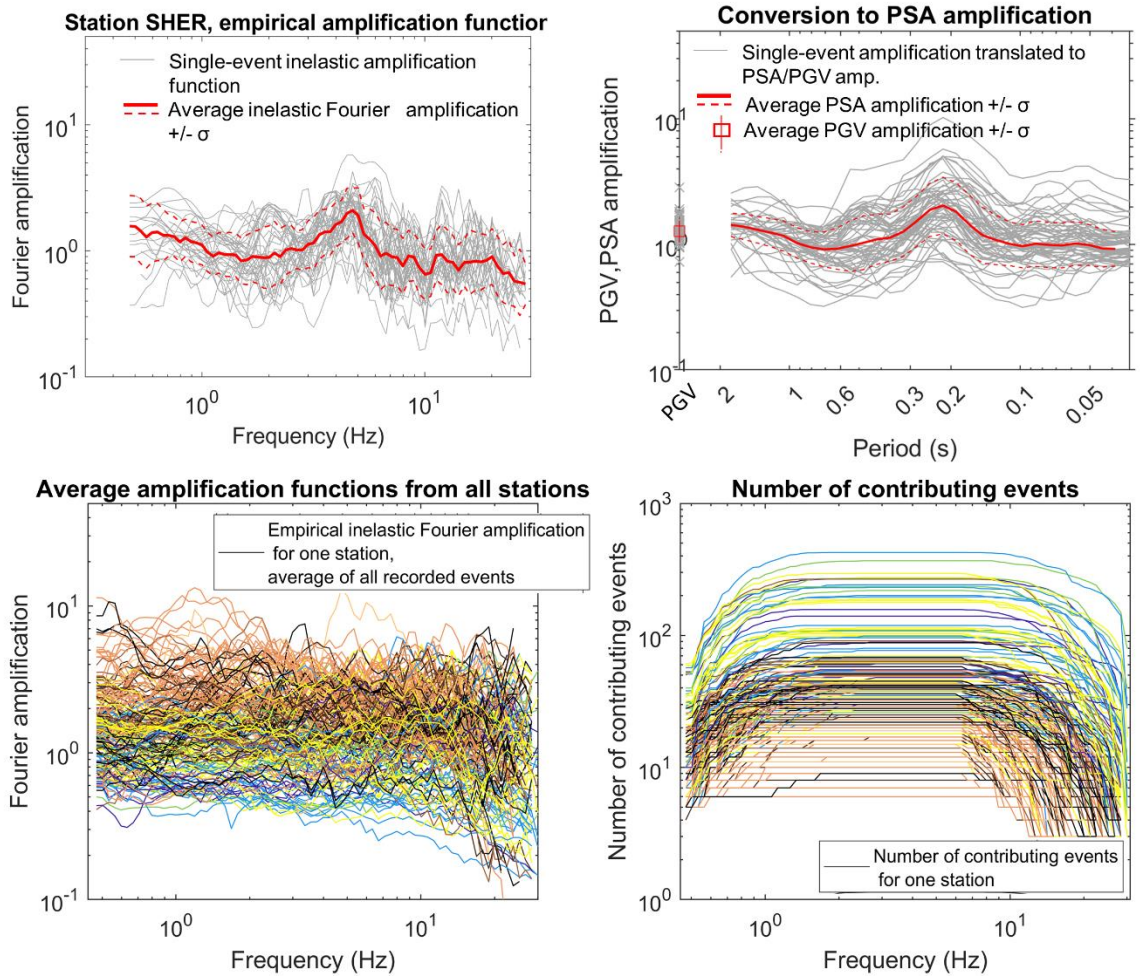
Figure 3.1. Top left: empirical Fourier amplification function obtained using the empirical spectral modelling technique for the strong motion station SHER (Hérémence, SW Switzerland). Top right panel: conversion of the Fourier amplification into *PGV*, *PSA* amplification with random vibration theory. In both panels the amplification functions derived from an individual earthquake are represented as grey lines, their global average and ± σ interval as red continuous and dashed lines respectively. Bottom left panel: average Fourier empirical amplification functions extracted at ~260 (urban) free-field stations in Switzerland and constrained by at least five events in the range 0.5–10 Hz. Bottom right panel: number of events contributing to the average amplification function at each considered frequency for all stations. In both lower panels the data for each station are represented in a colour corresponding to the local lithotype (same colour legend as Figure 3.3, upper panel).
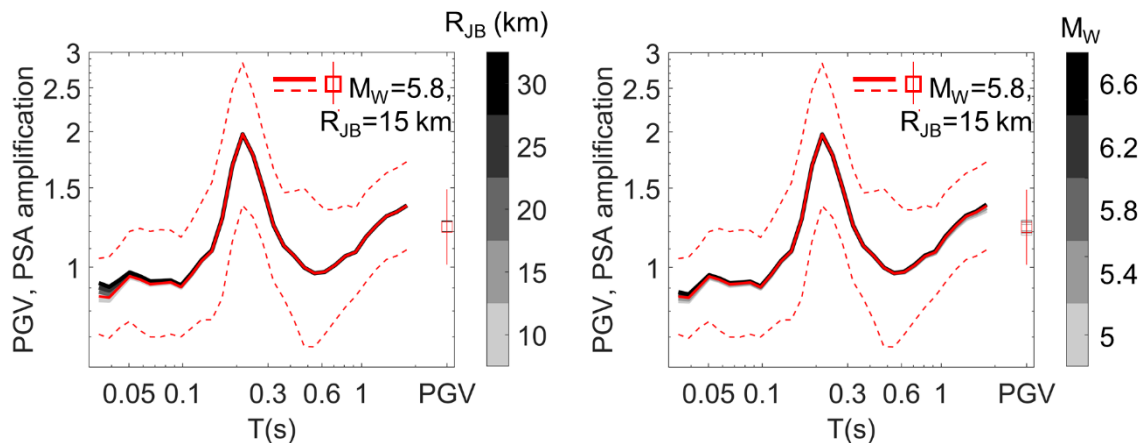
Figure 3.2. Sensitivity analyses on the dependence of the *PGV,PSA* amplification of station SHER on the magnitude – distance scenario employed for the RVT conversion from Fourier aggravation to spectral response. Left: sensitivity analysis fixing $M_W = 5.8$ and increasing R_{JB} from 10 to 30 km, by 5 km steps (obtained *PGV,PSA* amplification functions in greyscale). Right: sensitivity analysis fixing $R_{JB} = 15$ km and increasing M_W from 5 to 6.6, by steps of 0.4 (obtained *PGV,PSA* amplification functions in greyscale). Red lines and symbols are the same as Figure 3.1, top right panel.

3.2.2   Layers of site condition indicators

For the extrapolation of the high-quality (but local) information provided by the empirical amplification functions from instrumented sites, we used site condition proxies (SCPs) as predictor variables. Several studies have evidenced the correlation between topographical or geological indicators and geophysical parameters related to site response (e.g. V_{S30}, Wald and Allen, 2007) as well as site amplification itself (Weatherill et al., 2020). Based on existing literature and our own studies dedicated to Switzerland (Bergamo et al., 2019, 2021a, 2022c), we selected the following SCPs:

-   A bespoke *lithological classification of Switzerland*, based on the 1:500'000 national geological map (Swisstopo, 2005; Figure 3.3, upper panel). We also tested alternative classifications based on the 1:200,000 geotechnical map of Switzerland (Swisstopo 1967) and the 1:25,000 geological atlases (Swisstopo 2017). However, the former had issues related to the recent digitisation of the map and the latter had to be abandoned because of inconsistencies among the 220 different atlases covering Switzerland.

-   *Multi-scale maps of the topographical slope* (e.g. Figure 3.3, lower left panel), derived from the digital height model DHM25 (Swisstopo, 1999) covering Switzerland with a regular grid of 25 x 25 m cells. We computed the topographical slope at seven spatial scales between 75 and 3600 m. A sensitivity analysis correlating *PGV* and *PSA* amplifications with the topographical slopes identified the slope at 275 m scale as the one achieving the highest correspondence with *PGV* and *PSA*(0.3s) amplification, and the slope at 600 m scale as the one best correlating with *PSA*(1.0s) and *PSA*(0.6s) amplification.

-   The *depth to bedrock* as estimated by the bedrock model by Swisstopo (2019), covering most of Switzerland (Figure 3.3, lower right). The reliability of this dataset was assessed by comparing it with ~225 V_S profiles from site characterisation surveys (Michel et al., 2014, Hobiger et al., 2021). The comparison highlighted good reliability for predicted values of bedrock depth larger than a few metres; areas with predicted depths < 3 m were therefore discarded from the map (grey area in Figure 3.3, lower right).
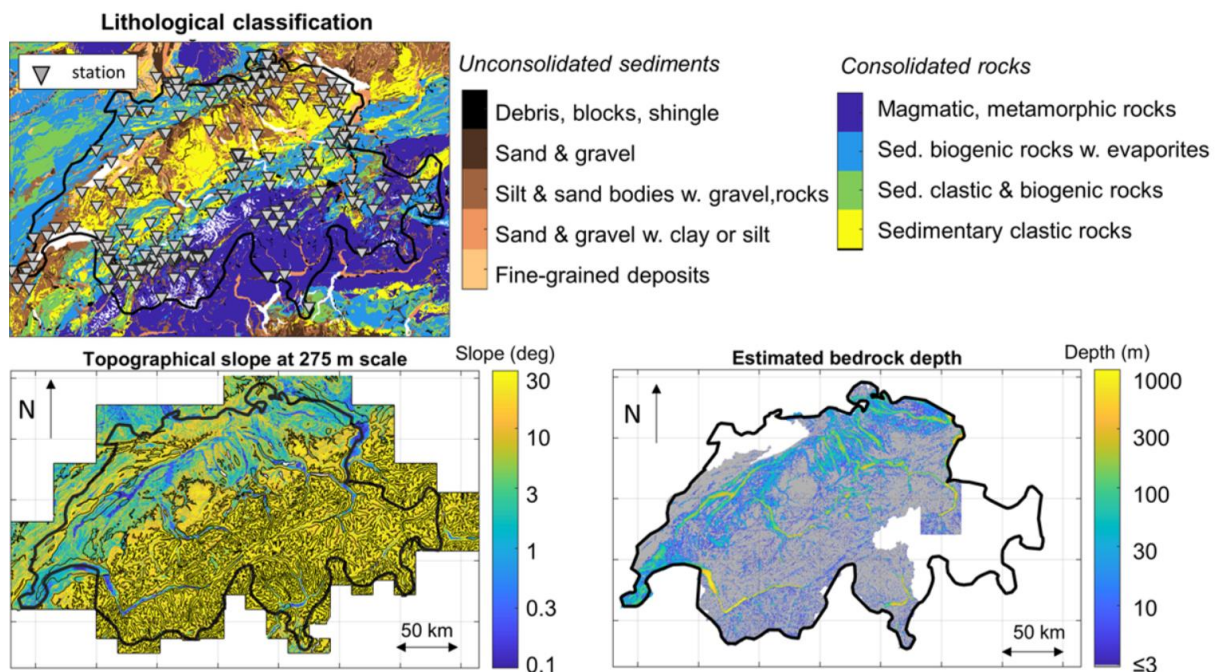
Figure 3.3. Employed site condition indicators. Top left: map of the adopted simplified lithologic classification and location of the ~260 (urban) free-field stations with empirical amplification function. Bottom left: topographical slope at the spatial scale of 275 m. Bottom right: map of bedrock depth derived from the Swisstopo 2019 model; predictions < 3 m are not considered reliable and are highlighted in grey. Blank areas are not covered by the Swisstopo model.

3.2.3 Workflow for the mapping of soil amplification

Once compiled, the joint datasets of measured site amplifications and layers of local condition parameters (3.2.1, 3.2.2) were combined for the mapping of the *PGV*, *PSA*(1.0s, 0.6s and 0.3s) amplification across the whole of Switzerland. As anticipated, the method we employed for the areal prediction of soil response was the regression kriging-algorithm (RK, Hengl et al., 2007). Besides RK, we also tested other strategies – based on machine learning – for forecasting local amplification. The Neural Network (NN) approach turned out to require a training dataset of several hundred seismic stations (Bergamo et al., 2021a, 2022c), which however is not available for Switzerland. As an alternative, the possibility of implementing a Bayesian Network (BN) strategy was explored too; although BN performed reasonably well in the testing phase, the platform used for its implementation (GeNIe Modeler, www.bayesfusion.com/genie) proved inadequate for large-scale predictions. Eventually, the RK strategy was selected as it makes it possible to i) regionally constrain the spatial prediction to local empirical measurements and ii) model the prediction variability in a consistent fashion. For each ground-motion parameter, the RK algorithm involves three successive steps:

- First*,* amplification-*vs*-slope and amplification-*vs*-bedrock depth relationships are derived for each lithotype (e.g. Figure 3.4, top row). Only for one lithotype, 'sand and gravel with clay or silt', hosting the highest number of stations (about 60), a bivariate correlation between amplification and both slope *and* bedrock depth could be reliably constrained.

- Secondly, an amplification prediction is attributed to each 25 x 25 m cell of a raster map covering Switzerland, entering the amplification-*vs*-proxy regressions with the values of slope and/or bedrock depth at the considered cell. If two concurring predictions are available (from topographic slope or bedrock depth), the one derived from the regression with higher r^2 is preferred. A joint map representing the uncertainty of the prediction is also created, filled with the values of standard deviations of uncorrelated residuals of the prediction relationships (see Section 3.4.1).
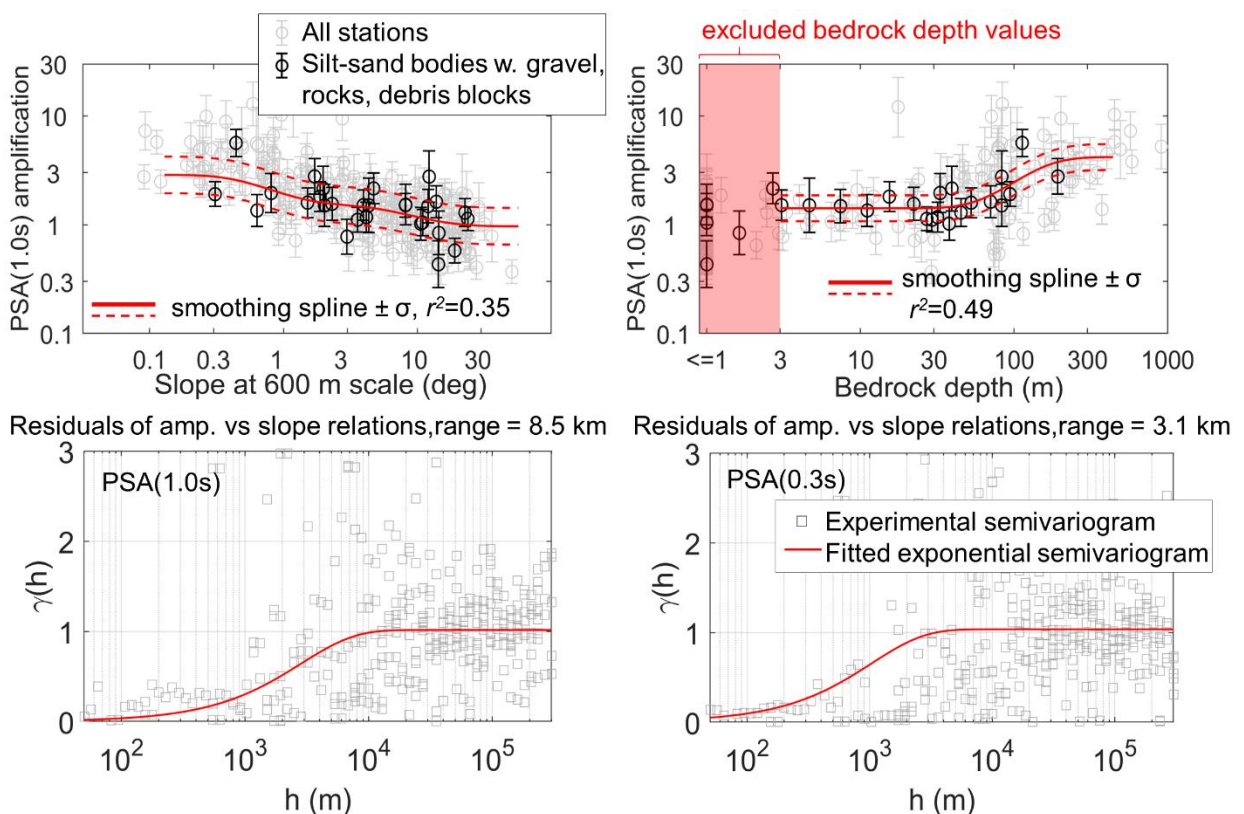
Figure 3.4. Top row: examples of amplification-*vs*-slope (left) and amplification-*vs*-bedrock depth (right) relationships for one sample lithotype. Bottom row: semivariograms of the residuals of amplification-*vs*-slope for *PSA*(1.0s) (left) and *PSA*(0.3s) (right).

- Finally, the spatial correlation of the residuals of the amplification-*vs*-proxy relationships is evaluated by computing their semivariograms (e.g. Figure 3.4, bottom row). We exploit this spatial correlation to implement a final correction of the amplification prediction for the map cells having a distance from the closest station(s) shorter than the semivariogram range. The local correction is performed following Hengl et al. (2007). This final step serves to locally constrain the amplification prediction to nearby measured values and to locally reduce the prediction uncertainty.

The four soil amplification maps obtained by applying this procedure are displayed in Figure 3.5, top row. They cover all of Switzerland with a spatial resolution of 25 m and portray the local amplification referred to the Swiss reference rock profile (V_{S30} = 1,105 m/s), the same standard rock condition adopted for the representation of the seismic hazard (Wiemer et al., 2016). The maps intend to primarily represent the effect of stratigraphic amplification; topographic effects are not explicitly modelled, although they are inevitably embedded at least in a part of the measured amplification functions used in input (Burjanek et al., 2014). Furthermore, given the data and procedure used to estimate such local response functions (Figure 3.1 and Figure 3.2), in the national amplification model a possible nonlinear behaviour (i.e. a strain-dependent increase of damping ratio and decrease of shear modulus in the near-surface at high levels of strain) is not accounted for. However, the most common scenarios with the highest contribution to hazard for return period = 475 years (generally $M_W \leq 6.2$, Bergamo et al., 2022b) and the tectonic regime of Switzerland (without subduction zones) suggest that such high strain levels may not occur over vast areas. Additionally, nonlinear behaviour affects only particular soil types in particular depositional conditions (Darendeli, 2001), and works such as Løviknes et al. (2021) indicate that – in generalised studies at large scales – nonlinear soil response, although relevant for specific sites, is 'diluted' in the dominant linear behaviour, and hence it does not emerge as globally significant. We therefore suggest specifically tackling the modelling of nonlinear soil response at the national level in a future development of the current study, starting for instance from the work of Janusz et al. (2022a).

In general, the local response maps predict a soil amplification ≤ 1 (i.e. equal to or lower than the one expected for the Swiss standard rock profile) for the mountainous areas of the Alps and the Jura; the alluvial or lacustrine sediments of the valley bottoms of the Alps and Jura display high amplification factors (around 4-5 and up to 10 for fine-grained sediments), particularly at low periods. Gravel terraces and moraines of the Swiss Foreland show moderate values of amplification (around 2-3), while the clastic sedimentary rocks of the Swiss Molasse present factors slightly higher than 1 (1.2-1.4).
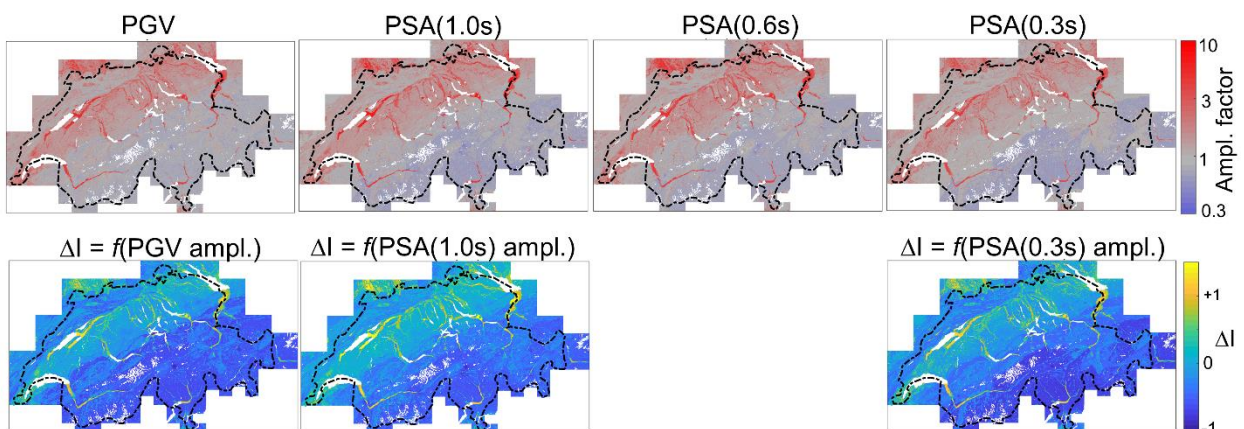
Figure 3.5. Top row: obtained maps of amplification of ground-motion intensity measures. The amplification is referred to the Swiss reference rock profile (V_{S30} = 1105 m/s). Bottom: macroseismic intensity aggravation (*ΔI*) maps derived from the ground-motion amplification layers by means of eq. 3.1; the maps are here referred to the soil conditions of the IPEs ($V_{S30} \approx 600$ m/s), using the central value of the correction factor ranges specified in the text.

3.2.4   Conversion to macroseismic intensity aggravation

The obtained amplification maps for *PGV* and *PSA* were also translated to macroseismic intensity aggravation layers. The conversion is based on the relations between macroseismic intensity and ground-motion measures of Faenza and Michelini (2010, 2011); the amplification in macroseismic intensity units *ΔI* (i.e. aggravation at the target site with respect to a reference I_{ref}) is computed following Michel et al. (2017) and Panzera et al. (2019):

$$\Delta I = I - I_{ref} = [a + b \log 10(PSA(T))] - [a + b \log 10(PSA_{ref}(T))] = b \log 10(A(T)) \qquad (3.1)$$

where *a, b* are the coefficients of the relations by Faenza and Michelini (2010, 2011), and *A(T)* is the *PSA* amplification at period *T* or the *PGV* amplification. Using equation 3.1, the maps of *PGV*, *PSA(1.0s)* and *PSA(0.3s)* amplification were translated to *ΔI* layers (Figure 3.5, bottom row; Faenza and Michelini (2011) do not provide any relation for *T* = 0.6s). *ΔI* obtained from eq. 3.1 is relative to the same reference condition of the ground-motion amplification maps in input, that is the Swiss standard rock profile (V_{S30} = 1,105 m/s). This soil condition, however, is not the same as that of the intensity prediction equations (IPEs) developed for Switzerland (Fäh et al., 2011), which define I_{ref}. The soil reference for these IPEs has been assessed in the framework of ERM-CH23 by Panzera et al. (2019, 2020) as a softer soil condition (V_{S30} ≈ 600 m/s). The same study also provides the range of the correction to be applied to the *ΔI* maps to shift their reference soil condition from V_{S30} = 1,105 m/s to the reference of the intensity prediction: for *ΔI(PGV)* the correction factor lies between -0.42 and -0.37 intensity units; for *ΔI(PSA(1.0s))* between -0.27 and -0.17*; for *ΔI(PSA(0.3s))* between -0.32 and -0.31*.

3.3   Local soil amplification models

As outlined in the introduction, for the soil amplification module we also developed a set of local ground-motion amplification models for the areas of Sion, Visp and Lucerne-Horw. The latter was selected because of its peculiar geological setting (3D basin with particularly soft sediments) and high exposure (population of ~80,000). Sion and Visp were chosen as two major towns in the area of Switzerland with the highest seismic hazard (canton of Valais); besides, they are both located in the deeply-incised Rhone Valley, where significant 2D/3D soil amplification effects are expected. The local soil amplification models were obtained by collecting a vast amount of geological and geophysical data, also through dedicated acquisition campaigns and the installation of temporary seismic networks. These data were processed to predict soil amplification by means of different methods.

The amplification models for Sion (Perron et al., 2022) and Lucerne-Horw (Janusz et al., 2022b) were derived using the hybrid standard spectral ratio (SSRh) technique (Perron et al., 2018). This method combines the spectral ratio on earthquake recordings (SSR, Borcherdt, 1970), performed for a few pairs of sites instrumented with seismic stations, and the spectral ratio on ambient noise recordings (SSRn, Kagami et al., 1982) computed between said stations and a spatially dense array of short-duration deployments. The SSR is used to estimate the local rock-relative amplification at a few selected locations and the SSRn is successively used to map the local response over a wide area. For the application of the SSRh technique, temporary seismic monitoring networks were installed in the middle and upper Rhone Valley (Sion model) and in the area of Lucerne; furthermore, about 300 and 100 noise recordings were acquired in Sion and Lucerne, respectively.
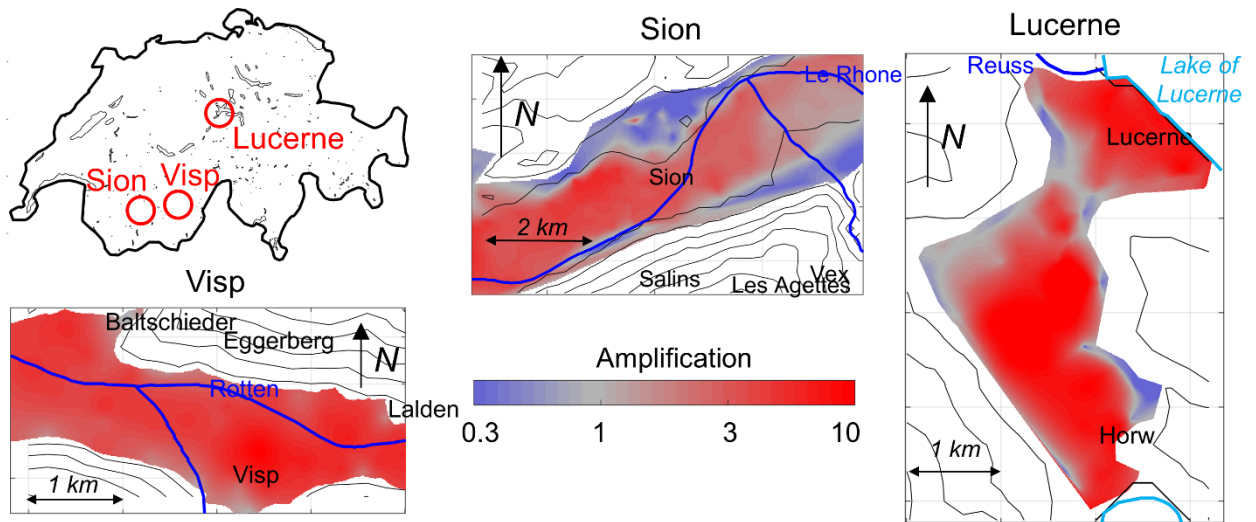
Figure 3.6. Ground-motion amplification maps at *T* = 0.6 s from the local models derived for Visp (using CC, left), Sion (centre) and Lucerne (right).

For the area of Visp, two concurring amplification models were estimated. The first is derived from a 3D joint geological-geophysical model. For this purpose, geophysical data collected in the past, as well as newly acquired data (within ERM-CH23), were employed. Overall, the geophysical dataset consists of ~500 single station noise measurements, velocity profiles from non-invasive surveys and seismic records from 14 seismic stations. Geophysical data were cross-referenced with geological information obtained through collaboration with Swisstopo (Volken et al., 2016). The developed 3D model of the Rhone Valley basin at Visp was used for a set of numerical ground-motion simulations, which allowed the local soil response to be estimated (Panzera et al., 2021b). The second amplification model for Visp was obtained by applying the statistical technique of the canonical correlation (CC, Cultrera et al., 2014) to map the correspondence between the horizontal-to-vertical spectral ratio of noise recordings (HVSRn) and earthquake local amplification functions obtained at seismic stations. The CC analysis was first calibrated on a Swiss-wide dataset of 172 instrumented sites; then the correlation was applied locally in the area of Visp, using a set of 86 HVSRns as a base for the prediction of the earthquake soil response (Panzera et al., 2021c).

The local models reported here, forming part of the final deliverable of module E, do not include the currently available soil amplification maps for Basel by Michel et al. (2017). The reason is that this model does not map the soil response at T = 0.6 s, a period selected in the overall architecture of ERM-CH23 for the ground-motion-based modelling of risk. Besides, the soil response maps of Michel et al. (2017) have a fine spatial resolution in the Rhine Valley bottom, but they are somewhat coarser for the hilly areas surrounding Basel, where a homogeneous amplification factor of 1 is imposed at all periods. The model by Michel et al. (2017) is currently being revised in the framework of the ongoing 'Earthquake Risk Model Basel' project.

3.4   Treatment of uncertainty

For the integration of the national site response layer in the wider framework of the ERM-CH23 model, a complete assessment of its uncertainties was carried out, and these were related to the variability terms of the Swiss stochastic ground-motion model of Edwards and Fäh (2013). This operation allowed the site response uncertainties to be incorporated in the adopted stochastic model for the prediction of ground motion, hence avoiding the double-counting of uncertainties. In the model of Edwards and Fäh (2013), the total uncertainty of the GMPE is composed of three items:

$$\sigma = \sqrt{\tau^2 + \varphi_{S2S}^2 + \varphi_{SS}^2} \tag{3.2}$$

where τ is the between-event variability, φ_{S2S} is the site-to-site variability and φ_{SS} is the single-site, within-event variability. We addressed the two terms related to local response, i.e. φ_{S2S} and

φ_{SS}. As illustrated in Section 3.2.3, the national ground-motion amplification layers were obtained by defining observed amplification-*vs*-slope and/or -bedrock depth relations for each lithotype; these relations were then mapped over the entire surface of Switzerland, with local constraints to the site amplification observed at seismic stations (regression-kriging, RK). Consistently with the RK approach, we identified the variability around the fitted smoothing splines of spatially uncorre- lated stations (e.g. Figure 3.4, top panels) as the model's site-to-site variability (φ_{S2S}). In other words, the variability observed within each lithotype, given the topographic slope and/or the bed- rock depth as predictor variable(s), is assumed as expressing the model's φ_{S2S}. As anticipated in Section 3.2.3, this variability is mapped jointly with the site amplification following the RK algo- rithm. While beyond the range of spatial correlation the soil amplification prediction relies on the amplification-*vs*-proxy relations, and its variability (=φ_{S2S}) is the standard deviations of uncorre- lated residuals, in the neighborhood of seismic stations the prediction is corrected with the values observed locally at the instrumented sites, and φ_{S2S} decreases collapsing to 0 at the stations' loca- tions (see an example for Basel in Figure 3.7, top panels). In this way, a national map of site-to- site variability (φ_{S2S}) is obtained for each ground-motion parameter (e.g. Figure 3.7, lower left panel).
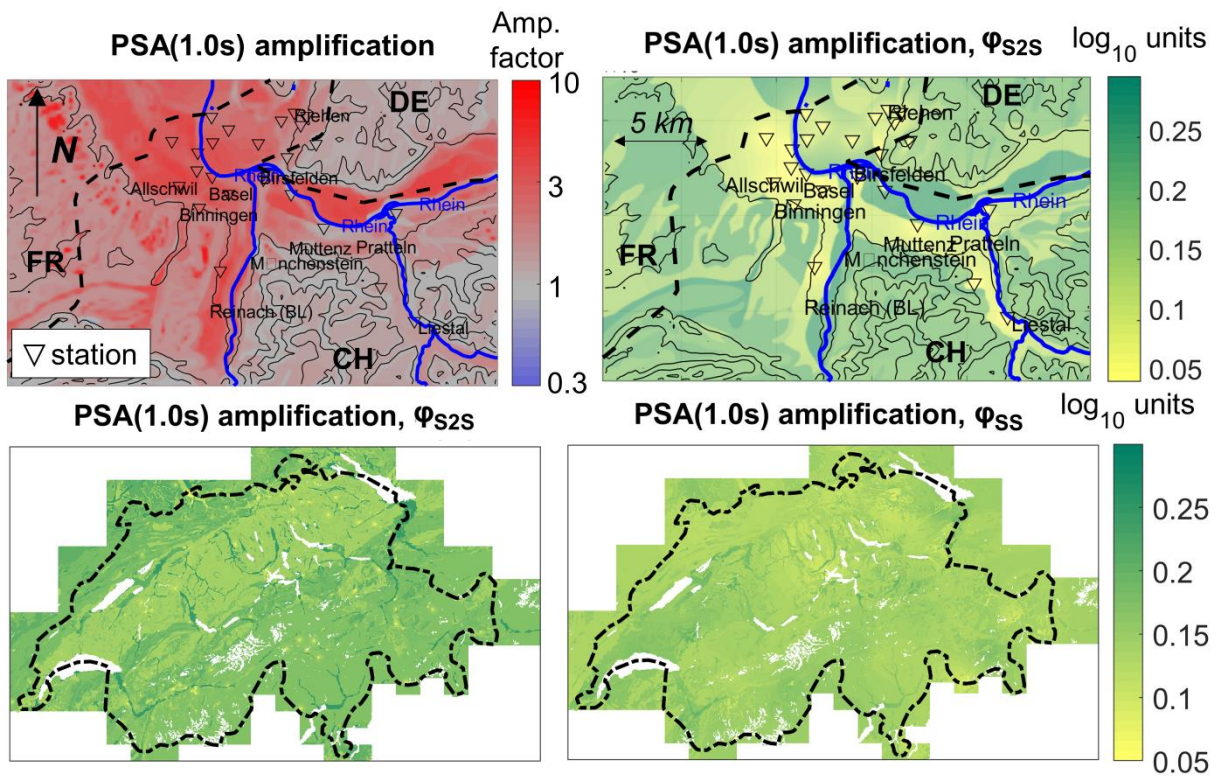
Figure 3.7. Top: example of regression-kriging (RK) local correction for the area of Basel. Left: *PSA*(1.0s) amplifica- tion (locally converging to the values observed at seismic stations); right: corresponding RK uncertainty (collapsing to 0 at stations' locations), identified as φ_{S2S}. Bottom: φ_{S2S} (left) and φ_{SS} (right) maps for *PSA*(1.0s) amplification.

For the representation of the single-site, within-event variability (φ_{SS}), we associated the latter with the variability observed across the single-event amplification functions estimated for the Swiss stations with empirical spectral modelling technique and RVT (e.g. Figure 3.1, upper right panel). We observed that the standard deviation over the single-event amplifications at the same site does not show any significant correlation with the continuous predictor variables employed for our model (multi-scale slope and bedrock depth); however, the standard deviation displays a slight correspondence with the lithotype, i.e. softer geomaterials have wider variability and con- versely stiffer lithologies have narrower uncertainties. Therefore, to map φ_{SS} we have attributed to each lithotype the average standard deviation of the empirical amplification functions of the sta- tions falling on that lithotype; this average was then corrected locally with ordinary kriging (Hengl et al., 2007) so that in the neighbourhood of seismic stations φ_{SS} gradually converges to the

standard deviation observed at the local instrumented sites. In this way, a national map of φ_{SS} is obtained for each ground-motion measure (e.g. Figure 3.7 units show a narrower variability (overall, they are comprised in the range 0.09-0.18 $\log_{10}$ units, compared to an interval of 0.05 to 0.3 for φ_{S2S}).

The uncertainty of the macroseismic intensity aggravation maps (Section 3.2.4) was also assessed; following eq. 3.1, the variability terms quantified for the ground-motion soil amplification would propagate into ΔI. However, it should be considered that the intensity prediction equations used to determine I_{ref} do carry their own uncertainty term, which also comprises the uncertainty related to site amplification. In fact, the IPEs available in the literature are based on datasets which do not take into account the local soil condition for the reported intensity observations. Consequently, to avoid a double-counting of uncertainty terms, the ΔI intensity maps have been released without corresponding standard deviation layers (Bergamo et al., 2020b).

The uncertainty for the soil amplification prediction was also evaluated for the four local models, consistently with the method employed to map the site response (Section 3.3). For the models produced by applying the SSRh technique (Sion, Lucerne), the uncertainty layer is derived by combining the variability observed in the earthquake as well as in the noise site-to-reference spectral ratios (Perron et al., 2022; Janusz et al., 2022b). As for the Visp model based on numerical simulations (Panzera et al., 2021b), the soil amplification uncertainty coincides with the standard deviation evaluated over multiple simulations. For the aforementioned models, it was considered that the computed uncertainties include both the epistemic and the aleatory components of variability; therefore they can be equated with the overall site response variability $\varphi=(\varphi_{S2S}{}^2+\varphi_{SS}{}^2)^{0.5}$. Finally, for the Visp model based on canonical correlation, the soil amplification uncertainty is estimated as the a-posteriori confidence interval of the least-square solution of the CC system of equations (eq. 5 in Panzera et al., 2021c); in this case, it was considered that the model uncertainty covers only the epistemic component of the site term variability, hence it can be equated with φ_{S2S}.

3.5   Verification and sanity checks

The validation of the national amplification model was carried out iteratively at every stage of its development and as soon as new benchmark datasets became available (Bergamo et al. 2020, 2021b). The conclusive validation of the final model was obtained by comparing it with three independent sets of data.

Comparison with soil amplification measured at instrumented sites. As described in Section 3.3, temporary networks of seismic stations were installed in the Swiss Rhone Valley and the area of Lucerne as tasks of the soil response module of ERM-CH23; these stations were employed in the stepwise development and validation of the local and national amplification models (Bergamo et al., 2020), and eventually used for the calibration of the final national amplification model. In fact, all available Swiss seismic stations satisfying the criteria listed in 3.2.1 were used to produce the final national model; however, we have identified a set of ~10 instrumented sites which – although not reaching the coverage of five events in the band 0.5 – 10 Hz – can be used as test sites for the assessment of the reliability of the national model. These stations, currently being installed, will record more earthquake data in the near future, thus becoming a reliable benchmark for the validation of the national model. Besides, this validation set of stations is also currently being integrated by temporary stations installed for the 'Risk Model Basel' project (Imtiaz et al., 2021). Comparisons with currently available data (e.g. Figure 3.8, top row) have shown a reasonable agreement between measured and predicted amplification, in particular for *PGV*.
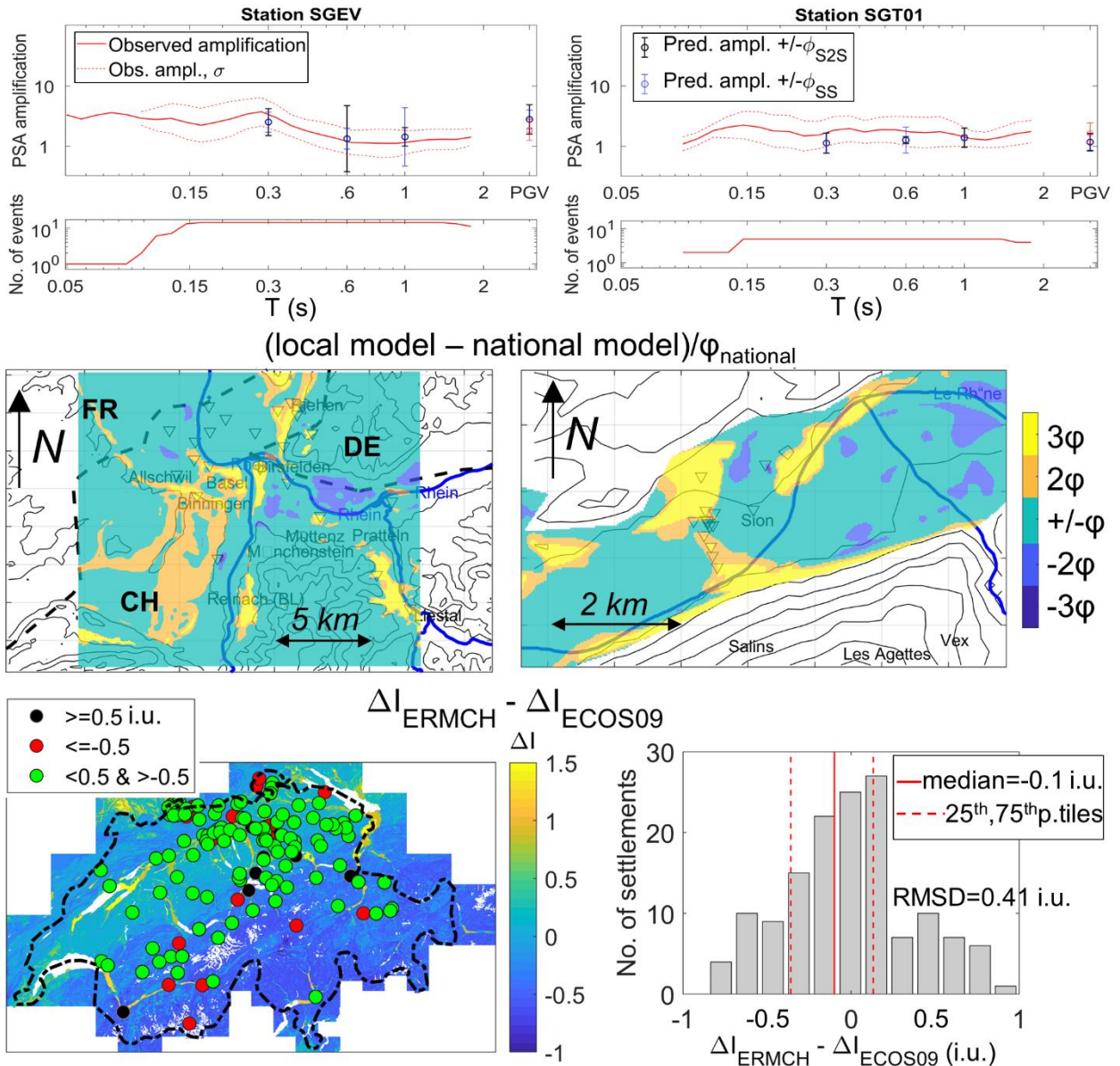
Figure 3.8. Verification of the national model. Top: comparison between predicted and measured site amplification at two sample seismic stations not included in the model calibration dataset. Centre: comparison between local and national amplification models for $T = 1s$ for the areas of Basel (left) and Sion (right). The difference between the models is normalised for the site response variability (φ) estimated for the national model. Bottom: comparison between the macroseismic aggravation map obtained from the $PSA(1.0s)$ amplification map from this study (ΔI_{ERMCH}, in the background) and the average ΔI residuals estimated for 146 Swiss settlements within the ECOS-09 project (ΔI_{ECOS09}).

Comparison with local amplification models. As the local models developed within ERM-CH23 were obtained from high-resolution, locally-sourced geophysical and seismological datasets, they were adopted as a benchmark for the validation of the national amplification model; for this validation, the local site response model for Basel by Michel et al. (2017) was also used. The comparison in general highlights a reasonable agreement between local and national models, with differences generally comprised within the overall uncertainty interval (φ) of the national model (e.g. Figure 3.8 middle row, examples from Basel and Sion). Areas of mismatch are mostly located at the borders between lithotypes of the classification employed for the national model (Section 3.2.2); in fact, this is based on the national geological map, which has a relatively coarse scale of 1:500,000. This aspect might be improved when a set of homogeneous 1:25,000 geological atlases for Switzerland becomes available. The local *vs.* national comparison for Lucerne-Horw also evidenced some discrepancies in the modelling of site response for fine-grained, lacustrine sediments, whose behaviour in the national model is represented by a relatively small number of sta-

tions (11). The validation of the local models was performed by comparing predicted and measured amplification at instrumented sites not used in the calibration of the models (see Panzera et al., 2021a,b; Perron et al., 2022; Janusz et al., 2022b). The 3D geophysical model for Visp was additionally validated by comparison between simulated and measured horizontal-to-vertical spectral ratios of ambient vibrations (Panzera et al., 2021a).

Comparison with macroseismic intensity observations from historical earthquakes. The macroseismic aggravation maps from this study (Section 3.2.1) were compared with a dataset of macroseismic intensity observations from historical earthquakes compiled for the project ECOS-09 (Fäh et al., 2011). For the validation, we used the average *ΔI* residuals computed by Fäh et al. (2011) for 146 Swiss settlements between reported macroseismic intensity observations and the predicted intensities from the IPE they developed for Switzerland. We compared these settlement-specific mean intensity aggravations (from ECOS-09) with the prediction extracted from the *ΔI* maps from our study at the coordinates of the corresponding postcode (e.g. Figure 3.8, lower panels). The results were quite positive: for the majority of the settlements the differences observed (ECOS-09) *vs.* estimated (ERM-CH23) local aggravations are comprised between -0.5 and +0.5 units; secondly, the medians over the 146 sites are close to 0 for all three *ΔI* maps of this study, suggesting that no systematic bias is present between the two datasets; finally, the overall root-mean-squared differences (*RMSD*) in observed *vs.* estimated local amplifications (*RMSD* = 0.41–0.42) are close to the *RMSD* (0.37) similarly computed for the *ΔI* map of Fäh et al. (2011), which was, however, calibrated on the very same ECOS-09 dataset.

References

Bergamo P. et al. (2019). SERA WP7 – Deliverable 7.4: Towards improvement of site condition indicators. http://www.sera-eu.org/export/sites/sera/home/.galleries/Deliverables/SERA_D7.4_IMPROVEMENT_SITE_INDICATORS-1.pdf

Bergamo P., et al. (2020). Provisional amplification maps for integration in the current implementation of the risk model. ERM-CH, Module E (site response) – Deliverable AM3.

Bergamo P. et al. (2021a). On the Relation between Empirical Amplification and Proxies Measured at Swiss and Japanese Stations: Systematic Regression Analysis and Neural Network Prediction of Amplification. BSSA **111** (1), 101–120.

Bergamo P. et al. (2021b). Amplification map with macroseismic and additional ground motion measures. ERM-CH, Module E (site response) – Deliverable AM4.

Bergamo P. et al. (2022a). Geophysical surveys for the characterization of the seismic local response at instrumented sites: a case study from a station of the Swiss strong motion network. 3rd European Conference on Earthquake Engineering and Seismology, Bucharest (Romania), 4th-9th September 2022, extended abstract no. 6478.

Bergamo P. et al. (2022b). Database for design-compatible waveforms. Deliverable: Disaggregation of the seismic hazard at return periods of 475 and 975 years. Report of the Swiss Seismological Service (SED) at ETH Zürich.

Bergamo P. et al. (2022c). Correspondence between site amplification and topographical, geological parameters: collation of data from Swiss and Japanese stations and neural networks-based prediction of local response. BSSA, doi: 10.1785/0120210225

Boore, D. (2003). Simulation of ground motion using the stochastic method. Pure and applied Geophysics, **160**, 635–676.

Borcherdt, R. D. (1970). Effects of Local Geology on Ground Motion Near San Francisco Bay. BSSA **60**(1), 29–61.

Brune, J. N. (1970). Tectonic stress and the spectra of seismic shear waves from earthquakes, J. Geophys. Res. **75**(26), 4997–5009.

Brune, J. N. (1971). Seismic sources, fault plane studies and tectonics, Eos Trans. AGU 52, no. 5, IUGG 178–IUGG 187.

Burjanek J. et al. (2014). NERA-JRA1 working group. Site effects at sites with pronounced topography: overview & recommendations. Research report for the EU project NERA, 64 pp., doi: 10.3929/ethz-a-010222426.

Cultrera G., et al. (2014). Statistical correlation of earthquake and ambient noise spectral ratios. BEE **12**, 1493–1514.

Darendeli, M. B. (2001). Development of a new family of normalized modulus reduction and material damping curves. PhD Thesis, The University of Texas at Austin.

Edwards, B. et al. (2010). Automatic computation of moment magnitudes for small earthquakes and the scaling of local to moment magnitude, Geophys. J. Int. **183**, 407–420.

Edwards, B. et al. (2013). Determination of site amplification from regional seismicity: Application to the Swiss National Seismic Networks, Seismol. Res. Lett. **84**(4) 611–621.

Edwards B. and Fäh, D. (2013). A stochastic ground-motion model for Switzerland. BSSA **103**(1), 78–98.

Fäh D, al. (2011) ECOS-09 earthquake catalogue of Switzerland release 2011. Report and database. Sed/Ecos/R/001/20110417, http://ecos09.seismo.ethz.ch/publications.html

Faenza L., & Michelini A. (2010). Regression analysis of MCS intensity and ground motion parameters in Italy and its application in ShakeMap. Geophys. J. Int. **180**(3), 1138–1152.

Faenza L., & Michelini A. (2011). Regression analysis of MCS intensity and ground motion spectral accelerations (SAs) in Italy. Geophys. J. Int. **186**(3), 1415–1430.

Hengl T. et al. (2007). About regression-kriging: From equations to case studies, Computers & Geosciences, **33**(10), 1301–1315.

Hobiger et al. (2021). Site Characterization of Swiss Strong-Motion Stations: The Benefit of Advanced Processing Algorithms, BSSA **111**(4), 1713–1739.

Imtiaz A. et al. (2021). Developing an integrated 3D geological-seismological model at urban scale in Basel, Switzerland. EGU General Assembly 2021, EGU21-12674, https://doi.org/10.5194/egusphere-egu21-12674.

Janusz P. et al. (2022a). Calibration of soil dilatancy parameters using CPT data – the case of Lucerne in central Switzerland. 3rd European Conference on Earthquake Engineering and Seismology, Bucharest (Romania), 4th-9th September 2022, extended abstract no. 5961.

Janusz, P., et al. (2022b). Combining Earthquake Ground Motion and Ambient Vibration Recordings to Evaluate a Local High-Resolution Amplification Model—Insight From the Lucerne Area, Switzerland. Front. Earth Sci. **10**, https://doi.org/10.3389/feart.2022.885724

Kagami, H., et al., (1982). Observation of 1-to 5-second microtremors and their application to earthquake engineering. Part II. Evaluation of site effect upon seismic wave amplification due to extremely deep soil deposits. BSSA **72**, 987–998.

Lachet, C. et al. (2016). Site effects and microzonation in the city of Thessaloniki (Greece) comparison of different approaches. BSSA **86**(6), 1692–1703.

Løviknes K. et al. (2021). Testing Nonlinear Amplification Factors of Ground-Motion Models. BSSA **111**(4), 2121–2137.

Michel C. et al. (2014). Assessment of Site Effects in Alpine Regions through Systematic Site Characterization of Seismic Stations, BSSA **104**(6), 2809–2826.

Michel C. et al. (2017). Site amplification at the city scale in Basel (Switzerland) from geophysical site characterization and spectral modelling of recorded earthquakes. Physics and Chemistry of the Earth Parts A/B/C **98**,27-40.

Panzera F., et al. (2016). Evaluation of building fundamental periods and effects of local geology on ground motion parameters in the Siracusa area, Italy. Journal of Seismology **20**, 1001–1019

Panzera F., et al., (2019). Assessment of the reference soil condition for the macroseismic amplification factors. ERM-CH, module E, deliverable of Task E12.

Panzera F. et al. (2020). Reference soil condition for intensity prediction equations derived from seismological and geophysical data at seismic stations. Journal of Seismology **5**, 163–179.

Panzera F. et al. (2021a). Database for design-compatible waveforms - Deliverable: Available database of waveforms and related meta-data, including the strategy for the selection of ground motions from observations and synthetics. Report of the Swiss Seismological Service at ETH Zurich.

Panzera F. et al., (2021b). Reconstructing a 3D model from geophysical data for local amplification modelling: The study case of the upper Rhone Valley, Switzerland. SDEE **155**, 107163.

Panzera, F., et al., (2021c). Canonical Correlation Analysis Based on Site-Response Proxies to Predict Site-Specific Amplification Functions in Switzerland. BSSA, **111**(4), 1905–1920.

Perron, V., et al. (2018). Can broad-band earthquake site responses be predicted by the ambient noise spectral ratio? Insight from observations at two sedimentary basins. GJI **215**(2), 1442–1454.

Perron V. et al. (2022). Site Amplification at High Spatial Resolution from Combined Ambient Noise and Earthquake Recordings in Sion, Switzerland. Seismological Research Letters, https://doi.org/10.1785/0220210289

Poggi, et al. (2011). Derivation of a reference shear-wave velocity model from empirical site amplification, BSSA **101**(1), 258–274.

Poggi V. & Fäh, D. (2015). A proposal for horizontal and vertical elastic design spectra - Input for the new Swiss code for dams. Technical Report SED/BFE/R/01/30072015Swisstopo, Swiss Federal Office of Topography (1967). Geotechnical Map of Switzerland 1:200000

Swisstopo, Swiss Federal Office of Topography (1999). Digital Height Model DHM25

Swisstopo, Swiss Federal Office of Topography (2005). Geological Map of Switzerland 1:500000 (GK500)

Swisstopo, Swiss Federal Office of Topography (2017). GeoCover V2

Swisstopo, Swiss Federal Office of Topography (2019). Grossezza da la crappa lucca da la Svizra, https://www.swisstopo.admin.ch/it/geodata/geology/models/unconsolidated-deposits.html

Shible, H. Et al. (2022). GITEC: A Generalized Inversion Technique Benchmark. BSSA **112**(2), 850–877.

Vilanova S. P. et al. (2018). Developing a Geologically Based Vs30 Site-Condition Model for Portugal: Methodology and Assessment of the Performance of Proxies, BSSA **108**(1), 322–337.

Volken S., et al., (2016). GeoQuat : developing a system for the sustainable management, 3D modelling and application of Quaternary deposit data. Swiss bulletin per la geologia applicata **21**, 3–16.

Wald, D. J., and T. I. Allen (2007). Topographic slope as a proxy for seismic site conditions and amplification, BSSA **97**(5) 1379–1395.

Weatherill, G., et al. (2020). Re-thinking site amplification in regional seismic risk assessment, Earthquake Spectra **36**(S1) 274–297.

Wiemer S. et al. (2016). Seismic Hazard Model 2015 for Switzerland (SUIhaz2015), Swiss Seismological Service (SED) at ETH Zurich.

4.   Exposure, a national building database

4.1   Introduction

Subproject F was managed by the federal office for the environment (FOEN). The product of sub-project F is a georeferenced database of all relevant building objects in Switzerland with necessary attributes for the ERM-CH23 model. This georeferenced database is called 'ERMCH_GEB01' and is based on the Federal Register of Buildings and Dwellings (RBD) kept by the Federal Statistical Office (FSO). Necessary attributes that are not contained in the RBD come from other sources or are modelled.

A detailed description of ERMCH_GEB01 as well as a description of the work processes and models for the building attributes are found in FOEN (2021) and Hügli et al. (2021). No uncertainties were considered on the building attributes in ERMCH_GEB01.

4.2   Overview of the national building database

The final version of ERMCH_GEB01 contains **2,320,716 building objects** with a volume above ground $\geq$ 200 m^3.[2] This includes 2,099,270 building objects from the RBD. As the RBD is not 100% complete for non-residential buildings, an additional 221,446 building objects were import-ed from the national database of building footprints (AV dataset). Objects with a volume less than 200 m^3 were removed because these very numerous objects (834,248) do not contribute signifi-cantly to the damage potential and risk, and lead to an overestimation of relevant damaged build-ings.

Table 4.1 gives an overview of the number and replacement value of buildings in ERMCH_GEB01 according to their main use category (residential or non-residential).

Table 4.1. Number and replacement value of residential and non-residential buildings in ERMCH_GEB01

Function category	Number of building objects	Modeled replacement value
Residential or mostly residen-tial (GKAT 1020 and 1030)	1,664,581	CHF 1,962 billions
Non-residential (GKAT 1040 and 1060)	656,135	CHF 983 billions
Total	2,320,716	CHF 2,945 billions

Table 4.2 gives an overview of the building attributes with a short definition, the source of infor-mation and the state of completeness. A detailed description or discussion of selected attributes (highlighted in green) in Table 4.2 is provided in Section 4.3.

---

[2] Buildings classed as temporary housing (bungalows, permanent caravans in camping sites) and special objects were not considered.

Table 4.2. Overview of the building attributes in ERMCH_GEB01. GWR = attribute imported from the Federal Register of Buildings and Dwellings (RBD); GIS = imported from another dataset through GIS spatial join; MOD = modelled attribute; COMP = degree of completeness; KGV = use of cantonal insurance data in the absence of an attribute value in the RBD.

#	Attribute (Number; abbreviation, type; description)			GWR	GIS	MOD	COMP	Remarks
1	ID-ERMCH	Integer	Building identifier in ERM-CH.	�－			100%	
2	Origin	Text	Object's origin	▢			100%	"GWR": national Building and housing registry of BFS "AV_cent": building footprint dataset (AV-dataset)
3	EGID	Integer	Federal building identification number	▢			81%	-9999 = object without EGID-number
4	AV_ID	Integer	AV-dataset ID				100%	ID of the corresponding building footprint in the AV-dataset
5	GDEKTg	Text	Abbreviation of cantons's name				100%	
6	GDENRg	Integer	BFS commune number				100%	
7	PLZ4g	Integer	ZIP-code				100%	
8	PLZZg	Integer	ZIP-code subdivision number				100%	
9	AREBAUZ	Integer	Building zone category		▢		100%	
10	GDETYP	Integer	Commune typology category		▢		100%	
11	GKODEg	Double	East coordinate / CH1903+_LV95	▢			100%	Projection coordinate system CH1903+_LV95
12	GKODNg	Double	North coordinate / CH1903+_LV95	▢			100%	Projection coordinate system CH1903+_LV95
13	GKAT	Integer	Main function category of the building	▢			100%	
14	GKLASdef	Integer	Detailed function category	▢	KGV		85%	0 = uknown including data of the cantonal insurances by missing information in GWR
15	GBAUJdef	Integer	Year of construction	▢	KGV		64%	0 = uknown including data of the cantonal insurances by missing information in GWR
16	GBAUPdef	Integer	Period of construction	▢	KGV		76%	0 = uknown including data of the cantonal insurances by missing information in GWR
17	GAREA_3g	Double	Area of the building footprint in m2	▢			99%	Data from GWR or through spatial join with the polygons of the building footprints of the AV_dataset footprints. Unknown (Surface = 0)
18	GASTW	Integer	Number of stories above ground	▢			63%	Low information quality. Can be checked and supplemented using GEBHAVE and GEBHMAX
19	GEBHOHE	Double	Average height above ground in m			▢	99%	modeled as GEBHOHE = GEBVOL / GAREA3_g
20	GEBHMAX	Double	Max building height over Terrain			▢	99%	Max building height over Terrain derived from DOM - DEM Model
21	GEBVOL	Integer	Building volume above terrain in m3			▢	99%	1) from digital elevation models (DOM - DEM) 2) GEBVOL = GAREA_3g * GASTW * 3m if 1) is not available. 3) GAREA_3g * 3.5 if GASTW is not available
22	NEIGDACH	Integer	Neigung des Daches / Roof inclination	▢			85%	1 = flat, 2 = inclined; 0 =uknown, From dataset www.sonnendach.ch (BFE)
23	ANZWHG02	Integer	Number of housing units	▢			100%	
24	KUMWAZIM	Integer	Sum of rooms in housing units	▢			100%	
25	KUMWAREA	Integer	Cumulative area of housing units in m2	▢			100%	
26	EINWMOD	Integer	Number of permanent inhabitants		▢		n/a	Agreggation at the building level of the georeferenced densus data of STATPOP (BFS).
27	VZAMOD	Double	Equivalent full time employees		▢		n/a	Agreggation at the building level of the georeferenced data of STATPOP.
28	BIN_SCHUL	Integer	Identificator for school buildings		▢		n/a	BIN_SCHUL = 1 : school buildings with students BIN_SCHUL = 0 : not a school building
29	SCHULMOD	Integer	Modeled numebr of students			▢	n/a	
30	BIN_HOS	Integer	Identificator for hospital buildings	▢			n/a	BIN_HOS = 1 : Hospital building BIN_HOS = 0 : Not a hospital building
31	ID_HOS_AREAL	Integer	Identificator of the hospital site				n/a	ID Spitalareal in SWISSTLM3d
32	SPITAL_Inst	Text	Name of the hospital institution				n/a	Link with "Krankenhausstatistik und der Medizinischen Statistik des Krankenhäuser des Bundesamtes für Statistik.
33	HOS_BET	Integer	Number of hospital beds			▢	n/a	
34	HOS_PAT	Double	Number of hospitalized patients			▢	n/a	
35	HOS_OUTPAT	Double	Average number of outpatients per day			▢	n/a	
36	GEBWERT	double	Replacement value in CHF			▢	99%	Modeled based on GEBVOL, GKAT, AREBAUZ, GDETYP. According to Röthlisberger et al. 2018
37	GEBWERTin	double	Modified Replacement value in CHF			▢	99%	GEBWERT multiplied by a factor for each canton so that the aggregated value per canton corresponds to the aggregated insurance value.
38	INHWERT	double	Value of mobile goods in CHF			▢	99%	Modeled as a percentage of the building value (GEBWERT). The percentage is variable with according to the attribute GKLAS.
39	INHWERTin	double	Modified Value of mobile goods in CHF			▢	99%	GEBWERTin multiplied by a factor for each canton so that the aggregated value per canton corresponds to the aggregated insurance value.
40	BWSMOD	double	Gross added value in CHF/year			▢	n/a	Modelled with VZAMOD and the statistic of the production account of BFS and the georeferenced STATENT data at the building level.
41	NOGA082_50	Text	Type of economic activity		▢		n/a	List of economic activities according to the NOGA082_50 classification system of BFS.
42	BAUW_KGV	Text	Flammability category		IRV		n/a	The indication is provided in 11 cantons., but the definition is not consistant between cantons **NO ACCESS TO THIRD PARTIES**

4.3   Description of selected building attributes

Attribute 9 / AREBAUZ / building zone category

The following characterisation of the building zone in which the building sits is determined through a GIS spatial join with the dataset of building zones of the Federal Office for Spatial Development (latest release in 2017). AREBAUZ is used in the model to compute the replacement value of the buildings (GEBWERT).

AREBAUZ	Code for building zones according to ARE 2017
0	outside of ARE zones
11	residential
12	commercial
13	mixed zone
14	urban center
15	public activity zone
16	construction zones with restrictions
17	tourism and recreational zones
18	transportation zones inside construction zones
19	other

Attribute 10 / GDETYP / commune typology category

The following characterisation of the commune in which the building sits is determined through a GIS spatial join with the dataset of the Federal Office for Spatial Development. GDETYP has no direct use so far in ERM-CH23.

GDETYP	Commune typology according to ARE
0	unknown
1	big urban centers
2	secondary urban centers of big urban centers
3	belt of big urban centers
4	middle-sized urban centers
5	belt of middle-sized urban centers
6	small urban centers
7	periurban rural communes
8	agricultural communes
9	touristic communes

Attribute 13 / GKAT / main function category

In the Federal Register of Buildings and Dwellings (RBD), the following main function categories are used:

GKAT	main function category
1020	Buildings exclusively for residential purpose
1030	Buildings mainly for residential purpose
1040	Buildings only partially for residential purpose
1060	Building with no residential purpose

Attribute 14 / GKLASdef / detailed function category

In the Federal Register of Buildings and Dwellings (RBD), the following detailed function categories are used:

GKLAS	detailed function category
0	unknown
1110	Individual homes
1121	Homes with 2 housing units
1122	Building eith 3 and more housing units
1130	Buildings for community housing
1199	Residential function without further distinction
1211	Hotels
1212	Other buildings for touristic accomodation
1219	Hospitality industry
1220	Office buildings
1230	Commercial buildings
1231	Restaurants and bars in buildings with no residential use
1241	Train stations, terminal buildings, communication buildings
1242	Garages
1251	Industrial buildings
1252	Reservoirs, silos and warehouses
1259	Industrial and/or commercial (code used by insurances)
1261	Building for recreational or cultural use
1262	Museums and libriaries
1263	Buildings for teaching and research
1264	Hospitals and health care buildings
1265	Sports halls
1271	Agricultural buildings
1272	Religiopus buildings
1273	Historical monuments
1274	Other buildings not otherwise classified
1276	Argricultural: buildings for raising animals
1277	Argricultural: buildings for vegetal cultivation (greenhouses)
1278	Argricultural: other uses (storage, …)
1275	Other buildings for collective housing
1279	Special public buildings

Attribute 17 / GEBAREA_3g / building footprint area

In a first step, the building footprint area was obtained from the RBD dataset. The values were then verified and supplemented using the dataset of building footprints from the official cadastral survey (AV dataset, centralised at Swisstopo). If the information from the AV dataset and RBD did not coincide, the information from the AV dataset was used. For 0.7% of the building objects, the building footprint area could not be determined.

Attribute 18 / GASTW / number of storeys above ground

Local checks revealed this information in the RBD to be very unreliable. Therefore, the height categorisation of buildings is based on the height above ground of buildings derived from digital surface (DOM) and digital terrain elevation (DEM) models.

Attributes 19 / GEBHOHE / average building height above terrain

GEBHOHE is modeled as the building volume above ground (GEBVOL) divided by the building footprint area (GAREA3g).

Attributes 20 / GEBHMAX / maximum building height above terrain

GEBHMAX is the difference between the highest point of the digital surface elevation model and the lowest point of the digital terrain elevation model over the building footprint. The default minimum value is set as 3.5 m (assumed height for a one-storey building).

Attribute 21 / GEBVOL / building volume above ground

The building volume above ground is modelled using different approaches depending on the available data as described in FOEN (2021) and Hügli et al. (2021). For 0.8% of the buildings in the database, it was not possible to approximate the building volume. Further information on the validation of the model for GEBVOL is provided in Section 4.5.1.

Attribute 22 / NEIGDACH / roof inclination category

The attribute 'roof inclination' (flat, inclined or unknown) was provided for 85% of the building objects using a GIS analysis and the roof geometry database of the Swiss Federal Office of Energy.

Attribute 26 / EINWMOD / number of permanent inhabitants

EINWMOD is newly obtained through the aggregation at the building level of the georeferenced housing statistics (STATPOP). 98.7% of the 1,553,322 STATPOP data points could be linked with a building object and 8.47 million inhabitants were distributed in 1,520,119 buildings.

Attribute 27 / VZAMOD / number of full-time equivalent employees

VZAMOD is obtained through the aggregation at the building level of the georeferenced employment statistics (STATENT). 97.3% of the 648,884 STATENT data points could be linked with a building object and 4.02 million full-time equivalent employees were distributed in 389,136 building objects.

It is expected that some single STATENT data points contain aggregated data for sites with multiple buildings or aggregated data for companies with multiple sites. These cases could not be identified and are a potential source of errors.

Attribute 28 / BIN_SCHUL / school identifier

17,432 buildings are considered school buildings in ERMCH_GEB01 (attribute BIN_SCHUL = 1). These are buildings with an attribute GKLAS = 1263 or buildings with GKLAS = unknown and falling into a school perimeter according to the terrain and surface model (SwissTLM3d) of the Federal Office of Topography (Swisstopo).

Attribute 29 / SCHULMOD / number of students

The number of students aggregated at the postcode level (PLZ) from the students statistics of the Federal Statistical Office were distributed among the school buildings (attribute BIN_SCHUL = 1) in each postcode area proportionally to their volume above terrain (GEBVOL). The attribute SCHULMOD is a crude approximation of the capacity of school buildings in terms of number of students. With this procedure, 1,393,430 students were distributed in 17,431 school buildings.

Depending on the number of buildings for teaching and research and their variability in volume and actual function in a postcode area, SCHULMOD may deviate significantly from the actual number of registered students in a school. BIN_SCHUL and SCHULMOD can be used to assess the aggregated number of impacted schools and students in a geographical region.

Attribute 30 / BIN_HOS / hospital building identifier

1'930 buildings are considered hospital buildings in ERM-CH_GEB01 (attribute BIN_HOS = 1). These are buildings with an attribute GKLAS = 1264 or with an attribute GKLAS = unknown that fall into a hospital perimeter according to the terrain and surface model (SwissTLM3d) of the Federal Office of Topography (Swisstopo).

Attributes 33, 34, 35 / HOS BET, HOS PAT, HOS OUTPAT / number of hospital beds; number of hospitalised patients; number of outpatients

Using the Federal Statistical Office's 2019 statistics on hospitals, the number of hospital beds, patients occupying a bed and outpatients per day in each hospital area were distributed among the buildings with an attribute BIN_HOS = 1 present in the hospital area proportionally to their volume. The results are:

- HOS_BET is the modelled estimated number of beds in the hospital building.

- HOS_PAT is the modelled estimated number of patients hospitalised.

- HOS_OUTPAT is the modelled average number of outpatients in the hospital per day.

These attributes can be used to assess the aggregated number of hospital beds and patients that are impacted in an event. The distribution of beds, patients and visitors amongst different buildings in a hospital area is not very reliable. Results of analyses for hospital buildings should be aggregated at the level of the hospital area (ID_HOS_AREAL) or institution (SPITAL_inst) to be meaningful.

Attribute 36 / GEBWERT / replacement value of building objects

The definition of the building replacement value corresponds to the definition used by insurance companies in Switzerland. It should be equivalent to the costs for reconstruction of the building as an individually constructed object of the same type and size, with the same standard of construction and at customary local prices on the day of the valuation. The building insurance value may differ significantly from the official value (used for property taxation) or the market value.

To compute GEBWERT, an approach developed by Röthlisberger et al. (2018) is used. This method requires the building volume (GEBVOL), the building's main purpose (derived from GKAT) and the construction zone category (derived from AREBAUZ) as the main input parameters. The building database ERMCH_GEB01 does not consider underground buildings or the volume of buildings that is underground. Nevertheless, the model used for GEBWERT implicitly includes the value of the underground portion of the buildings.

The aggregated modeled building replacement value (CHF 2,945 billion) nationwide is 3% higher than the aggregated insured value. Further information on the model for GEBWERT and on its validation is provided in Section 4.5.2.

The attribute 37 GEWERTin is computed as GEBWERT multiplied by a cantonal correction factor so that the aggregated GEBWERTin value at the cantonal level corresponds to the aggregated insured value from the insurance statistics. For consistency, it is advised to use GEBWERT (homogeneous national value model) for ERMCH analyses. GEBWERTin could be used for specific cantonal loss estimations of insured values.

Attribute 38 / INHWERT / replacement value of content

The replacement value of content is computed as a fraction of the building value (GEBWERT). Different ratios are used, based on a statistical analysis of private and cantonal insurance data.

The final ratios to compute INHWERT from GEBWERT in ERM-CH23 are as follows:

- INHWERT = **0.19** * GEBWERT for GKLAS 1110 to 1199 (residential buildings)

- INHWERT = **0.38** * GEBWERT for GKLAS 1211, 1212, 1220, 1230, 1241, 1242, 1261, 1262, 1263, 1264, 1265, 1271, 1272, 1273, 1274 (commercial buildings)

- INHWERT = **0.65** * GEBWERT for GKLAS 1251 and 1252 (industrial buildings)

- INHWERT = **0.27** * GEBWERT for other GKLAS values.

The total replacement value of contents amounts to CHF 788 billion. Further information on the model for INHWERT and on its validation is provided in Section 4.5.3.

The attribute 39 INHWERTin is computed as INHWERT multiplied by a cantonal correction factor so that the aggregated INHWERTin value at the cantonal level corresponds to the aggregated insured value from the insurance statistics. For consistency, it is advised to use INHWERT (homogeneous national value model) for ERM-CH23 analyses.

Attribute 40 / BWSMOD / gross added value

The gross added value per STATENT data point is computed as the number of full-time employees per type of economic sector multiplied by the national average gross added value per equivalent full time employee for this economic sector. BWSMOD per building is then obtained through the aggregation at the building level of the georeferenced STATENT data points containing the estimation of the gross added value. With this approach, CHF 681 billion of yearly gross added value was associated with the 389,136 buildings with modelled full-time equivalent employees.

Attribute 41 / NOGA082_50 / type of economic activity

For each building with full-time equivalent employees (VZAMOD > 0), the corresponding types of economic activity are listed in the attribute NOGA082_50 based on the information in the georeferenced employment statistics (STATENT) of the Federal Statistical Office. The categories are as follows:

NOGA82_50	Type of economic activity
1.3	Agriculture, forestry and fishing
5.9	Mining and quarrying
10.2	Manufacture of food products, beverages and tobacco products
13.5	Manufacture of textiles, apparel, leather and related products
16.8	Manufacture of wood and paper products, and printing
19.2	Manufacture of coke, chemicals and chemical products
21	Manufacture of basic pharmaceutical products and pharmaceutical preparations
22.3	Manufacture of rubber and plastics products, and other non-metallic mineral products
24.5	Manufacture of basic metals and fabricated metal products, except machinery and equipment
36	Manufacture of computer, electronic and optical products; watches and clocks
27	Manufacture of electrical equipment
28	Manufacture of machinery and equipment n.e.c.
29.3	Manufacture of transport equipment
31.3	Other manufacturing, and repair and installation of machinery and equipment
35	Electricity, gas, steam and air-conditioning supply
36.9	Water supply, sewerage, waste management and remediation
41.2	Construction of buildings and Civil engineering
43	Specialised construction activities
45	Wholesale and retail trade and repair of motor vehicles and motorcycles
46	Wholesale trade, except of motor vehicles and motorcycles
47	Retail trade, except of motor vehicles and motorcycles
49	Land transport and transport via pipelines
50.1	Water transport and Air transport
52	Warehousing and support activities for transportation
53	Postal and courier activities
55	Accommodation
56	Food and beverage service activities
58.6	Publishing, audiovisual and broadcasting activities
61	Telecommunications
62.3	IT and other information services
64	Financial service activities, except insurance and pension funding
65	Insurance, reinsurance and pension funding, except compulsory social security
66	Activities auxiliary to financial services and insurance activities
68	Real estate activities
69	Legal and accounting activities
70	Activities of head offices; management consultancy activities
71	Architectural and engineering activities; technical testing and analysis
72	Scientific research and development

73.5	Other professional, scientific and technical activities
77.2	Administrative and support service activities
78	Employment activities
84	Public administration and defence; compulsory social security
85	Education
86	Human health activities
87	Residential care activities
88	Social work activities without accommodation
90.3	Arts, entertainment and recreation
94.6	Other service activities
97.8	Activities of households as employers; undifferentiated goods- and services-producing activities of households for own use
99	Activities of extraterritorial organisations and bodies

4.4   Data summary

Table 4.3 presents the number of buildings, their aggregated modelled volume and replacement value as well as the aggregated number of permanent inhabitants and full-time equivalent employees for selected detailed function categories. The 15 function categories presented cover 95% or more of the total aggregated values over all (30) function categories. The ranking goes from the highest to lowest aggregated replacement value.

Table 4.3. Number of buildings, their aggregated modelled volume and replacement value as well as the aggregated number of permanent inhabitants and full-time equivalent employees for detailed function categories.

GKLAS	detailed function category	Numer of buildings		Volume above ground, m³		Value, millions CHF		Permanent inhabitants		Equ. full time employees	
1122	Buildings with 3 housing units or more	388'667	16.7%	1'258'258'022	27.3%	961'590	32.6%	4'783'129	56.5%	555'459	13.9%
1110	Individual homes	1'063'642	45.8%	900'138'252	19.5%	761'620	25.9%	2'474'784	29.2%	266'238	6.6%
1121	Homes with 2 housing units	212'170	9.1%	295'773'321	6.4%	222'975	7.6%	700'593	8.3%	140'309	3.5%
1251	Industrial buildings	53'066	2.3%	499'961'081	10.8%	193'388	6.6%	19'374	0.2%	688'798	17.2%
0	unknown	147'411	6.4%	291'094'552	6.3%	131'179	4.5%	101'500	1.2%	200'220	5.0%
1220	Office buildings	24'734	1.1%	213'425'816	4.6%	102'876	3.5%	19'773	0.2%	946'774	23.6%
1263	Buildings for teaching and research	15'327	0.7%	118'159'469	2.6%	91'959	3.1%	9'533	0.1%	175'202	4.4%
1230	Commercial buildings	15'310	0.7%	145'083'057	3.1%	64'553	2.2%	14'816	0.2%	253'550	6.3%
1271	Agricultural buildings	114'573	4.9%	189'635'859	4.1%	58'326	2.0%	4'352	0.1%	11'244	0.3%
1252	Reservoirs, silos and warehouses	42'376	1.8%	150'124'977	3.3%	58'176	2.0%	1'751	0.0%	71'228	1.8%
1199	Residential, without further distinction	38'979	1.7%	87'449'424	1.9%	45'487	1.5%	198'645	2.3%	129'416	3.2%
1274	Other buildings not otherwise classified	70'277	3.0%	90'889'032	2.0%	43'454	1.5%	10'074	0.1%	75'767	1.9%
1264	Hospitals and health care buildings	3'317	0.1%	43'769'272	0.9%	35'394	1.2%	25'397	0.3%	199'621	5.0%
1241	Train stations, terminal buildings	28'926	1.2%	72'229'278	1.6%	24'555	0.8%	1'931	0.0%	40'835	1.0%
1261	Building for recreational or cultural use	8'910	0.4%	37'214'855	0.8%	23'555	0.8%	2'676	0.0%	25'333	0.6%

4.5   Further information on models and their validation

4.5.1   Model building volumes

The modelled building volumes (GEBVOL) at the object level as well as aggregated at the postcode level and at the cantonal level were compared with the data from 17 cantonal insurers where this information was available. The detailed results are provided in Hügli et al. (2021). An overview of the comparison of the aggregated building volumes at the cantonal level is given in Table 4.4.

Table 4.4. Comparison of the aggregated building volumes with insurance data in 17 cantons.

	Aggregated volume of buildings in m³		
Canton	Insurances*	ERM_CH**	ERM/Ins
AG	408'835'046	372'269'003	91%
AR	36'416'013	34'595'602	95%
BE	652'144'003	573'268'861	88%
BL	151'966'599	140'758'806	93%
BS	108'078'259	85'522'234	79%
FR	206'133'750	184'308'826	89%
GL	31'790'862	28'723'730	90%
GR	178'304'515	160'174'868	90%
LU	275'105'278	270'647'244	98%
NE	98'163'775	98'282'724	100%
SG	318'039'940	297'638'262	94%
SH	53'498'991	48'414'536	90%
SO	164'060'862	157'263'223	96%
TG	199'734'748	177'246'302	89%
VD	408'912'902	426'234'378	104%
ZG	67'085'930	69'680'820	104%
ZH	698'174'378	634'821'733	91%
	4'056'445'851	3'759'851'152	93%
	* underground and above ground volumes		
	** above ground volumes only, volumes < 200 m3 ignored		

The canton of Basel-Stadt (BS) shows that, for a very urban area (the canton is basically a large city at the Swiss scale), the aggregated building volume above ground from digital elevation models computed in ERM-CH23 underestimates the total volume of insured buildings (including underground volumes) by approximately 20%. In all other cantons, the underestimation is 10% or less. In two cantons, ERM-CH23 overestimates the aggregated building volume by 4%. For the 17 cantons where building volume information is available from cantonal insurers, ERM-CH23 underestimates the total aggregated building volume by 7%.

4.5.2   Modelled building replacement value

The modelled building values (GEBWERT) aggregated at the postcode level and at the cantonal level were also compared with the data from the cantonal and private insurers. The detailed results are provided in Hügli et al. (2021). An overview of the comparison at the cantonal level is provided in Table 4.5.

The model used to compute the replacement value of buildings on a national scale is not able to capture the variations in replacement value models from the various cantonal and private insurers in Switzerland. The underestimation of the aggregated insured value is highest in very urbanised cantons like Basel-Stadt (BS), Geneva (GE) and Zurich (ZH). For less urbanised cantons, the model has a tendency to overestimate the aggregated insured replacement value. Globally, the relatively simple model in ERM-CH23 is able to model the aggregated replacement value within 3% of the total insured replacement value at the national level. It should also be noted that approximately 50% of the insured value in Switzerland is located in only four out of 26 cantons (ZH, BE, VD and AG).

The model used for the estimation of the building replacement value in ERM-CH23 is based on the analysis of building databases of 11 cantonal insurers (see Figure 4.1 and Röthlisberger (2018) for details).

Röthlisberger (2018) developed five different models (M1 to M5). In ERM-CH23, the most detailed and effective models, M4 and M5, which rely on the building volume above ground as the most relevant input parameter, were used. Model M5 was finally selected to compute the attribute GEBWERT as it provides the best fit with the aggregated insured building replacement values in Switzerland.

Model M4 uses constant average building replacement values per m^3, with a differentiation for residential and non-residential buildings, as well as for the category of land use (see Table 4.6).

Table 4.5. Overview of the comparison of the aggregated building replacement value against insurance data at the cantonal level.

| Canton | Insurance | Replacement value of buildings in CHF | | ERM/Ins |
		Insurances	ERM_CH	
AG	Cantonal	207'089'816'000	233'833'546'445	113%
AI	Private	3'630'097'000	6'550'040'196	180%
AR	Cantonal	21'901'377'753	21'958'520'558	100%
BE	Cantonal	382'196'648'951	359'390'703'232	94%
BL	Cantonal	90'680'484'000	93'159'265'601	103%
BS	Cantonal	79'944'134'000	58'375'625'830	73%
FL	Private	17'954'305'000	18'499'495'494	103%
FR	Cantonal	93'052'372'368	111'798'832'191	120%
GE	Private	135'227'822'049	112'715'594'892	83%
GL	Cantonal	16'124'941'990	17'771'775'742	110%
GR	Cantonal	110'156'189'135	102'495'624'580	93%
JU	Cantonal	23'810'282'258	33'946'915'176	143%
LU	Cantonal	120'596'856'000	158'001'837'612	131%
NE	Cantonal	57'112'358'174	63'418'565'968	111%
NW	Cantonal	13'868'758'700	15'015'241'078	108%
OW	Private	12'733'938'704	15'382'280'148	121%
SG	Cantonal	150'405'814'425	181'414'197'048	121%
SH	Cantonal	25'931'720'100	30'894'037'485	119%
SO	Cantonal	86'526'772'404	100'068'271'626	116%
SZ	Private	47'430'381'817	57'003'346'509	120%
TG	Cantonal	92'044'109'600	106'550'442'276	116%
TI	Private	128'976'427'225	143'648'172'960	111%
UR	Private	11'743'436'353	14'230'318'434	121%
VD	Cantonal	264'334'562'125	278'930'306'078	106%
VS	Private	125'888'209'336	144'638'213'646	115%
ZG	Cantonal	49'738'275'200	44'156'731'139	89%
ZH	Cantonal	492'839'244'400	421'517'215'274	86%
	Total	2'861'939'335'066	2'945'365'117'218	103%
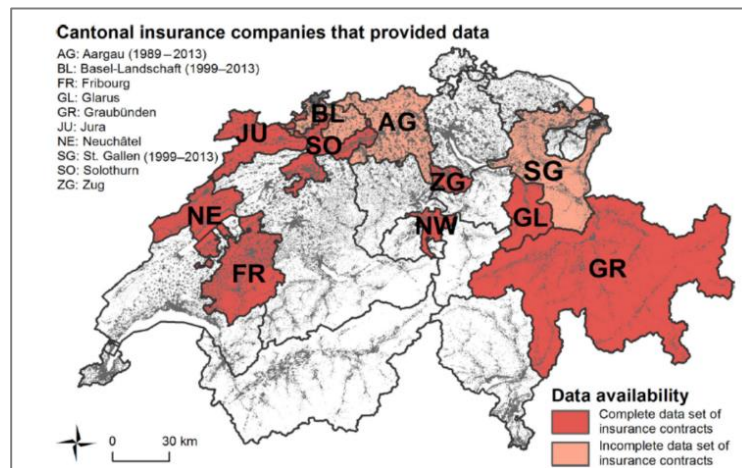
Figure 4.1. Overview of the cantonal data used for the development of building replacement value models in Röthlisberger (2018).

Table 4.6. Unit replacement values for buildings according to model M4 in Röthlisberger (2018).

Land-use zoning category	Attribute AREBAUZ in ERM-CH23	Unit repl. value, **Residential**	Unit repl. value, **Non-residential**
Residential	11	897 CHF/m^3	765 CHF/m^3
Urban centre	14	861 CHF/m^3	645 CHF/m^3
Mixed zone	13	801 CHF/m^3	584 CHF/m^3
Commercial	12	505 CHF/m^3	377 CHF/m^3
Public activity	15	984 CHF/m^3	818 CHF/m^3
Others	16-19	950 CHF/m^3	730 CHF/m^3
No zoning	0	596 CHF/m^3	376 CHF/m^3

In model M5, the replacement value per m^3 varies according to the absolute value of the volume above ground. Different regression laws were developed in Röthlisberger (2018) for residential and non-residential buildings with a differentiation according to the land-use zoning category. Table 4.7 gives an overview of the unit replacement values per m^3 for different building volumes above ground.

Table 4.7. Unit replacement values for buildings according to model M5 in Röthlisberger (2018).

	Unit replacement value for different building volumes above ground, **Residential**			Unit replacement value for different building volumes above ground, **Non-residential**		
Land use	1,000 m^3	10,000 m^3	100,000 m^3	1,000 m^3	10,000 m^3	100,000 m^3
Residential	906 CHF/m^3	734 CHF/m^3	594 CHF/m^3	610 CHF/m^3	711 CHF/m^3	830 CHF/m^3
Urban centre	835 CHF/m^3	683 CHF/m^3	560 CHF/m^3	401 CHF/m^3	473 CHF/m^3	558 CHF/m^3
Mixed zone	844 CHF/m^3	691 CHF/m^3	567 CHF/m^3	457 CHF/m^3	539 CHF/m^3	636 CHF/m^3
Commercial	754 CHF/m^3	485 CHF/m^3	312 CHF/m^3	393 CHF/m^3	365 CHF/m^3	339 CHF/m^3
Public activity	991 CHF/m^3	800 CHF/m^3	645 CHF/m^3	710 CHF/m^3	825 CHF/m^3	960 CHF/m^3
Others	884 CHF/m^3	757 CHF/m^3	647 CHF/m^3	506 CHF/m^3	624 CHF/m^3	769 CHF/m^3
No zoning	692 CHF/m^3	309 CHF/m^3	138 CHF/m^3	332 CHF/m^3	213 CHF/m^3	137 CHF/m^3

Table 4.8 compares the modeled building replacement value using model M5 in ERM-CH23 with the available insurance data. The comparison is made for all buildings as well as separately for residential and non-residential buildings. The territory covered is Switzerland and Liechtenstein.

Table 4.8. Comparison of the total number of buildings and their replacement value according to ERM-CH23 and insurance data.

	Number of buildings ERM-CH23*	Number of buildings Insurers	Building replacement value ERM-CH23	Building replacement value Insurers
All buildings	2,320,720	2,712,115	CHF 2,945 billion	CHF 2,861 billion
Residential	1,707,861	1,691,579	CHF 1,946 billion	CHF 1,775 billion
Non-residential	612,859	1,020,536	CHF 999 billion	CHF 1,086 billion

*Only buildings with a volume above ground ≥ 200 m^3

Model M5 overestimates the total insured replacement value of all considered buildings in Switzerland and Liechtenstein by 3%. It overestimates the aggregated insured replacement value of residential buildings by roughly 10% and underestimates the aggregated insured replacement value of non-residential buildings by roughly 8%. The number of considered non-residential buildings in ERM-CH23 is much lower than in the insurance datasets. The main reason is that only objects with a volume ≥ 200 m^3 are considered in ERM-CH23. The differences between ERM-CH23 and insurance data vary from canton to canton (see also Table 4.5).

Using model M5 of Röthlisberger (2018) in ERM-CH23 leads to an average replacement value of 783 CHF/m^3 (volume above ground) for residential and 450 CHF/m^3 for non-residential buildings. For residential buildings, the value is consistent with the expected construction costs for apartment buildings with normal construction standards according to simulations on the platform www.kennwerte.ch (780 CHF/m^3 [3]) as well as according to estimations from three Swiss architectural firms[4] (average of 820 CHF/m^3 [5]). For non-residential buildings, there is an expected large scatter of unit construction costs per m^3 depending on the possible sub-categories of use (from around 200 CHF/m^3 for agricultural buildings to around 1,200 CHF/m^3 for hospital buildings according to the same sources).

In conclusion, the relatively simple model used to compute the building replacement value GEBWERT leads to aggregated values and average values per m^3 that are globally in line with the data of insurers and estimations of actual construction costs. Future refinements of this model should consider a more extensive calibration dataset from the cantonal insurers and more categories of building use than residential and non-residential. A regionalisation of the model could also be envisaged, if warranted.

4.5.3   Modelled content value

The proposed ratios for computing the content value (INHWERT) from the modelled building replacement value (GEBWERT) initially came from a statistical analysis of the ratio of the total insured content value to the total insured building replacement value for the categories 'private', 'commercial' and 'industry' in the seven cantons where both contents and buildings are insured by private insurance companies and thus categorised as 'private', 'commercial' and 'industry' using the same criteria. For this analysis, the Swiss Insurance Association representing private insurers (SIA) provided the data from their latest global survey from December 2015. The results are presented in the figure below, from the report by Hügli et al. (2021). The originally selected ratios for ERM-CH23 correspond to total insured content value in the seven GUSTAVO cantons in relation to the total insured building replacement value for the categories 'residential' (*privat*), 'commercial' (*Gewerbe*) and 'industry' (*Industrie*).

Following a comment by the ERM-CH23 review team in July 2022, these ratios were re-evaluated with further analyses. The results and implemented modifications are described here.

The overall ratio of aggregated insured content value to aggregated insured building replacement value across Switzerland and Liechtenstein amounts to 0.27, which is slightly lower than the ratio of 0.28 in Figure 4.2. Consequently, the content value ratio for unknown and miscellaneous building use was changed to 0.27 in the final version of ERM-CH23.

The ratio for residential buildings, which was originally computed as noted above using aggregated data from private insurance companies in the seven GUSTAVO cantons where contents and buildings are insured by private insurers, leads to an overestimation of the aggregated content value for residential buildings in Switzerland and Liechtenstein of roughly 50%. The source of the problem is an apparent discrepancy in the calculation of the insured replacement value of residential buildings between private and cantonal insurers.

---

[3] Volume including volume under ground level.
[4] Survey conducted by SPF in the summer of 2021.
[5] Volume including volume under ground level.

Kanton	Anzahl PLZ	Summe Inhaltswerte				Summe Gebäudewerte			
		Privat	Gewerbe	Industrie	Total	Privat	Gewerbe	Industrie	Total
AI	6	700'558'000	353'014'390	407'684'610	1'461'257'000	1'568'909'000	1'696'440'713	226'391'287	3'491'741'000
GE	59	18'495'368'800	16'669'494'990	9'232'251'651	44'397'115'440	45'887'964'051	57'513'047'290	31'613'449'654	135'000'000'000
OW	16	1'615'262'271	975'999'118	1'017'619'863	3'608'881'252	5'946'078'510	4'975'804'567	1'690'070'413	12'611'953'490
SZ	48	6'467'610'329	3'567'208'229	3'245'435'392	13'280'253'951	21'951'776'169	19'314'809'137	5'669'552'323	46'936'137'629
TI	244	13'824'725'138	7'487'479'274	8'700'915'347	30'013'119'759	72'021'975'116	41'935'843'570	14'772'013'034	129'000'000'000
UR	25	1'433'795'471	935'644'914	1'159'765'516	3'529'205'900	5'363'756'889	4'753'976'375	1'495'987'277	11'613'720'541
VS	172	15'149'381'549	6'275'915'199	13'515'210'957	34'940'507'705	67'975'092'843	38'283'991'524	19'130'663'969	125'000'000'000
Total	570	57'686'701'558	36'264'756'113	37'278'883'337	131'230'000'000	220'716'000'000	168'474'000'000	74'598'127'958	463'788'000'000

Kanton	Anzahl PLZ	Summe Inhaltswerte / Summe Gebäudewerte			
		Privat	Gewerbe	Industrie	Total
AI	6	45%	21%	180%	42%
GE	59	40%	29%	29%	33%
OW	16	27%	20%	60%	29%
SZ	48	29%	18%	57%	28%
TI	244	19%	18%	59%	23%
UR	25	27%	20%	78%	30%
VS	172	22%	16%	71%	28%
Total	570	26%	22%	50%	28%

Figure 4.2. Data used to compute the INHWERT to GEBWERT ratios for ERM-CH23. Source: Hügli et al. (2021).

The insured replacement value per m^3 is systematically lower in cantons with a private insurance system (on average 538 CHF/m^3) than in cantons with a cantonal insurance system (on average 762 CHF/m^3). As the building replacement value model in ERM-CH is based on data from cantonal insurers, it was decided to recompute the ratio for content value of residential buildings based on cantonal insurance data in the 16 cantons where contents are insured by private insurers and buildings by cantonal insurers. The adapted ratio is computed as the aggregated insured content value ('private' category) in relation to the aggregated insured residential building replacement value from cantonal insurers, and amounts to 0.19. Consequently, the content value ratio for residential buildings was changed to 0.19 in the final version of ERM-CH23.

For industrial buildings, it was decided to remove the cantons of Appenzell Innerrhoden (AI) and Geneva (GE) from the analysis shown in Figure 4.2 and to add Liechtenstein. The removal of AI and GE was decided based on very inconsistent reported aggregated values in AI and an unrealistically low (outlier) content value ratio for industrial buildings of 0.29 in GE. The revised ratio for industrial buildings is computed as the aggregated insured content value and the aggregated building replacement value for the 'industry' category in the cantons of Uri (UR), Schwyz (SZ), Ticino (TI), Valais (VS) and Obwalden (OW) as well as Liechtenstein. Consequently, the content value ratio for industrial buildings was changed to 0.65 in the final version of ERM-CH23.

The private insurance companies report CHF 209 billion of insured content value for industrial buildings in Switzerland and Liechtenstein, excluding the cantons of Glarus (GL), Nidwalden (NW) and Vaud (VD) (which have special insurance regimes for contents). In ERM-CH23, the modelled content value for industrial buildings (GKLASdef = 1251 or 1252) over the same territory amounts to CHF 152 billion, underestimating the industrial insured content value reported by insurers by roughly 30%. A probable main cause for this underestimation is the lower number of buildings tagged as industrial in ERM-CH23 compared with the number of buildings in the 'industrial' category according to the private insurance data. In the seven GUSTAVO cantons and Liechtenstein, where a direct comparison is possible, there are 21,883 buildings identified as industrial by the insurers, whereas 10,256 buildings are considered as industrial in ERM-CH23 (GKLASdef = 1251 or 1252). There is unfortunately no way to resolve this classification discrepancy at his time. Thus, part of the 'missing' content value for industrial buildings in ERM-CH23 lies in the content value for other use categories (mainly commercial).

For the 'commercial buildings' category, the content value ratio of 0.22 from the initial analysis in Figure 4.2 was raised to 0.38 to compensate for an underrepresentation of industrial buildings (and therefore of industrial content value) in ERM-CH23 compared with the classification system of private insurance companies and for a general underestimation of the aggregated insured content value of non-residential buildings.

The final content value ratios to compute INHWERT from GEBWERT in ERM-CH23 are as follows:

- INHWERT = **0.19** * GEBWERT for GKLAS 1110 to 1199 (residential buildings)

- INHWERT = **0.38** * GEBWERT for GKLAS 1211, 1212, 1220, 1230, 1241, 1242, 1261, 1262, 1263, 1264, 1265, 1271, 1272, 1273, 1274 (commercial buildings)

- INHWERT = **0.65** * GEBWERT for GKLAS 1251 and 1252 (industrial buildings)

- INHWERT = **0.27** * GEBWERT for other GKLAS values.

The total content value modelled in ERM-CH23 amounts to CHF 788 billion. The private insurance industry reports CHF 698 billion of insured content value (at the end of 2015). Furthermore, CHF 72 billion of content value is insured by the cantonal insurer in VD, CHF 4.7 billion by the cantonal insurer in NW and CHF 2 billion by the cantonal insurer in GL (special insurance regimes; situation at the end of 2020). The total content value of CHF 788 billion modelled in ERM-CH23 is thus roughly 2% higher than the reported total insured content value of CHF 776 billion from insurance data. An overview of the comparison between computed content value and reported insured content value aggregated at the cantonal level is provided in Table 4.9. Geneva stands out as an outlier with an underestimation of the insured aggregated content value of 35%, suggesting a possible problem with data collection by the private insurers.

Table 4.9. Overview of the comparison of the aggregated content value against insurance data at the cantonal level.

Canton	Content value of buildings in CHF		ERM/Ins
	Insurances	**ERM_CH**	
AG	61'473'179'642	67'056'493'281	109%
AI	1'634'533'777	1'629'887'621	100%
AR	5'327'753'223	5'743'915'071	108%
BE	94'057'870'893	95'631'056'272	102%
BL	26'951'686'403	26'525'931'846	98%
BS	18'158'835'931	16'192'495'071	89%
FL	5'452'759'304	5'335'087'917	98%
FR	26'392'758'742	28'958'353'071	110%
GE	46'817'916'176	30'593'364'751	65%
GL	5'225'914'938	5'367'382'219	103%
GR	27'098'992'044	26'778'669'905	99%
JU	7'298'036'000	8'903'845'842	122%
LU	35'305'233'218	42'883'282'979	121%
NE	15'649'619'902	16'514'217'130	106%
NW	5'246'189'566	4'049'924'688	77%
OW	3'706'674'000	3'976'279'907	107%
SG	49'482'624'113	53'149'802'196	107%
SH	6'616'870'000	8'531'993'348	129%
SO	25'302'343'943	27'177'636'500	107%
SZ	13'642'468'259	13'830'692'149	101%
TG	26'320'413'584	31'170'122'954	118%
TI	30'474'778'047	35'151'277'542	115%
UR	3'664'423'181	3'467'972'565	95%
VD	71'547'375'995	72'556'714'348	101%
VS	35'548'552'042	34'566'900'815	97%
ZG	11'959'125'008	11'502'652'898	96%
ZH	116'051'410'678	111'116'242'256	96%
	776'408'338'608	788'362'195'141	102%

Table 4.10 shows a comparison between insured content value and modelled content value for the categories 'residential' and 'non-residential' for Switzerland and Liechtenstein excluding the cantons of VD, GL and NW (no data with distinction between residential and non-residential available). It shows a slight overestimation (12%) of the insured content value for residential buildings and a slight underestimation (6%) for non-residential buildings.

Table 4.10. Comparison of residential and non-residential content value between insurance data and ERM-CH23 valid for Switzerland + Liechtenstein excluding the cantons of VD, GL and NW.

Category	Insured content value	Content value ERM-CH23	ERM- CH23/Insured value
Residential	CHF 305 billion	CHF 341 billion*	112%
Non-residential	CHF 389 billion	CHF 365 billion**	94%

* Computed from GEBWERT of buildings tagged as residential or mostly residential in ERM-CH23

** Computed from GEBWERT of buildings tagged as non-residential in ERM-CH23

In summary, the content value ratios implemented in ERM-CH23 are based on limited insurance data but enable a satisfactory global estimation of content values in comparison with the aggregated insured content values in Switzerland.

4.6   Selected issues

Completeness and consistency of the building database

The Federal Register of Buildings and Dwellings (RBD) kept by the Federal Statistical Office is not yet 100% complete and also not fully compatible with the database of building footprints (AV dataset) of the Federal Office of Topography. The AV dataset is also not 100% complete in some regions. We expect that the number of missing relevant objects in ERMCH_GEB01 because of that situation to be very small (< 1%). The RBD and the AV dataset contain a large number of small objects that are irrelevant from a risk perspective. In the ERMCH project, we dealt with the problem by excluding objects with a volume smaller than 200 m³.

The completion and unification of the RBD and AV datasets (expected in 2024) will make it possible to perform checks in order to exclude objects that are not real building objects (tanks, silos, transformer housings, etc.). Through random checks, we identified that some of these special objects are present in ERMCH_GEB01. They could not be excluded in a systematic way. The impact of the presence of such non-standard building objects in ERMCH_GEB01 is probably negligible.

For future developments, it would be very helpful if insurance companies used the EGID number from the RBD as an identifier for building objects in their databases (see also Chapter 12).

Human occupancy

Permanent inhabitants, full-time equivalent employees, school and hospital capacities are the only attributes regarding human occupancy that are provided in ERMCH_GEB01. In light of the very high uncertainty associated with actual human occupancy of buildings and casualty estimation models, it was decided not to develop further models of human occupancy for ERMCH_GEB01.

References

FOEN (2021). Earthquake Risk Model Switzerland (ERM-CH) – Subproject F, Database of building objects - Deliverable DB4, report. SPG-SPD-0015.

Hügli, M., Zischg, A., Keiler, M. (2021). Modellierung von Gebäudeattributen im Rahmen des Projektes Erdbebenrisikomodell Schweiz – dritte Arbeitsphase. Bericht im Auftrag vom Bundesamt für Umwelt. EXT-TR-0017.

Röthlisberger, V. (2018). A comparison of building value models for flood risk analysis. Journal of natural hazards and earth system sciences. Natural Hazards and Earth System Sciences **18**(9):2431–2453.

5.   Building taxonomy and fragility models

5.1   Introduction

Subproject G is hosted by the Earthquake Engineering and Structural Dynamics Laboratory (EESD) at EPFL (École Polytechnique Fédérale in Lausanne). The general scope of this subproject is to analyse the seismic fragility of buildings in Switzerland. Macroseismic (i.e. intensity-based) and mechanical (i.e. Sa-based) approaches are two methodologies used to derive fragility models for the large-scale seismic vulnerability assessment. Intensity-based fragility curves are derived based on the empirical estimate of the fragility of European building typologies, together with engineering judgement about Swiss practice. The set of I-based fragility curves was also updated for better performance on their low-intensity sides. Regarding the mechanical approach, as masonry and reinforced concrete buildings represent the majority in Switzerland, different subclasses of those buildings are considered and their seismic performance is investigated by developing several numerical models with different numbers of storeys. Variation of material/mechanical characteristics is also captured and the obtained sets of capacity curves are then used for deriving Sa-based fragility curves. Those fragility curves are also compared with those from independent studies as well as with I-based fragility curves.

As structural building features are not available in the Swiss building dataset of subproject F, proxies to detect the structural building type are necessary and play a major role in seismic risk assessments on the national scale. We developed several mapping schemes from extensive surveys in different cities. The big dataset from visual surveys was also used for developing a machine learning-model to detect building typology by considering all building features, collected in subproject F.

5.2   Building taxonomy

As shown in previous studies (e.g. the ESRM20 project), an essential step for risk calculations at a large scale is to define an appropriate Building Taxonomy (BT). In other words, since the Swiss building inventory encompasses a considerable number of buildings (i.e. more than 2.8 million), defining a limited number of building types is essential; buildings with almost similar structural behaviour are grouped into one building type and the vulnerability of each building type is evaluated. This step plays a key role in risk assessment since the vulnerability of the exposure strongly depends on the defined building typologies and their attributed fragility curves. According to several surveys carried out in Switzerland (e.g. Thiriot, 2019), the BT proposed in Lagomarsino and Giovinazzi (2006) is suitable for and can therefore be applied to Switzerland with minor modifications. Accordingly, the BT presented in Table 1 is proposed for ERM-CH23.

5.3   Intensity-based fragility model

Intensity-based fragility is developed based on the mean damage value, μ_D, which can be obtained using:

$$\mu_D = \left[2.5 + 2.7 * tanh\left(\frac{I + 6.25V - 13.1}{Q}\right)\right] * \begin{cases} e^{(I-7)/2}, & I \ll 7 \\ 1, & I > 7 \end{cases} \qquad (5.1)$$

V and Q are vulnerability and ductility indices and I is the macroseismic intensity at the building location. Thus, I is the ground motion that corresponds to the reference rock conditions considered in the hazard calculations, and then locally corrected to account for the amplification factor from these reference rock conditions to the local ground surface.

Unreinforced masonry buildings with rigid floor (M6) and reinforced concrete shear wall (RCW) buildings account for a large portion of the exposure, and Swiss construction practice for these two building types is different from that in other European countries. It was therefore decided to re-evaluate vulnerability indices for these buildings based on the EMS-98 major vulnerability classes. In EMS-98, six major vulnerability classes (A to F) and the corresponding vulnerability indices for those classes are estimated based on the observed damage from past earthquakes. Based on engineering judgement on Swiss buildings, association rules between these major vulnerability classes and the two dominant building types are considered. 90% of the Swiss RCW buildings are constructed without earthquake-resistant provision (similar to RC1 in Bernardini et al., 2010), and the rest with a moderate level of earthquake-resistant design (similar to RC2 in Bernardini et al., 2010). In summary, the association of the EMS-98 classes to M6 and RCW is presented in Table **5.2**. Based on (1) the vulnerability indices for each EMS-98 major class and (2) the corresponding association rules from Table 5.2, the value of vulnerability indices for M6 and RCW is calculated and referred for mid-rise buildings. Vulnerability indices for different height classes are then evaluated based on the suggestion made by Lagomarsino and Giovinazzi (2006). Vulnerability and ductility indices (i.e. V and Q parameters) for M1-M5, steel and timber buildings are estimated based on the assumption made by Lagomarsino and Giovinazzi (2006), in which these indices have been calibrated based on observed damage in European countries. Vulnerability and ductility indices, V and Q, for all building types are summarised in Table 5.1.

**Table 5.1**. Building typological matrix with vulnerability indices

Building Type¥	Description	V⁻	V*	V⁺	Q
M1_L	Dry stone	0.73	0.79	0.9	2.3
M1_M		0.81	0.87	0.98	2.3
M2_L	Adobe (earth bricks)	0.69	0.84	0.98	2.3
M3_L	Rubble stone	0.57	0.66	0.75	2.3
M3_M		0.65	0.74	0.83	2.3
M3_H		0.73	0.82	0.91	2.3
M4_L	Dressed stone	0.41	0.54	0.71	2.3
M4_M		0.49	0.62	0.79	2.3
M4_H		0.57	0.7	0.87	2.3
M5_L	U masonry (old bricks)	0.57	0.66	0.75	2.3
M5_M		0.65	0.74	0.83	2.3
M5_H		0.73	0.82	0.91	2.3
M6_L	U masonry – RC floors	0.384	0.51	0.684	2.3
M6_M		0.464	0.59	0.764	2.3
M6_H		0.544	0.67	0.844	2.3
RCF_L	RC Frames	0.34	0.49	0.64	2.3
RCF_M		0.36	0.51	0.66	2.6
RCF_H		0.38	0.53	0.68	2.6
RCW_L	Shear walls	0.323	0.50	0.626	2.3
RCW_M		0.343	0.52	0.646	2.6
RCW_H		0.363	0.54	0.666	2.6
RCmix_L	Mixed shear wall and RC frame	0.332	0.495	0.633	2.3
RCmix_M		0.352	0.515	0.653	2.6
RCmix_H		0.372	0.535	0.673	2.6
S	Steel structures	0.17	0.324	0.48	2.3
T	Timber structures	0.207	0.447	0.64	2.3
Ind	Industrial structures	0.36	0.5	0.69	2.3

¥ Keys: _L: low-rise, _M: mid-rise, _H: High-rise.

Table 5.2. Probabilistic association of the EMS-98 classes to M6 and RCW.

	Weight					
	A	**B**	**C**	**D**	**E**	**F**
M6	0	0.27	0.64	0.09	0	0
RCW	0	0.081	0.585	0.307	0.027	0

It should be noted that the functional form of Equation (5.1) is comparable to suggestions by Lagomarsino et al. (2021) and Lagomarsino and Giovinazzi (2006). However, an adjustment is carried out to obtain a better estimate of damage at low intensities by following suggestions in Bernardini et al. (2010). As shown in Figure 5.1 (left), the mean damage values for the EMS-98 major vulnerability classes from the suggested formula by Lagomarsino and Giovinazzi (2006) (i.e. thick lines) are higher than the expected range of mean damage from observation in low intensities. However, the estimated mean damage values from the adjusted formula (i.e. Equation 5.1) lie within the expected range of mean damage for major vulnerability classes (Figure 5.1 right).
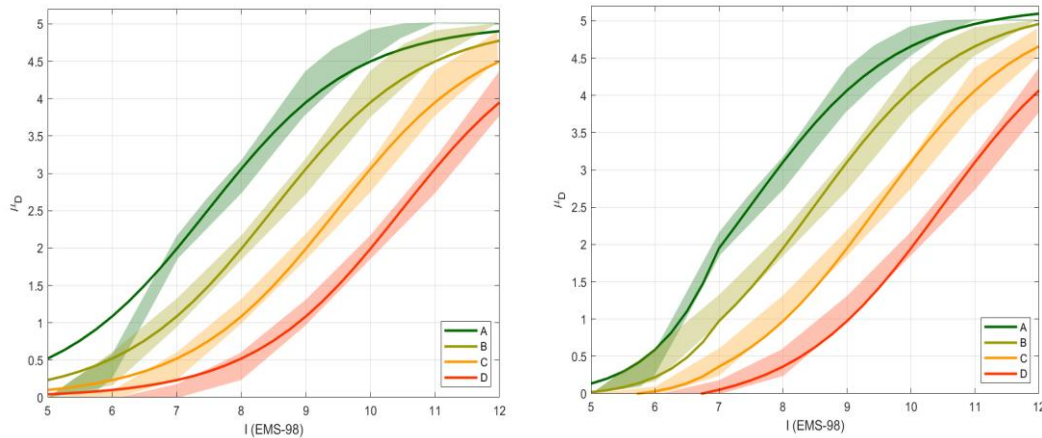
Figure 5.1. Shadows show the ranges of mean damage for major vulnerability classes from observation (Lagomarsino and Giovinazzi, 2006). Thick lines show (left) evaluation from the suggested formula by Lagomarsino and Giovinazzi (2006) and (right) our evaluation from the adjusted formula.

The probabilistic assessment of damage distributions is then evaluated based on the mean damage value (μ_D) by assuming a binomial distribution. The probability, p_{D_k}, of having a certain damage grade D_k (k = 0 … 5) is evaluated according to the following function:

$$p_{D_k} = \frac{5!}{k!(5-k)!}\left(\frac{\mu_D}{5}\right)^k\left(1 - \frac{\mu_D}{5}\right)^{5-k} \tag{5.2}$$

To capture uncertainty, the three values of the vulnerability index (i.e. V^*, V^-, and V^+) are considered and three empirical fragility models are presented. Whereas V^* is the best estimate of the vulnerability index, the V^-, V^+ can be considered as the probable value range of this index. As an example, fragility curves for M3_L (low-rise rubble stone masonry buildings) for different damage grades are depicted in Figure 5.2. Intensity-based fragility curves for M3_L (left) for all damage grades with V^*, and (right) with their uncertainties for DG1, DG3 and DG5.
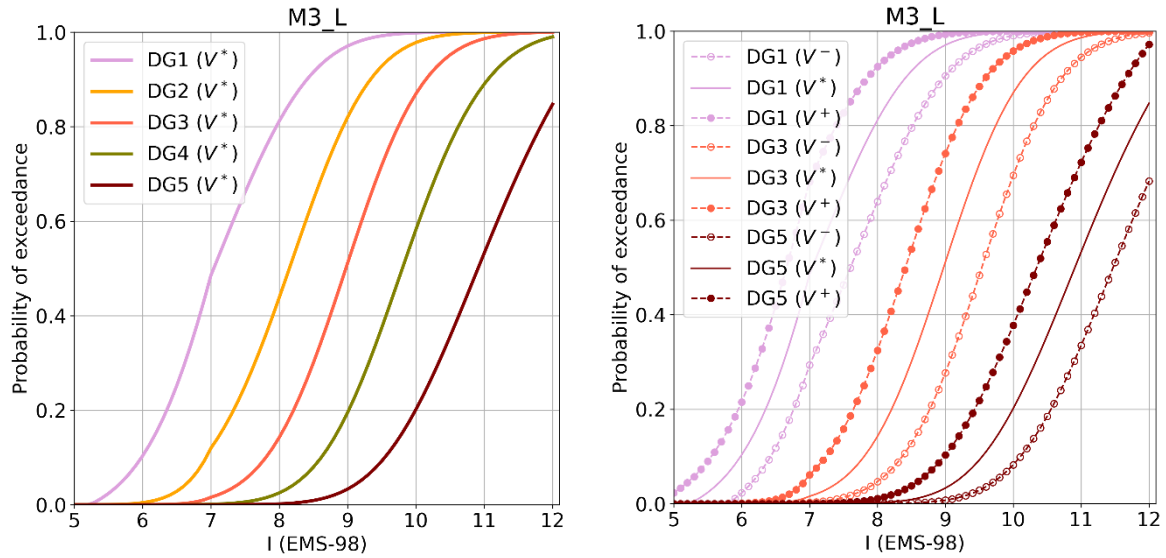
Figure 5.2. Intensity-based fragility curves for M3_L (left) for all damage grades with V^*, and (right) with their uncertainties for DG1, DG3 and DG5.

5.4   Sa-based fragility curves

Although there are already several fragility curves in the literature, direct implementation of such models in large-scale seismic risk analyses can be challenging as the methodologies and the considered damage criteria are often different. Moreover, the structural characteristics of some Swiss buildings are different from those of buildings investigated in other countries. It is also worth noting that empirical fragility models developed based on macroseismic intensity are usually hampered by the lack of sufficient datasets of recorded damage. Those models are, therefore, usually used for damage assessment of common scenarios whereas mechanical-based fragility functions can be a better option when it comes to calculating seismic risk in the probabilistic framework. The aforementioned factors demonstrate the necessity of a fragility model capable of overcoming the limitations. Therefore, as a parallel path to the intensity-based fragility model, a mechanical-based fragility model was developed. In the following, we first present different mechanical models, developed for the different building types. After an introduction of the method used here for finding performance points, fragility curves for different building types are presented and compared with the curves obtained by independent studies.

5.4.1   M3, M4 and M5 building typologies

Here, we focus on the most representative unreinforced masonry (URM) buildings with flexible floors located in Switzerland; two different height classes (low-rise: L and mid-rise: M) and three masonry types (rubble stone masonry: M3, dressed stone masonry: M4 and clay brick masonry: M5) are investigated in detail. According to the surveys and application of predictive models, these building types contribute ~35% to the exposure model of buildings in Switzerland. Numerical models of two- and four-storey buildings are generated as representative of low-rise and mid-rise buildings respectively. For the configuration (i.e. geometrical characteristics) of the representative buildings, we make use of the detailed statistical investigation of the building blueprint by Savoy (2019) so that numerical models represent the buildings with the average geometric characteristics (e.g. length of walls and openings). The three-dimensional equivalent-frame modelling approach is used to investigate the seismic behaviour of the masonry buildings. The technique provides an accurate modelling strategy for masonry buildings and is a practical compromise between complexity and computational cost.

To validate the modelling technique, we modelled a building, extensively monitored and investigated in Martakis et al. (2021), and modal analysis was performed. The difference between our results and the measurement is around 8% for the first mode, which is less than the corresponding differences evaluated from the models used in Martakis et al. (2021). There is also a good match between the numerical model and measurements in terms of mode shapes; the first mode is along the longitudinal direction and the third mode shape is a torsional mode. Moreover, the initial stiffness of the structure and maximum base shear of the building are consistent with the model in Martakis et al. (2021).
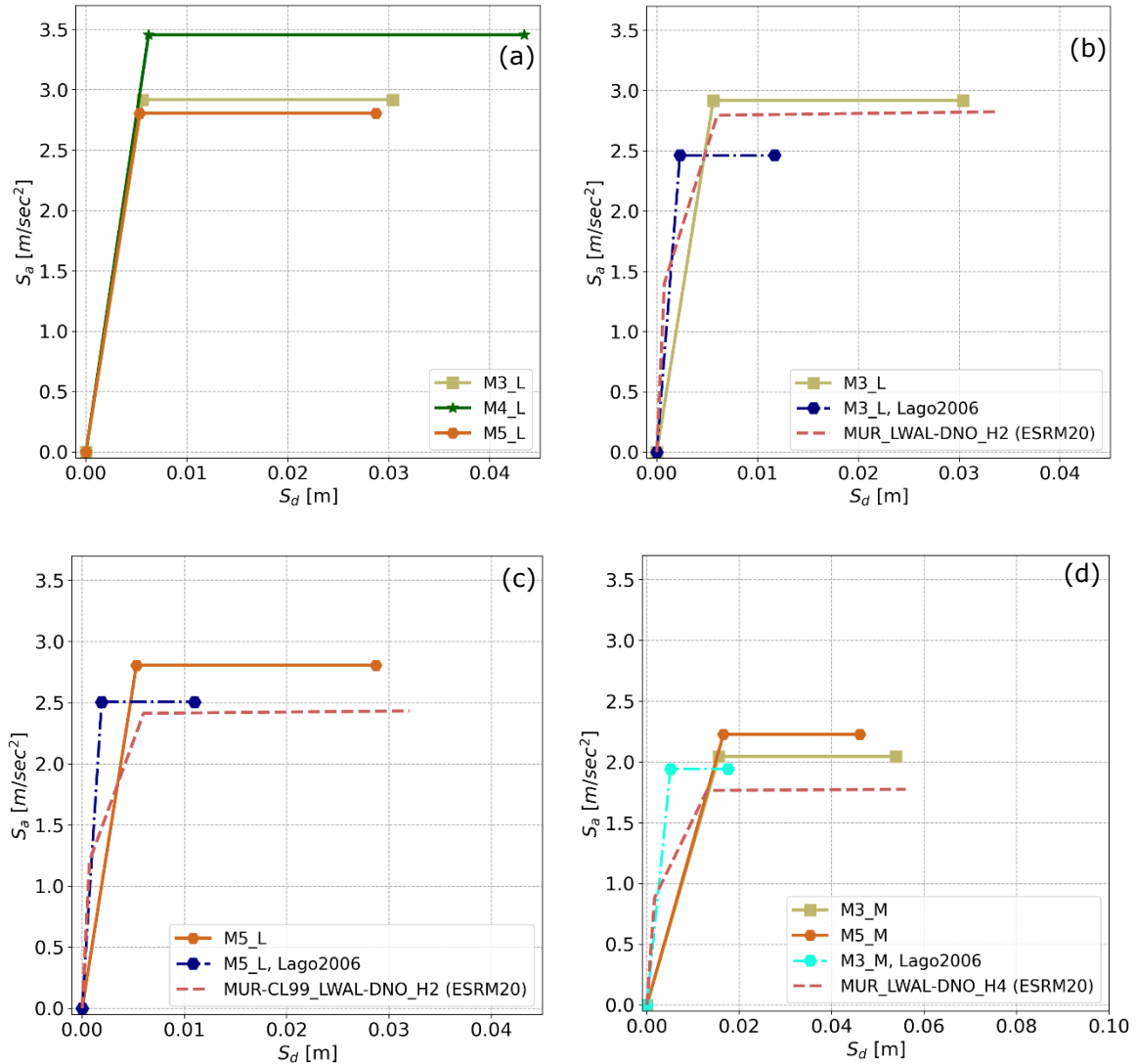
Figure 5.3. Capacity curves for masonry buildings and comparison with Lago2006:Lagomarsino and Giovinazzi (2006) and ESRM20: European Seismic Risk Model

Due to the natural variability of the masonry materials, their mechanical properties are subject to a range of uncertainties. Vanin et al. (2017) summarised a significant number of quasi-static shear-compression tests on stone masonry and provided input for displacement-based assessment of stone masonry building.

Concerning stone masonry, mechanical parameters are derived from Vanin et al. (2017). The masonry category C in Vanin et al. (2017) represents rubble stone masonry, and its properties are used for M3, and an average of category E-E1 in their study is selected for M4. Mechanical parameters, estimated by Sarhosis et al. (2015) from the experimental of brick masonry walls, are used in modelling of M5 buildings. Mean values (X_i) and covariance (CoV) of material properties and their references are summarised in Table 5.3.

Table 5.3. Material properties for M3-M4-M5 buildings.

		Elastic modulus [Mpa]	Cohesion [Mpa]	Friction coeff. [-]	Drift limits $\theta_{P,S}$, $\theta_{P,F}$	Residual $\beta_{P,S}$, $\beta_{P,F}$
M3 (rubble stone)	X_i	1740	0.054	0.275	low-rise: 0.006,0.013; mid-rise: 0.006, 0.009	0.4, 0.85
	CoV	0.15	0.15	0.15	0.6	-
M4 (dressed stone)	X_i	2800	0.106	0.330	low-rise: 0.015,0.023; mid-rise: 0.015, 0.021	0.4, 0.85
	CoV	0.15	0.10	0.10	0.6	
M5 (clay brick)	X_i	1340	0.075	0.477	low-rise: 0.0048,0.011; mid-rise: 0.0048, 0.0078	0.4, 0.85
	CoV	0.2	0.3	0.50	0.6	

$\theta_{P, (S/F)}$: Drift limits for piers elements, $\beta_{P, (S/F)}$: Residual strength for piers elements [shear (S) and flexural (F)]. References for drift limits and residual strength: Vanin et al. (2017), Petry and Beyer (2014) and Milosevic et al. (2020).

To take into account the variability of material/mechanical properties, several numerical models for M3, M4 and M5 masonry typologies with different heights (i.e. mid-rise and low-rise) were generated and nonlinear static analyses were performed. The idealised capacity curves for low-rise building types from models with the mean values of material properties are presented in Figure 5.3(a). As expected, dressed stone masonry buildings have the maximum capacity; they can tolerate more base shear and the highest ultimate displacement is achieved. A comparison between the obtained capacity curves for masonry buildings and the corresponding ones presented in the European Seismic Risk Model (ESRM20) and by Lagomarsino and Giovinazzi (2006) is also shown in Figure **5.3**(b-d). There is a good consistency between the obtained capacity curves and the ones from ESRM20. Generally, the maximum S_a values of ERM-CH23 capacity curves are higher in comparison to ESRM20, whereas the ultimate displacement is slightly lower. These discrepancies are mainly due to the modelling assumptions of diaphragms; the ERM-CH23 capacity curves are derived from full 3D equivalent-frame models, in which semi-flexible diaphragms are considered. However, in ESRM20, a different assumption of flexible floors is applied by estimating S_{du} from drift limits (Ahmad and Ali, 2017; Bal et al., 2010; Lagomarsino and Cattari, 2014), which results in a minor decrease in maximum shear capacity and an increase in structural ductility (see Jimenez-Pacheco et al. (2020) for more details). Concerning Lagomarsino and Giovinazzi (2006), the idealised fundamental period and maximum Sa value are comparable to ours and to ESRM20 results while there is a big underestimation of ultimate displacement for all building types.

We also developed a statistical framework for capturing uncertainties of capacity curves using a limited number of structural models. To take into account the variability of material, three different values (corresponding to mean and mean ± standard deviation) for parameters of Young modulus (*E*), cohesion (f_{vo}) and friction coefficient (*µ*) are considered, and 27 models are developed for each M3, M4 and M5 building type. As the capacity curves are idealised in a bilinear form, their uncertainties are then investigated by studying the variations of three parameters of Ty, Sdy, and Sdu. First, we investigate variation of T_y, which is expected to result mainly from the variation of Young's modulus (*E*). As an example, the distributions of Ty and Sdu for M4 low-rise building and the fitted lognormal distribution are shown in Figure 5.4. For all three masonry types, the

Kolmogorov-Smirnov goodness-of-fit test showed that the structural period (Ty) is lognormally distributed.

Figure 5.5 shows the histograms and correlations of idealised capacity curve parameters (i.e. Ty, Sdy and Sdu) for the M4 low-rise building type. The strong dependency between Sdy and Ty is observed, which is also reported in ERSM20 for a large dataset of capacity curves developed for European countries. The observed correlation between Sdy and Ty can be presented by using linear regression, as shown in that figure. However, the ultimate displacement, Sdu, is independent of Ty, and Sdu could be independently presented by a lognormal distribution (see Figure 5.4) when it comes to the material uncertainties, as the Kolmogorov-Smirnov test showed.

It is worth mentioning that drift limits also have a strong effect on the ultimate displacement. We assumed that uncertainties of material properties and drift limits are independent and the uncertainties from the two sources are coupled, as given below, and used in estimating the standard deviation of Sdu:

$$\sigma_{Sdu} = \sqrt{\sigma^2_{(E,\mu,f_{v0})} + \sigma^2_{(\theta_{P,S/P,F})}}$$

where σ(E,µ,fvo) represents the uncertainty from material properties and σ(θ (P,S/ P,F)) resulted from the variation of drift limits. The uncertainties of drift limits are evaluated using nine extra-models, in which values of material properties are fixed and drift limits are changed with the same pattern of variation as proposed by Milosevic et al. (2020). In summary, for each building type, we developed a statistical model, in which lognormal distributions of Ty and Sdu are defined and the correlation of yielding displacement and Ty is fully captured by considering linear relationship.
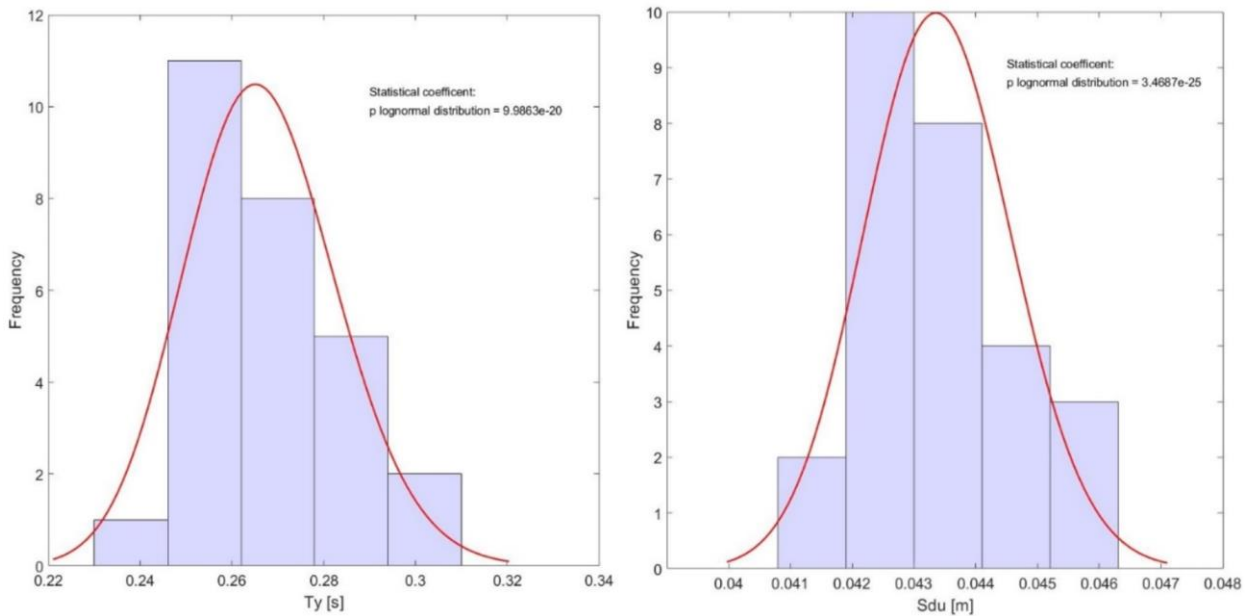
Figure 5.4. Distribution of (a) structural period, Ty [s] and (b) ultimate displacement, Sdu [m] for an M4 low-rise building. Also shown is the fitted lognormal distribution in red.
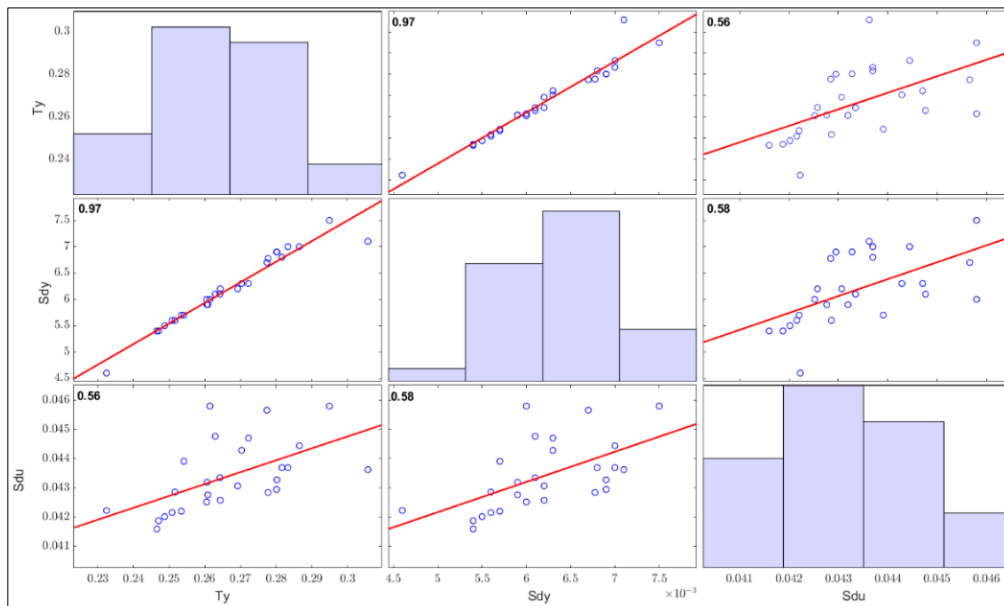
Figure 5.5. Correlation matrix of seismic response parameters for M4-L. T_y: structural period, S_{dy}: yielding displacement, S_{du}: ultimate displacement.
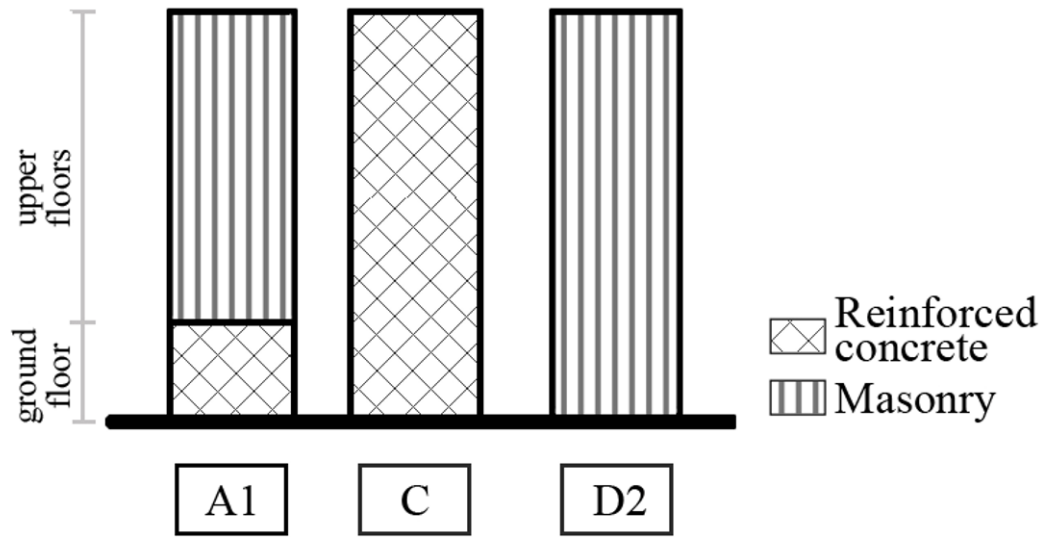
5.4.2   M6 and RCW building types

This section presents the outcome of comprehensive research carried out on different Swiss-specific building types and the corresponding capacity curves. Swiss cities were first surveyed using rapid visual screening, covering approximately 3,000 buildings in Sion and ~1,600 buildings in Martigny (Lucchini, 2016). A limited number of buildings were also analysed in depth using construction drawings from city archives. Surveys on Swiss cities showed that there are several kinds of brick masonry or RC structures, which are different from buildings commonly encountered in Europe. In summary, the main differences between M6 buildings and other masonry structures in European countries are:

- rigid floors (mainly RC flat slabs);
- brick dimensions (Swiss bricks thinner than those in southern Europe);
- very regular configurations with relatively long shear walls;
- basement floor in concrete;
- most masonry buildings in European countries are two- or three-storey structures while M6 are mostly constructed as four-storey buildings.

The detailed survey resulted in five specific building types with rigid floors (Luchini, 2016). Three of them (Figure 5.6) are widespread in the whole country and they are here considered as subclasses of M6 and RCW types defined in the ERM-CH23 taxonomy. Type A1 represents structures with reinforced concrete shear walls on the ground floor and URM walls on upper floors. Type C represents buildings with RC shear walls over the entire height of the building. Type D2 is characterised by URM shear walls, made of concrete blocks, and RC floors.

Considering the variety of construction/design methods for RC buildings, three construction time thresholds (1935, 1970, 1990) are considered and numerical models of the corresponding buildings (i.e. C1935, C1970 and C1990) generated. All subclasses with different heights (i.e. three to eight storeys) were investigated using the displacement-based vulnerability method (Lagomarsino and Cattari, 2013). Three capacity curves (i.e. minimum, average and maximum capacity curves), covering material uncertainties, are developed for each prototype building. Please refer to Lestuzzi et al. (2017) and Luchini (2016) for more details about the captured variability of material properties. Capacity curves for equally weighted building types of A1 and D2 are considered for deriving

fragility curves for M6, whereas models for C1935, C1970 and C1990, with their contributions on the exposure model (i.e. 0.23, 0.27 and 0.5 respectively), are used for RCW.


Figure 5.6. Building types, adopted from Lestuzzi et al., (2017) and considered as subclasses of M6 and RCW buildings.
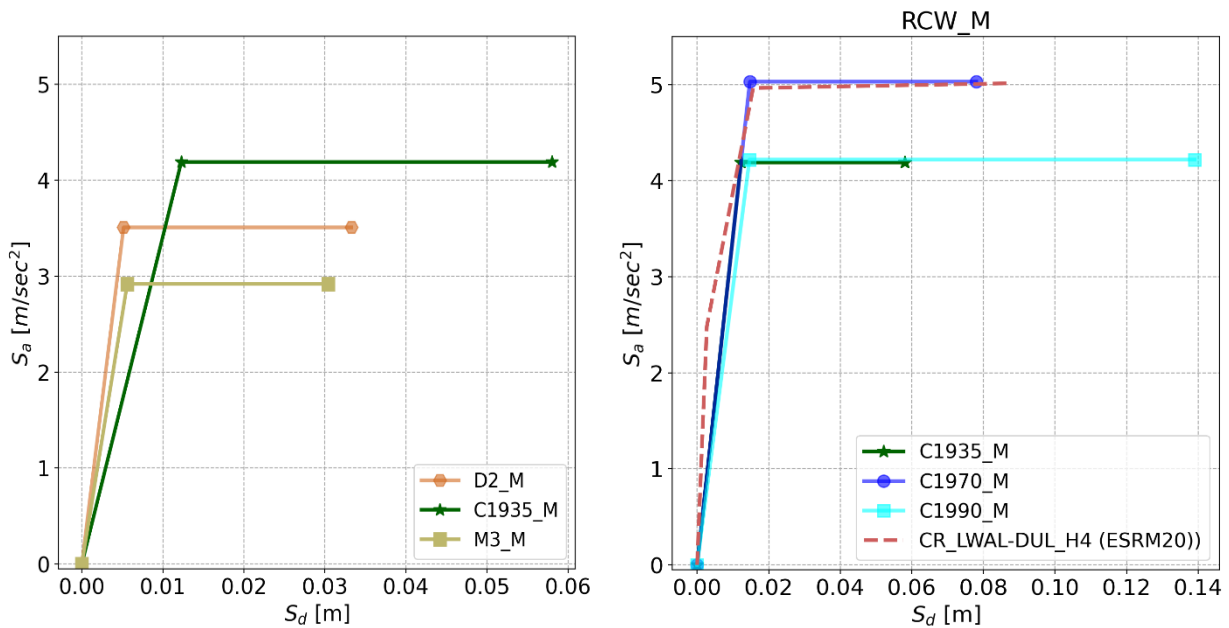
Figure 5.7. Capacity curves of different subclasses of D2 and C, and comparison with other independent investigations.

As an example, capacity curves for mid-rise (i.e. four-storey) D2 and C1935 buildings are shown in Figure 5.7 (left). C1935 has the highest idealised period and the highest ultimate displacement capacity. A higher capacity for D2_M in comparison with M3_M is obtained, mainly justifiable by rigid floor effect. In Figure 5.7 (right), all capacity curves for C1935, C1970 and C1990 buildings are depicted. Ductility of C1990 is much higher than that of the other two formats of Type C; the displacement capacity does actually increase with time. It is worth mentioning that C1970 has a great contribution in the exposure model and that there is a good consistency between capacity curves for C1970_M and the corresponding building typology in ESRM20.

To fully capture the entire possible uncertainty, 1,000 capacity curves for each building typology are generated using the statistical model, covering material uncertainties. With that procedure, truncation of uncertainties has been considered at the level of two standard deviations. As an example, Figure 5.8 shows 270 stochastic capacity curves for C1990_M building types. As expected, variability of the material properties has a considerable effect on maximum S_a, and ultimate displacement.
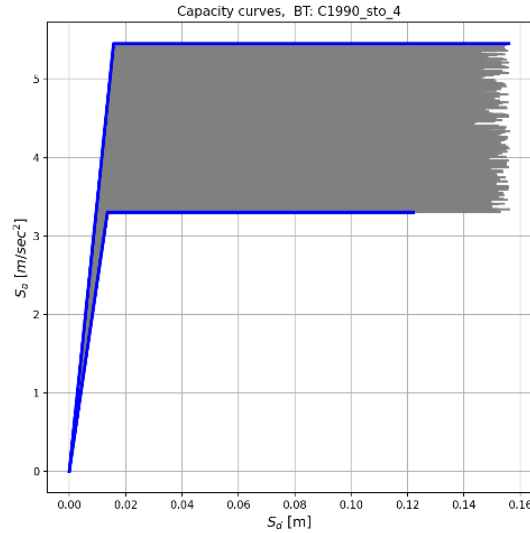
Figure 5.8. Stochastic capacity curves for a C1990_M building. The thick blue lines show the minimum and maximum curves while thin lines show the variability of capacity curves.

According to construction practice in Switzerland, most two-storey RCW buildings are comparable with M6 buildings as the majority of the lateral load-bearing system of the two-storey RCW buildings is masonry and no seismic provision is considered in designing RC walls. The fragility curves for RCW_L buildings are hence considered equal to those of M6_L buildings.

5.4.3   Methodology

The method used here for deriving fragility functions is primarily inspired by Michel et al. (2018) and developed to generate those functions at any given Intensity Measure Type (IMT). The main two inputs for this methodology are: (1) capacity curves and (2) response spectra. Regarding the former, the structural capacity of each building class is represented by a large number of equivalent single-degree-of-freedom (SDOF) systems, enabling the propagation of the building-to-building variability. Those capacity curves are taken from results of 3D numerical models of structures. Response spectra are generated from the GMPE of Akkar (2014a) for a given scenario (M_w 6.6 and R=10 km) and the record-to-record variability is captured by randomly selecting within the 1.5 standard deviation. The advantage of this method is that there is no need for record selection and matching to a reference spectrum, which would be challenging for a region like Switzerland, where no records from big events are available. Based on these two inputs, a set of structural responses is estimated by using the methodology of Lin and Miranda (2008), and the probability of exceedance for five damage grades is calculated. It should be noted that the Sa range is not limited to the 1.5 standard deviation of GMPE and we found the best fitted lognormal distributions, and the fragility function for each building type was then extrapolated up to the Sa value of 2 g. Within that process, we also modelled the building-to-building variability by considering the standard deviation, σ, according to the following equation:

$$\sigma = \sqrt[2]{\sigma_{rr}^2 + \sigma_{bb}^2}$$

where σ_{rr}^2 and σ_{bb}^2 are standard deviations due to record-to-record variability and building-to-building variability respectively. σ_{bb}^2 was assumed to be equal to 0.25, which is adopted from another regional seismic risk model at the European level (i.e. ESRM20).
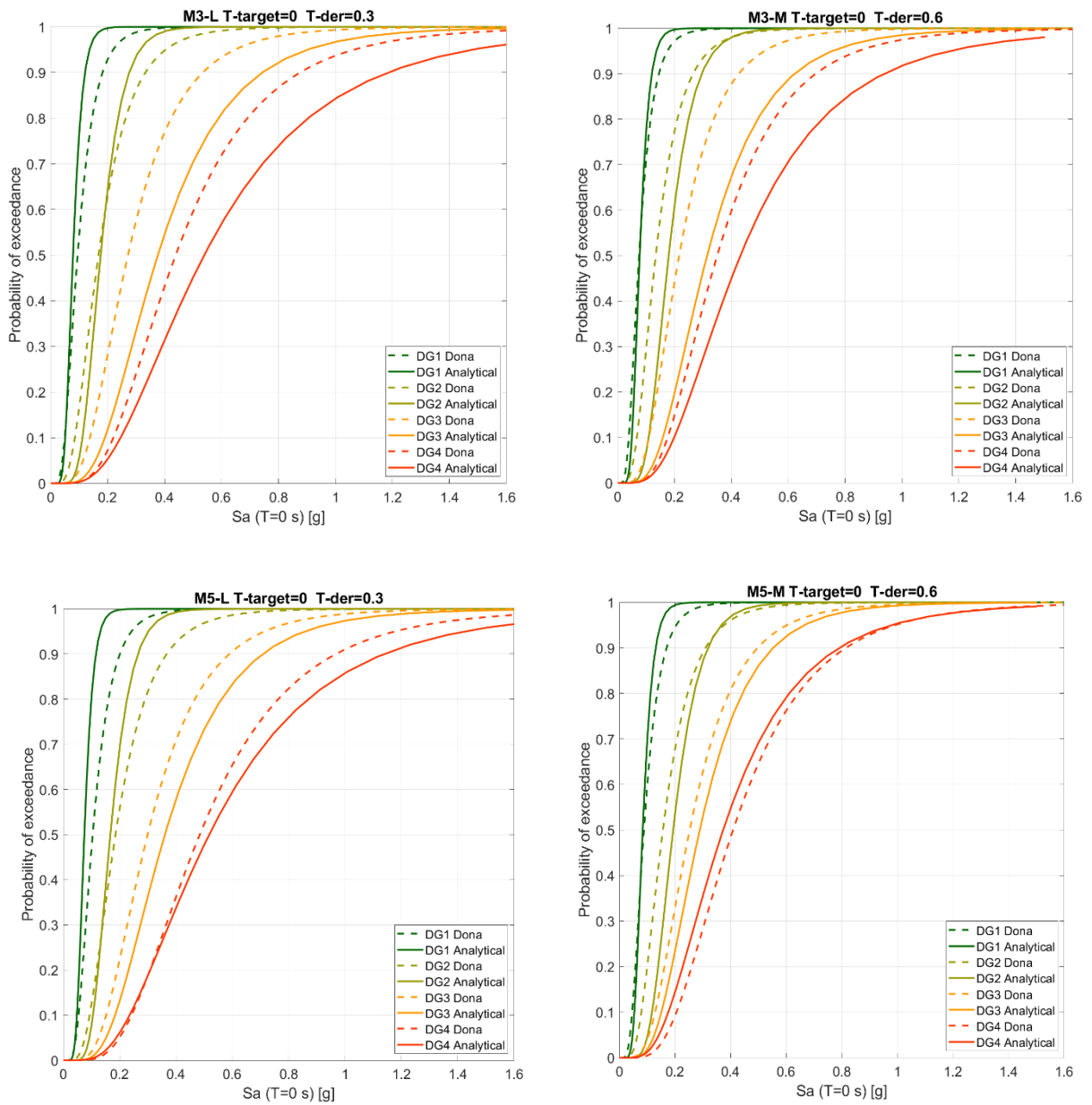
5.4.4   Fragility curves and comparison

To minimise the computational effort in risk calculations and to be compatible with other subprojects, specially site amplification (subproject E), all fragility curves are produced as a function of spectral ordinates at periods of 0.3 s and 0.6 s. In Table 5.4, the fundamental periods from numerical models and selected Intensity Measure Type (IMT) are summarised. To be compatible with previous versions of the site amplification models, a set of fragility curves as a function of spectral ordinates at 0.2 s and 0.4 s is also available.

Here, we mainly focus on comparing the obtained results with other independent investigations. We make use of the response spectra, used in deriving the fragility function, when the IMT considered in the independent study is not identical to our suggestion. For instance, in order to compare the derived fragility curves for the M3, M4 and M5 types with those of an independent study such as Donà et al. (2020), the conversion from Sa(0.3) or Sa(0.6) to Sa(0) is carried out. As shown in Figure 5.9, a good consistency is observed, especially for DG1 and DG2 where the mean values and shape of the curves are close.

Table 5.4. Fundamental period from numerical models and selected IMT.

| Building type	Fundamental period [sec]	IMT
M3_L	0.28	Sa (0.3)
M4_L	0.27	Sa (0.3)
M5_L	0.27	Sa (0.3)
M3_M	0.55	Sa (0.6)
M4_M	0.44	Sa (0.3)
M5_M	0.54	Sa (0.6)
M6_L	0.12	Sa (0.3)
M6_M	0.20	Sa (0.3)
M6_H	0.37	Sa (0.3)
RCW_L	0.12	Sa (0.3)
RCW_M	0.36	Sa (0.3)
RCW_H	0.53	Sa (0.6)

Figure 5.9. The obtained fragility curves for M3 and M5 compared with those from Donà et al. (2020).

Figure 5.10 shows a comparison between fragility curves for M6 buildings and the corresponding ones from Lagomarsino et al. (2021). Considering ERM-CH23 fragility curves for M6 low-rise buildings, we expect less severe damage from small events that cause peak ground acceleration of 0~0.6 g. However, both fragility curve sets for different height classes are generally comparable although different methodologies were used. A comparison between fragility curves for RCW and the corresponding ones from GEM is also shown in Figure 5.11. In comparison to the curves from the GEM model, ERM-CH23 fragility curves result in more vulnerability, especially for DG1 and DG2. This difference primarily results from different displacement thresholds for damage grades. For instance, the displacement threshold for DG2 in our model is equal to 1.5 times the yielding displacement, while DG2 in the GEM model is defined as a function of both yielding and ultimate displacements of capacity curves.
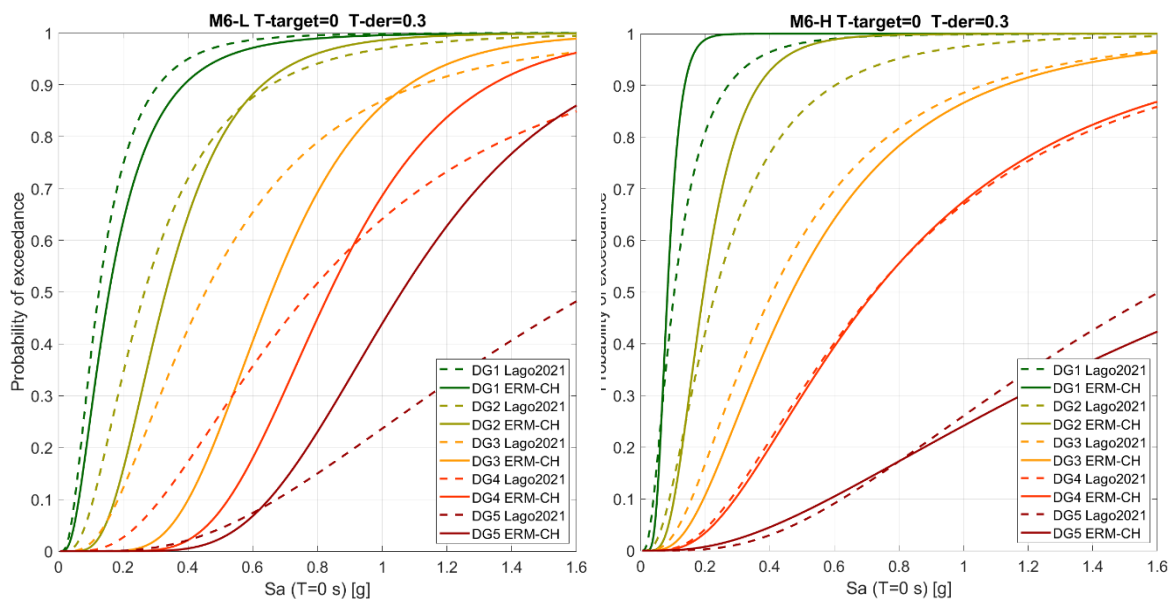
Figure 5.10. Fragility curves for M6 buildings and the corresponding ones from Lagomarsino et al. (2021).
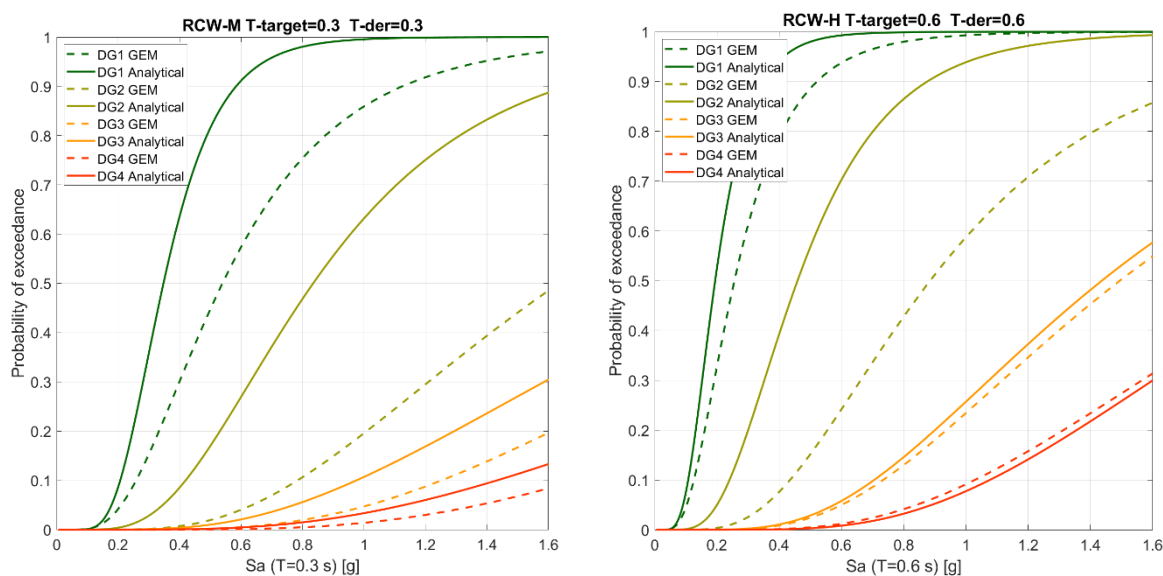
Figure 5.11. Fragility curves for RCW buildings and the corresponding ones from GEM (Silva et al., 2018).

More than 95% of buildings registered in the exposure model are covered by the developed fragility curves. For the rest of the building types, we consider fragility curves from the most up-to-date European-scale practice (i.e. investigation in the framework of the European Seismic Risk Model, ERSM20) or from existing studies (see Table 5.5).

Table 5.5. Suggested fragility curves from literature for building types with low contribution in the exposure model.

Building type	# of buildings¥	Suggested fragility curve	
		ERSM20 building type	**IMT ɣ**
RCmix_L	18184	CR_LDUAL-DUL_H2	Sa (0.3)
RCmix_M	1750	CR_LDUAL-DUL_H4	Sa (0.6)
RCmix_H	650	CR_LDUAL-DUL_H7	Sa (0.6)
S	3316	S_LFINF-DUM_H4	Sa (0.3)
T	11619	W_LFM-DUL_H2	Sa (0.3)
M1_L	8756	MUR-ADO_LWAL-DNO_H2	Sa (0.6)
		ERM-CH23 building type	**IMT**
M1_M	538	M1_L	Sa (0.6)
M3_H	4175	M3_M	Sa (0.6)
M4_H	677	M4_M	Sa (0.3)
M5_H	174	M5_M	Sa (0.6)
		Reference	**IMT**
Ind	-	T6 and T9 (Babič and Dolšek, 2016)	Sa (0.3)

¥ Number of buildings is from the rate-based model (i.e., application of mapping scheme) for the whole country.

ɣ IMTs are identical to the ones selected in the final release of ESRM20.

5.5   Exposure analyses

5.5.1   Rate-based (RB) model

As summarised in Table 5.6, buildings in different cities are analysed through visual surveys, and a building type of the project taxonomy is assigned to each individual building by taking into consideration certain characteristics (e.g. the façade features, the presence of balconies). These ground truth datasets are then subdivided into subsets using two fields of the Swiss building database (Chapter 4): 'period of construction' and 'height classes'. The distribution of building types is a mapping scheme we use for the structural building types in other cities. Having mapping schemes for different cities helps us to cover geographical differences in building type distribution over the entire country. The mapping scheme for the city of Basel is used to detect the structural type of buildings in the big cities, i.e. any city with a population greater than 40,000, such as Zurich, Geneva, Bern, Lausanne and Lucerne. The mapping scheme of Sion, Martigny, Neuchâtel, Yverdon-les-Bains and Solothurn is applied to the city for which it was developed. The average of the mapping schemes for Sion, Neuchâtel, Yverdon-les-Bains and Solothurn is applied to the rest of the country.

Table 5.6. Number of surveyed buildings in different cities

City	# of buildings surveyed
Basel	2706
Neuchâtel	3533
Yverdon	2808

Solothurn	3283
Sion	2504
Visp	307

5.5.2   Random Forest (RF) model

We developed several deep-learning models for building type detection based on all building features, available from the database of subproject F. The Random Forest (RF) method, a supervised learning algorithm, is implemented and the surveys' outcome is used as ground-truth data for training and validation. Two models, which are separately trained and tested on the building datasets of Neuchâtel and Yverdon-les-Bains, are first developed and their performance is then evaluated by using three accuracy measures. The accuracy measure corresponding to building type distribution varies between 81% and 90%. Moreover, another RF model is trained based on the concatenated datasets of Neuchâtel and Yverdon-les-Bains and applied to three other Swiss cities (Basel, Solothurn and Visp) in order to evaluate the performance of the model when applied to other cities. The accuracy of the application of the model to the different cities is comparable for the two models, which are separately trained and tested on the building datasets of Neuchâtel and Yverdon-les-Bains. The decent accuracy of the methodology, even in relation to cities not used in the training phase, showed the robustness of the RF models, paving the way for its application to the whole country. Hence, it is proposed to implement the second branch of the exposure model based on a prediction of building types from the RF model. The RF model is assigned a weight of 0.75 in the logic tree, compared with 0.25 for the RB method.

5.5.3   Industrial buildings

Subproject F's database is in essence a database of residential and commercial buildings. However, some of the buildings are labelled as having an industrial function as they are part of industrial zones. Regarding these buildings:

- 50% are expected to be administrative buildings. The building types already assigned to them based on RF or RB models are kept.

- 50% are actual industrial buildings, where production processes are carried out, and fragility curves corresponding to industrial buildings (i.e., building type = Ind, see Table 5.5) are used in damage/risk calculations.

5.6   Treatment of uncertainty

The uncertainties of exposure and fragility models are two major factors that should ideally be considered in nationwide seismic risk assessment. Regarding exposure modelling, we considered two different methodologies for attributing structural building types; the RB and RF models cover the epistemic uncertainty in exposure modelling. Random assignment of structural building typology based on the mapping schemes will cover aleatory uncertainty. To include possible regional differences in building type distribution, a combination of mapping schemes for Sion, Neuchâtel, Solothurn and Yverdon-les-Bains is suggested in risk calculations. Regarding the intensity-based fragility model, uncertainties are evaluated from observed damage in past earthquakes; three different values for the vulnerability index of each building type have been proposed. Considering the Sa-based fragility model, building-to-building variability is captured by considering subclasses (i.e. [A1, D2] and [C1935, C1970, C1990]). Uncertainties about material properties, which play a major role in masonry buildings, are investigated using several numerical models of prototype buildings (see Section 5.4.1 for more details). Uncertainty of strong ground motions is also taken into account by sampling from the selected GMPE.

5.7   Validation

Two products of subproject G are (a) models for building typology association and (b) fragility models. These are validated based on the available independent studies. For the former, the outcomes of two models (i.e. the RB and RF models) are generally consistent (see 2021 annual report of subproject C) although different methodologies are implemented and data from surveys are input/used in a different way. As mentioned in Section 5.5.2, the performance of the RF model is also validated by testing on the cities from which the training dataset is collected, or even on other cities with different sizes (e.g. Basel, Solothurn and Visp). For the latter, derived Sa-based fragility curves are in agreement with other independent studies (see Section 5.4.4), indicating the robustness of the fragility model. Sa-based fragility curves are converted using the relationship specified by Gomez Capera et al. (2015) and compared with the I-based ones. The results of mechanical models are shown to be within the uncertainty range of observed damage (see Figure 5.12).
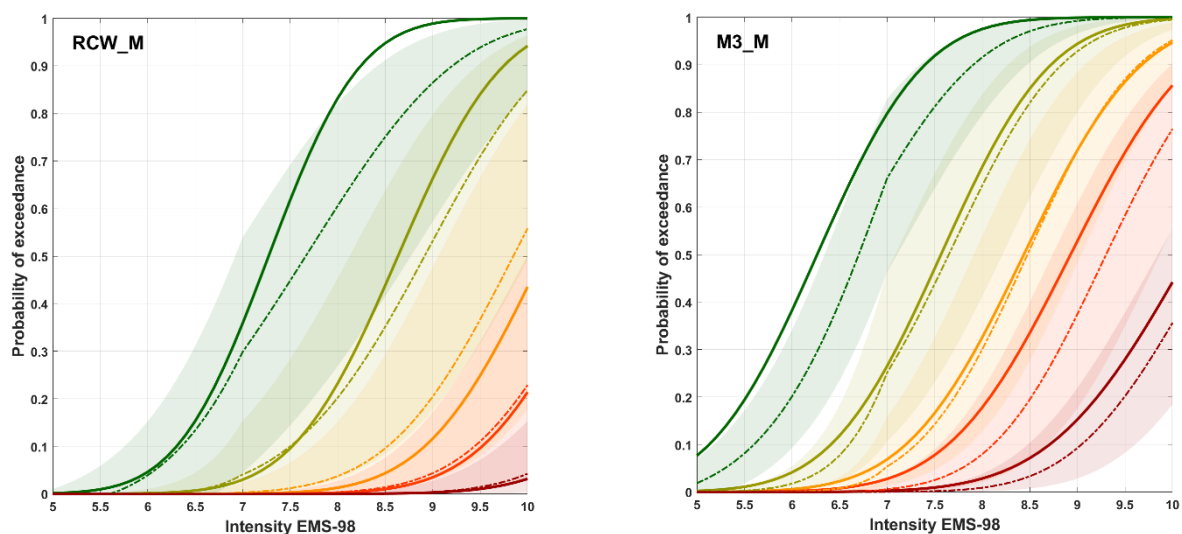
Figure 5.12. I-based fragility curves (dashed lines) and their uncertainties (shadows), in comparison to converted Sa-based fragility curves (solid lines). Green to dark red colours are used for damage grades of 1 to 5.

References

Ahmad, N., Ali, Q. (2017). Displacement-based seismic assessment of masonry buildings for global and local failure mechanisms. Cogent Engineering **4**(1). https://doi.org/10.1080/23311916.2017.1414576

Babič, A., Dolšek, M. (2016). Seismic fragility functions of industrial precast building classes. Engineering Structures **118**, 357–370. https://doi.org/10.1016/J.ENGSTRUCT.2016.03.069

Bal, I. E., Bommer, J. J., Stafford, P. J., Crowley, H., Pinho, R. (2010). The influence of geographical resolution of urban exposure data in an earthquake loss model for Istanbul. Earthquake Spectra **26**(3), 619–634. https://doi.org/10.1193/1.3459127

Bernardini, A., Lagomarsino, S., Mannella, A., Martinelli, A., Milano, L., Parodi, S., Troffaes, M. (2010). Forecasting seismic damage scenarios of residential buildings from rough inventories: a case study in the Abruzzo Region (Italy). Proceedings of the Institution of Mechanical Engineers **4**(4), 279–296. https://doi.org/10.1243/1748006XJRR305

Donà, M., Carpanese, P., Follador, V., Sbrogiò, L., da Porto, F. (2020). Mechanics-based fragility curves for Italian residential URM buildings. Bulletin of Earthquake Engineering, 0(0123456789). https://doi.org/10.1007/s10518-020-00928-7

Gomez Capera, A., Locati, M., Fiorini, E., Bazurro, P., Luzi, L., Massa, M., Puglia, R., Santulin, M. (2015). Macroseismic and ground motion: site specific conversion rules. In DPC-INGV-S2, Project 2015,.

Jimenez-Pacheco, J., Gonzalalez-Drigo, R., Pujades-Beneit, L. G., Barbat, A. H., Calderon-Brito, J., Jiménez-Pacheco, J., González-Drigo, R., Pujades Beneit, L. G., Barbat, A. H., Calderón-Brito, J. (2020). Traditional High-rise Unre-

inforced Masonry Buildings: Modeling and Influence of Floor System Stiffening on Their Overall Seismic Response. International Journal of Architectural Heritage **15**(10), 1–38. https://doi.org/10.1080/15583058.2019.1709582

Lagomarsino, S., Cattari, S. (2014). Fragility functions of masonry buildings. In: Pitilakis K, Crowley H, Kaynia AM (eds) SYNER-G: typology definition and fragility functions for physical elements at seismic risk: elements at seismic risk, geotechnical, geological and earthquake engineering. (Chapter 5), pp 111–156.

Lagomarsino, S., Cattari, S., Ottonelli, D. (2021). The heuristic vulnerability model: fragility curves for masonry buildings. In Bulletin of Earthquake Engineering **19**(8). Springer Netherlands. https://doi.org/10.1007/s10518-021-01063-7

Lagomarsino, S., Giovinazzi, S. (2006). Macroseismic and mechanical models for the vulnerability and damage assessment of current buildings. Bulletin of Earthquake Engineering **4**(4), 415–443. https://doi.org/10.1007/s10518-006-9024-z

Lin, Y.-Y., Miranda, E. (2008). Noniterative Equivalent Linear Method for Evaluation of Existing Structures. Journal of Structural Engineering **134**(11), 1685–1695. https://doi.org/10.1061/(asce)0733-9445(2008)134:11(1685)

Martakis, P., Reuland, Y., Chatzi, E. (2021). Amplitude-dependent model updating of masonry buildings undergoing demolition.

Milosevic, J., Cattari, S., Bento, R. (2020). Definition of Fragility Curves through Nonlinear Static Analyses: Procedure and Application to a Mixed Masonry-RC Building Stock. Vol. 18. Springer Netherlands.

Petry, S., Beyer, K. (2014). Influence of Boundary Conditions and Size Effect on the Drift Capacity of URM Walls. Engineering Structures **65**, 76–88.

Sarhosis, V., Garrity, S. W., Sheng, Y. (2015). Influence of Brick-Mortar Interface on the Mechanical Behaviour of Low Bond Strength Masonry Brickwork Lintels. Engineering Structures **88**, 1–11.

Savoy, R. (2019). Seismic Vulnerability Assessment at Large Scale - City of Basel. The École polytechnique fédérale de Lausanne (EPFL).

Silva, V., Amo-Oduro, D., Calderon, A., Dabbeek, J., Despotaki, V., Martins, L., Rao, A., Simionato, M., Vigano, D., Yepes, C., Acevedo, A., Crowley, H., Horspool, N., Jaiswal, K., Journeay, M., Pittore, M. (2018). Global Earthquake Model (GEM) Risk Map. https://doi.org/10.13117/GEM-GLOBAL-SEISMIC-RISK-MAP-2018

Thiriot, J. (2019). Seismic vulnerability assessment at large scale. ENAC, EPFL.

Vanin, F., Zaganelli, D., Penna, P., Beyer, K. (2017). Estimates for the Stiffness, Strength and Drift Capacity of Stone Masonry Walls Based on 123 Quasi-Static Cyclic Tests Reported in the Literature. Bulletin of Earthquake Engineering **15**(12), 5435–5479. doi:10.1007/s10518-017-0188-5.

6.   Consequence model

6.1   Introduction

Overview

This report describes the features of the consequence model of the ERM-CH23 risk model, developed as part of SPD. The model provides estimates of three separate categories of loss as per the EMS-98 damage scale:

- **direct economic loss** due to cost of repairing damaged structural and non-structural components, as well as contents;

- **downtime** caused by damage;

- **human loss** (casualties) – injuries, fatalities and displacement as a result of damage

Figure 6.1 provides a snapshot of inputs and outputs of the consequence model. Features shown here will be elaborated in the following.
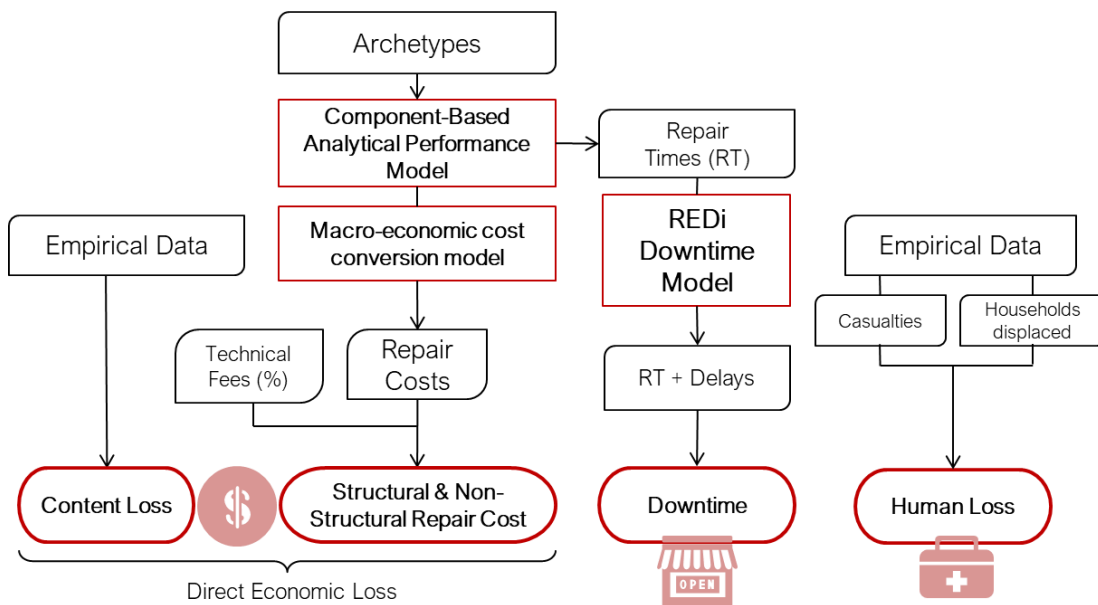
Figure 6.1. I/O of the consequence functions

The establishment of the **direct economic loss** consequence functions borrows the loss estimation methodology of the FEMA P-58 project: given distributions of demand (e.g. peak storey drifts or floor accelerations), simulate damage, then consequences, using individual component fragility and consequence functions in terms of repair costs and times. **Content** loss functions have been set out separately using HAZUS (FEMA, 2010) estimates.

Downtime was defined as the time elapsing from the moment of the asset being damaged to its re-occupancy. Following the REDi downtime estimation framework (Almufti and Willford, 2013), the final estimates are computed as functions of repair time and delays associated with post-earthquake inspection, engineering mobilisation, contractor mobilisation, financing and permitting.

Human loss comprised casualties (injuries and deaths) and households displaced. The former estimates were based on the HAZUS manual (FEMA, 2010), the Italian National Civil Protection Department (NCPD, 2018) and Spence (2007), whereas the latter were adopted from the empirical data harmonised by the NCPD (2018). Furthermore, the model assumed that households might be displaced in either the *short* or *long term* (mutually exclusive and collectively exhaustive states of displacement). While the former indicates the expected percentage of households forced to

move out of their houses for a duration shorter than a year, the latter points to the percentage of people who will be either temporarily (for longer than a year) or permanently displaced.

Taxonomy representation

Listed in Table 6.1 are archetype models used to develop repair cost and repair time functions, which are components of direct economic loss and downtime functions respectively:

- M3 low-rise
- M3 mid/high-rise
- M5 low-rise
- M5 mid/high-rise
- M6 low-rise
- M6 mid/high-rise
- RCW mid/high-rise
- Steel mid-rise commercial office

Note that the low-rise versions of M3, M5 and M6 are simply one-storey versions of the original designs of their mid/high-rise counterparts with small modifications to component quantities such as slab/floor systems (low-rise buildings do not employ these) and number of chimneys per unit footprint area. Key characteristic features including the number of storeys, total gross floor areas of the buildings, assumed replacement (reconstruction) values in CHF and references for Engineering Demand Parameters (EDPs) associated with EMS-98 damage scale are presented in Table 6.2.

Table 6.1. Model coverage in terms of direct representation of construction classes through dedicated archetype models and analysis

Construction class	Class ID	Full ID (class + rise)	FLM2
Rubble stone	M1	M1-L	
		M1-M	✓
Adobe	M2	M2-L	✓
Simple stone	M3	M3-L	✓✓
		M3-M	✓✓
		M3-H	✓
Massive stone	M4	M4-L	✓
		M4-M	✓
		M4-H	✓
Unreinforced masonry (Old bricks)	M5	M5-L	✓✓
		M5-M	✓✓
		M5-H	✓
Unreinforced masonry (Concrete blocks / RC floors)	M6	M6-L	✓✓
		M6-M	✓✓
		M6-H	✓
RC Frame	RCF	RCF-L	✓
		RCF-M	✓
		RCF-H	✓
Shear walls	RCW	RCW-L	
		RCW-M	✓✓
		RCW-H	✓
Mixed shear walls and frame	RCM	RCM-L	✓
		RCM-M	✓
		RCM-H	✓
Steel	S	S	✓✓
Timber	T	T	✓

✓: Implicit representation extrapolating function developed for an archetype belonging to another class.

✓✓: Explicit representation through archetype belonging to class

Table 6.2 sets out characteristic features of building archetypes used to develop direct economic loss (repair cost) and repair time consequence functions. Functions for other loss categories, as indicated in Figure 6.1, did not make use of these archetypes and their models.

Table 6.2. Key features of the modeled archetypes

Archetype ID	Number of storeys	Total gross floor area (m²)	Assumed reconstruction costs per m² (CHF)°	EDP thresholds associated with EMS-98 damage levels
M3-L	1	178	3,000	(Michel et al. 2018)
M3-M	4	858	2,500	(Michel et al. 2018)
M5-L	1	312	3,000	(Calvi 1999) [$]
M5-M	5	1,248	2,500	(Calvi 1999) [$]
M6-L	1	407	3,000	(Michel et al. 2018)[*]
M6-M	5	2,035	2,500	(Michel et al. 2018)[*]
RCW	6	2,800	2,559	HAZUS (FEMA 2010)
S-COM	5	3,568	3,550	HAZUS

[*] Calvi did not provide threshold values for all four damage states. As such, the median function parameter for heavy damage was deduced from other relevant studies (including but not limited to Magenes and Calvi, 1997; Mouyiannou et al., 2014).
[$] Adopted HAZUS recommended values for peak floor accelerations (PFAs) for low-code masonry construction class,
[°] Reconstruction costs are only used to compute loss ratios and not to inform the broader model on what this number should be when determining asset reconstruction costs
EDP: Engineering Demand Parameter

6.2   The consequence model parts

6.2.1   Direct economic loss

Direct economic loss is expressed in terms of the ratio between the actual repair cost of restoring a building to its original state and its total replacement cost. We will hereafter call this ratio the Repair Cost Ratio (RCR). Distributions of RCR are modelled employing the component-based approach of FEMA P-58 (Mahoney et al., 2018). The methodology estimates the associated repair cost of a damaged building as a function of the make-up of its component types and quantities. Components are categorised into *Component Groups* (CGs) – alternatively referred to as *Fragility Groups* in the text. A CG is composed of:

▪ a fragility function to estimate the likelihoods of different prescribed levels of damage as a function of an engineering demand parameter such as peak storey drift;

▪ a consequence function to estimate the cost of repair as a function of damage.

Collectively, CGs make up the so-called *performance model*, and the performance model is combined with a component inventory consisting of component counts to estimate the cost of repairing a building. Several additions and modifications have been made herein to the existing component fragility and consequence function database of P-58 to establish the present *performance model* as input for establishing the final ERM-CH23 direct economic loss consequence functions. We gathered, created and collated an extensive list of fragility and consequence functions for damageable structural and non-structural components.

Direct economic losses can finally be estimated for given prescriptive damage states as per the EMS-98 scale by introducing associated structural demand thresholds, which are listed in Table 6.2 for all archetypes subject to analysis.

6.2.1.1 Component groups (CG) and their fragility functions

Fragility functions express probabilities of damage given increasing levels of a select engineering demand. As alluded to earlier, while the fragility functions for a large portion of the present performance model established here leveraged many of the existing component groups in P-58, several other CGs that were missing – the Swiss buildings in question had components for which no CG was available in P-58 – were collated using other sources. Table 6.3 shows a short list of such CGs introduced to the performance model.

Table 6.3. List of select important component groups added to the performance model in this work

| Component group (CG)	Country of source	Reference	Remark(s)
Unrestrained floor/slabs in masonry buildings	Italy	Rossi et al. (2021)	▪ Fragility function parameters are set to those of the masonry walls – e.g., unseating is assumed to occur at the same (average) level of demand as brick wall collapsing
External infill walls with/without windows, infills with/without doors	Italy	Cardone and Perrone (2015), Cardone (2016)	▪ Adopted the fragility function parameters ▪ Repair costs have been adapted to the Swiss context.
Brick masonry piers; Brick spandrels - wooden lintel; Brick spandrels arch lintel	Italy	Ottonelli et al. (2020)	▪ Adopted the fragility function parameters ▪ Cost functions are adapted to Switzerland
Generic floor finish Ceramic floor finish	USA	P58, FIXR[*] database	▪ Repair cost consequences cross-checked with Italian construction works data (Comune di Milano and Regione Lombardia 2021) as well Swiss ones in CRB[6], reflecting as-new costs data, to the extent possible. ▪ Cost functions then adapted to Switzerland using the macro-economic cost conversion model. ▪ Damageability constituted by the damage fragility functions and their parameters set to follow brick wall crushing and collapse functions.
Concrete blocks masonry	Italy	Mixed	▪ Fragility function parameters established by synthesising data reported in Avila et al (2012), Mouyiannu et al (2014), and Magenes and Calvi (1997). ▪ Given nearly identical definitions of damage states and the associated repair operations, and comparable cost of material and labour, adopted the repair costs reported in Ottonelli et al. (2020) for brick masonry walls.

* USA repairs: https://www.fixr.com/costs/repair-floor

6.2.1.2 Component consequence functions

While the damageability of a building is not sensitive to economic conditions that characterise the region where it is located, the cost of repairing is – and it needs to be defined accordingly in relation to the construction market. As such, cost functions of an FG that is defined in the *performance model* have been, when necessary, adjusted using a macro-economic model in view of the

---

[6] Swiss works datasets. https://www.crb.ch/

construction dynamics between the reference country (from which cost functions were available) and Switzerland. The process is illustrated in Figure 6.2.
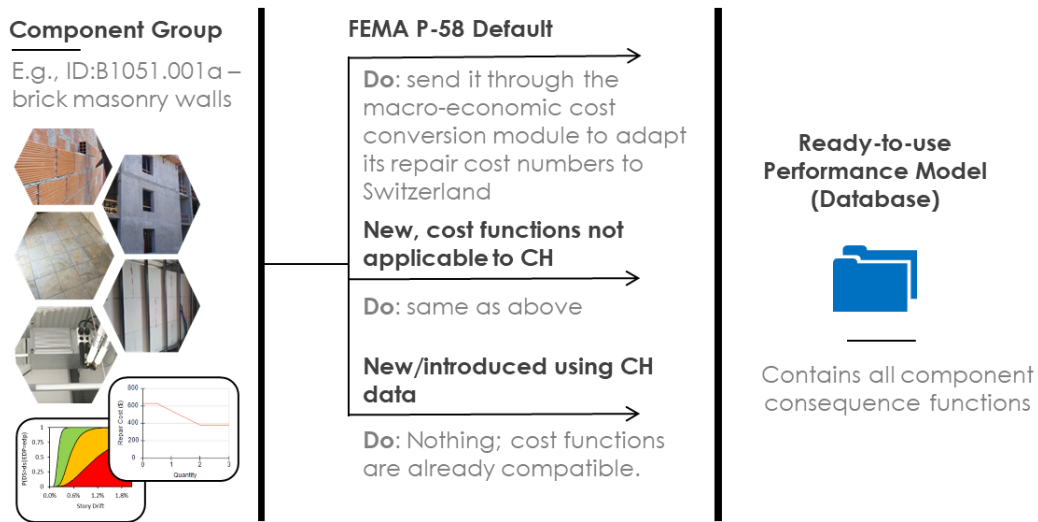
Figure 6.2. Collating relevant component groups into the performance model.

A repair cost multiple, r, which is the number that the reference repair cost needs to be multiplied by, is calculated by the macro-economic repair cost conversion formula shown in Equation (6.1)

$$r = \left(r_{labour} \cdot f_{labour} \,/\, r_{productivity}\right) + \left(r_{material} \cdot f_{material}\right) + \left(r_{m\&p} \cdot f_{m\&p}\right) \tag{6.1}$$

Here, f_{labour}, $f_{material}$ and $f_{m\&p}$ represent the proportion of the total repair cost associated with labour, materials, and margins and preliminaries, respectively, in the reference country (from which the cost is being adapted). r_{labour}, $r_{material}$ and $r_{m\&p}$ denote estimated ratios of the costs of labour, material, and margins and preliminaries between Switzerland (numerator) and the reference country (denominator). These parameters were determined following an extensive survey of both national and international sources including, but not limited to, the statistics bureaus of Italy, Switzerland and the United States; Turner and Townsend (2019); ARCADIS (2019); and Raetz et al. (2020).

The initial estimate that needs to be put in place is the ratio of the cost incurred from one of these three components to the total repair cost (i.e. either f_{labour}, $f_{material}$ or $f_{m\&p}$). Construction market surveys suggest a range of 20-40% depending on the nature of the work, and of course country of reference. Considering the labour-intensive nature of most repairs – as opposed to as-new construction work – and the market dynamics in the evaluated reference countries of the US and Italy, f_{labour}=0.425 and 0.35 respectively were deemed appropriate. The remaining f parameters are worked out using available comparative data in the above-mentioned references: $f_{m\&p}$ already known, f_{mat} is derived (1-$f_{m\&p}$-f_{lab}) and the r parameters computed in accordance with data using Turner and Downsend (2019) and Italian costs data (Comune di Milano and Regione Lombardia, 2021). Table 6.4 lists the used cost conversion function input parameters.

Table 6.4. Repair cost conversion model parameters

	r_{lab}	r_{mat}	$r_{m\&p}$	f_{lab}	f_{mat}	$f_{m\&p}$	RCR
USA-to-CH	0.81	1.65	1.06	0.425	0.40	0.175	1.40
ITA-to-CH	2.06	2.20	1.52	0.35	0.545	0.105	2.73

$r_{productivity}$ in Equation (6.1) denotes the difference in labour productivity between countries, and it can be simply expressed as

$$r_{productivity} = {c_{productivity,target}}\big/{c_{productivity,reference}} \qquad (6.2)$$

where $c_{productivity}$ represents labour productivity in a given country. This coefficient is calculated as a function of Gross Value Added (GVA) to the construction sector divided by the number of persons employed in the construction sector multiplied by the hourly associated worker compensation. Simply put, it represents value added per dollar spent on labour. These inputs were collected from the public databases of EUROSTAT[7], the OECD[8] and the Federal Statistical Office of Switzerland. Thus, we compute $c_{productivity}$ as

$$\boldsymbol{c_{productivity}} = \frac{GVA}{\# \ of \ persons \ employed \ \times \ average \ workers'compensation} \qquad (6.2)$$

Accordingly, $r_{productivity}$ is computed as 0.52 when converting costs from Italy to Switzerland, and 0.66 from the United States to Switzerland.

Next, the P-58 component fragility functions adapted for the purposes of this work needed to be adjusted for inflation because they were representative of prices in 2012. As such, the 2012-2019 construction price inflation (in US$ terms) in West Coast California was determined as the average of DGS-CA-GOV(1.19)[9], Ed Zarenski[10] (1.40/1.34) and Turner Construction[11] (1.36), equalling 1.32.

Finally, the P-58 methodology does not account for technical/professional fees that arise on top of the operational costs of repairs. Previous research has shown that they can constitute up to 14% of the operational expenses (Di Ludovico et al., 2017a, b). As such, the percentage cost of technical fees added on top of our estimated repair costs was determined as 5% for DS1 and DS2, and 13% for the rest, in recognition of relevant national data on such fees reported in ETH Zurich (2015).

6.2.1.3   Component inventory

Quantities of structural elements such as load-bearing masonry walls, spandrels and slabs were established using archetype blueprints. The P-58 *quantity estimator tool* is used to determine the non-structural component quantities with uncertainty.

6.2.1.4   The functions

Direct economic loss functions were in the form of both lognormal function parameters and equivalent discrete probability mass functions. Figure 6.3 shows median plus/minus two standard deviations of analysis loss realisations for all archetypes previously listed in Table 6.2. We observe the following:

- The masonry archetypes M3, M5 and M6 exhibit comparable loss ratios across the first two damage states: slight and moderate.

- While the loss ratios of the low-rise counterparts tend to be higher for the first three damage levels, this trend reverses for the very heavy damage level. This dynamic is in large part attributed to the (high) proportion of the chimney repair costs at lower damage levels in relation to the total reconstruction costs for low-rise archetypes, and floor/slab system repairs for mid-rise ones.

---

[7] https://ec.europa.eu/eurostat/web/products-datasets/. Note that you need to search for the metric you are interested in.
[8] https://stats.oecd.org/Index.aspx?DataSetCode=ALFS_EMP
[9]https://www.dgs.ca.gov/RESD/Resources/Page-Content/Real-Estate-Services-Division-Resources-List-Folder/DGS-California-Construction-Cost-Index-CCCI
[10] US Construction market expert. https://edzarenski.com/2016/10/24/construction-inflation-index-tables-e08-19/
[11] https://www.turnerconstruction.com/cost-index

- The RCW archetype, at slight to moderate states, tended to exhibit lower loss ratios compared to other archetypes except S-COM, mainly because of the lack of widespread damage across shear walls – damage occurs only on the first two storeys. At substantial and very heavy damage states, however, it fared similarly to others because of the counteracting factor of the higher costs involved in repairing RC elements and joints. Figure 6.4 provides an interesting benchmark using earthquake damage data from Italy for RC versus masonry buildings, where comparable damage (in prescriptive terms) translates into higher loss ratios for RC.

- While faring comparably to other archetypes at substantial damage and beyond, the steel commercial archetype (S-COM) exhibited significantly smaller repair cost ratios at slight and moderate damage levels because of the composition of its damageable components. The façade made of curtain walls (i.e. glazing), which replace exterior masonry infills, mostly does not get damaged at drift demands linked to slight and moderate damage levels. Although the internal partition walls made of drywalls (gypsum partitions) do experience damage, they are significantly cheaper and faster to repair compared to their masonry infill counterpart.
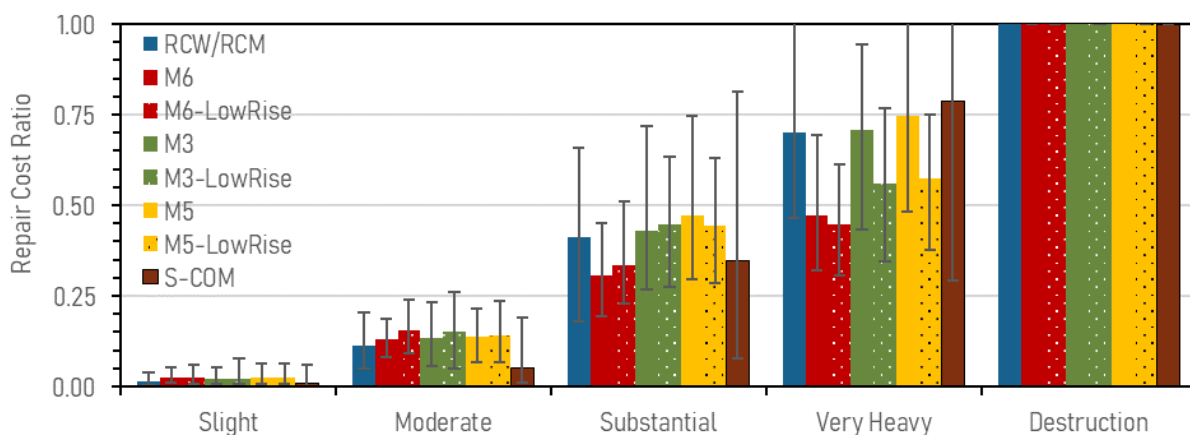
Figure 6.3. Direct economic loss estimates as ratios of repair cost to total reconstruction costs of the archetypes.

6.2.2   Downtime

Downtime is defined as the time required for a building damaged after an earthquake to achieve re-occupancy and regain the facility's primary function. Downtime is herein assumed to be constituted by the so-called *impedance factors* that delay repair operations from starting, and the repair times following the downtime assessment methodology of the REDi (Almufti and Willford, 2013). Delay parameters comprise utility disruption, inspection, engineering review, financing, contractor mobilisation, and permitting. A snapshot of the workflow is illustrated in Figure 6.5.

Some of these individual delay function parameters are sensitive to secondary attributes (see Table 8 of the REDi manual). In the absence of explicit knowledge of such attributes (e.g. we do not know which households would have access to insurance), final function parameter values were determined by weighing amongst mutually exclusive alternatives shown in Table 6.5, and the final model parameters in terms of the said impedance factors and utility disruption are listed in Table **6.6** and Table 6.7 respectively.
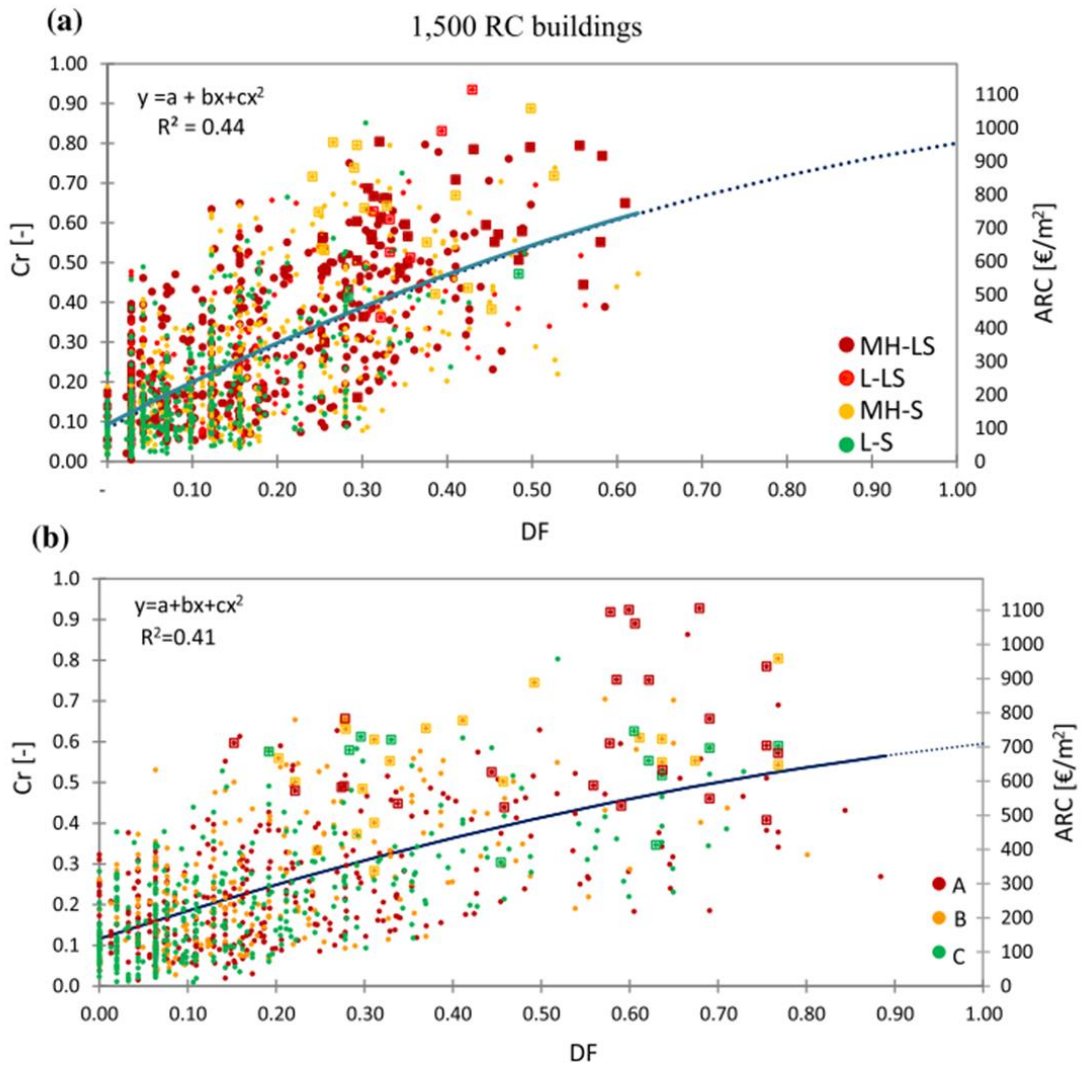
Figure 6.4. Damage Factor (DF) – Cost Ratio (Cr) relationship of (a) RC and (b) masonry buildings. Excerpt from De Martino et al. (2017).
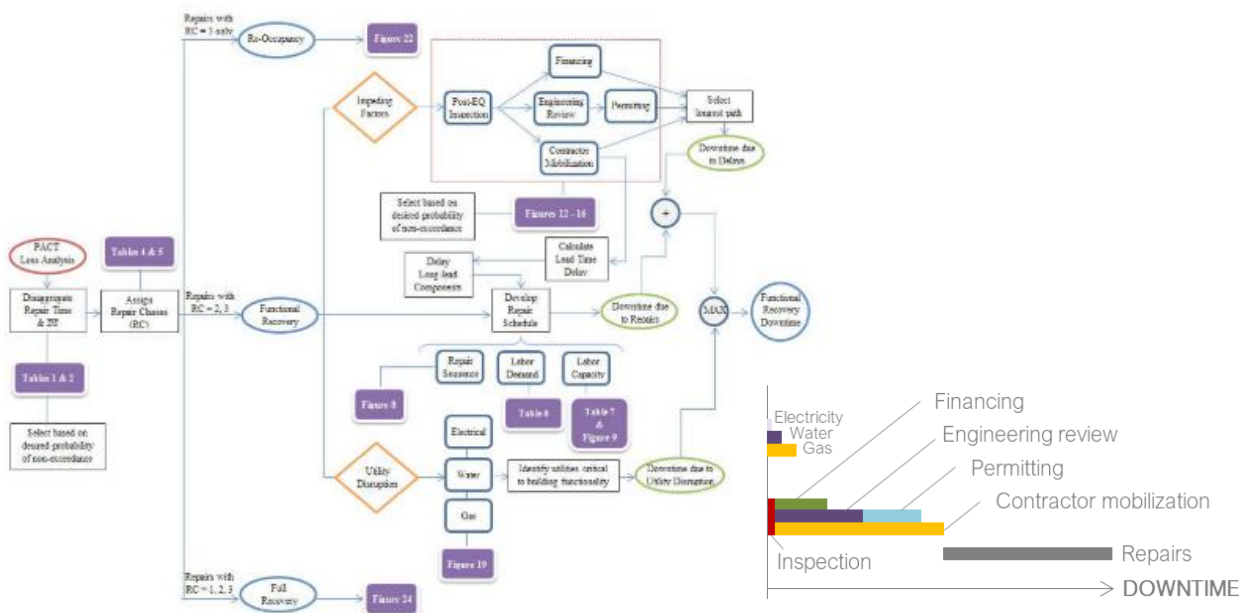

Figure 6.5. Left: flow chart for downtime computation (excerpt from REDi manual; Almufti and Willford, 2013); right: a Gantt-chart equivalent of the shown workflow.

Table 6.5. Determination of delay function parameters. Parameter values shown under 'Branches' are the REDi recommended values representative of the US context. The 'Final weighted parameters' column shows values adopted for use here.

Impeding factor	Mitigation measure	Branches		Weighted			Final weighted parameters$	
		Weight	Damage	θ	β		θ	β
Post-EQ inspection	-	1	-	5	0.54		**5**	**0.54**
Engineering mobilisation, review and re-design	Engineer on contract	0.05	DS=1	14	0.4		**14**	**0.4**
			DS=3	28	0.4		**41**	**0.4**
			DS>=4	206*	0.32		**81**	**0.4**
	-	0.95	DS=1	42	0.4		**243**	**0.32**
			DS=3	84	0.4			
			DS>=4	245*	0.32			
Financing	Pre-arr. credit lines	0.55		7	0.54		**7**	**0.70**
	Insurance	0.10		42	1.11		**67**	**0.70**
	Private Loans	0.30		105	0.68			
	SBA-backed loans	0.05		336	0.57			
Contractor mobilization	GC on contract	0.10	DS=1	21	0.66		**21**	**0.66**
			DS=3	49	0.35		**71**	**0.46**
	-	0.90	DS=1	77	0.43		**150**	**0.40**
			DS=3	161	0.41			
Permitting			DS=1	7	0.86		**7**	**0.86**
			DS=3	56	0.32		**56**	**0.32**

Geometric parameters of the lognormal function, θ: median; β: dispersion
* Adjusted as 70% of REDi-recommended values in view of current project's context
$ Full list and definition of model parameters are presented in Table 6.6

Table 6.6. Impedance factors: lognormal LN function parameters

Damage State	Post-EQ inspection		Engineering review		Contractor mobilisation		Financing		Permitting	
	θ	β	θ	β	θ	β	θ	β	θ	β
Slight	5	0.54	14	0.4	21	0.66	7	0.70	7	0.86
Moderate	5	0.54	41	0.4	71	0.46	67	0.70	7	0.86
Substantial	5	0.54	81	0.4	150	0.40	67	0.70	56	0.32
Very Heavy	5	0.54	162	0.32	150	0.40	67	0.70	56	0.32
Destruction	5	0.54	243	0.32	150	0.40	67	0.70	56	0.32

Geometric parameters of the lognormal distribution, θ: median; β: dispersion

Table 6.7. Utility disruption function parameters

Damage State	Water systems		Gas systems		Electricity systems	
	θ	β	θ	β	θ	β
Slight	4	0.56	10	1.0	3	1.12
Moderate	4	0.56	10	1.0	3	1.12
Substantial	21	1.15	42	0.6	3	1.12
Very Heavy	21	1.15	42	0.6	3	1.12
Destruction	21	1.15	42	0.6	3	1.12

Geometric parameters of the lognormal distribution, θ: median; β: dispersion

Repair times, which had been simulated as the direct output of the previously detailed P58 methodology, are also defined as lognormal variables and they are assumed to be independent of the delay parameters. Computed individually for each of the analysed archetypes, these functions are shown in Table 6.8. It should be noted that repair time estimates are sensitive to assumed repair sequence and the maximum number of workers per unit floor area. We assumed the former to be serial, and the latter to be one worker per 1,000 square foot (sf). Repairs are assumed to be carried out in series across floors as opposed to in parallel. The former is a higher-bound – and more conservative – idealisation of reality, which should fall somewhere between the two. The number of workers, on the other hand, can be appropriately assumed to be between one worker per 500 and 2,000 sf according to P-58. Our assumption, once again, errs on the conservative side in view of Switzerland's scarce history of earthquakes.

Table 6.8. Repair time function parameters

		Slight	Moderate	Substantial	Very Heavy	Destruction
[M6]	θ	12.1	51.1	115.7	171.2	360
	β	0.33	0.24	0.2	0.2	0.1
[M6L]	θ	3.68	13.9	28	37.42	200
	β	0.45	0.27	0.22	0.185	0.1
[M5]	θ	9.2	39.7	104.8	154.8	360
	β	0.45	0.26	0.25	0.2	0.1
[M5L]	θ	3.7	12.2	30.53	39.41	200
	β	0.5	0.26	0.2	0.165	0.12
[M3]	θ	11.6	44	110.7	176.3	360
	β	0.45	0.38	0.25	0.19	0.08
[M3L]	θ	3.28	14.4	28.92	34.27	200
	β	0.59	0.38	0.155	0.165	0.1
[RCW]	θ	9.66	56.8	179	239.4	480
	β	0.6	0.35	0.25	0.19	0.1
[St-COM]	θ	2.8	12.6	55	131	420
	β	0.95	0.8	0.67	0.5	0.1

The output of the downtime estimation methodology in the form of downtime realisations is demonstrated in Figure 6.6 for the M5-M subclass in moderate damage state. When we look at the same figures available for all archetypes, we see that downtime is governed in most cases by delays; these can account for as much as 90-95%, and as little as 35% of downtime. Lognormal downtime function parameters are provided in Table 6.9, and a comparison of median values can be found in Figure 6.7.
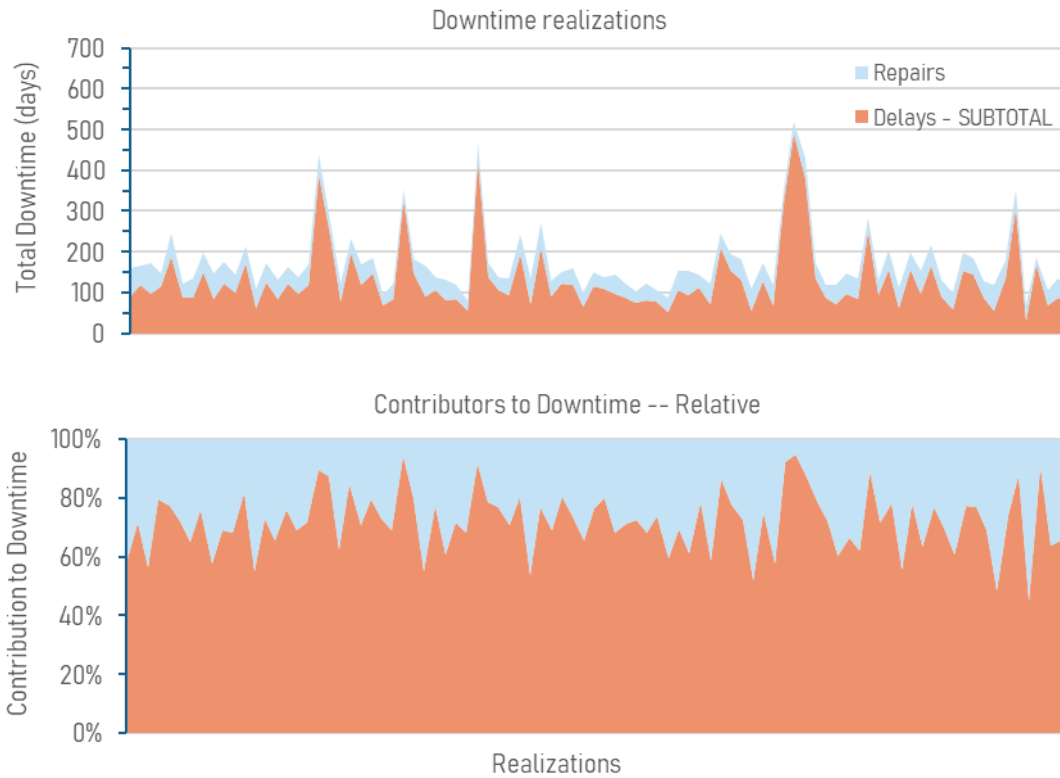
Figure 6.6. Downtime realisations for M5-M subclass in moderate damage state

Table 6.9. Lognormal downtime function parameters computed for the analysed archetypes

Damage State	[M6]		[M6L]		[M5]		[M5L]		[M3]		[M3L]		[RCW]		[St-COM]	
	θ	β	θ	β	θ	β	θ	β	θ	β	θ	β	θ	β	θ	β
Slight	49	0.26	40	0.31	47	0.27	40	0.31	50	0.26	40	0.31	50	0.28	41	0.32
Moderate	161	0.36	118	0.45	149	0.39	115	0.46	156	0.38	122	0.45	173	0.36	125	0.46
Substantial	315	0.19	222	0.26	307	0.20	225	0.26	314	0.2	224	0.26	384	0.18	267	0.27
Very Heavy	433	0.15	284	0.21	416	0.16	285	0.21	439	0.15	280	0.21	506	0.14	403	0.22
Destruction	689	0.12	526	0.14	689	0.12	525	0.15	687	0.11	526	0.14	813	0.11	752	0.11
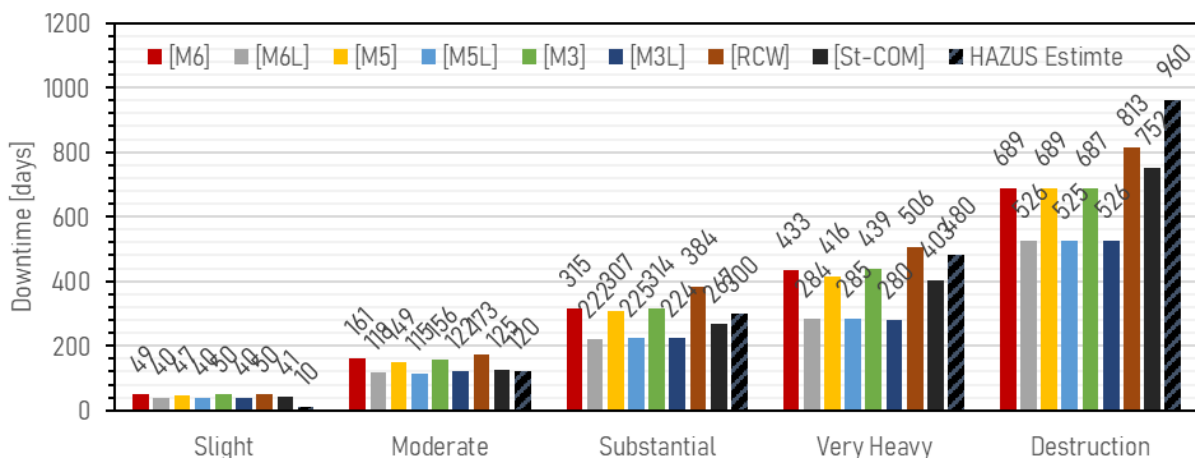
Figure 6.7. Median downtime estimates compared with HAZUS' downtime to re-occupancy

6.2.3   Human loss

Human loss comprises casualties (injuries and fatalities) and households displaced. The former estimates are based on the works of HAZUS (for DS3 only; FEMA 2010), the Italian National Civil Protection Department (NCPD 2018, for DS4 injury and fatality rates) and Spence (2007, for DS5, collapse) while the latter are adopted from the empirical data harmonised by the NCPD (2018). Expected injury and fatality rates adopted in the model are shown in Table 6.10.

Table 6.10. Injury and fatality rates for the human loss consequence functions

DS3-Injury	DS4-Injury	DS4-Fatality	DS5-Injury	DS5-Fatality
2.1-2.5%*	5%	1%	52-81%*	2-28%*

* Depends on rise and load resisting system. Masonry types and high-rise subclasses have larger % values. Percentages are those of inhabitants present at the time of event

The model assumes that households might be displaced in either the *short* or *long term* (mutually exclusive and collectively exhaustive states of displacement). While the former indicates the expected percentage of households forced to move out of their houses for a duration shorter than a year, the latter points to the percentage of people who will be either temporarily (for longer than a year) or permanently displaced. The current model does not estimate what percentage of the long-term displaced would fall into which category. Finally, these estimates do not replace, and should not be conflated with, the number of people looking for shelter after an earthquake, which is not provided herein.

It is worth noting that there are significant discrepancies between the estimates for the households displaced based on NCPD (2018) and those made by HAZUS. Specifically, besides providing different estimates based on the type of dwelling (i.e. single- or multi-family), HAZUS suggests households in a very heavily damaged (EMS-98, DS4) single-family dwelling would not be displaced; and 90% of inhabitants in a multi-family dwelling would be displaced. HAZUS further states that no households would be displaced in a substantially damaged (EMS-98, DS3) building. These estimates were deemed less realistic, or at least, not to reflect what would transpire in a European country under such circumstances. As such, HAZUS estimates are not considered in this consequence model for the displaced.

Table 6.11. Consequence function for households displaced

% Displaced	DS-1	DS-2	DS-3	DS-4	DS-5
Short-term	0	40	40	0	-*
Long-term	0	0	60	100	-*

* The number of people displaced is computed by subtracting the estimated number of deaths from the number of inhabitants in the given building

6.3   Treatment of uncertainty

The uncertainties associated with the estimation of losses have been taken into account across the submodel components. Besides aleatory and epistemic uncertainties, coverage of parametric and model uncertainties under the former are often looked at within catastrophe risk modelling circles. A *parametric* uncertainty, for example, may refer to incomplete knowledge of a function parameter (e.g. the quantity of partition walls in a building). On the other hand, a *model* uncertainty may refer to whether a given model is an appropriate means of estimating loss; hence, blending it with an alternative would incorporate this type of uncertainty. Table 6.12 shows uncertainty coverage by the consequence model in this regard.

Table 6.12. Uncertainty consideration by the consequence model

	Epistemic uncertainty		Aleatory uncertainty
Model Component	**Parametric**	**Model**	
Direct economic loss			
Structural & non-structural	✓	✗	✓
Contents	✓	✗	✓
Human loss			
Injury and fatality rates	✗	✗	✗
Displaced households	✗	✗	✗
Downtime	✓	✗	✓

6.4   Limitations

▪ Unique demand profiles (i.e. displaced shape and acceleration profiles across floors) and potential mechanisms as a cause and result of damage are not fully captured in the present model. We start from global demand maxima in terms of drifts and accelerations, and assume a uniform distribution across floors/storeys to estimate damage in the absence of probabilities of occurrence of different respective damage modes and demand patterns.

▪ Repair cost and time functions of repairs are insensitive to storey level and access difficulty. The methodology allows for such intricacies to be taken into account; however, it was decided not to pursue this path in the absence of convincing empirical data and relevant research about them.

▪ Extreme situations that can significantly affect downtime estimates have been neglected. A couple of examples of this would be the additive cordon-induced downtime and possibility of relocation.

▪ Repair time estimation is heavily dependent on the assumptions of sequence of repairs and the maximum number of workers per unit floor area, both of which can exhibit significant uncertainties.

▪ The functions we provide do not take into account possible surges of costs, repair times and downtime in general following a large/damaging event. This is often referred to as 'demand surge' and it is a result of a sudden spike in demand not met by the existing supply. The current model neglects the potential effects of this phenomenon since current understanding of the phenomenon is limited, and the proposed models in the literature lack validation.

▪ In the absence of local information largely due to Switzerland's scarce history of earthquakes, downtime delay parameters have been based on post-earthquake data from the US.

6.5   Verification and sanity checks

Modelled repair cost ratios, i.e. the repair cost normalised by the building replacement cost, are compared with empirically-based direct loss (repair cost) consequence functions reported in the literature as part of a validation exercise (Figure 6.8).

A holistic validation of the model estimates in terms also of casualties, downtime and content loss remained a challenging task given the lack of complete datasets outside the fragmental data that the current model already leverages (e.g. delays constituent of downtime and component repair cost figures).
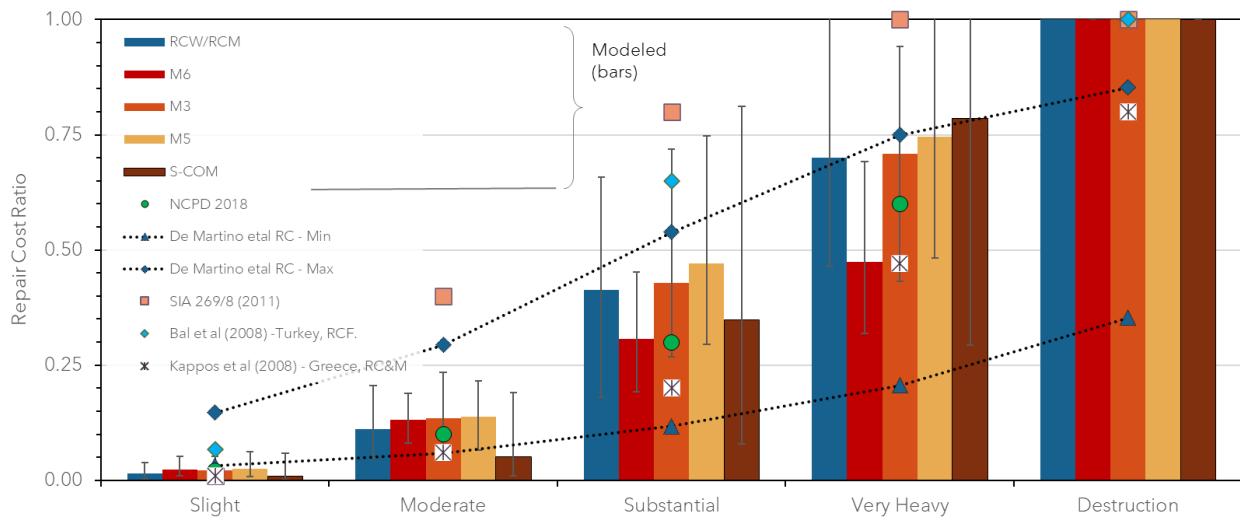
Figure 6.8. Direct economic loss: modeled (ERM-CH23) estimates versus empirically-based functions in the literature. SIA269 is the expert-judgement based estimate of the Swiss code for existing structures.

References

Ahmad, N., Ali, Q. (2017). Displacement-based seismic assessment of masonry buildings for global and local failure mechanisms. Cogent Eng 4. https://doi.org/10.1080/23311916.2017.1414576

Almufti, I., Willford, M. (2013). REDi ™ Rating System: Resilience-based Earthquake Design Initiative for the Next Generation of Buildings

ARCADIS (2019). International Construction Costs

Avila, L., Vasconcelos. G., Lourenço, P.B., et al. (2012). Seismic Response Analysis Of Concrete Block Masonry Buildings: An Experimental Study Using Shaking Table. In: 15WCEE. Lisboa

Babič, A., Dolšek, M. (2016). Seismic fragility functions of industrial precast building classes. Eng Struct **118**, 357–370. https://doi.org/10.1016/J.ENGSTRUCT.2016.03.069

Bal, I.E., Bommer, J.J., Stafford, P.J., et al. (2010). The influence of geographical resolution of urban exposure data in an earthquake loss model for Istanbul. Earthq Spectra **26**, 619–634. https://doi.org/10.1193/1.3459127

Bernardini, A., Lagomarsino, S., Mannella, A., et al. (2010). Forecasting seismic damage scenarios of residential buildings from rough inventories: a case study in the Abruzzo Region (Italy). Proc Inst Mech Eng **4**, 279–296. https://doi.org/10.1243/1748006XJRR305

Calvi, G.M. (1999). A displacement-based approach for vulnerability evaluation of classes of buildings. J Earthq Eng **3**, 411–438. https://doi.org/10.1080/13632469909350353

Cardone, D. (2016). Fragility curves and loss functions for RC structural components with smooth rebars. Earthq Struct **10**, 1181–1212. https://doi.org/10.12989/eas.2016.10.5.1181

Cardone, D., Perrone, G. (2015). Developing fragility curves and loss functions for masonry infill walls. Earthquakes Struct **9**. https://doi.org/10.12989/eas.2015.9.1.000

Comune di Milano, Regione Lombardia (2021). Public Works Pricelist. Prezzario regionale delle opere pubbliche, edizione 2021, Volume 1.1. Milano

De Martino, G., Di Ludovico, M., Prota, A., et al. (2017). Estimation of repair costs for RC and masonry residential buildings based on damage data collected by post-earthquake visual inspection. Bull Earthq Eng **15**, 1681–1706. https://doi.org/10.1007/s10518-016-0039-9

Di Ludovico, M., Prota, A., Moroni, C., et al. (2017a). Reconstruction process of damaged residential buildings outside historical centres after the L'Aquila earthquake: part I-''light damage'' reconstruction. Bull Earthq Eng **15**, 667–692. https://doi.org/10.1007/s10518-016-9877-8

Di Ludovico, M., Prota, A., Moroni, C., et al. (2017b). Reconstruction process of damaged residential buildings outside historical centres after the L'Aquila earthquake: part II—"heavy damage" reconstruction. Bull Earthq Eng **15**, 693–729. https://doi.org/10.1007/s10518-016-9979-3

Donà, M., Carpanese, P., Follador, V., et al. (2020). Mechanics-based fragility curves for Italian residential URM buildings. Bull Earthq Eng 0: https://doi.org/10.1007/s10518-020-00928-7

ETH Zurich (2015). Design And Building Process

FEMA (2010). Multi-hazard Loss Estimation Methodology Earthquake Model Hazus®-MH MR5: Technical Manual. Washington, D.C.

Gomez Capera, A., Locati, M., Fiorini, E., et al. (2015). Macroseismic and ground motion: site specific conversion rules. In: DPC-INGV-S2, Project 2015,

Jimenez-Pacheco, J., Gonzalalez-Drigo, R., Pujades-Beneit, L.G., et al. (2020). Traditional High-rise Unreinforced Masonry Buildings: Modeling and Influence of Floor System Stiffening on Their Overall Seismic Response. Int J Archit Herit 00, 1–38. https://doi.org/10.1080/15583058.2019.1709582

Lagomarsino, S., Cattari, S. (2014). Fragility functions of masonry buildings. In: Pitilakis K, Crowley H, Kaynia AM (eds) SYNER-G: typology definition and fragility functions for physical elements at seismic risk: elements at seismic risk, geotechnical, geological and earthquake engineering. (Chapter 5), pp 111–156

Lagomarsino, S., Cattari, S., Ottonelli, D. (2021). The heuristic vulnerability model: fragility curves for masonry buildings. Bull Earthq Eng. https://doi.org/10.1007/s10518-021-01063-7

Lagomarsino, S., Giovinazzi, S. (2006). Macroseismic and mechanical models for the vulnerability and damage assessment of current buildings. Bull Earthq Eng **4**, 415–443. https://doi.org/10.1007/s10518-006-9024-z

Lin, Y-Y., Miranda, E. (2008). Noniterative Equivalent Linear Method for Evaluation of Existing Structures. J Struct Eng **134**, 1685–1695. https://doi.org/10.1061/(asce)0733-9445(2008)134:11(1685)

Magenes, G., Calvi, G.M. (1997). In-plane seismic response of brick masonry walls. Earthq Eng Struct Dyn **26**, 1091–1112. https://doi.org/10.1002/(SICI)1096-9845(199711)26:11<1091::AID-EQE693>3.0.CO;2-6

Mahoney, M., Rojahn, C., Heintz, J.A., et al. (2018). FEMA P-58-6: Guidelines for Performance-Based Seismic Design of Buildings. Washington, D.C.

Martakis, P., Reuland, Y., Chatzi, E. (2021). Amplitude-dependent model updating of masonry buildings undergoing demolition

Michel, C., Karbassi, A., Lestuzzi, P. (2018). Evaluation of the seismic retrofitting of an unreinforced masonry building using numerical modeling and ambient vibration measurements. Eng Struct **158**. https://doi.org/10.1016/j.engstruct.2017.12.016

Mouyiannou, A., Rota, M., Penna, A., Magenes, G. (2014). Identification of suitable limit states from nonlinear dynamic analyses of masonry structures. J Earthq Eng **18**, 231–263. https://doi.org/10.1080/13632469.2013.842190

NCPD (2018). National risk assessment: Overview of the potential major disasters in Italy: seismic, volcanic, tsunami, hydro-geological/hydraulic and extreme weather, droughts and forest fire risks

Ottonelli, D., Cattari, S., Lagomarsino, S. (2020). Displacement-Based Simplified Seismic Loss Assessment of Masonry Buildings. J Earthq Eng **24**, 23–59. https://doi.org/10.1080/13632469.2020.1755747

Raetz, H., Forscher, T., Kneebone, E., Reid, C. (2020). The Hard Costs of Construction: Recent Trends in Labor and Materials Costs for Apartment Buildings in California. California

Rossi, A., Morandi, P., Magenes, G. (2021). A novel approach for the evaluation of the economical losses due to seismic actions on RC buildings with masonry infills. Soil Dyn Earthq Eng **145**, 106722. https://doi.org/10.1016/j.soildyn.2021.106722

Savoy, R. (2019). Seismic Vulnerability Assessment at Large Scale - City of Basel. The École polytechnique fédérale de Lausanne (EPFL)

Silva, V., Amo-Oduro, D., Calderon, A., et al (2018). Global Earthquake Model (GEM) Risk Map. https://doi.org/10.13117/GEM-GLOBAL-SEISMIC-RISK-MAP-2018

Spence, R., So, E., Ameri, G., et al. (2007). Earthquake Disaster Scenario Prediction and Loss Modelling for Urban Areas. Pavia

Thiriot, J. (2019). SEISMIC VULNERABILITY ASSESSMENT AT LARGE SCALE. ENAC, EPFL

Turner and Townsend (2019). International construction market survey - 2019

7.   The different types of uncertainty and their treatment

7.1   Introduction

Uncertainties are an inherent part of science. The real world is an extraordinarily complex and interconnected system and we use numerical models that attempt to characterise it. In the earth-related sciences, probabilistic frameworks and statistical models are used to describe apparently random and unpredictable natural events such as earthquakes.

In the background of any numerical model-building process are a few essential questions regarding the quality of input data used to develop subcomponents or these models, the stability of assumptions and the accuracy of the results. A complete uncertainty analysis would involve two phases: i) comprehensive identification of all sources of uncertainty that contribute to the joint probability distributions of each input or output variable; ii) propagation of uncertainty in model parameters and model structure to obtain confidence statements for the estimate of risk and to identify the model components of dominant importance.

Furthermore, these two phases lead to standard procedures for handling complex uncertainties associated with site-specific seismic hazard assessment (i.e. SSHAC guidelines), and these procedures can be extrapolated to probabilistic seismic risk analyses too. Such guidelines clearly indicate the framework and procedures to be followed given the goals and budget of such site-specific studies. From the procedural point of view, we follow a simplified procedure (inspired by SSHAC levels 1 and 2) in the development of the model, by establishing a core team, a participatory, advisory technical committee, a steering committee, as well as an international review panel of experts in the field of seismic hazard and risk.

In the adopted probabilistic framework, we aim to capture the uncertainties of available datasets, input subcomponents and/or main parameters, and the uncertainties adopted herein are classified as knowledge (or epistemic) uncertainties, natural (i.e. aleatory) variability, and decisional uncertainties (see Figure 7.1).

Epistemic uncertainties, also known as knowledge or modelling uncertainties, arise from the fact that predictive models do not have access to all the data they require, and that different experts may interpret data differently. Hence, in this project, the principal investigators were encouraged to explicitly handle and document the epistemic uncertainties at the data and subcomponent level.
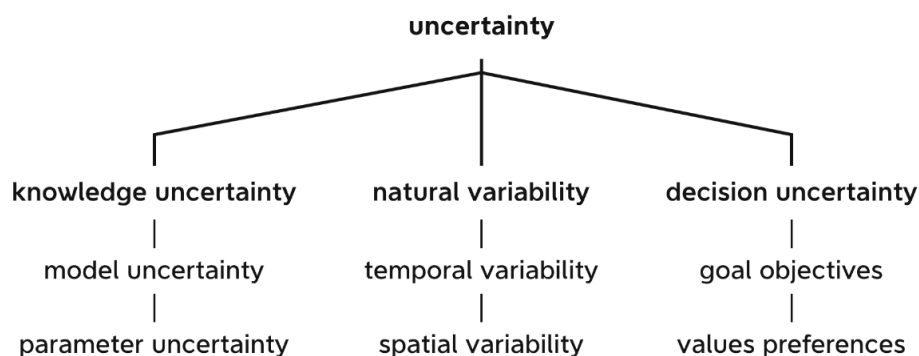
Figure 7.1. Theoretical uncertainty classification (adapted after Baecher et al., 2000).

The randomness that results from predicting an outcome from a specific model, assuming the model is accurate, is known as aleatory variability. The standard deviation of a GMPE is the most common randomness in a probabilistic seismic hazard framework. However, in order to assess seismic risk, aleatory uncertainty must be identified at the level of each subcomponent.

Aleatory and epistemic uncertainties are both considered in probabilistic risk calculations. While epistemic uncertainty is explicitly considered through the use of alternative hypotheses and mod-

els, aleatory uncertainty is directly considered through the generation of stochastic events and realisations of ground motion fields and damage/loss.

Alternative hypotheses are described by logic tree structures, which consist of a number of decisional nodes, depicting alternative input parameter values or model representations, and branches that display potential discrete states of evaluation. Each option receives one of two types of relative likelihood ratings as a weighting factor or level of uncertainty. How much one model is favoured over another can be seen in the weights on the logic tree and extends to the last category of uncertainties in our framework, i.e. decisional uncertainty.

Such uncertainty reflects knowledge of the study's general scientific context, local particularities, and analysis goals. Decisional uncertainties are related to the existence of information from a previous seismic risk study, the study's lifespan, how long such a study will be relevant, updating mechanisms, and so on.

In the context of ERM-CH23, the core team is responsible for model development and implementation decisions, and the uncertainty associated with their subjectivity is addressed by i) consulting committees, ii) conducting internal and external review meetings, and iii) providing transparent documentation of the model-building process.

In addition, some of the prerequisites associated with the project's early managerial decisions (such as the use of the SUIhaz15, community standards, and software such as OpenQuake) can also be considered decision uncertainties. A few important decisions were made during the project's preparation phase, which established the path to the current model development philosophy:

- Use of SUIhaz2015's (Wiemer et al., 2016) seismogenic source and ground motion models, without changes. This constraint has the advantage of allowing us to use the reference and authoritative seismic hazard model for Switzerland. Furthermore, it is worth noting that the seismic hazard components are not utilised in the same way for seismic risk as they are for seismic hazard assessment. In the traditional seismic hazard analysis, all relevant seismic sources and ground motion models are combined to obtain the hazard curves at a given site, whereas in the seismic risk assessment, stochastic event sets or synthetic catalogues can be generated from earthquake rate forecasts, and for each synthetic event, ground motion fields are then explicitly generated at all sites.

- The macroseismic intensity-based model provides a different perspective on the difficult problem of modelling earthquake effects on the built environment. Macroseismic data and information depict a longer observational time span, which is useful in connecting the effects of historical earthquakes with the built environment of today. The macroseismic intensity-based model is built as an alternative model to capture ground shaking characteristics, such as source, path and site, as described by the EMS-98 intensity scale (Grünthal et al., 1998); thus, when combined with the seismogenic source model, it can be viewed as a stand-alone model to evaluate seismic risk.

- The use of a community and open-source software (i.e. OpenQuake, Pagani et al., 2014). Although OpenQuake is a collection of various libraries for seismic hazard and risk calculations, several limitations exist, primarily on the use of logic trees for seismic risk assessment, i.e. event-based calculators. The current version's limitation is the inability to handle epistemic uncertainties associated with exposure and vulnerability subcomponents. Furthermore, the current event-based calculator cannot combine acceleration and intensity-based models in a single calculation, necessitating a post-processing task.

Consequently, the purpose of this chapter is to discuss some of the inherent uncertainties associated with the model, thereby facilitating comprehension of the model's implementation and calculation.

The framework for assessing seismic risk consists of several subcomponents: earthquake rate forecasting, ground motion characteristic models, site amplification, vulnerability and fragility models, consequence models, and exposure. Each of these components was independently derived, and the inherent uncertainties are described in the chapter devoted to them; therefore, their description is not repeated here. Note that many of the decisions made during this development process are supported by sensitivity analyses, which are also provided in the report.

7.2   Overall uncertainty model and main logic tree

As stated previously throughout this report, two alternative approaches were used to develop the computational model for assessing the seismic risk in Switzerland: the spectral acceleration-based model (hereinafter SAM) and the macroseismic intensity-based model (hereinafter MIM). Both strategies result in two distinct developments and computational pathways.

The seismogenic source model and the mapping techniques to assign building types to the exposure portfolio, as outlined in the main logic tree, are shared by both approaches (see Figure 7.2). The ground motion models, amplification and fragility components are specific to each of the two models, i.e. SAM and MIM, hence of great interest when assessing the weights of these two approaches.

It should be noted that the principal investigators of subprojects propose the weights assigned to each branch of the logic tree for their subcomponents (i.e. the weights of the IPEs or the weights of the amplification branches), whereas the final weights of the two approaches (SAM and MIM) were determined by the consensus proposal of the core team.

Next, the source model and the buildings' mapping scheme, which are the same for both SAM and MIM, are summarised first; the ground motion and site amplification, specific to each approach, are then discussed.
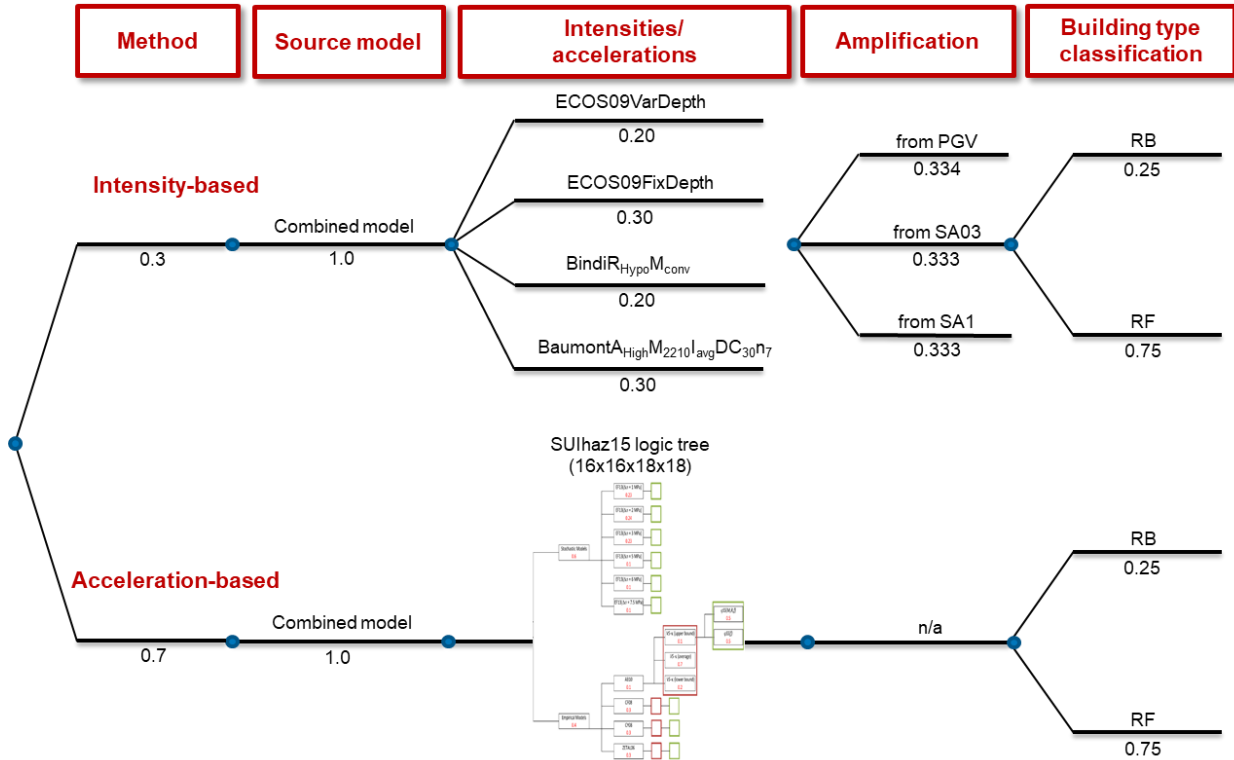
Figure 7.2. ERM-CH23 overall logic tree

7.2.1   Earthquake rate forecast

The seismogenic source model's logic tree is identical to SUIhaz2015's, with one branching level depicting 2.5th, 16th, 50th, 84th and 97.5th earthquake rate forecast models. The assigned weights are 68% for the 50th earthquake rate model, 13.5% for the 16th and 84th, and 2.5% for the 2.5th and 97.5th (Chapter 2).

In ERM-CH23, a weighted earthquake rate model was used to remove the simultaneous assumption of above- or below-average seismic activity across all seismogenic sources in the region (resulting in extreme high or low risk estimates). Further sensitivity analyses confirmed this observation, and it was agreed that synchronously assigning implausible rates (e.g. in the 2.5th or 97.5th quantile rate branches) across the nation introduces bias that should be avoided. Hence, a single 'weighted' or 'collapsed' earthquake rate model branch is used by averaging the five original earthquake rate models (SUIhaz2015, Wiemer et al., 2016).

The 'collapsed' earthquake rates provide both the temporal and spatial variability of the stochastic earthquake ruptures for use in the event-based calculation of the seismic risk. The controlling factors, i.e. length of the stochastic catalogue and number of ground motion logic tree samples, were optimised by sensitivity analyses. Naturally, this 'collapsed' earthquake rates model is given unity weight.

7.2.2   Mapping building typologies

A georeferenced database of all relevant building objects in Switzerland, comprising more than 2 million building objects, along with the attributes required for the ERM-CH23 model (Chapter 4) was compiled within this project. The link between this georeferenced dataset and the building typologies is done by two classification techniques: a rate-based and a random-forest approach.

Both techniques are based on datasets obtained from fieldwork investigations and walk-down surveys of building typologies in multiple cities, yielding a correlation matrix between certain building characteristics (e.g. facade features, presence of balconies), heights, footprint, volume, materials, and year of construction. In the case of the rate-based approach, the data were used to obtain statistics of different building types based on two variables, namely the building height and its construction period. These statistics were then used to randomly sample the building typology of all 2.2 million buildings in the database. The second technique is a statistically supervised learning algorithm used to solve classification and regression problems; the technique is based on ensemble learning and numerous decision trees to depict the attributes of the database object. The two techniques were weighted differently by the model developers, with a preference for the random-forest algorithm (0.75 vs. 0.25).

It should be noted that no uncertainty was associated with the object attributes during the development of the existing buildings database. Furthermore, certain attributes, such as replacement value, content replacement value, permanent inhabitants, full-time equivalent employees, occupancy type, owner category, and types of economic activity, were modelled because they are not directly available in ensembled databases. Chapter 4 described this modelling while the risk implementation section (next chapter) describes some of the additional assumptions and their implementation.

Furthermore, the spatial aggregation of the building portfolio within a geographical region is a critical aspect of the seismic risk calculation, as the individual buildings are often aggregated at a regional scale, i.e. administrative zones or postal codes. Such aggregation will assume that all aggregated buildings will have correlated ground motion and amplification features.

7.2.3   Ground motion characterisation

To handle the epistemic uncertainties, two alternative ground motion models are delivered with SAM and MIM (see Chapter 2).

Acceleration-based models depict both the recorded ground motion (portrayed by the empirical models and the simulated records (represented by the stochastic models); the reference site conditions are known (Vs30=1,100 m/s); the sigma of the equations is calibrated to remove the local-site conditions (a partially non-ergodic model); the models are adjusted to low-magnitude effects and provide a full range of intensity measure types that can be linked with the structural periods of the buildings. The extrapolation of the GMPEs to large magnitudes (M>6.5) is one of the main limitations of the acceleration-based models.

Intensity-based models depict the regional variability of the path effects, in particular the ECOS-09 intensity prediction equations (IPEs). Furthermore, the IPEs provide a link to the moderate- and large-magnitude events, which are not available in the ground motion dataset. Also, there is a direct link between the IPEs and the observed damage of historical earthquakes based on the Swiss-specific building typologies.

The large uncertainties associated with depth, the unknown site conditions, the restriction to point-source ruptures also for large-magnitude earthquakes and the substantial standard deviations are some of the major limitations of intensity-based models. The most significant of these are the unknown site conditions, which convey a large uncertainty when compared to the acceleration-based models. Other limitations are the magnitude conversion of the Bindi et al. (2011) IPE and the fact that we assign the standard deviation model of Beaumont et al. (2018) to all IPEs.

An additional limitation associated with the realisations of the ground motion fields in the current model implementation is the absence of spatial correlation. Jayaram and Baker (2009) noticed that distance affects the correlation between intra-event residuals at two sites for a given earthquake, i.e. the greater the distance, the lower the correlation. Additionally, cross-correlation is required when various intensity measure types are used to define the fragility functions of various building typologies (Baker and Cornell, 2006; Crowley et al., 2008).

Altough an important aspect for the current configuration of the computational model, neither the spatial correlation nor the cross-correlation features of the intra-event residuals for SAM and MIM are used due to complexity of the model.

7.2.4   Site amplification

A site amplification model for SAM was developed and adapted for use with MIM. The recently developed amplification model provides four national amplification maps for PGV and spectral acceleration at 0.3, 0.6 and 1 s (Chapter 3, Bergamo et al., 2022; Panzera et al., 2021). For Sion, Visp and Lucerne, more precise models of amplification are provided, which are then used to validate the independently derived national model.

For SAM, the spatially variable amplification factors are converted to natural logarithms and added to the predicted logarithmic spectral accelerations by the corresponding GMPEs. In addition, the random component of the GMPEs was updated to consider the updated site-to-site and single-station variability provided by the amplification model. The latter two are presented as raster maps, and the model incorporates a site-specific definition of uncertainty.

These amplification maps for PGV and PSA (0.3 and 1 s) are converted to macroseismic intensity aggravation layers for the MIM with the empirical relations of Faenza & Michelini (2010, 2011); the amplification in macroseismic intensity units (i.e. aggravation at the target site with respect to a reference intensity, i.e. Iref) is computed following Michel et al. (2017) and Panzera et al. (2019). The resulting aggravation layers are equally weighted, reflecting the lack of preference for any intensity proxy parameter.

Overall, the underlying data and methodology for site amplification are advanced and among the best practice in the field. When combined with ground motion models, SAM amplification models appear to have the advantage of applying directly to individual GMPEs, whereas MIM involves additional conversions, which introduces additional uncertainties, both epistemic and aleatory. Given that models with lower aleatory variability are generally preferred, there is a slight preference for SAM amplification since MIM amplification is inflated by the conversion to intensity.

7.2.5   Fragility and vulnerability models

Following the development of SAM and MIM, two independent pathways were used to assess the vulnerability of Switzerland's building portfolio: an intensity-based fragility model for MIM and a mechanical model, i.e. spectral-acceleration-based, for SAM.

The intensity-based fragility curves are derived from empirical fragility curves of European building typologies, adjusted to Swiss specificities and regional engineering practice. The use of intensity-based fragility curves is justified by the need to expand current knowledge on earthquake damage observation and data in neighbouring countries, specifically France, Austria, Germany and Italy. The latter has a long history of damaging earthquakes, which provides a foundation for using macroseismic intensity for fragility and vulnerability modelling, especially when based on observed damage and loss data.

Fragility models are typically subject to great uncertainties and they are often seen as one of the least well-constrained components of earthquake risk models. Therefore, capturing and propagating associated epistemic uncertainties is a worthwhile objective. Despite this, extending logic tree structures to the fragility level is not common practice, either in academic literature or in commercial models. The reasons behind this vary from increased model complexity to lack of relevant data/models. Fragility/vulnerability models should generally capture the characteristics of the local building practice, and therefore it is challenging to use global data.

Moreover, the development of analytical models for a range of different building typologies constitutes a cumbersome task that often also requires considerable and varied expertise. Deriving multiple fragility models that capture different epistemic views is therefore a very challenging demand.

A simpler but practical approach would be a judgement-driven ad-hoc 'shift' of the vulnerability curves to model some uncertainty. This would result in low- and upper-end curves along with the best-estimate ones. Unfortunately, the challenge then becomes how to objectively combine such models for different building types. In other words, each logic tree branch represents one plausible view of reality.

Assuming there is no justified reason that all the vulnerability curves (i.e. for all building typologies) are under- or over-estimated, then one would need to construct logic tree branches that enumerate all possible combinations of low/best/upper curves for each of the 23 building typologies of the ERM-CH23 taxonomy (for a total of 223 branches). This is unfeasible due to computational constraints.

Of equal importance is the calibration of these fragility models with past earthquakes and even more important is their adjustment at low intensity levels, as described in Chapter 5.

The SA-based fragility models are derived based on mechanical/numerical representation of different building typologies, further classified by material type and number of storeys. A capacity-spectrum method was used to evaluate the structural performance of the buildings of a given typology. Different capacity curves are obtained for combinations of material, mechanical characteristics, variable number of storeys and ground motion variability. The aleatory uncertainties of the SA-based fragility models are driven by several factors including the definition of capacity curves, which covers material and building-to-building uncertainty, as well as record-to-record variability (albeit referring to a single earthquake scenario).

As stated in Chapter 5, both fragility models have strengths and limitations, and efforts are being made to calibrate these models using both data and engineering judgement.

These fragility models are equally adequate for the current implementation, and, as with the ground motion, the SA-based fragility models have a slight advantage over the intensity-based ones. Overall, the SA-based fragility models are based on state-of-practice methodology, accounting for structural response of building typologies rather than expert opinion-based correlation of vulnerability classes with specific building typologies, as is the case with intensity-based fragility models.

7.3   Conclusions

To conclude, given these strengths and limitations, as summarised in Table 7.1, a consensus was achieved towards the assumption that the acceleration-based approach is a more robust approach than the intensity-based ground motion model. The final SAM and MIM weights were set at 0.7 and 0.3 respectively. These weights also reflect the preference of the external experts involved in the review process. It should be noted that the uncertainties of each model subcomponent are described in their respective chapters of this report. Table 7.2 gives an overview of the different components and types of uncertainty in ERM-CH23.

The choices made for the model's implementation and calculation are discussed in the following chapter. Last but not least, the uncertainties should be reduced over time with the acquisition of new data, new models, and new software development; undoubtedly, this is the goal to be set for the next update of the model.

Table 7.1. Summary of the strengths and limitations of the three subcomponents specific to the two main approaches SAM and MIM, used to guide the final assignment of weights of the two models.

Model	Component	Relative strengths	Relative weaknesses
MIM	Ground shaking	IPEs derived based on historical observations	Arguably very slow attenuation with possibly spurious predictions at long distances (possibly due to data incompleteness).
		Macroseismic intensity data and information that are Swiss-specific	Use of R_{epi} or R_{hypo} distance metrics which do not capture finite spatial extent of ruptures
		Extrapolation to larger magnitudes	Macroseismic intensity is a spatial metric that here is applied to individual locations. Arguably, there might be some inconsistency between the IPE derivation and how they are used in a loss calculation.
		Sigma model (total/inter/intra components) of the Baumont et al. 2018 IPE was adopted for all IPEs. Refer to Section 2.5 for more insights.	3/4 IPEs did not feature distinction of inter/intra event variability, therefore the uncertainty model of the Baumont et al. IPE was adopted for all.
			A reference soil correction had to be applied to the IPEs.
			Large uncertainties of the macroseismic data with epicentral area; poor extrapolation of intensity with hypocentral depth
			2 IPEs are derived for different intensity scales: MSK64 for Bindi et al. 2011; MCS and MSK for Baumond et al. 2018.
	Site conditions		Inferred from ground motion proxies and a conversion equation
			Inflated sigma due to ground motion to intensity conversion of the amplification factors
	Fragility	Free of modelling assumptions, based on textual description of the EMS-98 damage scale and expert-opinion based association of building typologies to EMS-98 vulnerability classes	Judgement-based association of building typologies to EMS-98 vulnerability classes

				Macroseismic intensity as intensity measure cannot describe the frequency content of a particular earthquake scenario and capture the dynamic properties dependent response of different building typologies.
SAM		Ground shaking	Use of R_{rup} distance metric which can capture finite spatial extent of ruptures	Lack of large-magnitude observations for model calibration
			Complex logic tree capturing a wide range of GMPEs both stochastic and empirical	Arguably extreme individual ground motion field simulations in very near field sites
			Reference soil conditions known (vs30=1100m/s)	Use of the stochastic models: low stress-drop for large magnitudes, and vice-versa, use of high stress-drop for low to moderate magnitudes
		Site conditions	Site-specific model of amplification factor, single-station sigma and site-to-site sigma	Amplified sigma due to amplification factors (Section 3.4)
		Fragility	Data/mechanics-driven modelling	Use of simplified models (capacity spectrum method, bilinear capacity curves)
			Explicit modelling of different uncertainty sources	Some models sourced from literature, possible inconsistencies
			Two intensity measures (SA03, SA06) used to better describe the response of different building typologies	Limited modelling of record-to-record variability (single scenario)
				Limited/implicit-only modelling of building-to-building variability
				Damage state definition match to EMS-98 damage grades not ensured
				Variability pertaining to building height within class definition (low-/mid-/high-) not modelled, capacity curves of single height were used

Table 7.2. Summary of the uncertainty components in ERM-CH23, by type, approach and component.

Component	Aleatory uncertainties		Epistemic uncertainties	
	MIM	**SAM**	**MIM**	**SAM**
Source model	Poisson process of earthquake recurrence		None	None
Ground shaking	Normal distribution truncated at 1 sigma. Uncertainty model from Baumont et al. IPE.	Lognormal distribution truncated at 2 sigmas. Site-specific single-station and site-to-site sigma.	Four alternative IPE branches	16x16x18x18 branch GMPE logic tree
Site amplification	Assumed included in the ground shaking uncertainty	Assumed included in the ground shaking uncertainty	Three branches of alternative intensity amplification factors obtained from different ground motion amplification proxies	None
Vulnerability	Beta distribution of loss ratio given intensity for structural/non-structural and content loss types. None for human loss types	Beta distribution of loss ratio given intensity for structural/non-structural and content loss types. None for human loss types	None within MIM or SAM, although different independent models used in each of the two.	
Exposure	None	None	Two branches pertaining to different typology mapping schemes	

References

Akkar, S., Sandıkkaya, M.A., Bommer, J.J. (2014). Empirical ground-motion models for point- and extended-source crustal earthquake scenarios in Europe and the Middle East. Bulletin of Earthquake Engineering **12**, 359–387. https://doi.org/10.1007/s10518-013-9461-4

Baecher, G., Christian, J. (2000). Natural variation, limited knowledge, and the nature of uncertainty in risk analysis." In Proceedings of the Risk-Based Decision making in Water Resources IX, Santa Barbara, CA, USA, 15–20 October 2000.

Baker, J.W., Cornell, A.C. (2006). Spectral shape, epsilon and record selection. Earthquake Engineering Structural Dynamics **35**(9), 1077–1095.

Baumont, D., Manchuel, K., Traversa, P., Durouchoux, C., Nayman, E., Ameri, G. (2018). Intensity predictive attenuation models calibrated in Mw for metropolitan France. Bulletin of Earthquake Engineering **16**, 2285–2310. https://doi.org/10.1007/s10518-018-0344-6

Bergamo P. et al. (2022). SPE – Deliverable AM3 - Provisional amplification maps for integration in the current implementation of the risk model. ERM-CH report.

Bindi, D., Parolai, S., Oth, A., Abdrakhmatov, K., Muraliev, A., Zschau, J., 2011. Intensity prediction equations for Central Asia. Geophysical Journal International **187**, 327–337. https://doi.org/10.1111/j.1365-246X.2011.05142.x

Crowley, H., Bommer, J.J., Stafford, P. (2008). Recent developments in the treatment of ground-motion variability in earthquake loss models. Journal of Earthquake Engineering, Special Issue, **12**(S2), 71–80.

Faenza L., & Michelini A. (2010). Regression analysis of MCS intensity and ground motion parameters in Italy and its application in ShakeMap. Geophys. J. Int. **180**(3), 1138–1152.

Faenza L., & Michelini A. (2011). Regression analysis of MCS intensity and ground motion spectral accelerations (SAs) in Italy. Geophys. J. Int. **186**(3), 1415–1430.

Grünthal, G. (ed.) (1998). European Macroseismic Scale 1998 (EMS-98). Cahiers du Centre Européen de Géodynamique et de Séismologie **15**, CEGS, Luxembourg, 99 pp.

Jayaram, N., Baker, J.W. (2008). Statistical tests of the joint distribution of spectral acceleration values. Bulletin of the Seismological Society of America **98**(5), 2231–2243.

Michel, C., Fäh, D., Edwards, B., Cauzzi, C. (2017). Site amplification at the city scale in Basel (Switzerland) from geophysical site characterization and spectral modelling of recorded earthquakes. Physics and Chemistry of the Earth Parts A/B/C **98**,27–40.

Pagani, M., Monelli, D., Weatherill, G., Danciu, L., Crowley, H., Silva, V., Henshaw, P., Butler, L., Nastasi, M., Panzeri, L., Simionato, M., Vigano, D. (2014). OpenQuake Engine: An Open Hazard (and Risk) Software for the Global Earthquake Model. Seismological Research Letters **85**, 692–702. https://doi.org/10.1785/0220130087

Panzera, F., Bergamo, P. & Fäh, D., 2021. Reference soil condition for intensity prediction equations derived from seismological and geophysical data at seismic stations. J Seismol 25, 163–179 (2021). https://doi.org/10.1007/s10950-020-09962-z

Wiemer, S., Danciu, L., Edwards, B., Marti, M., Fäh, D., Hiemer, S., Wössner, J., Cauzzi, C., Kästli, P., Kremer, K. (2016). Seismic Hazard Model 2015 for Switzerland (SUIhaz2015). https://doi.org/10.12686/A2.

8.   Risk implementation and computational aspects

8.1   Introduction

This chapter details the technical implementation of ERM-CH23 and summarises methodologies, assumptions and choices made during the integration of the various raw subcomponents and datasets. The resulting final model subcomponents are also presented and critically analysed.

8.2   Probabilistic framework

To assess the earthquake risk over a spatially distributed exposure, a so-called event-based approach based on Monte-Carlo simulations is typically required. An event-based probabilistic earthquake risk assessment starts with the generation of a large number of stochastic earthquake catalogues, by sampling according to the rates and probabilistic recurrence model of the underlying seismogenic source model. The stochastic catalogues are meant to represent alternative realisations of seismicity over a pre-specified temporal interval.

An associated random ground motion field is then also sampled for each rupture in the catalogue by means of a ground shaking intensity model (GSIM). The latter takes as arguments rupture and site parameters (e.g. magnitude, rupture-to-site distance, site conditions) and returns a distribution of the relevant ground shaking intensity measure (e.g. spectral acceleration at a certain period of vibration or macroseismic intensity). A random ground motion field constitutes a joint (across all sites of interest, i.e. locations of building assets) Monte-Carlo simulation of the intensity measure.

The simulated intensity values at each site are then passed on to the relevant vulnerability functions associated with the building typologies located at said site according to the exposure model. The exposure model is a dataset of the modelled buildings with information such as their location, building typology (e.g. stone masonry, reinforced concrete wall), replacement cost, number of occupants, etc. A vulnerability curve refers to a single building typology and relates ground motion intensity to loss ratio (loss divided by total value). A vulnerability curve can be deterministic, i.e. return a single mean value of loss ratio for each intensity level, or probabilistic, i.e. return a distribution of loss ratio. In the latter case, when the simulated ground motion intensity value is passed to it, another Monte-Carlo simulation is performed to return a realisation of the loss ratio.

The obtained loss ratios are multiplied by the relevant value (economic structural replacement cost, content replacement cost, number of occupants) to obtain the asset-specific loss. To compute the exposure-wide loss for a given stochastic earthquake, the individual asset losses are added up. Repeating this for all simulated earthquake ruptures results in a stochastic catalogue of event losses, often referred to as an event loss table (ELT). This loss catalogue or sample can then be used to obtain standard risk metrics, such as the average annual loss (AAL) or a loss exceedance frequency (LEF) curve. In the presence of a logic tree, this analysis is performed separately for each logic tree branch. This results in a collection of AALs and LEF curves, which represent the epistemic range of loss estimates and can be used to obtain relevant statistics, such as mean estimates and quantiles of the relevant metrics.

Except for the event-based probabilistic risk assessment, analyses specific to scenario ruptures are also carried out. In those cases, the same procedure is followed with the exception that a single pre-specified earthquake rupture is used instead of a stochastic catalogue meant to represent a temporal interval.

All calculations are carried out using the open-source OpenQuake Engine v3.14 (Pagani et al., 2014) developed by the Global Earthquake Model (GEM) foundation. The probabilistic event-based risk assessment makes use of the OpenQuake 'event_based_risk' calculator, while the 'scenario_damage' and 'scenario_risk' calculators are used for the scenario damage and loss assessments.

8.3   Risk metrics

This section summarises the main output of the model. The following metrics are obtained from the probabilistic event-based risk calculations for the characterisation of earthquake risk and presented in this report:

- Average Annual Loss (**AAL**) [12]: the expectation of the annual loss.
- Loss Exceedance Frequency (**LEF**) curves or Probable Maximum Loss (**PML**) curves: the LEF curves show the annual frequency of loss exceedance versus the associated loss. If the return period of exceedance (i.e. the reciprocal of the exceedance frequency) of a certain event loss is shown against loss, then the curve is referred to as PML.

Here, we note the distinction of the LEF curves from other risk measures, used primarily in the insurance sector, such as the Occurrence Exceedance Probability (OEP) and Aggregate Exceedance Probability (AEP). OEP refers to the probability that the maximum event loss in a year exceeds a given level, while AEP describes the probability that the sum of event losses in a year exceeds a given level. Since all those measures can be expressed as probabilities, frequencies or return periods of loss exceedance, it is important not to conflate them. OEP and AEP estimates could also be readily derived from ERM-CH23, but will not be further referenced in this report.

All risk metrics have been computed at different scales, namely:
- country-wide;
- canton level;
- municipality level;
- postcode level;
- 2 km x 2 km regular grid;
- by building occupancy;
- by building structural typology.

It should be noted that the term 'loss', throughout this report, refers to any of the following loss types:
- economic loss related to the damage sustained by structural and nonstructural building components;
- economic loss related to damage to building contents;
- fatalities;
- injuries;
- displaced population.

8.4   Seismic hazard modelling

The modelling of seismic hazard requires three main ingredients, namely a seismogenic source model (Chapter 2), a ground shaking intensity model (Chapter 2) and a site amplification model (Chapter 3). Since details on these individual components are given in their dedicated chapters, here we only report on technical aspects pertaining to their implementation and integration in the risk model.

---

[12] Note that the "average" in AAL refers to the aleatory year-to-year randomness. The quantification of epistemic uncertainty by means of a logic tree results in multiple estimates of AAL (one for each logic tree branch). In this report, we report the average (over the epistemic distribution) AAL, as well as its full epistemic distribution.

8.4.1   Generation of stochastic catalogues

The seismogenic source model used in ERM-CH23 comes from the Swiss 2015 Seismic Hazard Model (SUIhaz2015). As reported in Chapter 2, a single 'collapsed' source model branch is used in ERM-CH23, derived by averaging the rates of the five source model branches in SUIhaz2015. The rationale behind this is laid out in Chapter 2. The source model is used by the OpenQuake Engine to define all possible ruptures and their rate of occurrence and subsequently generate multiple one-year-long stochastic catalogues. This is repeated for each logic tree branch realisation in the model. The number of stochastic catalogues to be generated depends on the risk metrics of interest and the desired convergence to be achieved (Silva 2018). To achieve good convergence of the mean loss estimates up to the 1,000-year return period, the number of stochastic catalogues to be generated was set to 20,000 for each of the 24 logic tree branch realisations of the macroseismic intensity submodel of ERM-CH, and to 10,000 for each of the sampled 400 logic tree branch realisations of the spectral acceleration submodel (further details on the logic tree configuration are given in Section 8.6 below). This resulted in 4.48 million simulated one-year-long stochastic catalogues. Figure 8.1 illustrates the spatial distribution of hypocentres in the generated stochastic catalogues and resulting magnitude sample distribution.
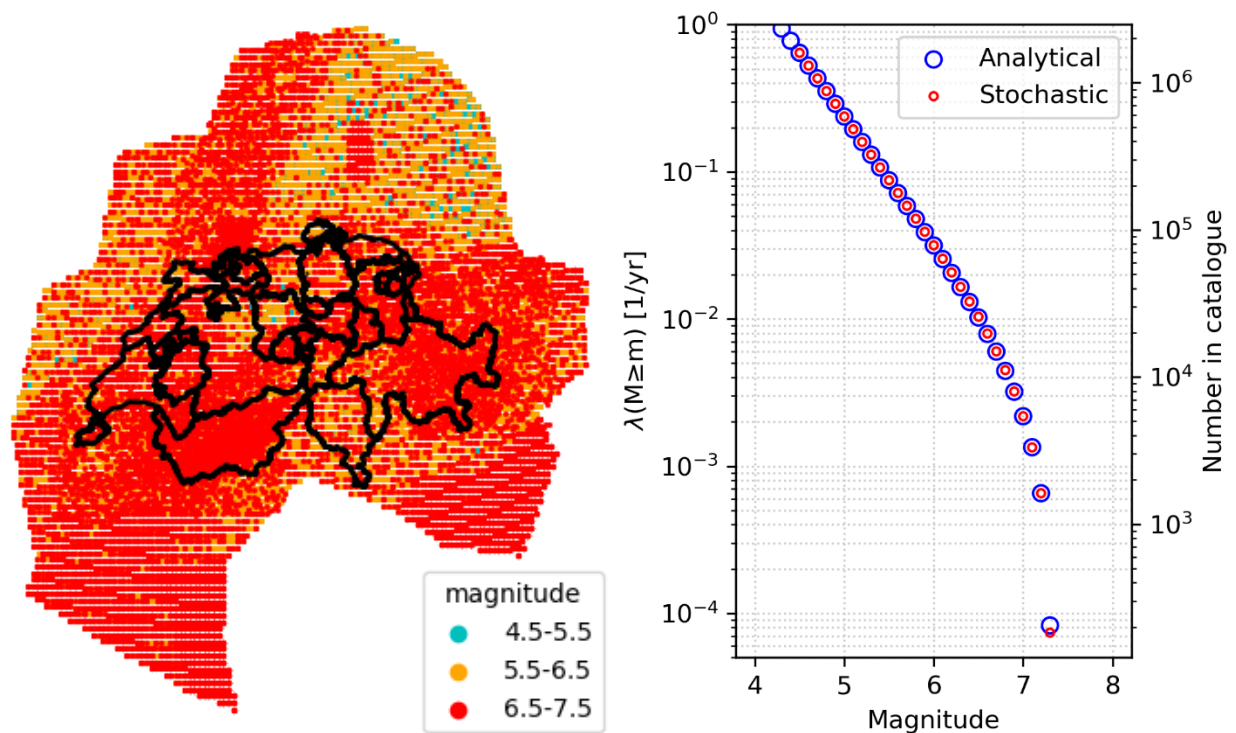
Figure 8.1. Left: generated stochastic event catalogues (combined from all logic tree branches); right: magnitude-frequency distribution of combined stochastic catalogues against analytical rates of the underlying source model.

8.4.2   Random ground motion fields

As mentioned before, a random ground motion field is generated for every rupture in the stochastic catalogue using the GSIM that is associated with each given logic tree branch realisation. As described in Chapter 2, the OpenQuake GSIMs are adjusted to cater for the ERM-CH requirements in terms of modelling the site amplification and uncertainty.

The intensity prediction equations (IPEs) are modified as follows:

- Given that the employed IPEs provide estimates for unknown soil-reference conditions, an additive correction factor ΔI_v is applied to the mean predicted intensity to convert to rock

conditions according to the specifications of the amplification model (Chapter 3). The correction factor applied is equal to -0.39, -0.31 or -0.22 intensity units, depending on the amplification model used (from PGV, SA(0.3s) or SA(1s) respectively).

- A site-specific additive amplification factor ΔI_{AF} is also applied to bring the intensity estimate to the specific site conditions for the considered location. The mean intensity predicted is thus $E(I) = E(I_{IPE}) + \Delta I_{AF} + \Delta I_v$.

- The aleatory uncertainty in intensity prediction is modelled with a Gaussian distribution. The inter- and intra-event variability is taken from the Baumont et al. (2018) model as described in Chapter 2. We chose to apply a truncation at 1 sigma, to avoid the sampling of values deemed unrealistic. The use of a very detailed amplification model provides another argument for reducing the allowed range of uncertainty.

The ground motion prediction equations (GMPEs) are modified as follows:

- A site-specific additive amplification factor ΔI_{AF} is applied to bring the acceleration estimates to the specific site conditions for the considered location. The mean acceleration predicted is thus $E(\ln SA) = E(\ln SA_{GMPE}) + \Delta I_{AF}$.

- The inter-event variability of the GMPEs as used in SUIhaz2015 is retained, while the intra-event variability is substituted with the site-to-site variability and single-station variability estimates φ_{s2s} and φ_{ss} described in Chapter 3. The intra-event variability at each site is computed as $\varphi = \sqrt{\varphi_{ss}^2 + \varphi_{s2s}^2}$. A truncation at 2 sigmas was implemented with similar justification as in the case of IPEs.
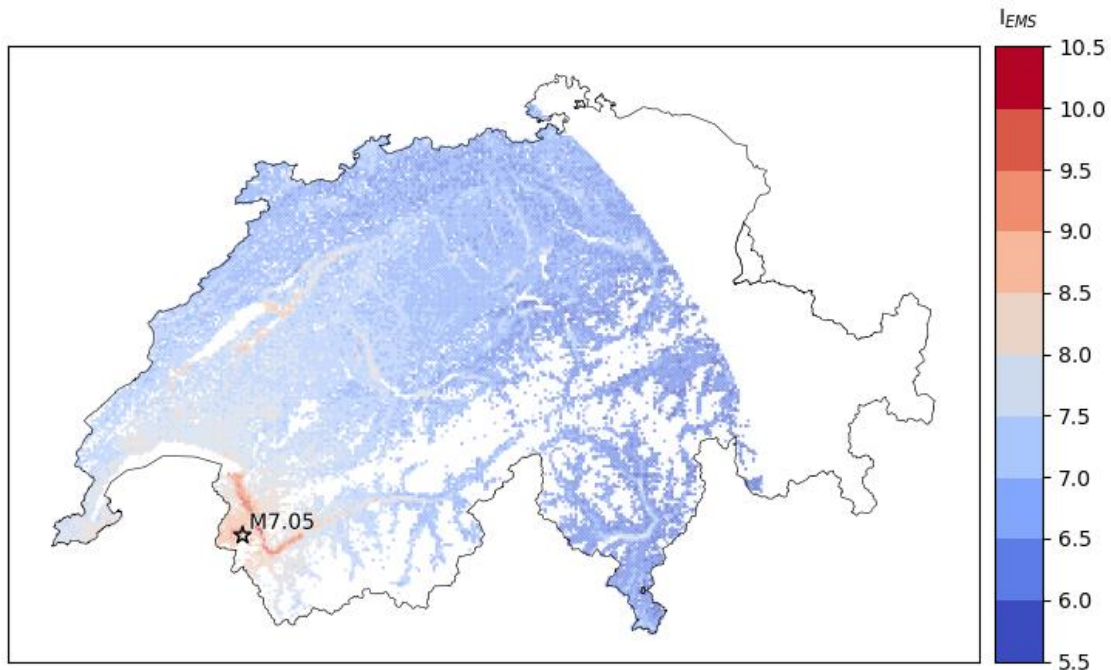
Figure 8.2. Example ground motion field from the MIM model associated with a loss equal to the 2,000-year return period estimate.

For each rupture, a sampled residual of the inter-event variability is applied to all sites, whereas the intra-event residual is sampled at each individual location. A maximum rupture-to-site distance of 200 km was set up to which ground motion is computed. It was assumed that damage is unlikely to occur at longer distances. Spatial correlation of intra-event ground motion residuals was not considered because (1) no such model is available for macroseismic intensity, (2) the computational complexity is prohibitive for a national scale calculation, and (3) it is unclear whether it should be applied in cases of aggregated exposure where an implicit correlation is in-

troduced anyway. Figure **8.2** illustrates an example random ground motion field in terms of macroseismic intensity from the generated catalogue.

8.5   Exposure modelling

The ERM-CH23 exposure model is built based on the building database described in Chapter 4, the typology mapping scheme described in Chapter 5 and the data curation and assumptions detailed in the sections below.

8.5.1   Curation of building database

The building database, described in Chapter 4, numbers 3'154'964 building entries, distributed across Switzerland. Out of these over 3 million entries, 834'244 structures with zero or small volume (<200 m^3) were removed. These small volume structures (such as storage sheds, machinery installations, etc.) comprised a very small portion of the total building stock value, and were removed to avoid obtaining misleading estimates of certain earthquake impact metrics (e.g. number of damaged buildings). Also, 69,350 buildings with unclassified function thought to consist of bus shelters, public toilets, garden huts, etc. were removed, leaving 2,251,370 buildings in our dataset. The development of the exposure model using this subset of the database as the basis is summarised below.

8.5.1.1   Number of storeys and construction period

The number of storeys of each individual building was determined based on the height (GEBHOHE), maximum height (GEBHMAX; difference between the highest point of the digital elevation model and the lowest point of the terrain surface model over the building footprint) and number of storeys (GASTW) attributes of the building database. Due to possible inconsistencies in the GASTW field, the number of storeys was by priority determined from the height (GEBHOHE) field. Entries with building height between 1.5 and 6 m were assigned one storey, while a floor division with 3 m was used to compute the number of storeys for entries with height > 6 m. When the height was not available or in cases of height < 1.5 m, the maximum height (GEBHMAX) field was used with the same criterion for assigning storeys. Finally, if the maximum height was also not available or smaller than 1.5 m, the GASTW (number of storeys) field was consulted. The construction period of each building was obtained from the GBAUJ (year of construction) and GBAUPdef (period of construction) fields of the database. For a very small portion of buildings with unknown construction period, cantonal statistics were used to sample a value

8.5.1.2   Building occupancy type

The building database contains fields that describe the function of each building: GKLASdef (function category), BIN_SCHUL (flag for school buildings) and BIN_HOS (flag for hospitals). Using this information, we distinguished five main occupancy categories, i.e. Residential (RES), Commercial and Public (COMPUB), Industrial (IND), Agricultural (AGR) and Historical Monuments (MON). The 'Historical' buildings, which numbered just 19, were dropped and not used subsequently. Around 145,000 buildings could not be assigned an occupancy based on the aforementioned fields. Around 8,000 of them were treated as residential, since they were assigned a 'habitation use' code in the GKAT (building category) field of the database. The remaining buildings were assumed to be in either one of the IND, COMPUB or AGR categories and their occupancy was sampled. To this end, statistics were obtained of known 'Industrial', 'Agricultural' and 'Commercial and Public' buildings in bins of building volume and AREBAUZ (building zone category) field values (Table 8.1).

To test the performance of this sampling, we split the database entries with known occupancy into a training (80%) and testing (20%) set, and compared the actual occupancy values with the randomly sampled ones (Figure 8.3). The 'correct' or benchmark occupancy here is the one determined from GKLASdef (function category), although it should be acknowledged that errors in this

regard might be present in the dataset. In general, we see the majority of agricultural and commercial buildings are correctly assigned, although with a significant number also incorrectly determined. For industrial buildings the performance is worse, with many buildings being assigned as commercial. That said, the opposite is also true (i.e. a similar number of commercial buildings is assigned as industrial), and the overall number of buildings of each typology is generally well preserved. This is also shown in Figure 8.4.

Figure 8.3. Proportion of non-residential buildings classified as 'Agricultural', 'Industrial' or 'Commercial and Public' by building zone category tag and volume bin. The value range in each row refers to the building volume in m^3, while the number in parenthesis refers to the number of buildings in each bin used to obtain the statistics.

Table 8.1. Number of buildings in each occupancy type.

Occupancy type	Initial count based on GKLASdef, BIN_SCHUL, BIN_HOS	Count after factoring in GKAT	Final count after random sampling
Residential	1,706,685	1,714,399	1,714,399
Commercial and Public	172,782	172,782	230,030
Industrial	94,631	94,631	122,862
Agricultural	132,216	132,216	184,060
Historical	19	19	19
Unknown	145,037	137,323	0
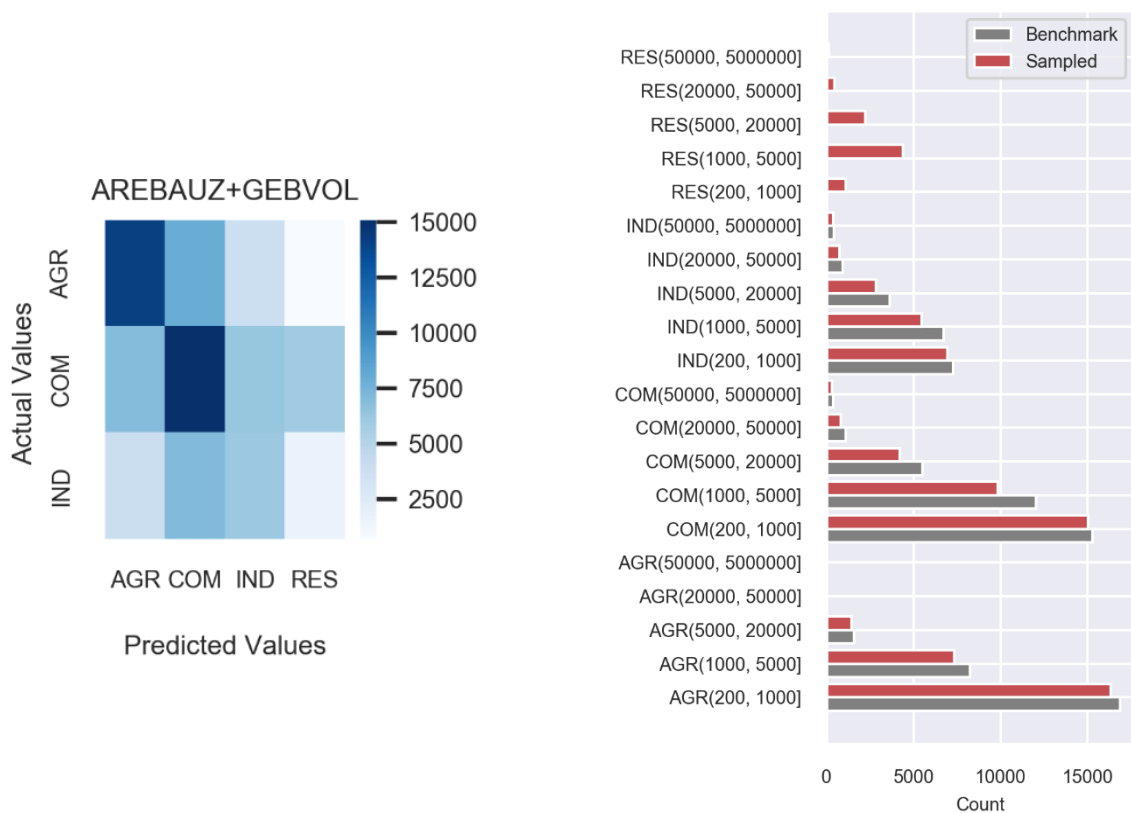
Figure 8.4. Left: confusion matrix for the sampling of occupancy in the testing subset; right: comparison between the GKLASdef-benchmark and sampled (based on building zone category and volume) overall number of buildings in each occupancy-volume bin. The value range in each row refers to the building volume in m^3.

8.5.1.3   Replacement cost and number of occupants

The definition of the structural and content replacement costs of each building is described in Chapter 4 and individual values are given for each building as attributes of the building database. As regards the building occupants, they are set by using the following database fields:

- EINWMOD (number of inhabitants);
- ANGMOD (full-time equivalent employees);
- HOS_PAT (number of patients in hospitals at night time);
- HOS_OUTPAT (average number of outpatients during a day);
- SCHULMOD (number of students in school buildings);

First, we break the day into three eight-hour intervals, which we refer to as 'night' (21:00 to 5:00), 'day' (8:00 to 16:00) and 'transit' (remaining hours). Since high-resolution/precision information on population movement is not available, to assign a number of occupants in each building for each time interval, we make some general assumptions regarding the time spent in different activities. First of all, we assume that employees work 42 h/week (which translates to 6 h/person-day since we do not differentiate weekdays and weekends), students spend 8 h at school (i.e. 5.7 h/person-day accounting for the weekends), and outpatient visits last 1 h (i.e. 0.7 h/person-day if 0 visits are assumed at weekends).

We also need to assign a fraction of time that people spend outdoors or in travelling/commuting. According to the Federal Statistical Office, about 80% of employed persons in Switzerland commute to work with an average trip time length of 29 minutes (one way).[13] Diffey (2011) tried to estimate typical times per day spent outdoors (including in transit on a bike or motorcycle) during the summer season, by combining data from different studies and countries. His analysis yielded estimates of 1.43 h and 2.38 h per day for weekdays and weekends respectively. One of the studies considered included a small sample from Switzerland (Basel), for which a mean time spent outdoors of 2.1 h was assessed for the months of January and December. Klepeis et al. (2001) present a survey conducted in the US on the time spent on different activities. In general, they find mean estimates of time spent outdoors and in a vehicle of 109 and 79 minutes respectively (3.1 h in total). On the basis of the above, we decided to assume 2.5 hours/person-day spent outdoors/commuting.

We then split these activities (employment, school, hospitalisations, medical visits, outdoors/commuting) into each of the three 'day', 'night', 'transit' time intervals as per Table 8.2. The estimates given in these tables are set through qualitative interpretation of literature data, such as those provided by Klepeis et al. (2001), referring to US data, as well as our judgement and experience.

Table 8.2. Distribution of time by activity

Time interval	Outdoor/transit [%] (time = 2.5 h /person-day)	Employees [%] (time = 6 h/person-day)	Students (time = 5.7 h/person-day)	Patients (time = 24 h/person-day)	Outpatients (time = 0.7 h/person-day)
Night	7.5%	2.0%	0.0%	33.3%	0.0%
Day	55.0%	76.0%	100.0%	33.3%	80.0%
Transit	37.5%	22.0%	0.0%	33.3%	20.0%

The number of occupants in each given building in the exposure is then set for the 'night', 'day' and 'transit' time periods, as well as for a time-agnostic case. For each time period *tp*, the number of employees, students and patients (ANGMOD, SCHULMOD, HOS_PAT, HOS_OUTPAT), multiplied by the total duration of these activities (6 h, 5.7 h, 24 h, 0.7 h) and the time period percentage Pct_{tp} (2% / 76% / 37.5%, 0% / 100% / 0%, 33.3% / 33.3% / 33.3%, 0% / 80% / 20%), is first added up.

Since OpenQuake's event-based calculator, unlike the scenario calculator, cannot model occupant variability throughout the day, a fixed number of occupants was assigned to each building, as the average of the night, day and transit time periods. That number for each building *i* and for each time period *tp* is computed as follows:

---

[13] https://www.bfs.admin.ch/bfs/en/home/statistics/mobility-transport/passenger-transport/commuting.html (last accessed: 03/02/2023)

$$Transient\ occupants\ in\ bldg\ i\ for\ time\ period\ tp\ (TO_{tp}^i) = \quad ANGMOD^i \cdot \frac{6}{24} \cdot Pct_{tp,EMPL} +$$

$$HOS_{PAT}^i \cdot \frac{24}{24} \cdot Pct_{tp,PAT} +$$

$$HOS_{OUTPAT}^i \cdot \frac{0.7}{24} \cdot Pct_{tp,OUTPAT} +$$

$$SCHULMOD \cdot \frac{5.7}{24} \cdot Pct_{tp,STUD}$$

$$Residents\ present\ in\ bldg\ i\ for\ time\ period\ tp\ (RP_{tp}^i) =$$

$$EINWMOD^i \cdot \sum_{j=1}^{N}(EINWMOD^i - EINWMOD^i \cdot \frac{2.5}{24} \cdot Pct_{tp,OUTDOOR} - TO_{tp}^i)$$

$$/ \sum_{j=1}^{N}(EINWMOD^i)$$

$$No\ occupants\ for\ bldg\ i\ for\ time\ period\ tp = RP_{tp}^i + TO_{tp}^i$$

8.5.1.4   Building typology mapping schemes

Two alternative strategies for determining the building material and overall lateral load-resisting system (LLRS) classes are provided. The two options are used as separate logic tree branches in the ERM-CH23 framework.

In the first one, henceforth referred to as **RB** (rate-based), the LLRS is randomly sampled based on the prevalence of each LLRS. The latter is quantified by means of field surveys, carried out in the cities of Basel, Solothurn, Sion, Yverdon, Neuchâtel and Martigny, and detailed in Chapter 5. These datasets quantify LLRS prevalence in each city by two attributes, the construction period and the building height. The LLRS together with the number of storeys of each given building determine the building typology class, as per the taxonomy detailed in Section 5.2. The following rule was used for the random sampling of LLRS:

- Municipalities (communes) with population > 40,000 → Sampling based on Basel survey prevalence statistics;

- Solothurn, Sion, Yverdon, Neuchatel, Martigny municipalities → Sampling based on Solothurn, Sion, Yverdon, Neuchâtel and Martigny survey prevalence statistics respectively;

- Other municipalities with population < 40'000 → Sampling based on prevalence statistics obtained as average of the Solothurn, Sion, Yverdon and Neuchâtel surveys.

The second option, henceforth referred to as **RF** (random forest) has been described in Chapter 5. The RF algorithm takes as input the various database fields described in Chapter 4, and returns the assigned LLRS. The RF algorithm did not have a sufficient training sample size to predict infrequent building typologies, therefore certain LLRSs (M1, S, T) of the ERM-CH23 taxonomy would be absent from the second exposure branch. To avoid this, it was decided to keep the M1, S and T assignments from the RB branch, and only apply the RF mapping to the remaining buildings.

Finally, an 'industrial' building typology was assigned as a last step to buildings of industrial occupancy. Given that a lot of such buildings are used for administrative purposes, it was decided to randomly assign the 'industrial' building typology to 50% of the industrial occupancy buildings. The building typology assignment for the remaining 50% of industrial buildings followed the previous RB/RF rules.

8.5.2   Spatial aggregation

With more than 2 million individual buildings in the building inventory, it is necessary to perform a spatial aggregation of the exposure dataset, in order to overcome computational constraints. The use of an aggregated exposure is common practice in regional or portfolio risk analyses and has been studied by several authors (Bal et al., 2010; Bazzurro and Park, 2007; Dabbeek et al., 2021; Scheingraber and Käser, 2018). Different spatial resolutions were explored for the aggregation. Moreover, we examined two alternative approaches for performing the spatial aggregation. The first one, henceforth referred to as average amplification (AA), involved (1) placing all buildings within a grid cell at its centroid, (2) merging all buildings of a given typology/occupancy/postcode within a grid cell into one macro-asset, by totalling their values and occupants (the distinction by occupancy and postcode was made to allow a computation of risk by occupancy or postcode tag), and (3) defining the amplification factor (and intra-event sigma in the case of SAM) to be assigned at the grid cell centroid, as the average of the amplification (and sigma) values at the locations of all buildings in the grid cell (as obtained from the relevant site model maps). The second approach, henceforth referred to as the n-cluster approach (CL_n), which was in the end deemed preferable, is illustrated in Figure 8.5, and works as follows:

1. A K-means clustering algorithm is applied on the site parameters of the locations of all buildings within each cell. The parameters to be clustered are: (MIM) the amplification factors obtained from PGV, SA(0.3s) and SA(1.0s) proxies; (SAM) the amplification factors, site-to-site sigmas and single-station sigmas for SA(0.3s) and SA(0.6s). We opted for three clusters in the case of MIM and five clusters in the case of SAM (due to the higher number of parameters and the results of the performance evaluations shown below).

   In the case of MIM, a choice was made to define multivariable clusters, i.e. to cluster simultaneously all three maps in order to have a single exposure/site model rather than three different ones. This choice was backed by the very satisfactory reduction of aggregation errors, as illustrated later. In the case of SAM, the six parameters had to be jointly clustered since they are used together within one realisation.

2. The buildings belonging to each of the three (MIM) or five (SAM) clusters are placed near the cell centroid in adjacent locations (a few metres apart).

3. For each cluster, all buildings of a given typology/occupancy/postcode are merged into one macro-asset, by totalling their values and occupants (the distinction by occupancy and postcode was made to allow a computation of risk by occupancy or postcode tag).

4. The associated K-means cluster centroid site parameter values are assigned to the three or five aggregation locations.

Moreover, since aggregation also involves the merging of buildings into macro-assets, the loss ratio variability across all aggregated buildings is implicitly assumed as perfectly correlated. While some mild correlation is expected to be present, an extra step was taken to remove this effect. More precisely, we estimated vulnerability curves for macro-assets of 1, 4, 20 and 85 buildings and used them for macro-assets of 1, 2-9, 10-39 and ≥40 buildings. This was done as follows:

➢ Equal replacement value was assumed for all buildings comprising a macro-asset.

➢ For each intensity level:

  o For each of 2,000 simulations:

    ▪ The loss ratio is sampled 1/4/20/85 times, the single-building losses are added up to get the macro-asset loss, and then the macro-asset loss ratio is estimated and saved.

  o The coefficient of variation of the 2,000 macro-asset simulated loss ratios is computed to define the loss ratio aleatory distribution (Figure 8.6).

We refer to this aggregation approach as AGV. Figure 8.6 (left) shows a schematic illustration of the reduced uncertainty in macro-assets representing multiple buildings. In the middle and right panels, the quantiles and coefficient of variation of the loss ratio are shown for different macro-assets of the M5_L typology as an example.
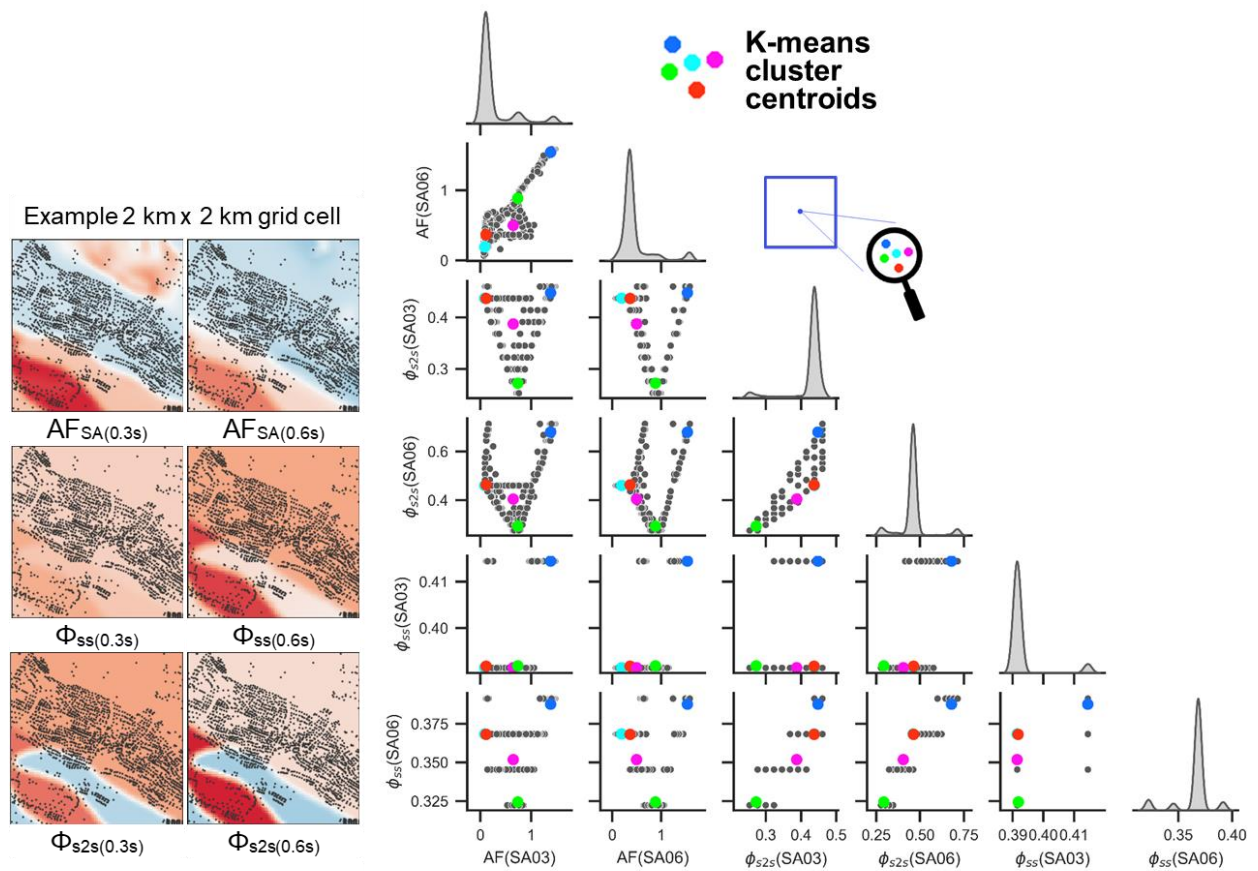
Figure 8.5. K-means clustering approach for minimising errors pertaining to mismatch of site conditions. Example referring to a 2 x 2 km gridcell.

To understand the impact of exposure aggregation, a number of sensitivity analyses were conducted. Results obtained with an aggregated exposure were compared with results obtained with a building-by-building exposure. To enable this analysis, we looked at individual cantons and used only a subset of the logic tree branches of the MIM and SAM models. More precisely, in the case of MIM, we used only the RF exposure branch and an average amplification branch. In the case of SAM, we again only used the RF exposure branch and only two GMPEs per tectonic regime, namely the ChiouYoungs2008SWISS01 and EdwardsFah2013Alpine75Bars for the Alpine regions and CauzziFaccioli2008SWISS08 and EdwardsFah2013Foreland50Bars for the Foreland regions.

Figure 8.7 (MIM) and Figure 8.8 (SAM) show the effect of exposure aggregation on structural/non-structural average annual loss (AAL) estimates by municipality for the cantons of Zurich and Valais. The various panels in Figure 8.7 show the errors obtained when different aggregation strategies were used. More precisely, in the case of MIM, the panels refer to aggregation with the (1) AA approach on a 1 x 1 km grid, (2) CL₃ approach on a 2 x 2 km grid, (3) CL₃ + AGV approach on a 2 x 2 km grid. In the case of SAM, the panels refer to aggregation with the (1) AA approach on a 1 x 1 km grid, (2) CL₃ approach on a 2 x 2 km grid, (3) CL₃ + AGV approach on a 2 x 2 km grid, (4) CL₅+ AGV approach on a 2 x 2 km grid.
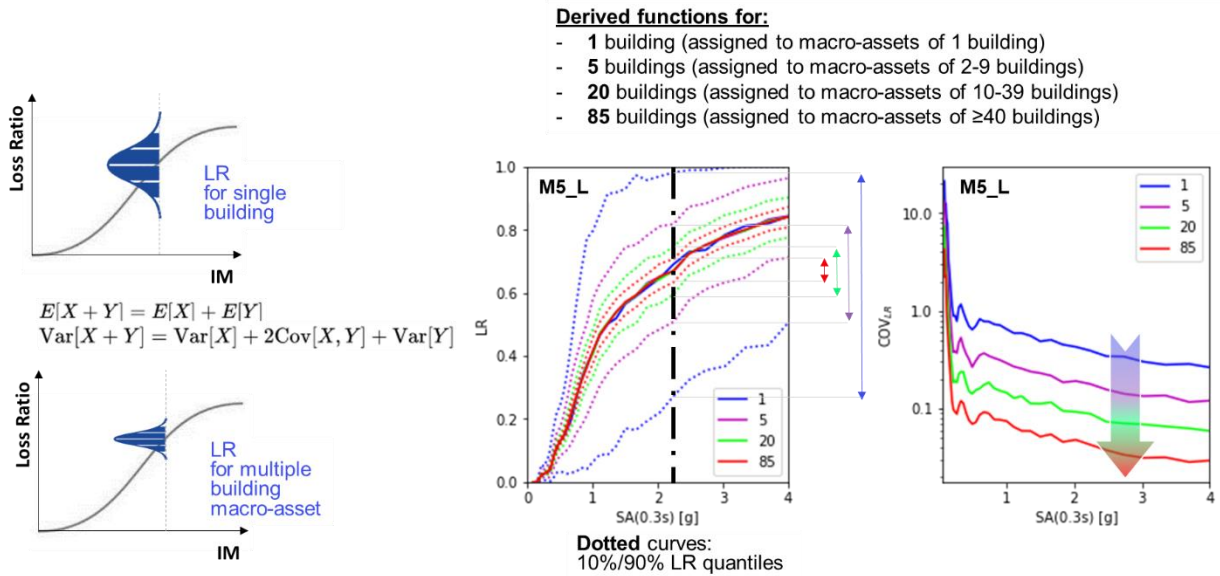
Figure 8.6. Illustration of vulnerability aggregation with typology M5_L used as an example.
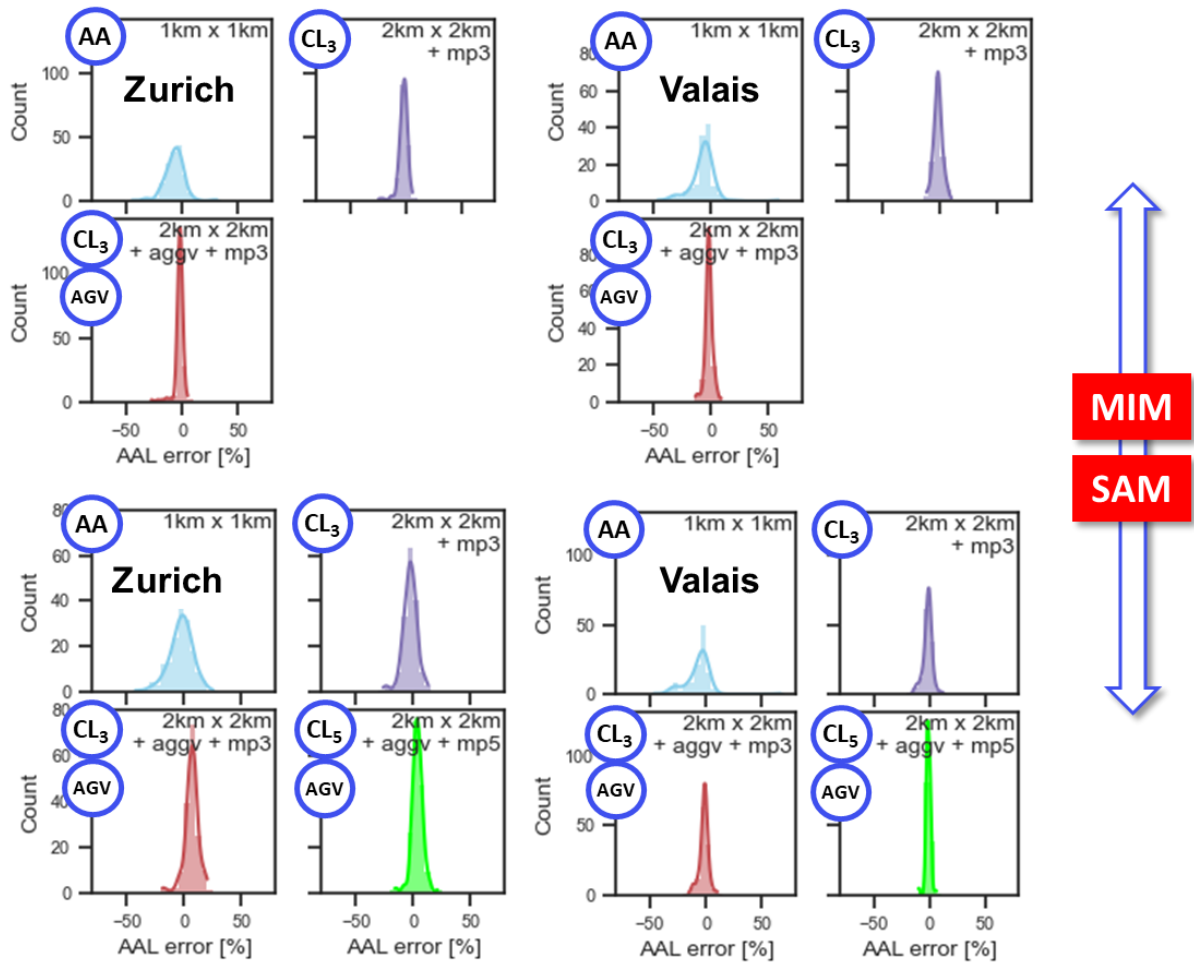
Figure 8.7. Effect of exposure aggregation on structural/non-structural AAL by municipality for the cantons of Zurich and Valais in the case of MIM (top) and SAM (bottom). The aggregation resolution is indicated within the panels. The blue circles indicate the aggregation approach: AA stands for average amplification, CL$_n$ for n K-means clusters, AGV for aggregated vulnerability.

The average amplification approach on a 1 km x 1 km grid provides a good compromise between efficiency and accuracy, with errors limited to <20% for most municipalities. As others have found (Dabbeek et al., 2021), the errors are even smaller at higher spatial scales, i.e. at the cantonal and especially at the country level. However, using the CL_n approach on a 2 x 2 km grid greatly limits any errors at essentially the same computational cost.

We also investigated the impact of the exposure aggregation on loss exceedance curves. Figure 8.9 (MIM) and Figure 8.10 (SAM) show the effect of exposure aggregation on structural/non-structural losses for specific return periods by municipality. As expected, the errors generally show a trend of underestimation for short return periods and overestimation for longer ones. This is a result of the implicit correlation of (1) ground motion and (2) loss ratio realisations among the aggregated buildings. In the case of SAM, the errors are larger, likely as a result of the larger aleatory variability of the ground motion, which follows a lognormal distribution (heavier tail, skewed) and is truncated at 2 sigmas, as opposed to the macroseismic intensity Gaussian distribution that is truncated at 1 sigma. Note that in the building-by-building analysis used as a benchmark here, neither the spatial correlation of ground motion residuals nor any vulnerability correlation were modelled. Therefore, to some extent, the introduction of some correlation is even desirable (Bazzurro and Park, 2007).

When the AGV approach is used, the aforementioned trend is removed to some extent, especially in MIM where the mismatch compared to the building-by-building case becomes minimal. In SAM, some mismatch remains due to the importance of the implicit ground motion correlation, but it mostly affects the low loss range and to some extent might even be desirable as explained above. Following this analysis, it was decided to follow the CL_3+AGV and CL_5+AGV approaches for MIM and SAM respectively.
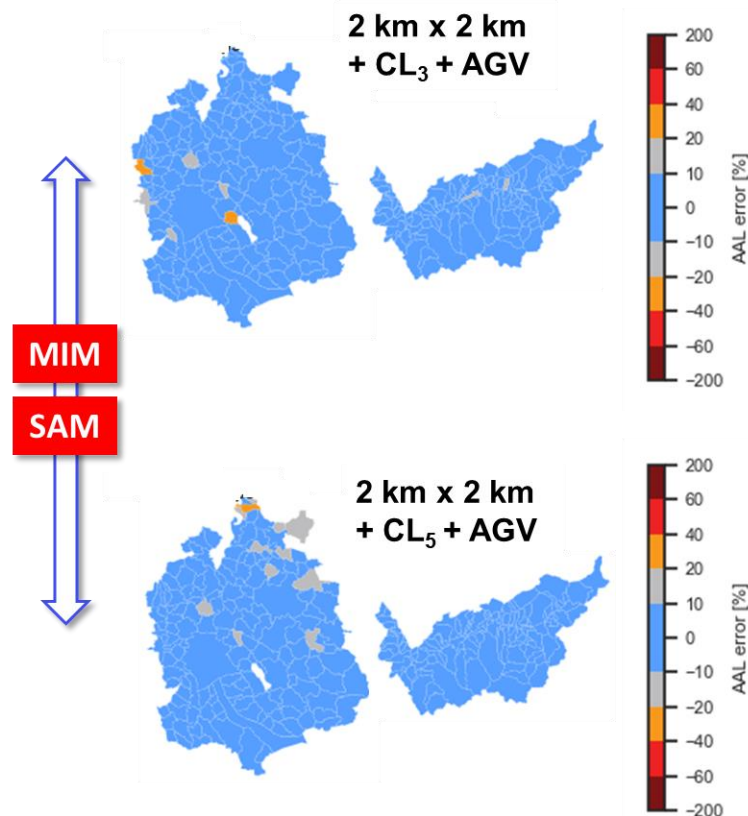
Figure 8.8. Maps of the effect of exposure aggregation on structural/non-structural AAL by municipality for the cantons of Zurich and Valais in the case of MIM (top) and SAM (bottom). The aggregation here was done on a 2 x 2 km grid with three (MIM) and five (SAM) clusters, along with aggregated vulnerability.
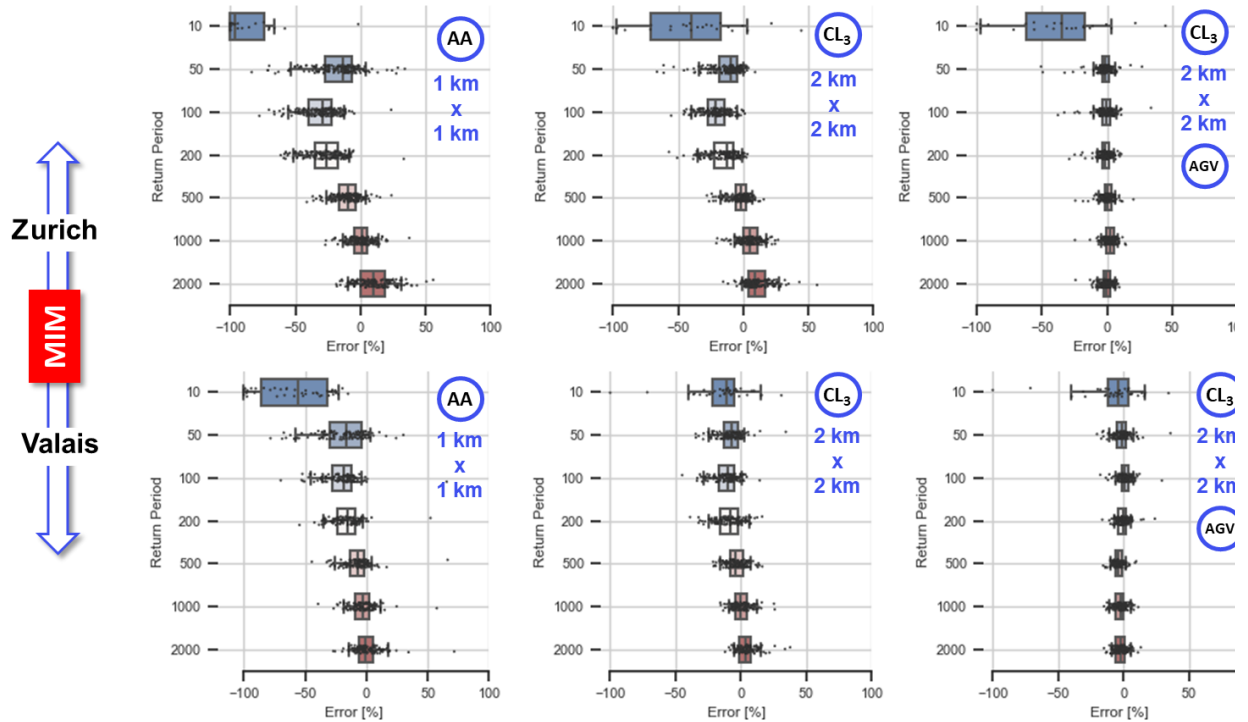
Figure 8.9. Effect of exposure aggregation with different methods on structural/non-structural loss exceedance curves by municipality for the cantons of Zurich (top) and Valais (bottom) in the case of MIM. The whiskers refer to 5%/95% quantiles. Municipality data points with loss < CHF 2,000 were omitted from the plot.
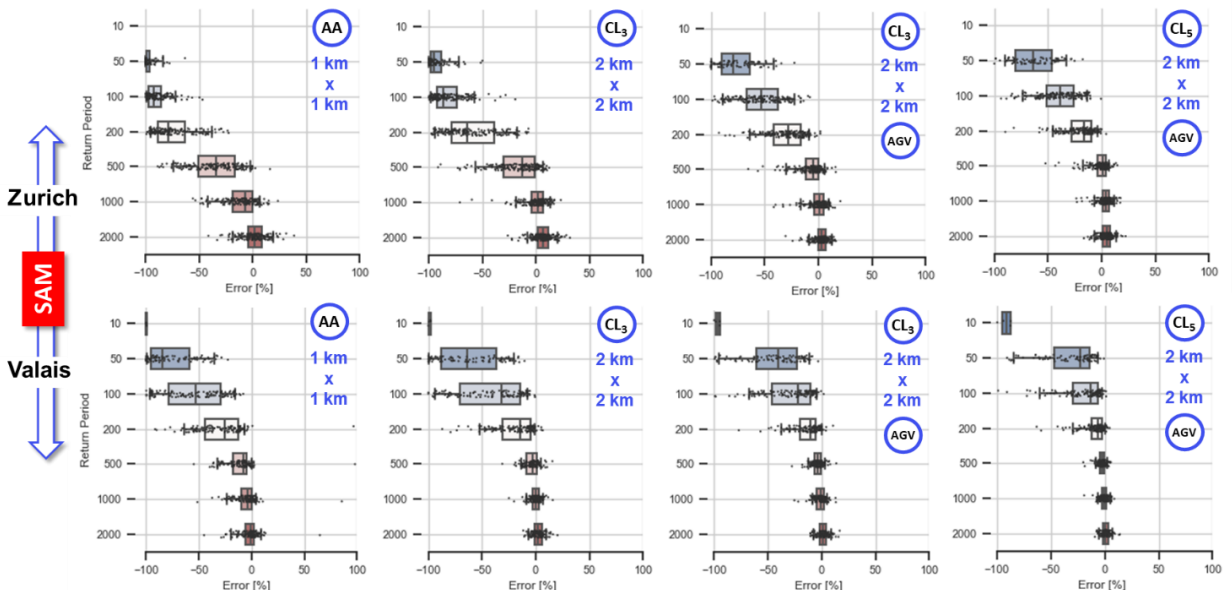
Figure 8.10. Effect of exposure aggregation with different methods on structural/non-structural loss exceedance curves by municipality for the cantons of Zurich (top) and Valais (bottom) in the case of SAM. The whiskers refer to 5%/95% quantiles. Municipality data points with loss < CHF 2,000 were omitted from the plot.

8.5.3   Summary of ERM-CH23 exposure model

In total, the ERM-CH exposure model contains around 2.25 million buildings, with a total structural/non-structural and content replacement value of about CHF 2,904 billion and CHF 837 billion respectively. Figure 8.11 shows the distribution (in logarithmic y-axis) of replacement cost and occupants among the 2.25 million buildings.
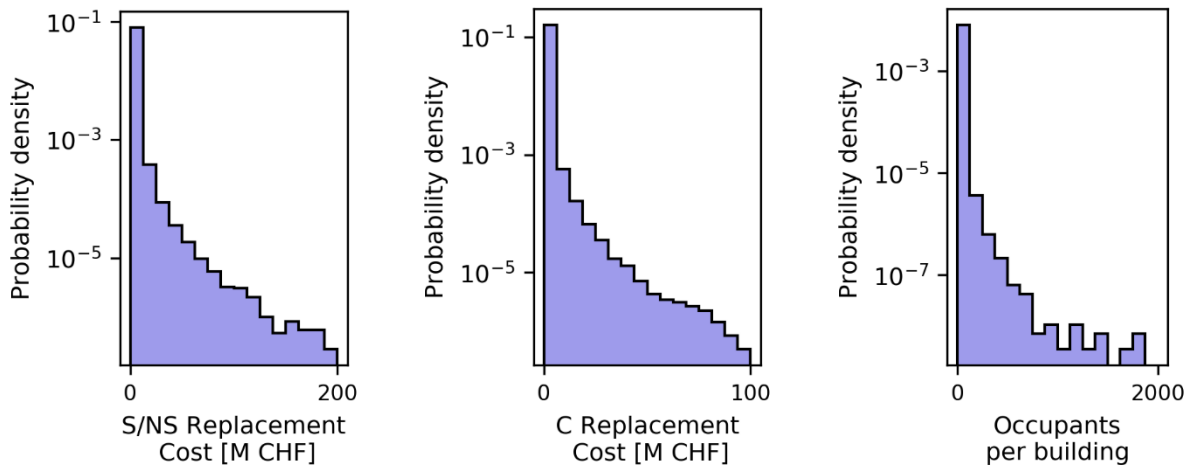
Figure 8.11. Left: distribution of structural/non-structural replacement cost among buildings; middle: distribution of content replacement cost among buildings; right: distribution of assigned occupants among buildings.

Figure 8.12 shows the composition of the building stock in terms of height and construction period. It can be seen that a large proportion of the buildings were constructed between 1946 and 1990. A significant number also date from the <1919 and 1919-1945 periods, indicating a notable portion of old buildings. The vast majority of Swiss buildings are low-rise with three or fewer storey.
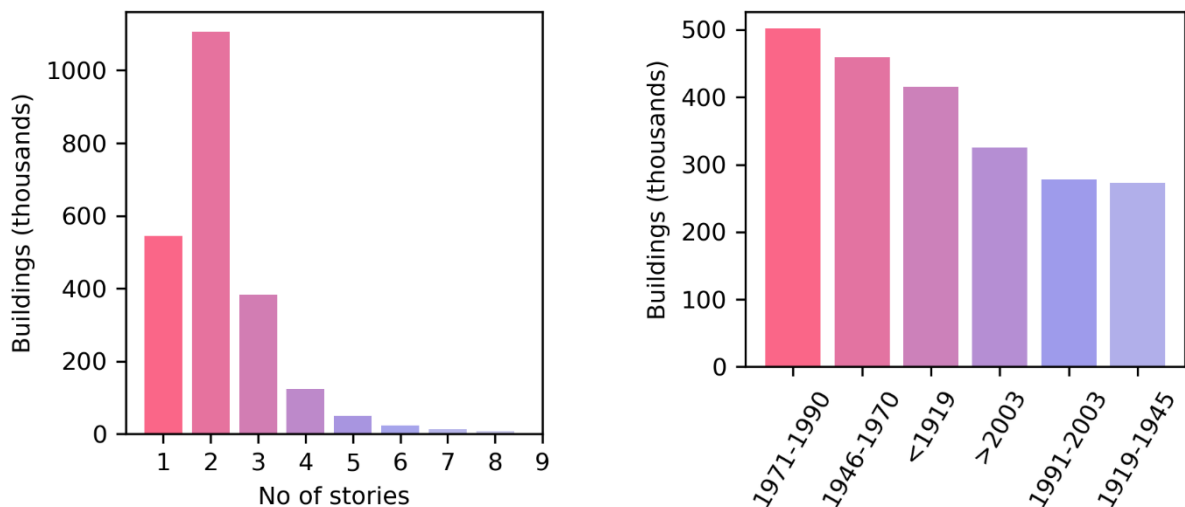
Figure 8.12. Left: number of buildings by number of storeys; right: number of buildings by construction period.

Spatial heterogeneities in the construction period and building height are demonstrated in Figure **8.13** and Figure 8.14. In the former, each panel shows the spatial variation of the percentage of buildings built within a certain time period at each location. While the significance of individual grid cells in mountainous and sparsely populated areas should not be overinterpreted, we do see some notable differences between different parts of the country, especially when it comes to buildings built before 1919, as well as between 1919 and 1945. This highlights the added value of using a detailed geolocalised building database. The frequency of buildings constructed in different time periods can also be seen at the cantonal level in Figure 8.16.
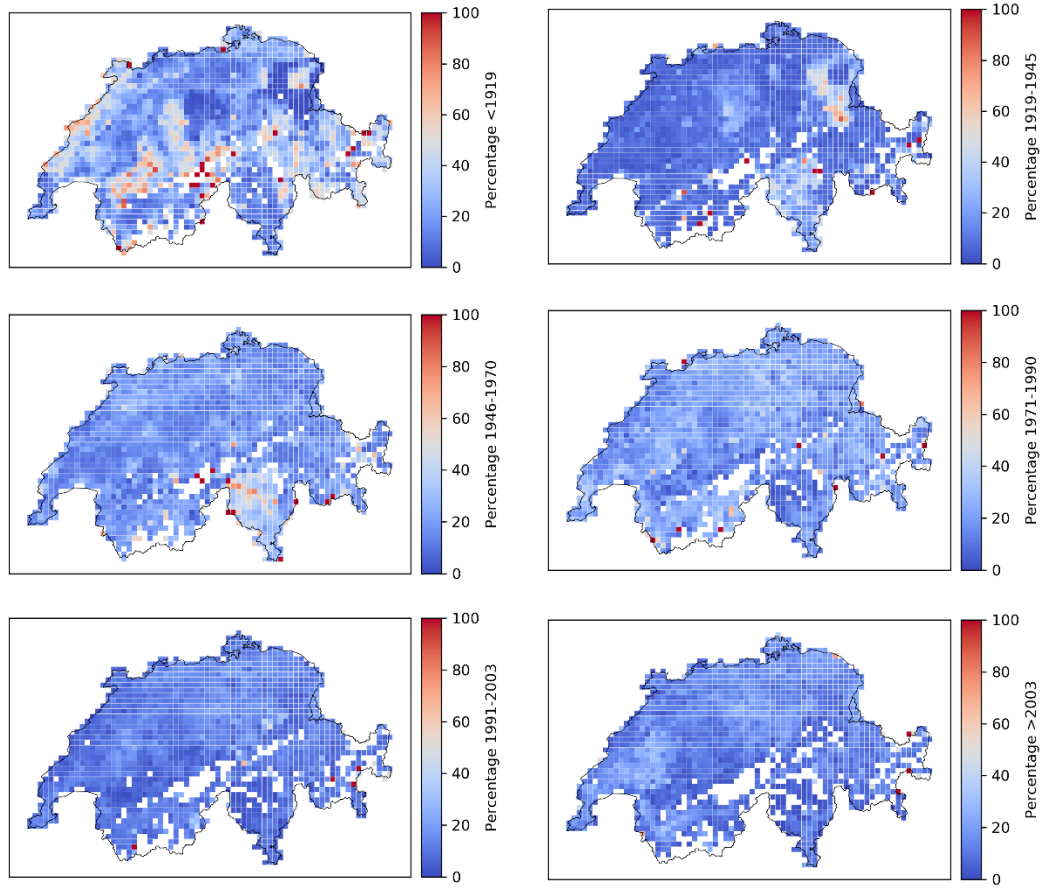
Figure 8.13. Spatial variation of building construction period.
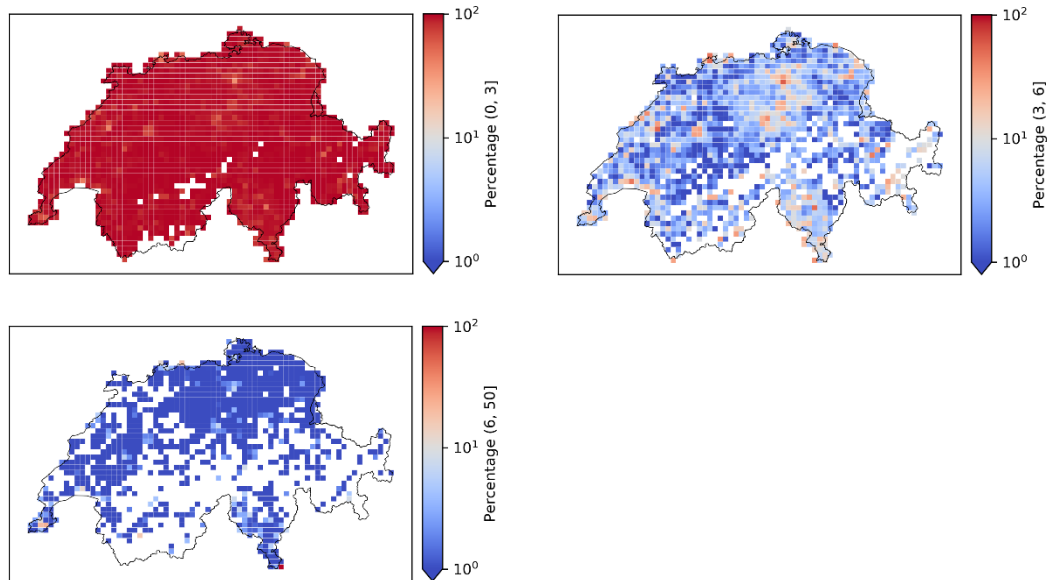
Figure 8.14. Spatial variation of building height; top left: ≤3 storeys, top right: 4-6 storeys, bottom left: ≥7 storeys.

With respect to the building height, Figure 8.14 shows the predominance of low-rise (1-3 storeys) buildings throughout the country. It is also interesting to note the higher proportion of mid- and high-rise buildings in urban centres (Zurich, Geneva, Basel, etc).

Buildings with residential function, as expected, make up the biggest share in terms of value, number and occupants (Figure 8.15) in the exposure. Industrial buildings are the fewest in number, while agricultural buildings are assessed as the lowest in value and occupants. Figure 8.16 shows the proportion of buildings of different occupancy in each canton. While residential buildings predominate throughout the country, some insights can be gained, e.g. the apparent increased relative frequency of agricultural buildings towards the south of Switzerland.

a.   **b.**   **c.**   **d.**
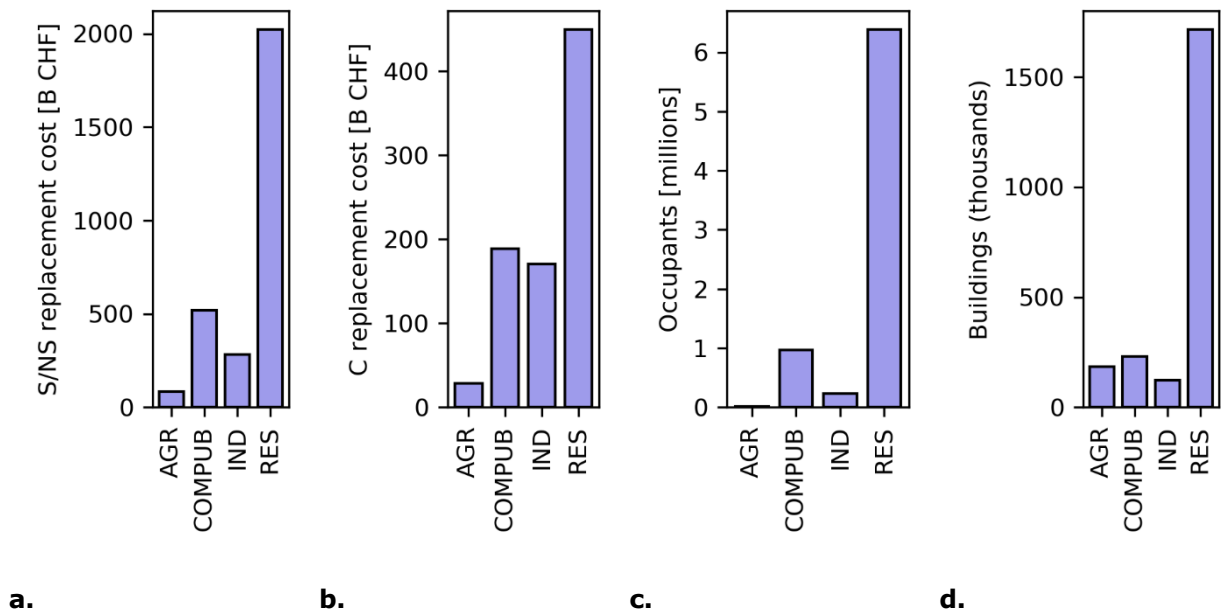
Figure 8.15. a. total structural/non-structural replacement cost by occupancy type; b. total content replacement cost by occupancy type; c. total number of occupants by occupancy type; d. total number of buildings by occupancy.
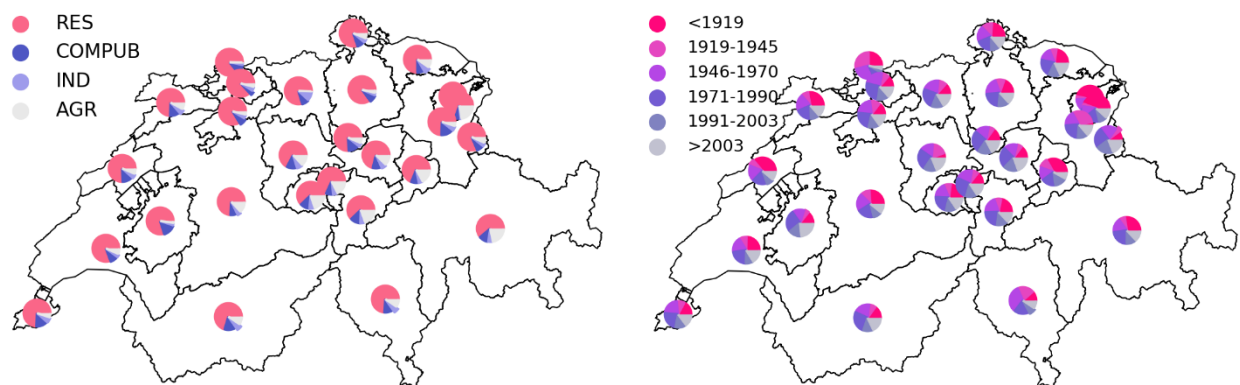
Figure 8.16. Left: prevalence of buildings of different occupancy types in each canton; right: prevalence of buildings constructed in different time-periods in each canton.

The spatial distribution of buildings, value and occupants is presented in Figure 8.17 by canton and on a 5 km x 5 km grid. Bern appears to be the canton with the most buildings, while Zurich has the most occupants and highest replacement value. The grid plots illustrate the distribution of buildings and occupants in the major urban centres such as Zurich, Geneva, Basel and Bern.
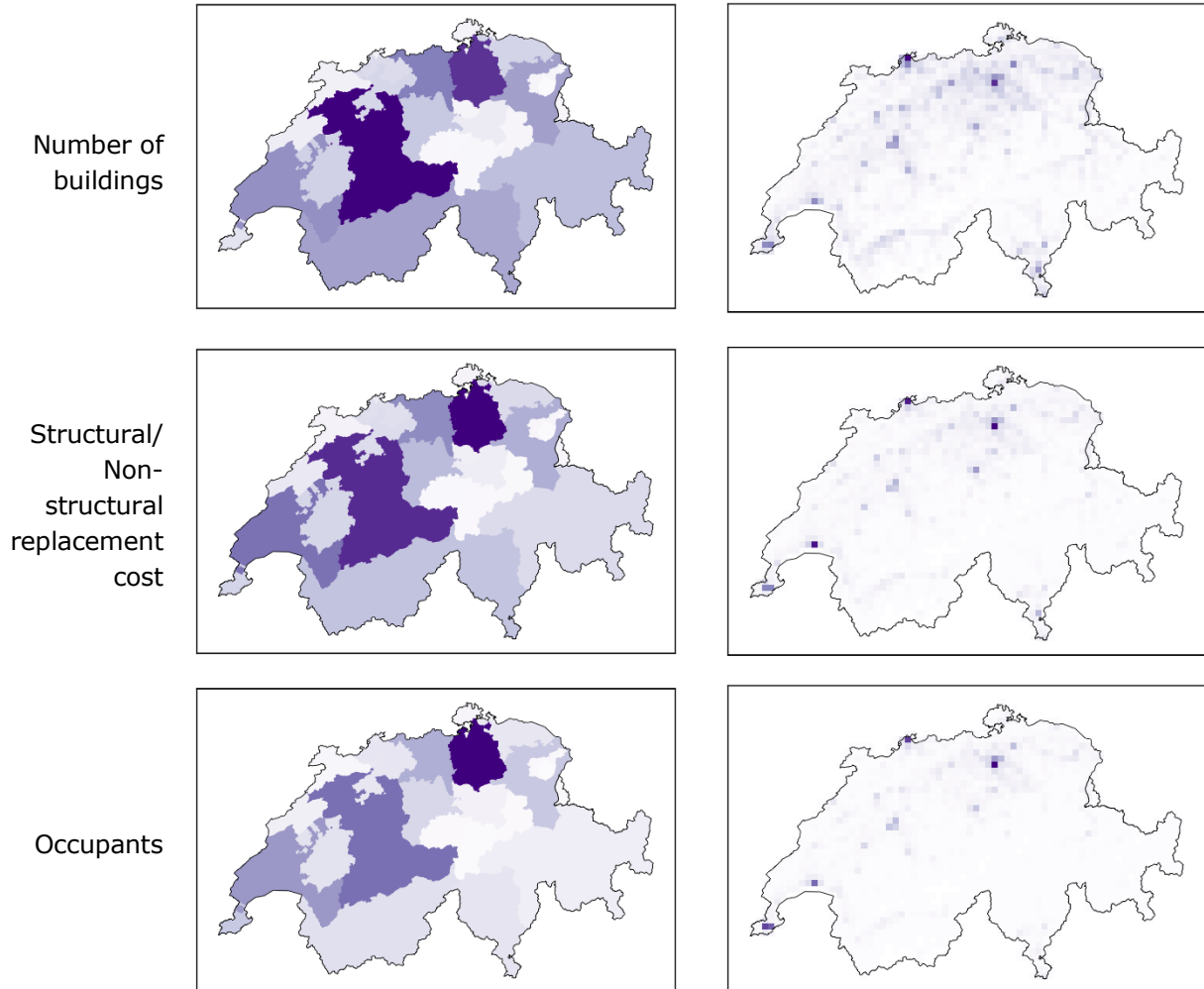
Figure 8.17. Spatial distribution of buildings, structural/non-structural replacement cost and occupants.

Last but not least, we look at the prevalence of different building typologies in the ERM-CH exposure model. Figure 8.18 and Table 8.3 show the assigned prevalence of different typologies as a result of the RB and RF mapping schemes. Overall, masonry buildings comprise the largest portion of the building stock. The M6 and M3 masonry types (see taxonomy in Chapter 5) are the most frequent, with M5 also present in significant numbers, especially in smaller municipalities. Reinforced concrete buildings comprise about one third of the exposure, with a somewhat greater frequency in smaller municipalities compared to larger urban centres. The differences between the two RB and RF mapping schemes are explored in Figure 8.18. Overall, RF assigns more M5 and less RCW LLRS, although the differences are starker locally.
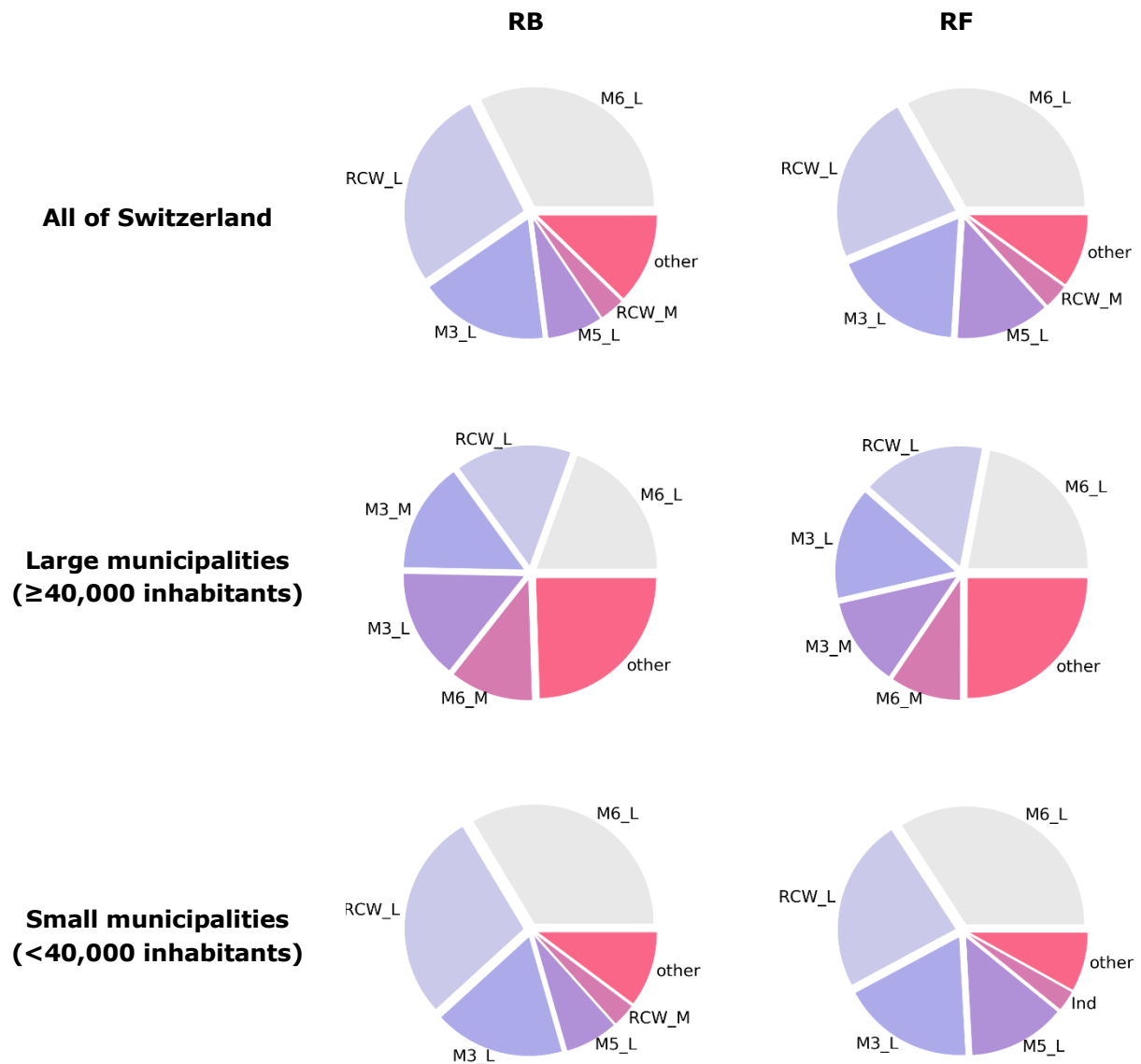
Figure 8.18. Distribution of building typologies in RB and RF exposure models. The pie charts show the five most prevalent typologies in each case, whit the rest grouped under 'other'.

Table 8.3. Prevalence of different typologies in RB and RF exposure models.

RB		RF	
Typology	Percentage	Typology	Percentage
Ind	2.7%	Ind	2.7%
M1_L	0.4%	M1_L	0.4%
M1_M	0.0%	M1_M	0.0%
M3_H	0.2%	M3_H	0.2%
M3_L	17.4%	M3_L	17.8%
M3_M	2.2%	M3_M	2.3%
M4_H	0.0%	M4_H	0.0%
M4_L	1.7%	M4_L	0.1%
M4_M	0.3%	M4_M	0.2%
M5_H	0.0%	M5_H	0.0%
M5_L	7.4%	M5_L	12.7%
M5_M	0.2%	M5_M	0.1%
M6_H	0.2%	M6_H	0.1%

M6_L	32.4%	M6_L	33.2%
M6_M	2.4%	M6_M	2.6%
RCW_H	0.5%	RCW_H	0.6%
RCW_L	27.2%	RCW_L	23.1%
RCW_M	3.3%	RCW_M	3.3%
RCmix_H	0.0%	RCmix_H	0.0%
RCmix_L	0.8%	RCmix_L	0.0%
RCmix_M	0.1%	RCmix_M	0.0%
S	0.1%	S	0.1%
T	0.5%	T	0.5%
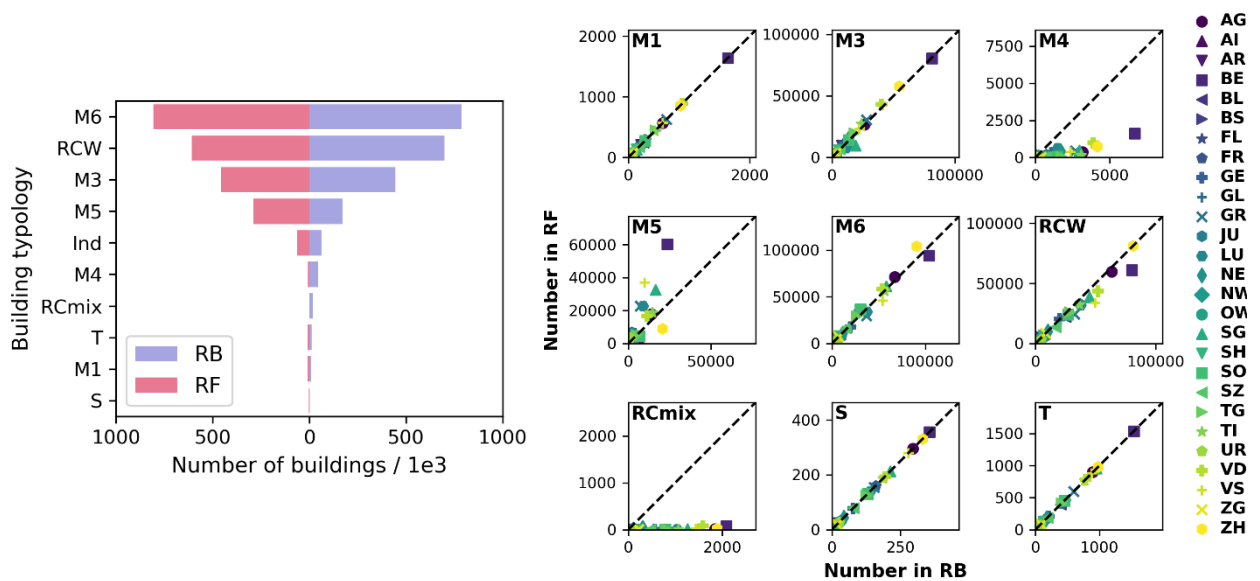
Figure 8.19. Left: comparison of number of buildings of each LLRS in RB and RF exposure models; right: Comparison of number of buildings of each LLRS in RB and RF exposure models by canton.

8.6   Vulnerability modelling

The fragility models (described in Chapter 5) and consequence models (described in Chapter 6) were convolved to derive vulnerability functions, i.e. functions that relate ground shaking intensity to loss ratio. The consequence models referring to structural/non-structural loss and contents loss are probabilistic, i.e. the loss ratio associated with each damage state is modelled as a random variable. To compute the structural/content loss vulnerability function for a given building typology from its fragility and consequence models, a Monte-Carlo simulation approach is employed as follows:

For each intensity level:

For each one of N=2,000 simulations:

> Extract from the fragility functions the probabilities of being in each particular damage state (DS0-DS5).

> Sample a damage state according to the probability mass function obtained in the previous step.

> Sample a loss ratio value from the consequence model distribution associated with that damage state. In the case of contents loss, a beta distribution is defined based on the

mean value and coefficient of variation given in the consequence model. In the case of structural loss, the non-parametric distribution, obtained from the procedure described in Chapter 6, is used to sample from.

> Save the loss ratio.

> Compute the mean loss ratio for the given intensity and its associated coefficient of variation.

If on the other hand the consequence model is deterministic (as is the case for the fatality, injury and displaced population models), the following procedure is followed:

> For each intensity level:

> Extract from the fragility functions the probabilities of being in each particular damage state (DS0-DS5).

> Compute the mean loss ratio for the given intensity by adding up the products of each damage state probability and associated mean loss ratio for that damage state.

The collection of vulnerability curves for all building types and loss variables is presented in Figure **8.20** in terms of macroseismic intensity and in Figure 8.21 in terms of spectral acceleration. The fatality curves are also shown individually in Figure 8.22 and Figure 8.23 with rescaled axes for better clarity.

In the case of structural and content loss, the aleatory variability of the loss ratio is modelled as a beta distribution within the OpenQuake computational workflow, while in the case of human losses no aleatory variability is considered. Figure 8.24 and Figure 8.25 show the beta distribution 10% and 90% quantile loss ratio curves along with the mean estimates for structural and content loss.

Given the significant variability of the loss ratio, the coefficient of variation was cut to zero for low intensities (up to I_{EMS98} = 6.0 and up to 0.10 g/0.06 g for SA(0.3s)/SA(0.6s)), in order to avoid the occasional sampling of unrealistically high loss ratios in areas far away from the earthquake rupture, as a consequence of the chosen mathematical modelling.
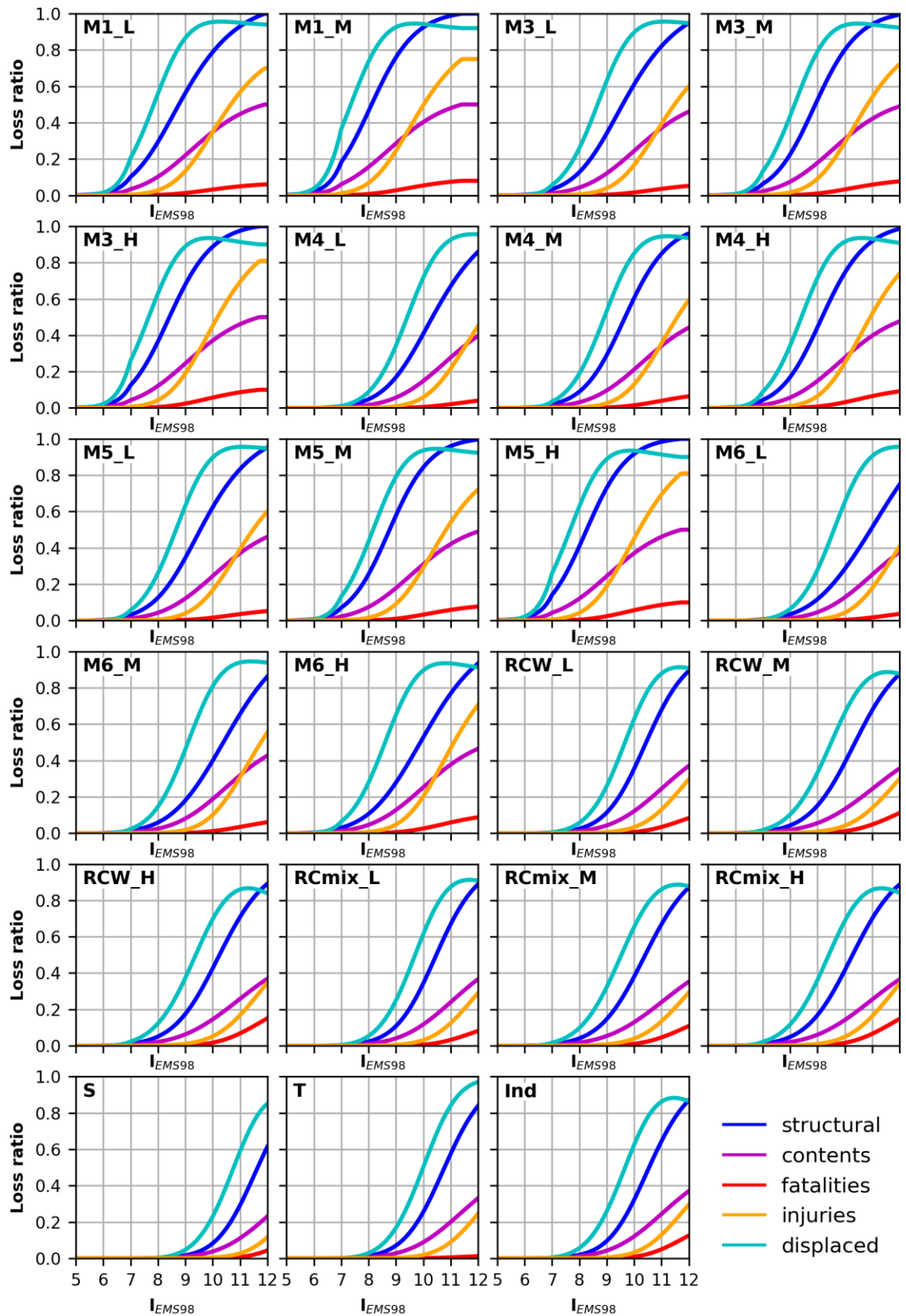
Figure 8.20. Mean vulnerability curves in terms of macroseismic intensity for structural loss, contents loss, fatalities, injuries and displaced population.
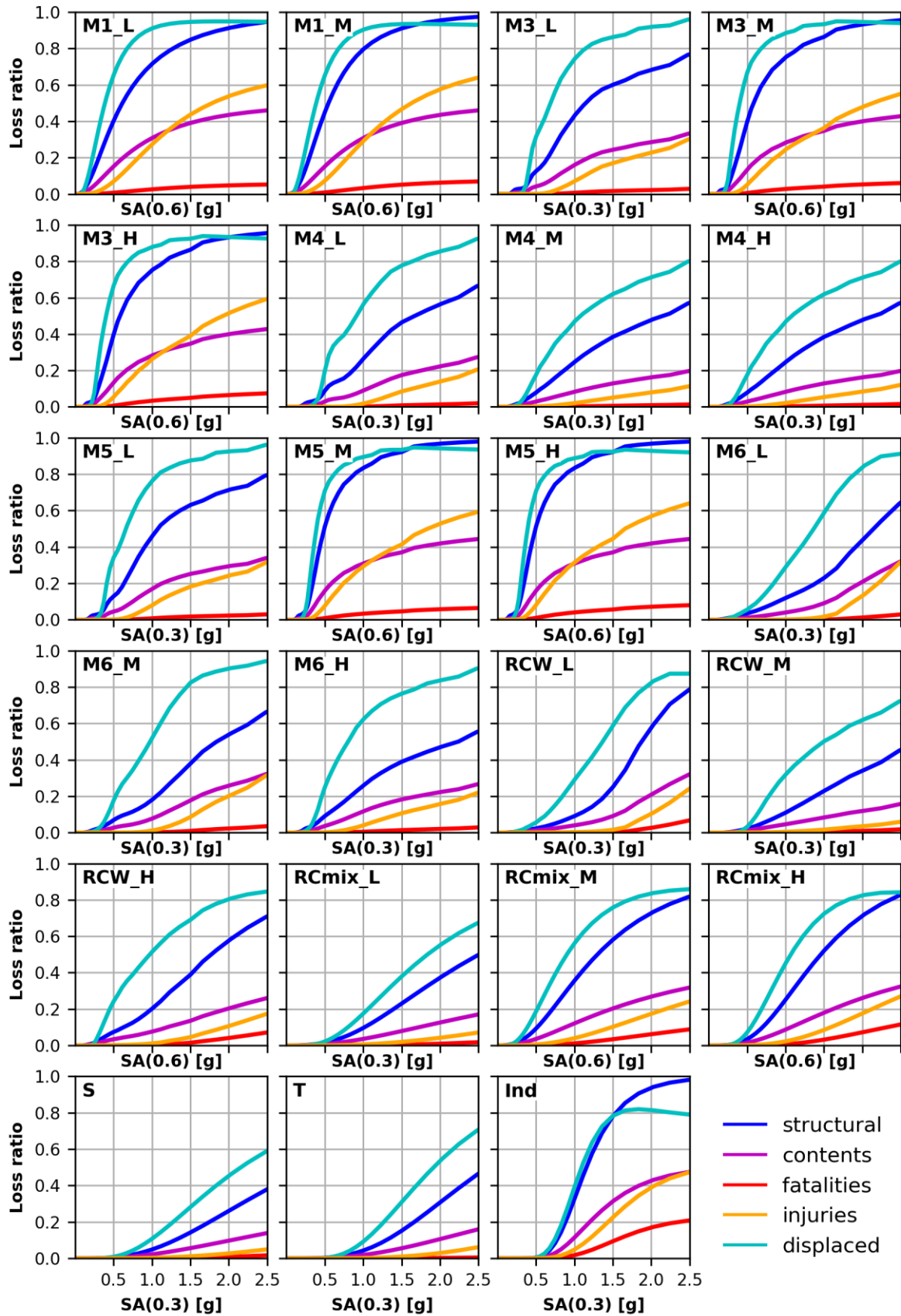
Figure 8.21. Mean vulnerability curves in terms of spectral acceleration at 0.3 s or 0.6 s for structural loss, contents loss, fatalities, injuries and displaced population.
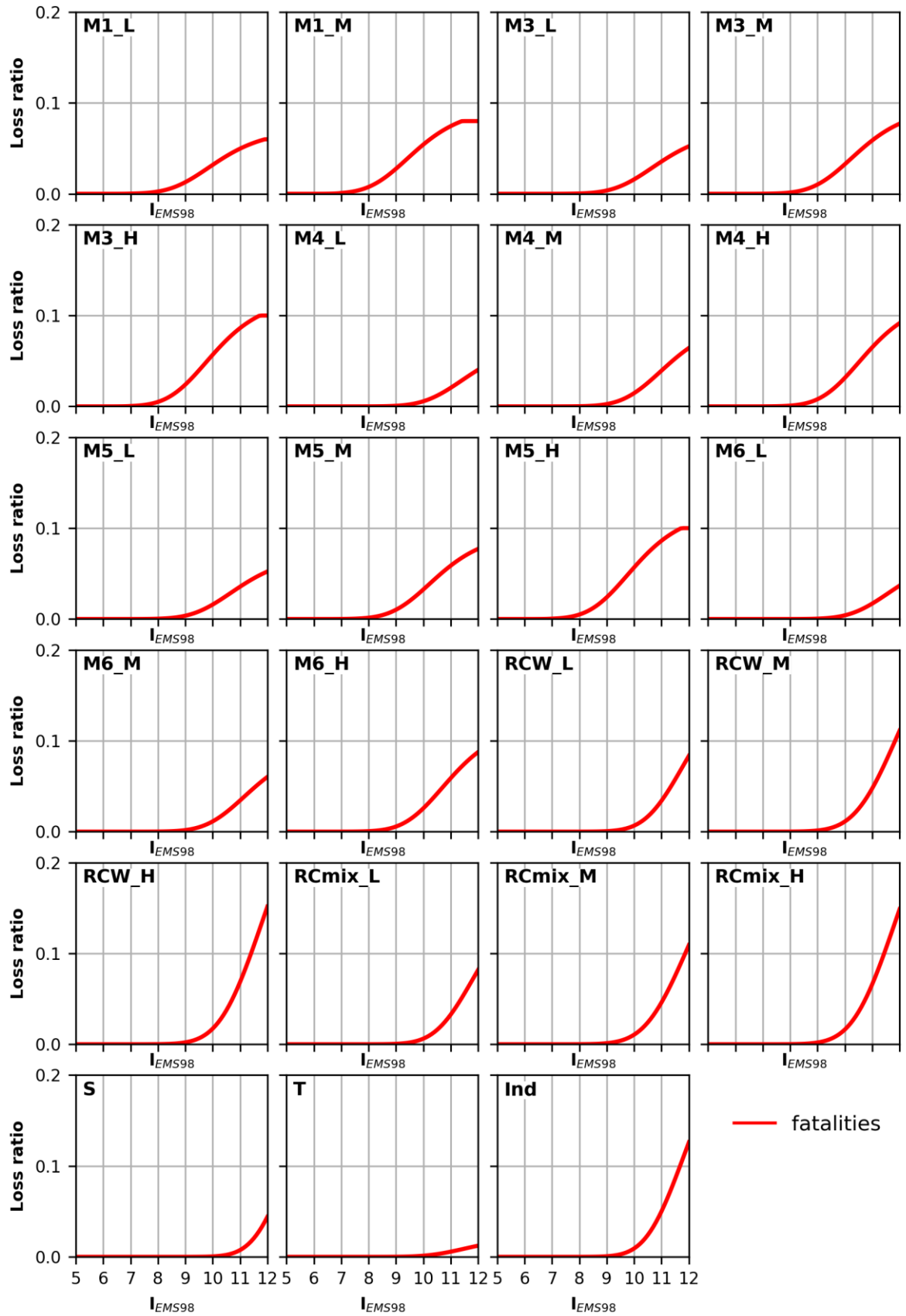
Figure 8.22. Mean fatality vulnerability curves in terms of macroseismic intensity.
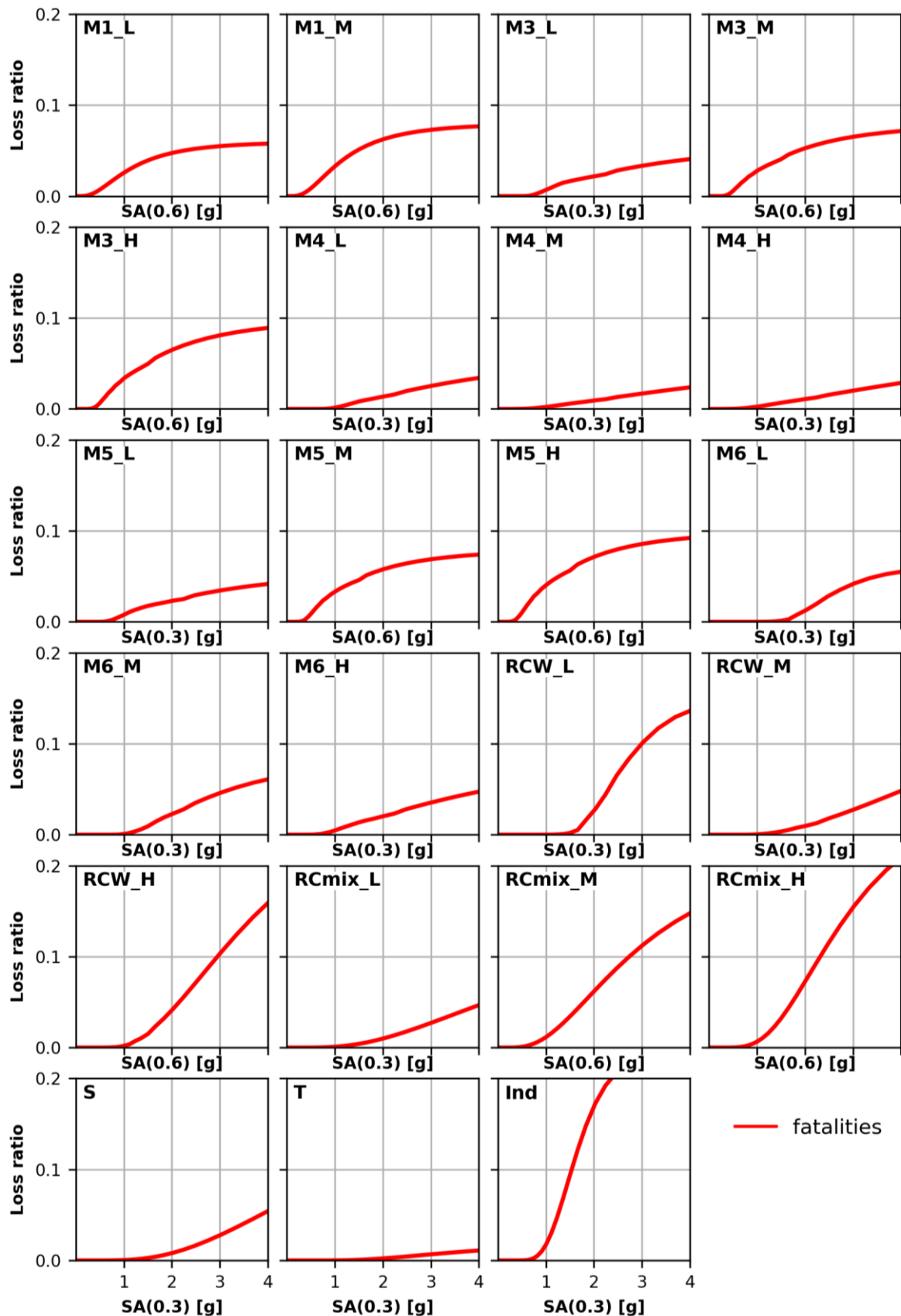
Figure 8.23. Mean fatality vulnerability curves in terms of spectral acceleration at 0.3 s or 0.6 s.
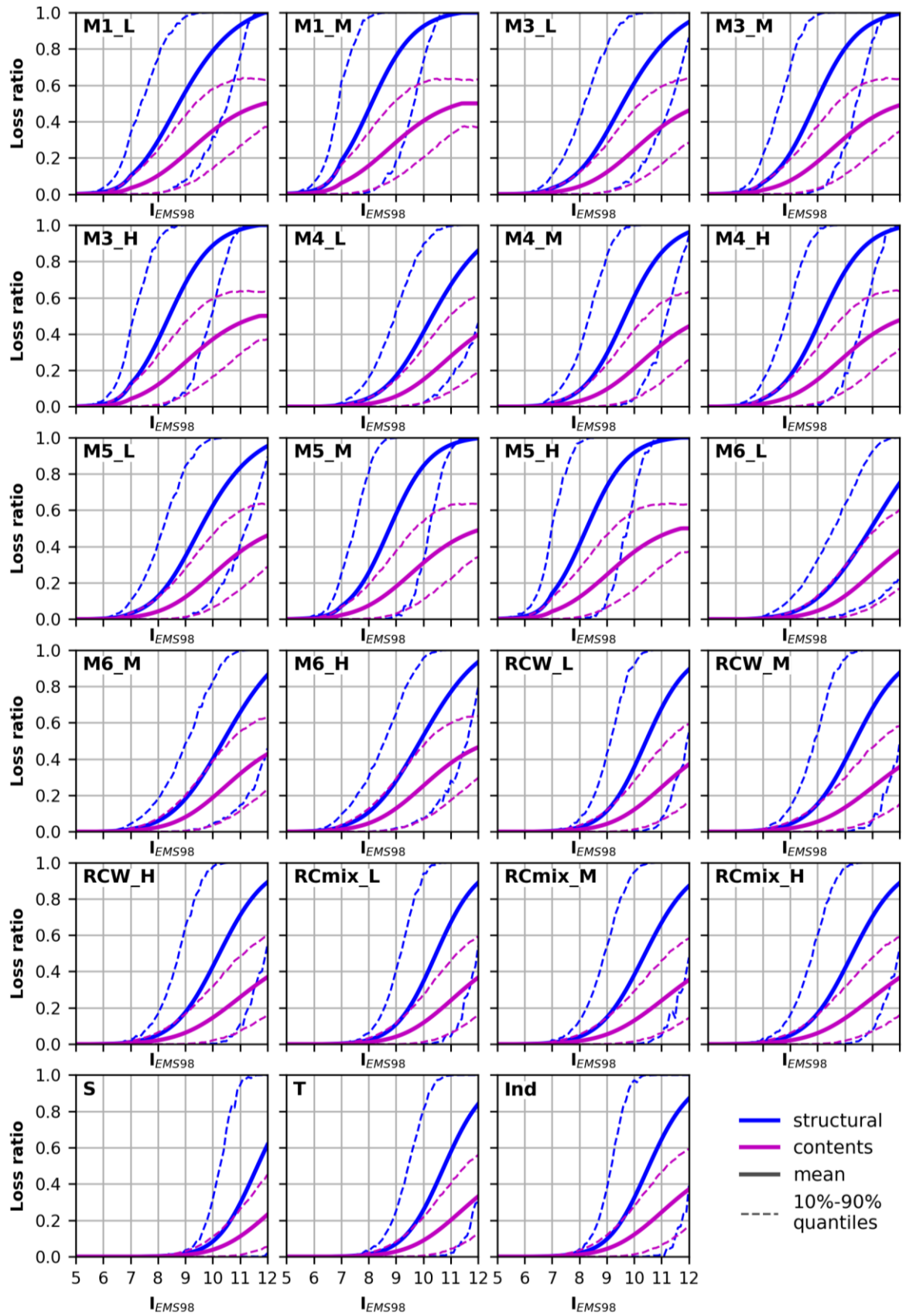
Figure 8.24. Mean and quantile structural and content loss vulnerability curves in terms of macroseismic intensity.
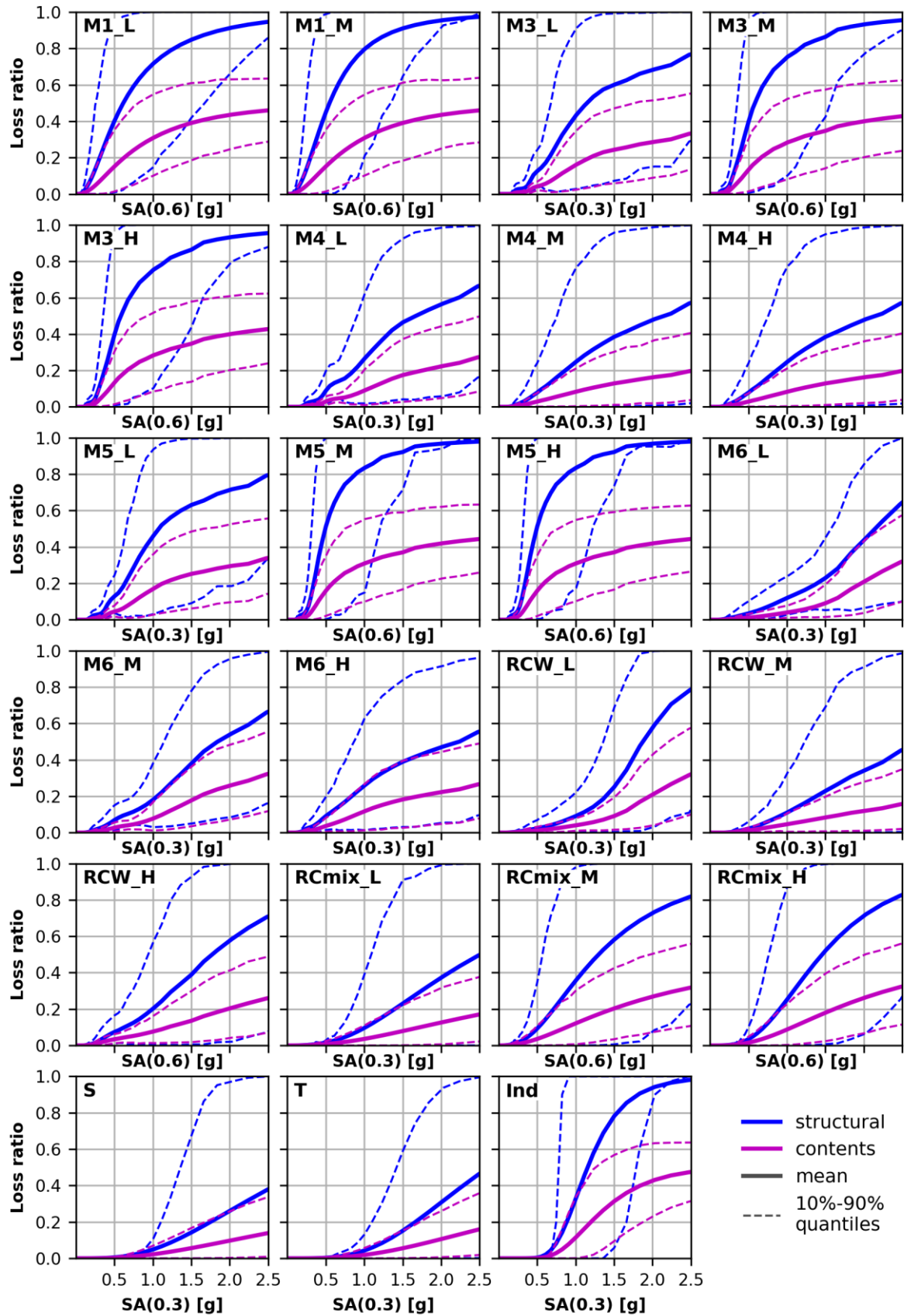
Figure 8.25. Mean and quantile structural and content loss vulnerability curves in terms of spectral acceleration at 0.3 s or 0.6 s.

8.7   Risk analysis configuration

As mentioned at the beginning of the chapter, two types of analyses, namely event-based risk and scenario risk/damage analyses, are carried out. Figure 7.2 in the previous chapter presents the overall model logic tree that branches into the two main submodels (the macroseismic intensity model MIM and the spectral acceleration model SAM) and then into different GSIM, amplification and exposure branches as described earlier on. In total, the MIM part of the model features 24 logic tree branches (4 IPEs x 3 amplification models x 2 exposure models), while the SAM part features 165,888 branches (16x16x18x18 GMPEs for 4 tectonic regimes x 2 exposure models).

As regards the IPE logic tree, the weights were assigned as follows:

- ECOS-09 Fixed depth: 0.3
- ECOS-09 Variable depth: 0.2
- Bindi et al. (2011): 0.2
- Baumont et al. (2018): 0.3

As outlined in the relevant chapter, these IPEs performed better in explaining historical data. The weights were split 50/50 to IPEs derived from Swiss data (ECOS-09) and others. Then, we assigned somewhat larger weights to the ECOS-09 fixed depth model, since it performed better in explaining observations, and to the Baumont et al. model, since the use of the Bindi et al. IPE involved converting the magnitude type which is likely to induce some error.

For the GMPE logic tree, the GMPE logic tree of SUIhaz2015 and its weights were adopted without changes. Following the recommendations of their developers, the three amplification models in the case of MIM were assigned equal weights, while a preference was given to the RF exposure model with a 0.75, compared with 0.25 for RB. Finally, the weights assigned to MIM and SAM were set at 0.3 and 0.7 respectively.

For the event-based risk assessment, all 24 MIM branches are enumerated and 50,000 one-year-long stochastic catalogues are generated for each one of them. In contrast, since it is computationally unfeasible to process 165,888 SAM branches, 400 samples are drawn and 10,000 one-year-long stochastic catalogues are generated for each one of them.

In the case of scenario calculations, we enumerate all the branches and generate 50 realisations for each of the 24 MIM branches and 280 realisations for each of the 32 or 36 (depending on the tectonic regime) SAM branches. Given that the scenario rupture is specified, the SAM logic tree is simpler as the four alternative tectonic regime GSIM trees do not need to be combined.

References

Bal, I.E., Bommer, J.J., Stafford, P.J., Crowley, H., Pinho, R. 2010. The Influence of Geographical Resolution of Urban Exposure Data in an Earthquake Loss Model for Istanbul. Earthquake Spectra **26**(3), 619–634.

Bazzurro, P., Park, J. 2007. The Effects of Portfolio Manipulation on Earthquake Portfolio Loss Estimates. in *10th international conference on applications of statistics and probability in civil engineering*. Tokyo, Japan.

Dabbeek, J., Crowley, H., Silva, V., Weatherill, G., Paul, N., Nievas, C.I. 2021. Impact of Exposure Spatial Resolution on Seismic Loss Estimates in Regional Portfolios. Bulletin of Earthquake Engineering (0123456789).

Diffey, Brian L. 2011. An Overview Analysis of the Time People Spend Outdoors. British Journal of Dermatology **164**(4), 848–854.

Klepeis, N.E., William, C.N., Wayne, R.O., Robinson, J.P., Tsang, A.M., Switzer, P., Behar, J.V., Hern, S.C., Engelmann, W.H. 2001. The National Human Activity Pattern Survey (NHAPS): A Resource for Assessing Exposure to Environmental Pollutants. Journal of Exposure Science & Environmental Epidemiology **11**(3), 231–252.

Pagani, M., Monelli, D., Weatherill, G., Danciu, L., Crowley, H. Silva, V., Henshaw, P., Butler, L., Nastasi, M., Panzeri, L., Simionato, M., Vigano, D. 2014. OpenQuake Engine: An Open Hazard (and Risk) Software for the Global Earthquake Model. Seismological Research Letters **85**(3), 692–702.

Scheingraber, C., Käser, M.A. 2018. The Impact of Portfolio Location Uncertainty on Probabilistic Seismic Risk Analysis. Risk Analysis 2.

Silva, V. 2018. Critical Issues on Probabilistic Earthquake Loss Assessment. Journal of Earthquake Engineering **22**(9), 1683–1709.

9.   ERM-CH23 results

9.1   Introduction

This chapter presents the results obtained from the two envisaged types of analyses described in the previous chapter, i.e. the event-based probabilistic risk and the scenario risk/damage analyses.

9.2   Probabilistic risk assessment

9.2.1   Country-wide risk estimates

Table 9.1 reports the mean (over the epistemic uncertainty) AAL and AALR estimates obtained for each of the five loss types. ERM-CH23 yields a Switzerland-wide AAL of CHF 245 million and CHF 28 million in structural/non-structural and contents economic loss respectively, while the AAL for fatalities is estimated at 7.6. We observe that MIM yields larger (compared to SAM) AAL estimates for economic loss and displaced population, but smaller for fatalities and injuries.

Figure 9.1 presents the epistemic distribution of the AAL estimates. The contributions of MIM and SAM to the overall model uncertainty are shown in different colours. The area in the probability density plots corresponding to each model is dictated by the weight assigned to each of them, i.e. 0.3 for MIM and 0.7 for SAM. However, one can also discern the within-submodel range of uncertainty. For instance, MIM estimates appear more uncertain (more spread out and less peaked) compared to SAM for economic loss and displaced population, while the opposite is true for fatalities and injuries.

Table 9.1. Country-wide mean average annual loss estimates for each of the five considered loss types.

	MIM		SAM		Weighted average	
	AAL	AALR [‰]	AAL	AALR [‰]	AAL	AALR [‰]
Structural	CHF 295.8 M	0.10	CHF 223.8 M	0.077	**CHF 245.4 M**	**0.084**
Contents	CHF 32.1 M	0.04	CHF 26.3 M	0.031	**CHF 28.0 M**	**0.033**
Fatalities	1.8	0.00024	10.1	0.0013	**7.6**	**0.001**
Injuries	31.5	0.0042	71.5	0.0094	**59.5**	**0.0078**
Displaced	1,373.8	0.18	953.7	0.13	**1079.7**	**0.14**
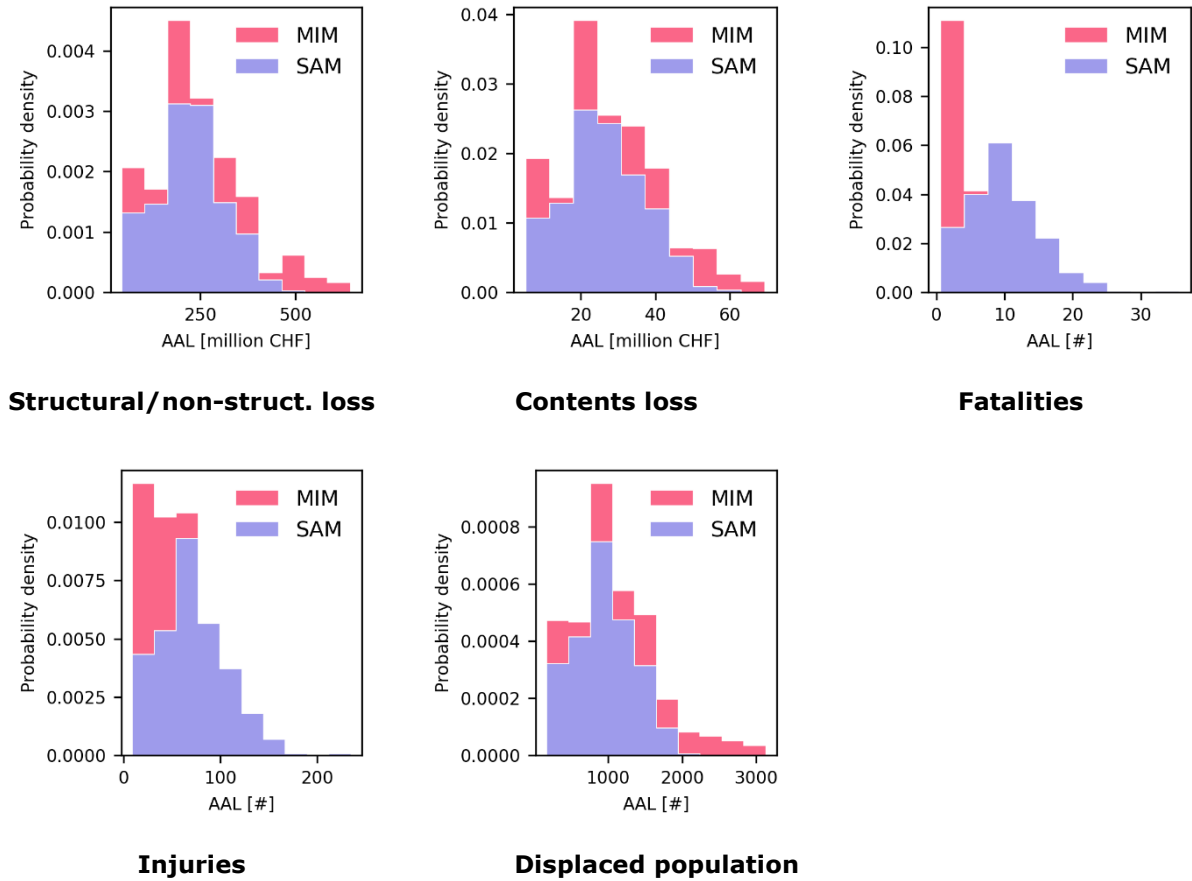
Figure 9.1. Average annual loss (AAL) epistemic distributions for each of the five considered loss types. The contributions of the MIM and SAM models are stacked, i.e. the MIM and SAM histograms are not superimposed. At each x-axis bin, the relative heights of the SAM and MIM bars indicate the contribution of the two models at the particular loss value.

Table 9.1 to Table 9.6 report the mean (over the epistemic uncertainty) loss estimates for a number of return periods of exceedance. These estimates are also plotted in Figure 9.2, along with epistemic quantiles.

Table 9.2. Country-wide mean structural/non-structural (S/NS) loss estimates for selected return periods.

	MIM		SAM		ERM-CH23	
Return period	S/NS loss [B CHF]	S/NS loss ratio [‰]	S/NS loss [B CHF]	S/NS loss ratio [‰]	**S/NS loss [B CHF]**	**S/NS loss ratio [‰]**
5	0.026	0.01	0.003	0.00	**0.01**	**0.00**
10	0.168	0.06	0.065	0.02	**0.10**	**0.03**
25	0.922	0.32	0.520	0.18	**0.64**	**0.22**
50	2.540	0.87	1.738	0.60	**1.98**	**0.68**
100	6.016	2.07	4.653	1.60	**5.06**	**1.74**
200	12.15	4.18	9.949	3.43	**10.61**	**3.65**
500	26.70	9.19	21.72	7.48	**23.21**	**7.99**
1000	41.43	14.26	34.86	12.00	**36.83**	**12.68**
2000	57.96	19.96	52.41	18.05	**54.08**	**18.62**

Table 9.3. Country-wide mean content (C) loss estimates for selected return periods.

Return period	MIM		SAM		ERM-CH23	
	C loss [B CHF]	C loss ratio [‰]	C loss [B CHF]	C loss ratio [‰]	**C loss [B CHF]**	**C loss ratio [‰]**
5	0.003	0.00	0.000	0.00	**0.00**	**0.00**
10	0.018	0.02	0.007	0.01	**0.01**	**0.01**
25	0.101	0.12	0.059	0.07	**0.07**	**0.09**
50	0.279	0.33	0.198	0.24	**0.22**	**0.27**
100	0.658	0.79	0.536	0.64	**0.57**	**0.68**
200	1.326	1.58	1.161	1.39	**1.21**	**1.45**
500	2.867	3.42	2.565	3.06	**2.66**	**3.17**
1000	4.442	5.30	4.158	4.97	**4.24**	**5.07**
2000	6.217	7.42	6.314	7.54	**6.28**	**7.51**

Table 9.4. Country-wide mean fatality estimates for selected return periods.

Return period	MIM		SAM		ERM-CH23	
	Fatalities	Fatality ratio [‰]	Fatalities	Fatality ratio [‰]	**Fatalities**	**Fatality ratio [‰]**
5	0.0	0.000	0.0	0.000	**0.0**	**0.000**
10	0.0	0.000	0.0	0.000	**0.0**	**0.000**
25	0.9	0.000	2.5	0.000	**2.0**	**0.000**
50	4.7	0.001	22.8	0.003	**17.3**	**0.002**
100	18.3	0.002	121.0	0.016	**90.2**	**0.012**
200	55.6	0.007	398.6	0.053	**295.7**	**0.039**
500	194.0	0.026	1'184.3	0.156	**886.5**	**0.117**
1000	396.6	0.052	2'214.1	0.292	**1668.7**	**0.220**
2000	686.7	0.090	3'902.0	0.514	**2937.4**	**0.387**

Table 9.5. Country-wide mean injury estimates for selected return periods.

Return period	MIM		SAM		ERM-CH23	
	Injuries	Injury ratio [‰]	Injuries	Injury ratio [‰]	**Injuries**	**Injury ratio [‰]**
5	1.5	0.00	0.2	0.00	**0.6**	**0.00**
10	10.0	0.00	3.6	0.00	**5.5**	**0.00**
25	61.9	0.01	44.0	0.01	**49.3**	**0.01**
50	192.5	0.03	235.8	0.03	**222.8**	**0.03**
100	509.5	0.07	993.8	0.13	**848.5**	**0.11**
200	1,187.2	0.16	2,919.2	0.38	**2,399.6**	**0.32**
500	3,127.7	0.41	8,163.7	1.08	**6,652.9**	**0.88**
1000	5,491.7	0.72	14,967.7	1.97	**12,124.9**	**1.60**
2000	8,439.3	1.11	25,648.9	3.38	**20,486.0**	**2.70**

Table 9.6. Country-wide mean displaced population estimates for selected return periods.

Return Period	MIM		SAM		ERM-CH23	
	Displaced	Displaced ratio [‰]	Displaced	Displaced ratio [‰]	**Displaced**	**Displaced ratio [‰]**
5	48.0	0.01	2.5	0.00	**16.1**	**0.00**
10	439.4	0.06	125.6	0.02	**219.7**	**0.03**
25	3,266.8	0.43	1,783.1	0.23	**2,228.2**	**0.29**
50	10,516.3	1.39	6,915.2	0.91	**7,995.7**	**1.05**
100	27,462.1	3.62	19,715.8	2.60	**22,039.7**	**2.90**
200	59,449.6	7.83	43,713.9	5.76	**48,434.6**	**6.38**
500	138,422.0	18.23	98,754.5	13.01	**110,654.7**	**14.57**
1000	218,496.4	28.78	160,278.0	21.11	**177,743.5**	**23.41**
2000	313,214.8	41.25	241,813.8	31.85	**263,234.1**	**34.67**
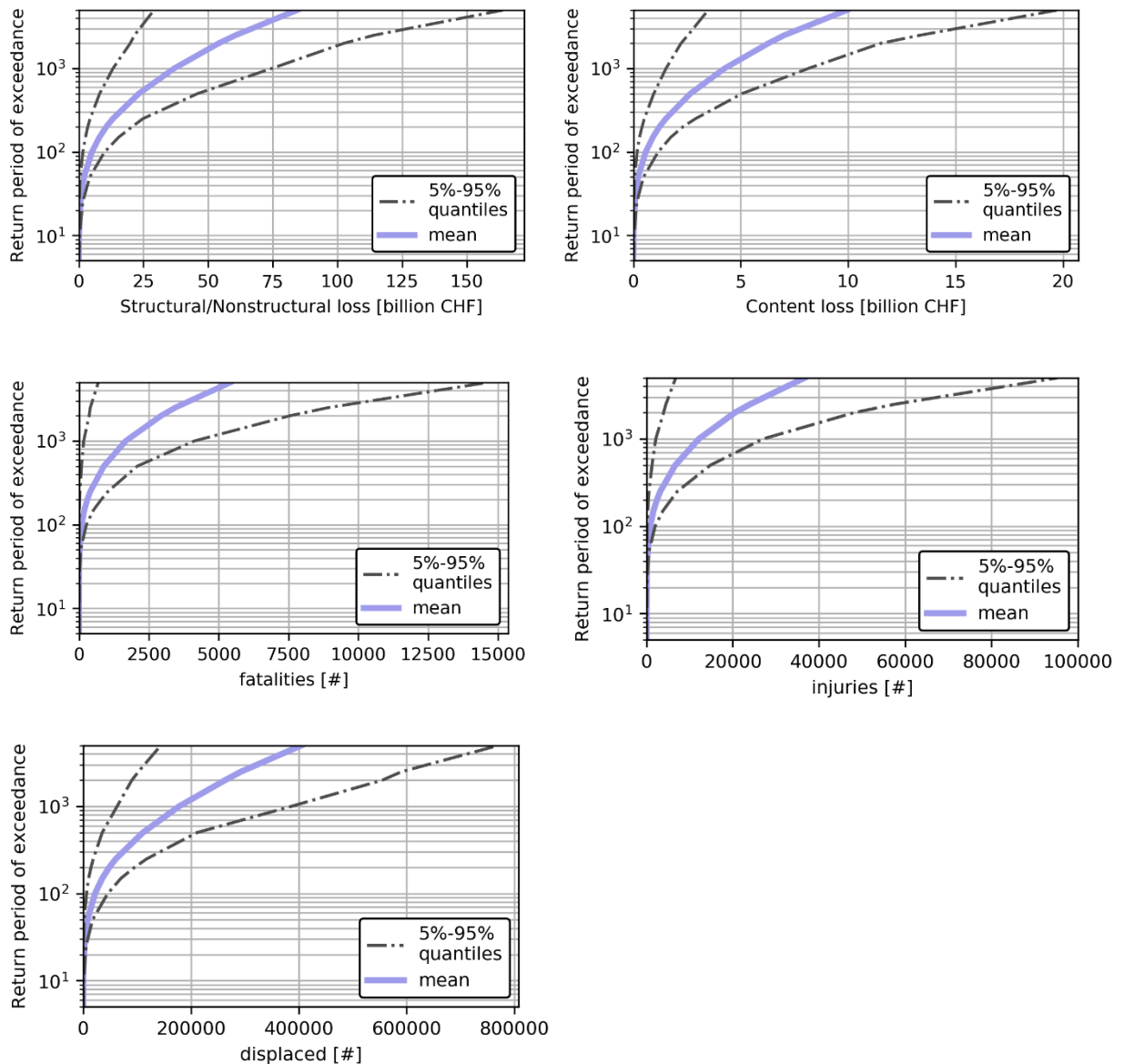
Figure 9.2. PML curves for each of the five considered loss types.

9.2.2   Risk estimates by canton

The cantonal view of AAL estimates for structural/non-structural economic loss and fatalities is shown in Figure 9.3 and Figure 9.4 respectively. The cantons of Basel-Stadt (BS) and Valais (VS) feature at the top of the AALR list, largely driven by the increased seismicity rates in these regions compared to the rest of the country. As regards the non-normalised AAL estimates, we also see the populous cantons of Zurich (ZH) and Bern (BE) feature among the top spots. This is of course a result of the larger exposure that is concentrated in these areas. The canton of Geneva (GE) is also quite high, as a result of its high exposure, but also its relatively high hazard on soil. The latter is mostly seen in the MIM submodel, as shown in Figure 9.5, which compares the MIM and SAM structural/non-structural AAL cantonal estimates.
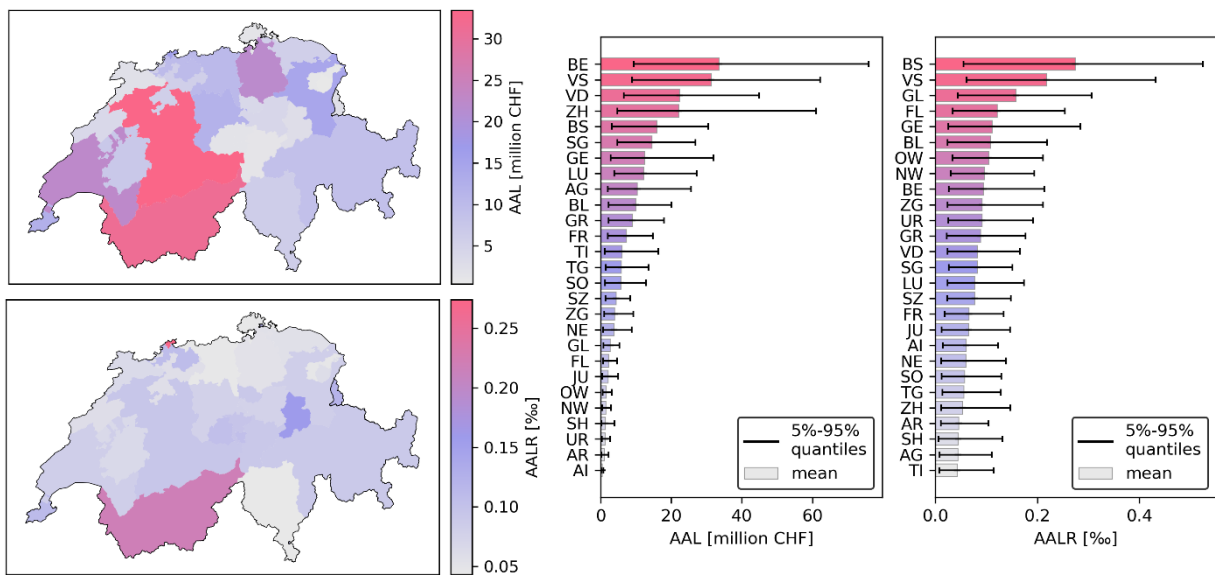
Figure 9.3. Structural/non-structural AAL and AALR estimates by canton.
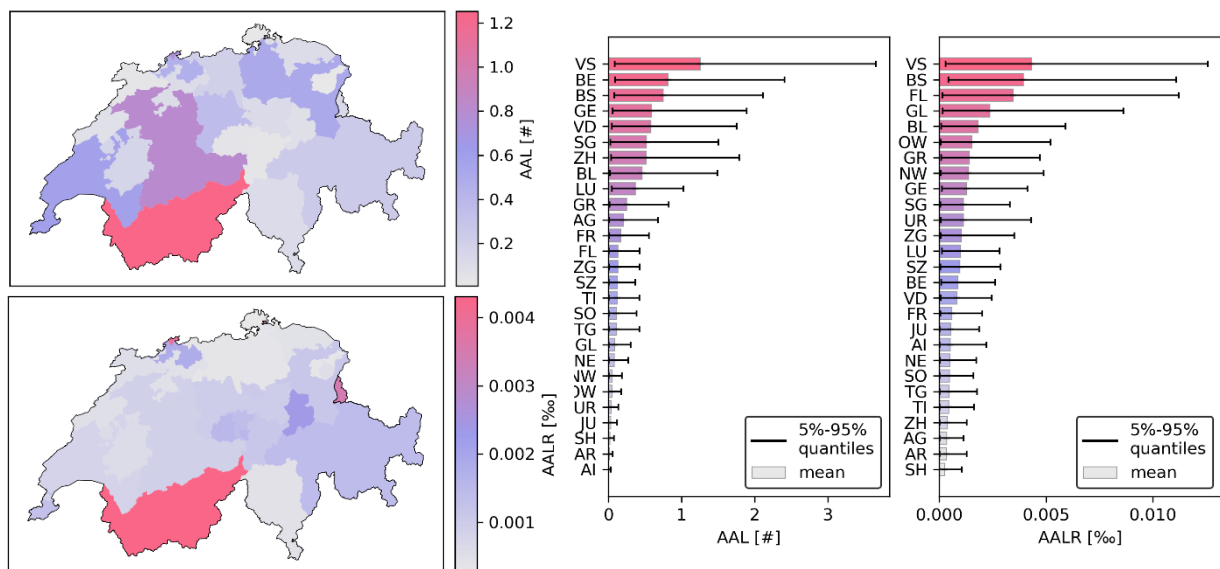
Figure 9.4. Fatality AAL and AALR estimates by canton.
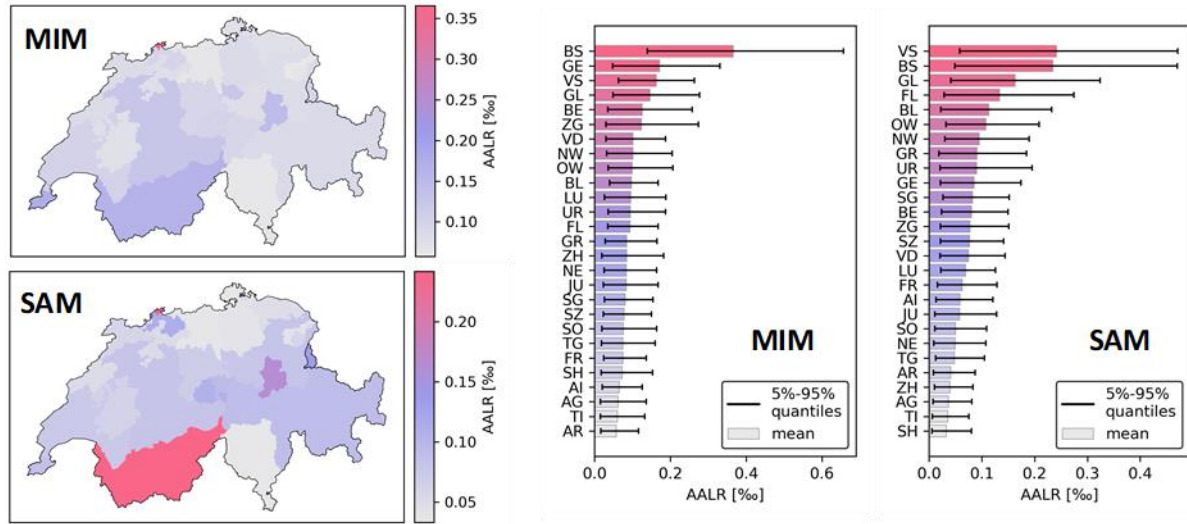
Figure 9.5. Comparison of cantonal structural/non-structural AALR estimates in MIM and SAM.

9.2.3   Risk estimates by municipality

Figure 9.6 and Figure 9.7 illustrate the AALR and AAL estimates, respectively, at the municipality level for all loss types. This resolution highlights the increased AALR estimates across e.g. the Rhone Valley, owing to expected site effects and elevated seismic hazard. Likewise, in Figure 9.7, the major urban centres stand out, a result of the concentration of the exposure therein.
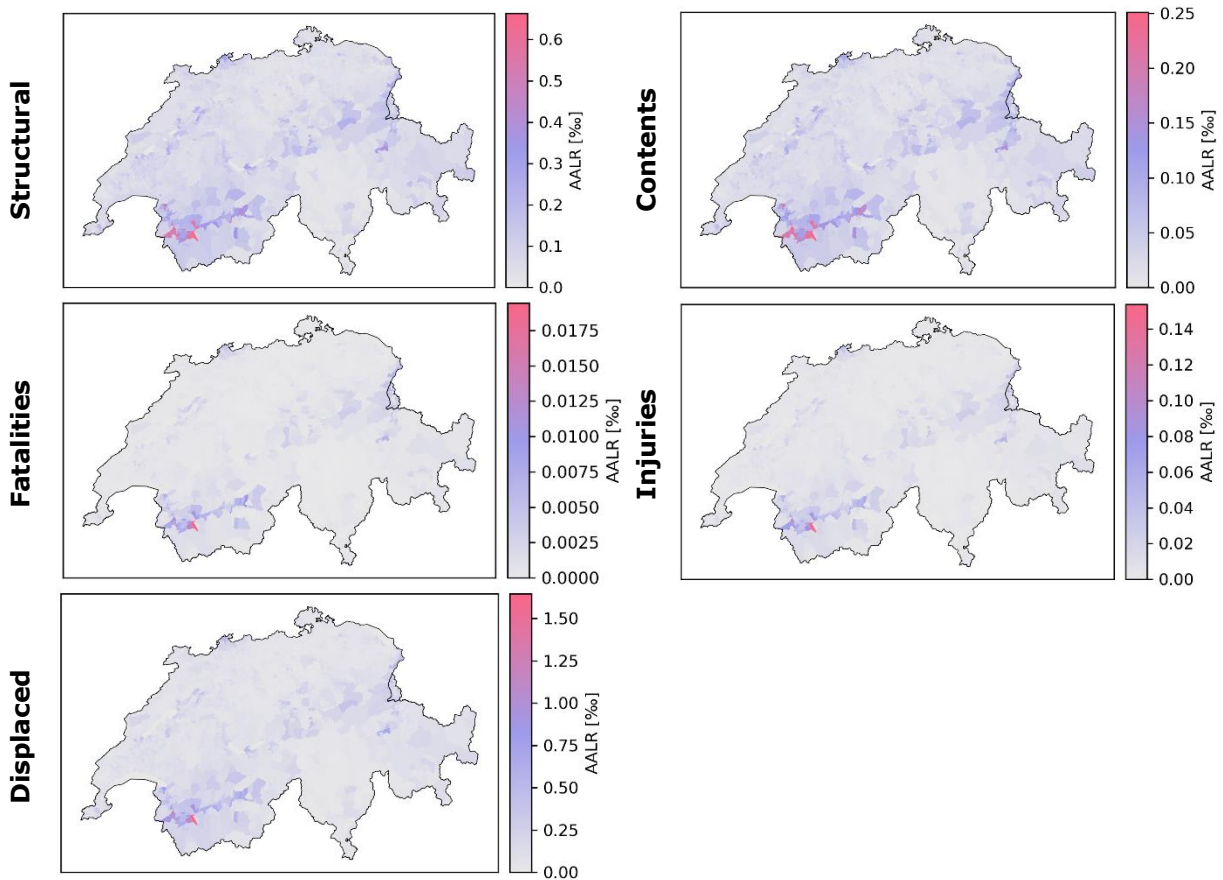
Figure 9.6. Mean AALR estimates by municipality for five loss types.
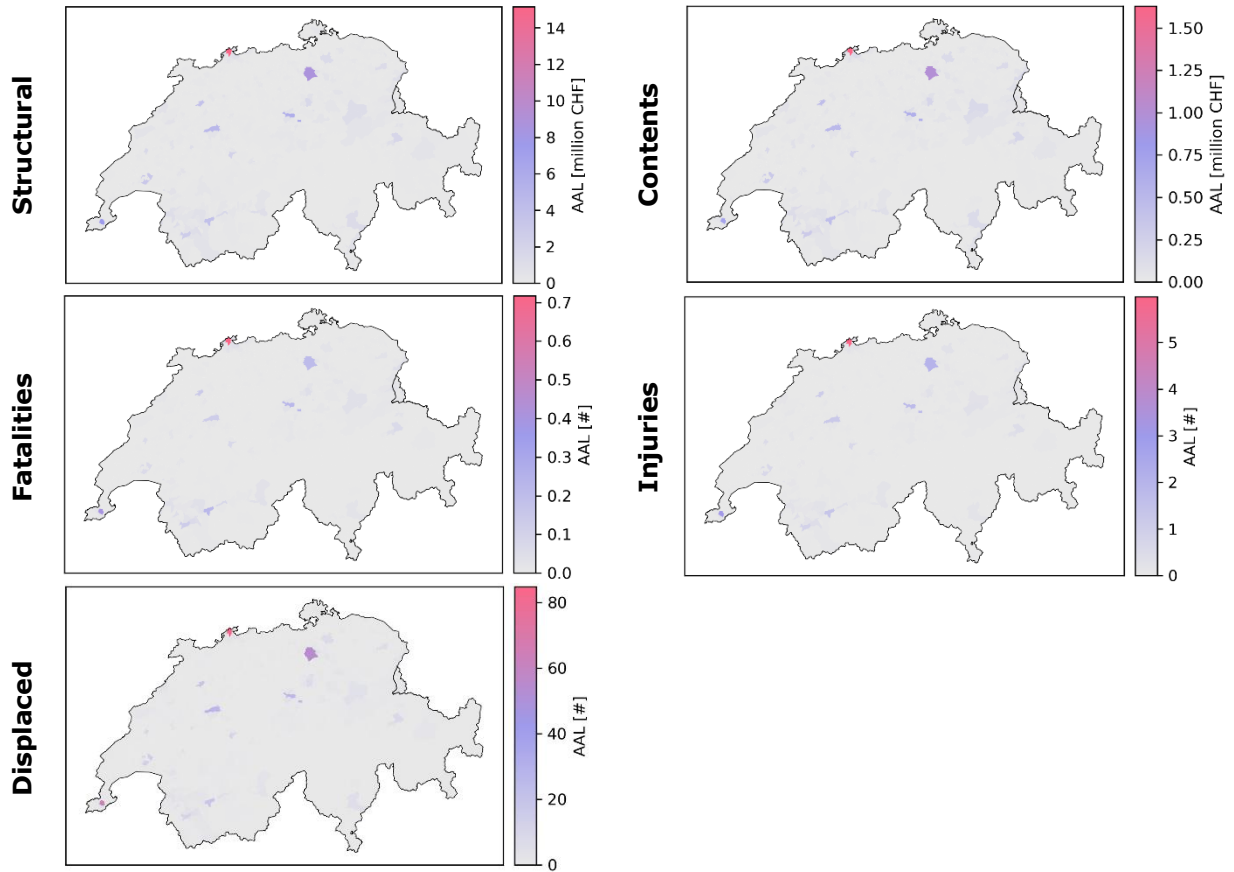
Figure 9.7. Mean AAL estimates by municipality for five loss types.

9.2.4   Risk estimates by grid cell (2 km x 2 km)

Finally, maps of structural/non-structural AAL and AALR on a 2 km x 2 km regular grid are also provided in Figure 9.8. It should be emphasised that results at such resolution should be interpreted cautiously due to the lack of appropriate resolution in the model inputs (e.g. in the building typology mapping or vulnerability). Nevertheless, they can provide qualitative insights if the aforementioned limitations are kept in mind.
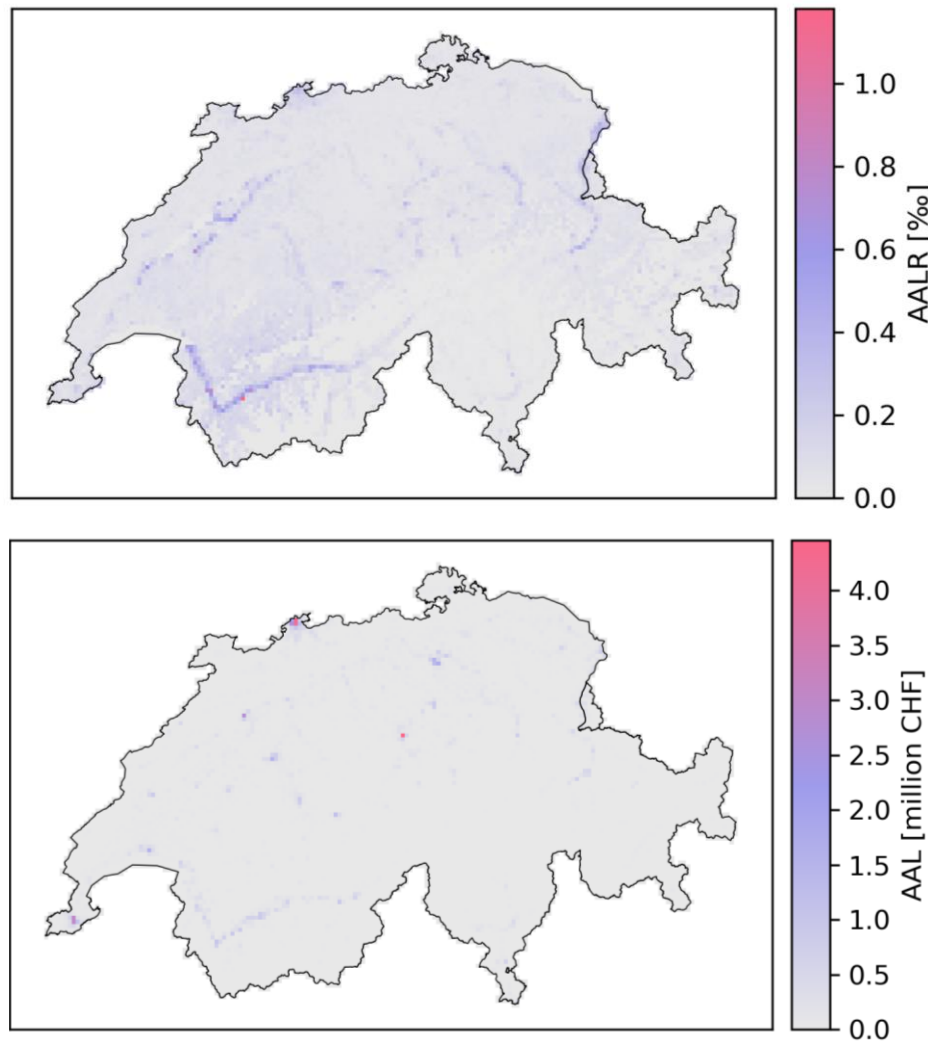
Figure 9.8. Mean structural/non-structural AAL (top) and AALR (bottom) estimates on a 2 km x 2 km grid.

9.2.5   Risk estimates by building typology

Figure 9.9 reports AAL/AALR estimates for structural/non-structural loss and fatalities per structural typology. AAL is heavily impacted by the prevalence of each building typology in the exposure, aside from its inherent vulnerability. As a result, frequent typologies such as low-rise M3, M6 and RCW feature towards the top. Of course, low-rise buildings are expected to be less vulnerable than their high-rise counterparts, as can be seen in the AALR plots. There, as expected, masonry mid- and high-rise typologies feature at the top of AALR rankings, while reinforced concrete, steel and timber buildings are generally lower, i.e. at less risk.

Figure 9.10 compares typology AALR estimates between the MIM/SAM submodels. As regards the structural/non-structural loss estimates, both submodels place M1_M as the typology with the highest AALR. Overall, the MIM AALR estimates are higher for most (but not all) typologies. This is of course in agreement with the higher total AAL obtained in MIM compared to SAM and is a result of the combination of the different ground shaking, amplification and fragility modelling. The ranking of the typologies is generally deemed consistent between MIM and SAM, although with some notable differences (e.g. in MIM, the height of the building seems to play a larger role compared to SAM). Where fatalities are concerned, the picture is different, with SAM featuring considerably higher AALR estimates. This is considered to be a result of the likely more

conservative modelling of collapse fragility in SAM and the possibly higher intensities computed in the epicentral area by the SAM GMPEs as opposed to the MIM IPEs. Lastly, a striking difference is seen in the industrial building typology, which is identified as the most vulnerable (in terms of fatalities) in SAM but is far from that in MIM.
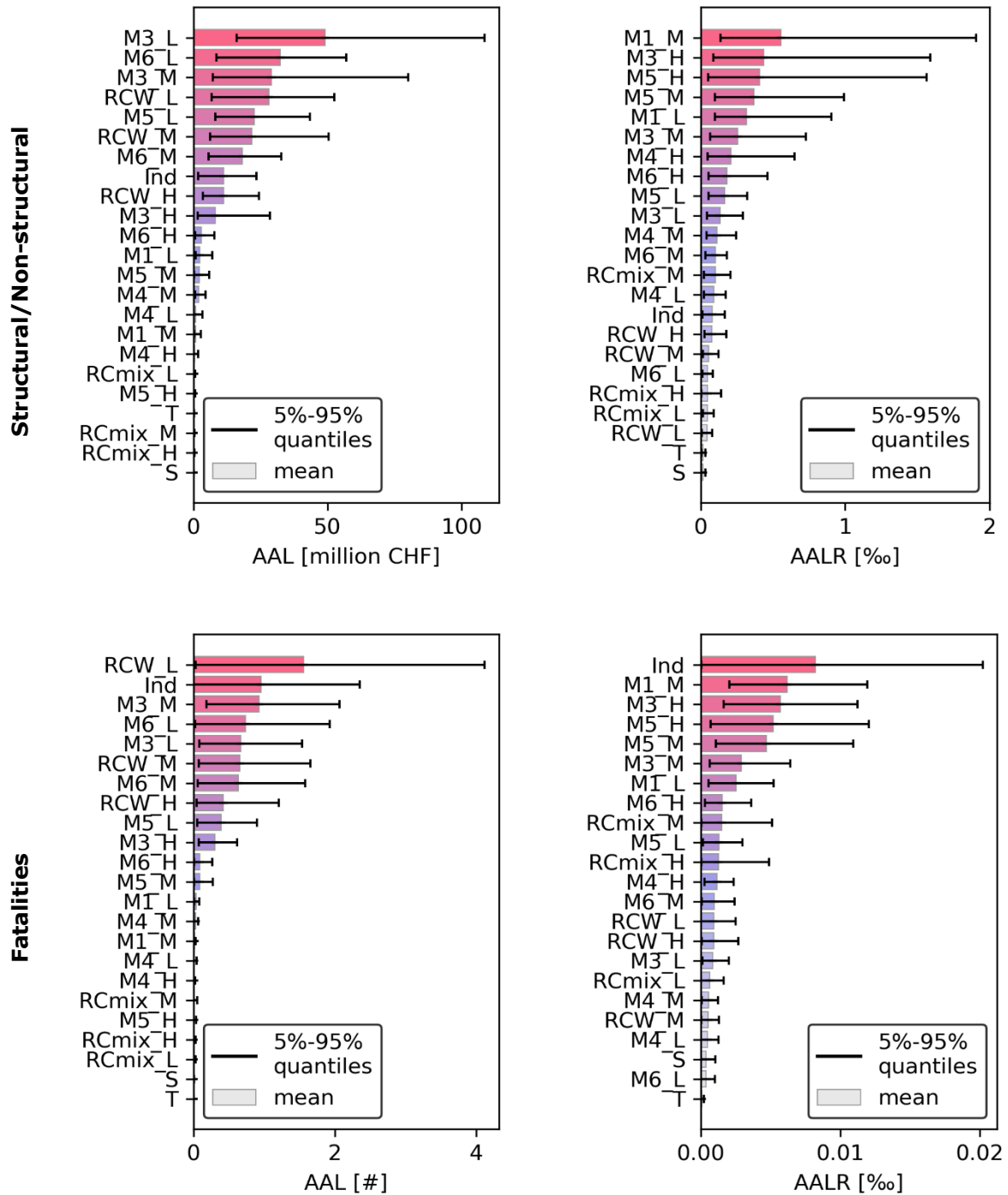
Figure 9.9. Structural/non-structural and fatality AAL and AALR estimates by building typology.
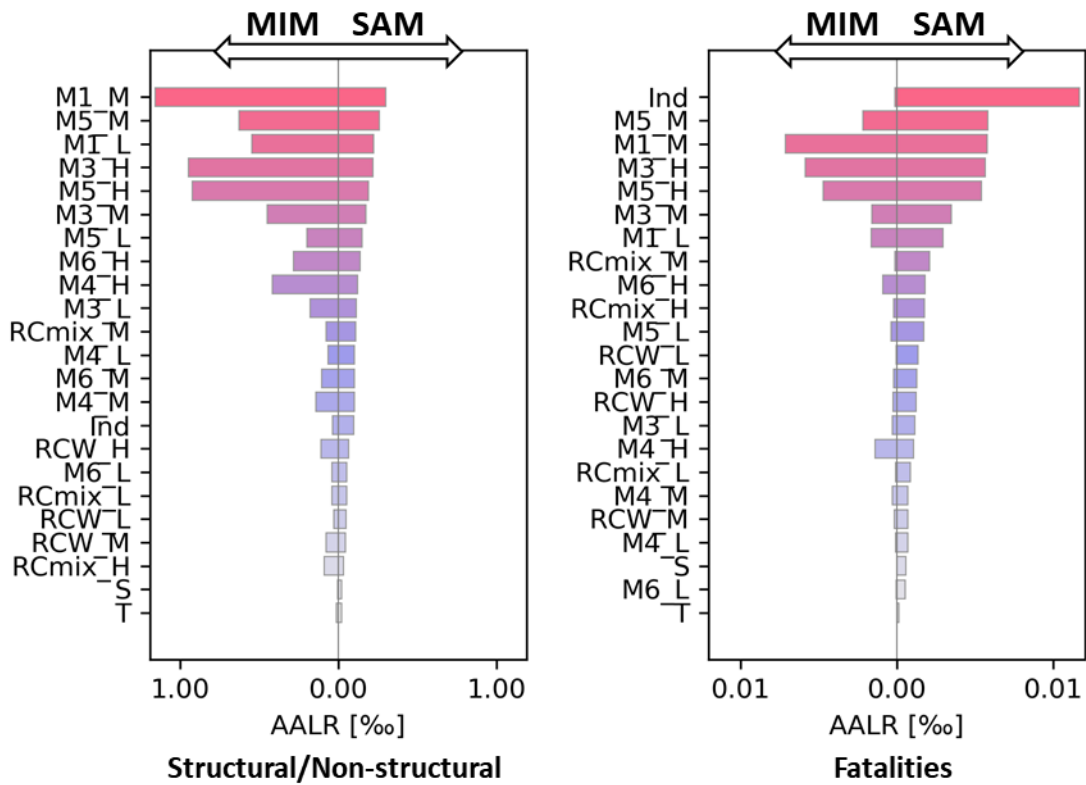
Figure 9.10. Comparison between MIM and SAM AALR estimates by structural typology for structural/non-structural economic losses (left) and fatalities (right). The bars on the left side of the panels refer to the MIM AALR values, the bars on the right side to the SAM AALR values.

9.2.6   Risk estimates by occupancy type

Finally, Figure 9.11 shows the structural/non-structural and contents AAL estimates by occupancy type. The residential building stock, comprising by far the largest part of the total value, is naturally also the main contributor to the total losses. The commercial, industrial and agricultural sectors follow in that order, with somewhat increased proportions when it comes to contents loss.
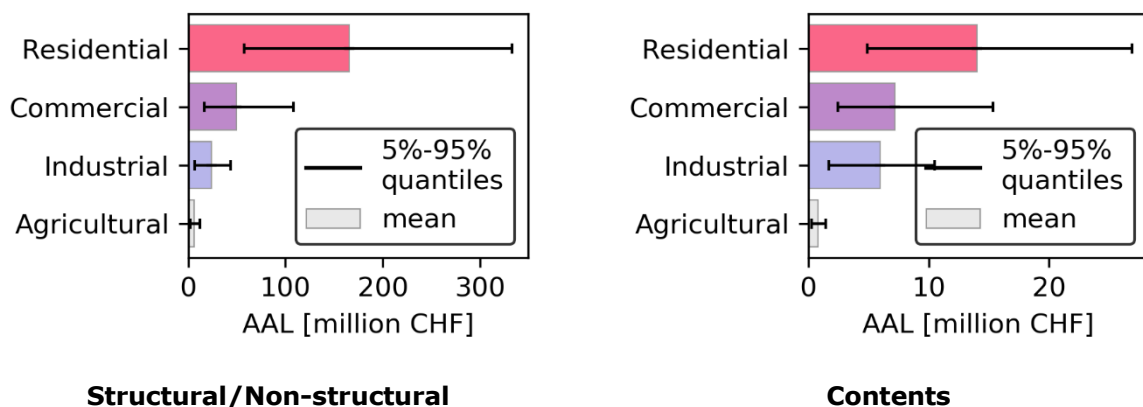
Figure 9.11. Structural/non-structural and content AAL estimates by occupancy type.

9.3   Scenario results

Except for the probabilistic risk products, a series of scenario damage and loss analyses with the ERM-CH23 model were conducted for the largest historical earthquakes to occur in Switzerland. A summary of the mean loss estimates obtained for these scenarios is given in Table 9.7 below. Note that these estimates refer to losses expected to be incurred if these earthquake events were to occur now, and therefore do not represent projections of their impact at the time of their occurrence.

Table 9.7. Mean loss estimates for historical scenarios.

Earthquake scenario	Structural/ Non-structural	Fatalities	Injuries	Displaced population
1584 Aigle Mw 5.9	CHF 7.2 B	286	20,052	30,193
1774 Altdorf Mw 5.7	CHF 2.2 B	57	488	8,386
1524 Ardon Mw 5.8	CHF 3.3 B	102	757	13,972
1356 Basel Mw 6.6	CHF 41.9 B	2,915	20,945	205,206
1755 Brig-Glis Mw 5.7	CHF 1.5 B	46	322	5,221
1295 Churwalden Mw 6.2	CHF 5.6 B	272	1,877	21,757
1622 Ftan Mw 5.4	CHF 105 M	0	7	211
1946 Sierre Mw 5.8	CHF 2.4 B	34	310	9,043
1855 Stalden-Visp Mw 6.2	CHF 5.6 B	141	1,016	18,974
1601 Unterwalden Mw 5.9	CHF 11.6 B	541	3,719	49,129

The following sections go into further detail on the results of two of these historical scenarios, namely the Basel Mw 6.6 earthquake and the Sierre Mw 5.8 earthquake.

9.3.1   Basel 1356 Mw 6.6

Figure 9.12 shows the mean EMS-98 intensity map for the Basel Mw 6.6 earthquake. The map has been derived as a weighted average of the MIM logic tree branches maps that were already expressed in intensity, and the SAM branches after converting SA (0.3 s) to intensity with the Faenza and Michelini (2011) conversion equation.

The estimated impact by municipality is shown in Figure 9.13. The impact of this earthquake is estimated to extend almost throughout Switzerland, with the highest damage and loss expected in Basel and the municipalities surrounding the epicentral area.
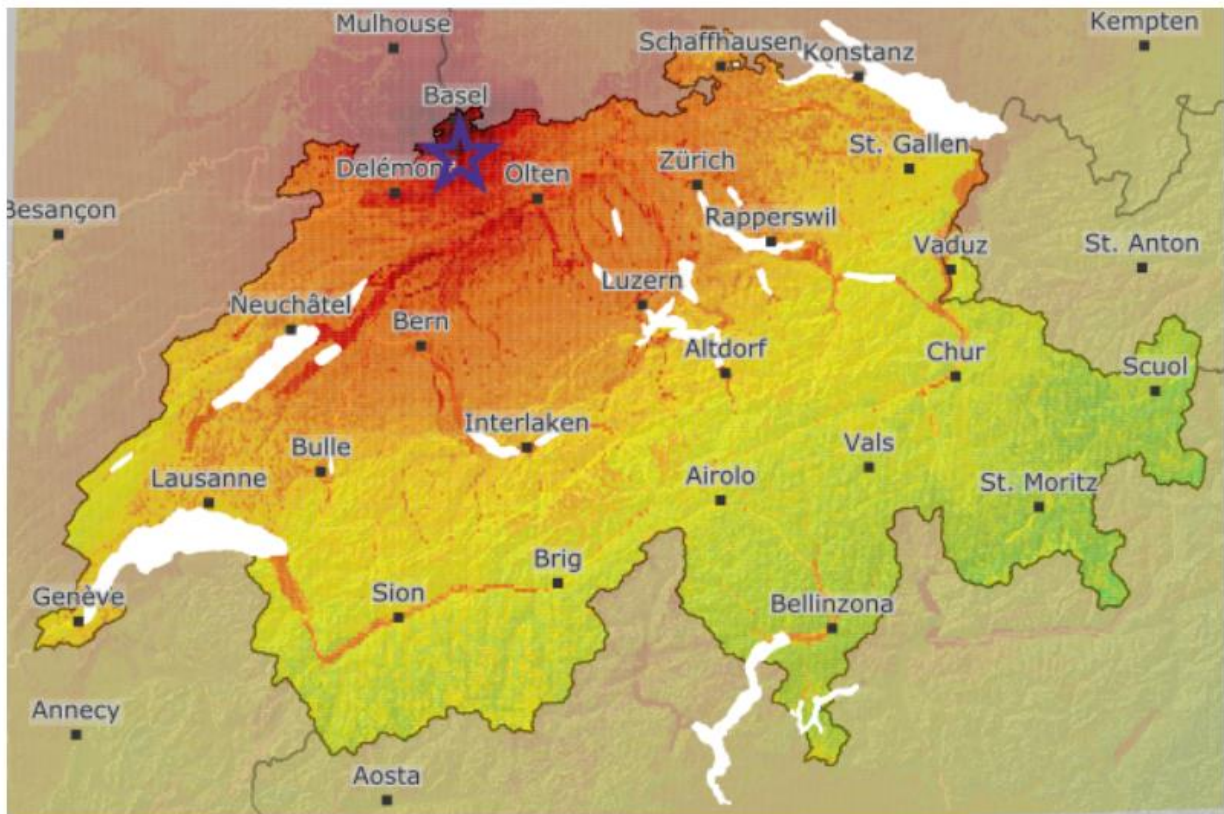
Intensity	II	III	IV	V	VI	VII	VIII	IX
Impact	scarcely felt	weak	largely observed	strong	slightly damaging	damaging	heavily damaging	destructive

**Figure 9.12**. Mean EMS-98 intensity map for the Basel Mw 6.6 earthquake.

Structural/non-structural loss ratio

Contents loss ratio

Fatalities

Injuries

Displaced population
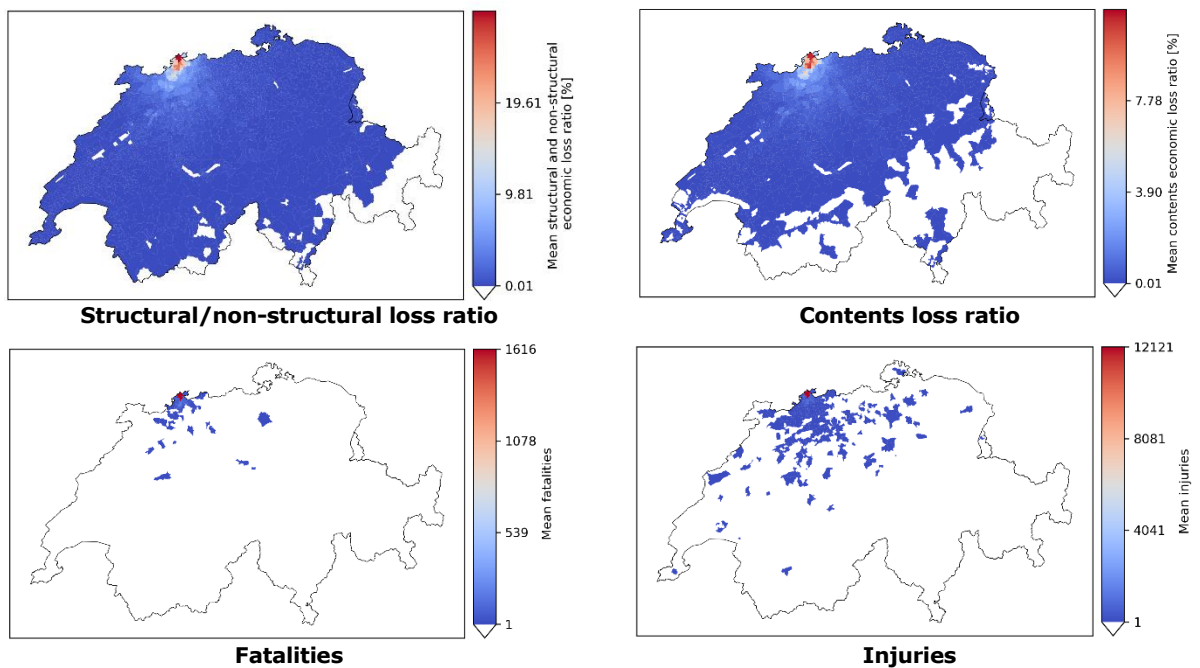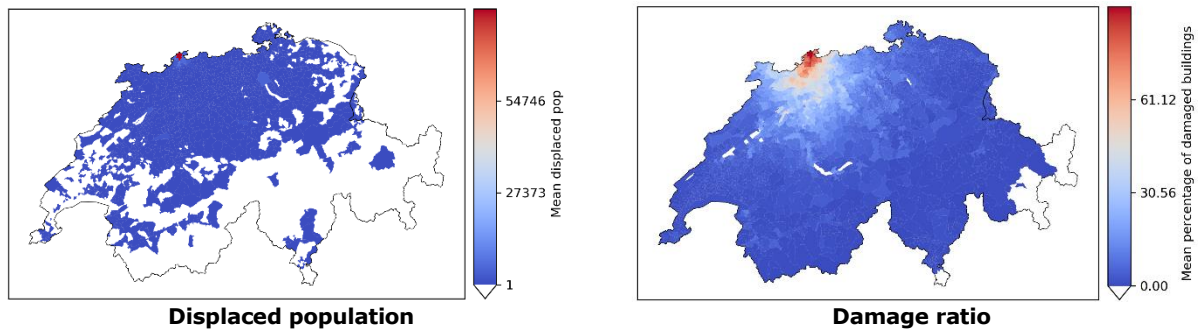
Damage ratio

Figure 9.13. Municipal views of average structural/non-structural loss ratio, contents loss ratio, fatalities, injuries, displaced population and percentage buildings in any damage state for the Basel Mw 6.6 earthquake scenario.

Table 9.8 compares the mean loss estimates of the two submodels, MIM and SAM. SAM yields somewhat higher economic losses and significantly higher injuries and fatalities. Moreover, the impact in SAM (at least for damage and economic losses) is limited to a smaller region than in MIM (Figure 9.14), as a result of the faster attenuation in the employed GMPEs. The impact attenuation is also faster on the fatalities side for SAM, although given the much higher estimated numbers compared to MIM, the area affected is still larger.

Table 9.8. Mean loss estimates for the Basel Mw 6.6 scenario.

Earthquake scenario	Sub-model	Structural/ Non-structural	Contents	Fatalities	Injuries	Displaced population
1356 Basel Mw 6.6	MIM	CHF 34.9 B	CHF 3.8 B	368	4,984	186,888
	SAM	CHF 44.9 B	CHF 5.5 B	4,007	27,786	213,056
	ERM-CH23	**CHF 41.9 B**	**CHF 5.0 B**	**2,915**	**20,945**	**205,206**

Structural loss ratio
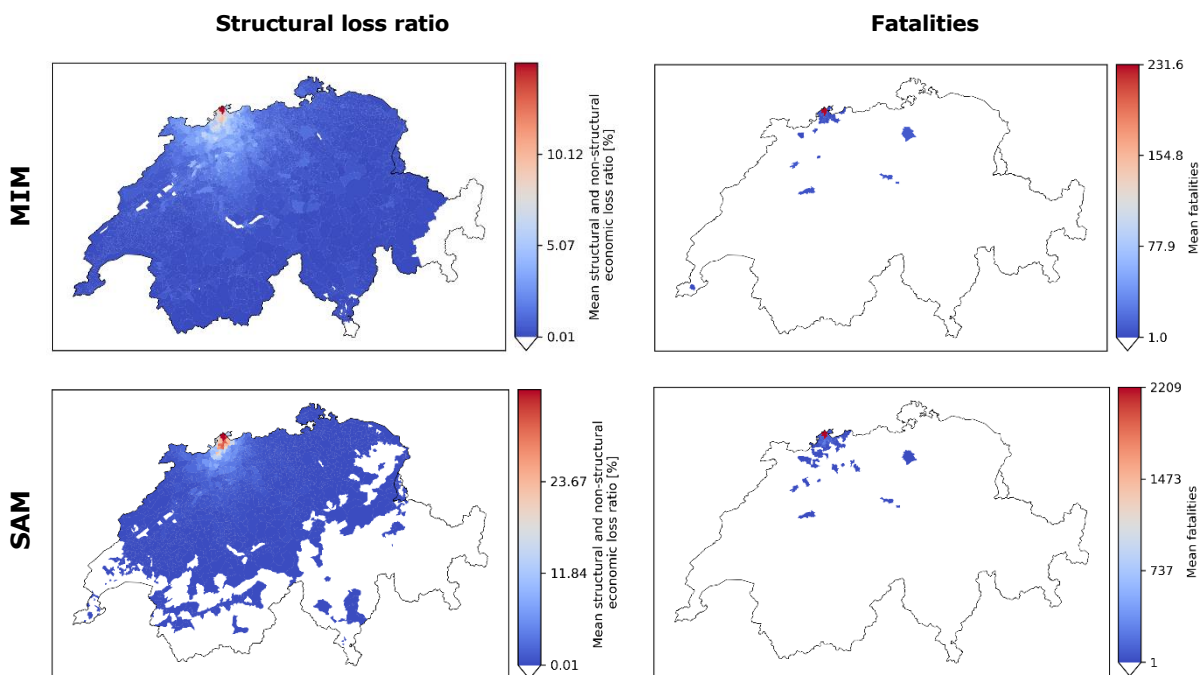
Fatalities

Figure 9.14. Comparison between MIM and SAM of mean structural/non-structural economic loss ratio [%] and mean number of fatalities by municipality for the Basel Mw 6.6 earthquake scenario.

Lastly, Figure 9.15 presents the distribution of the various loss types around the mean estimates previously given in Table 9.8. The black lines denote the kernel density estimate plots after combining the MIM and SAM distributions, while the coloured histograms denote the contributions obtained from each of the two submodels. Overall, the SAM estimates seem to extend over a wider range of the x-axis, although with a clear mode. The MIM estimates are bit less spread out, while in the case of injuries and fatalities they are clearly concentrated at much lower values compared to SAM.
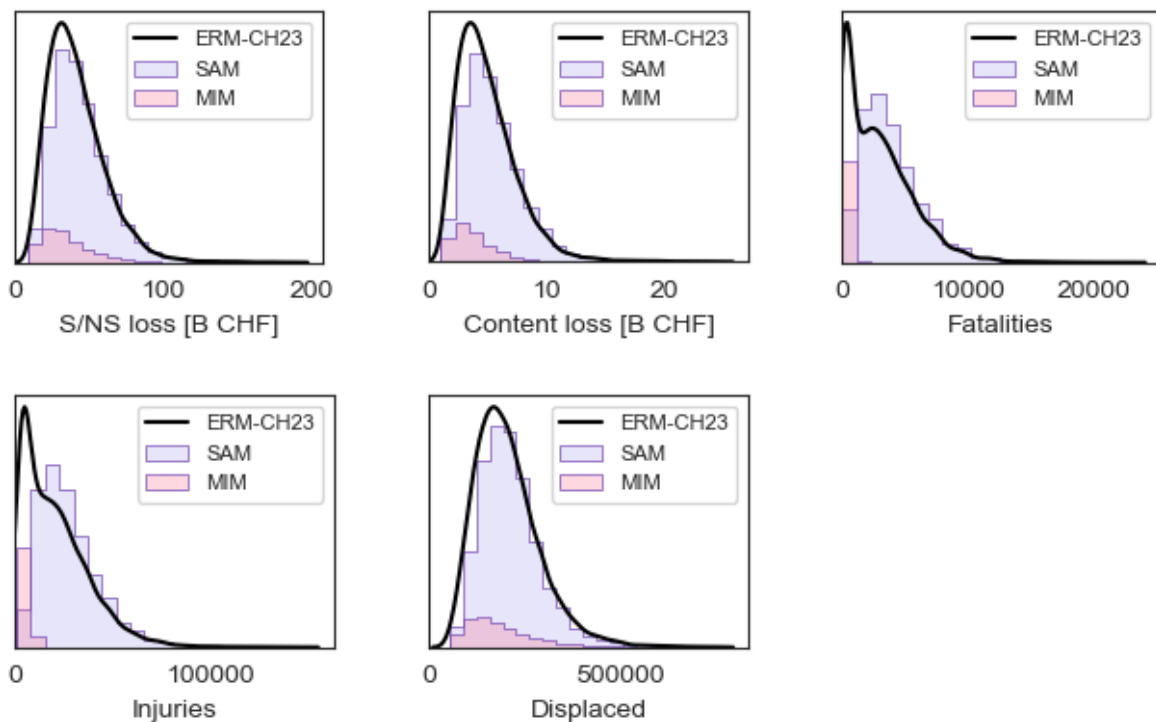
Figure 9.15. Distribution of loss estimates for the Basel Mw 6.6 earthquake. The black outline shows the overall ERM-CH23 distribution, while the coloured histograms show the contributions of the two submodels (MIM, SAM).

9.3.2   Sierre 1946 Mw 5.8

Figure 9.16 shows the mean EMS-98 intensity map for the Sierre Mw 5.8 earthquake. The map has been derived as a weighted average of the MIM logic tree branches maps that were already expressed in intensity, and the SAM branches after converting SA(0.3s) to intensity with the Faenza and Michelini (2011) conversion equation.

The estimated impact by municipality is shown in Figure 9.17. The impact of this earthquake is estimated to extend throughout western Switzerland, with the highest damage and loss expected in the Rhone Valley and surrounding areas.

Figure 9.16. Mean EMS-98 intensity map for the Sierre Mw 5.8 earthquake.

Displaced population

Damage ratio

Figure 9.17. Municipal views of average structural/non-structural loss ratio, contents loss ratio, fatalities, injuries, displaced population and percentage buildings in any damage state for the Sierre Mw 5.8 scenario.

Table 9.9 compares the mean loss estimates of the two submodels, MIM and SAM. In terms of economic losses, the two submodels give similar estimates. On the other hand, SAM predicts significantly higher injuries and fatalities, similarly to the Basel earthquake scenario. Similar observations to the previous scenario can also be made with regard to the attenuation of impact (Figure 9.18) and the overall uncertainty around the mean estimates (Figure 9.19).

Table 9.9. Mean loss estimates for the Sierre Mw 5.8 scenario

Earthquake scenario	Sub-model	Structural/ Non-structural	Contents	Fatalities	Injuries	Displaced population
1946 Sierre Mw 5.8	MIM	CHF 2.3 B	CHF 246 M	3.1	152	8,272
	SAM	CHF 2.5 B	CHF 269 M	46.9	377	9,374
	ERM-CH23	**CHF 2.4 B**	**CHF 261 M**	**33.8**	**310**	**9,043**

Structural loss ratio   **Fatalities**
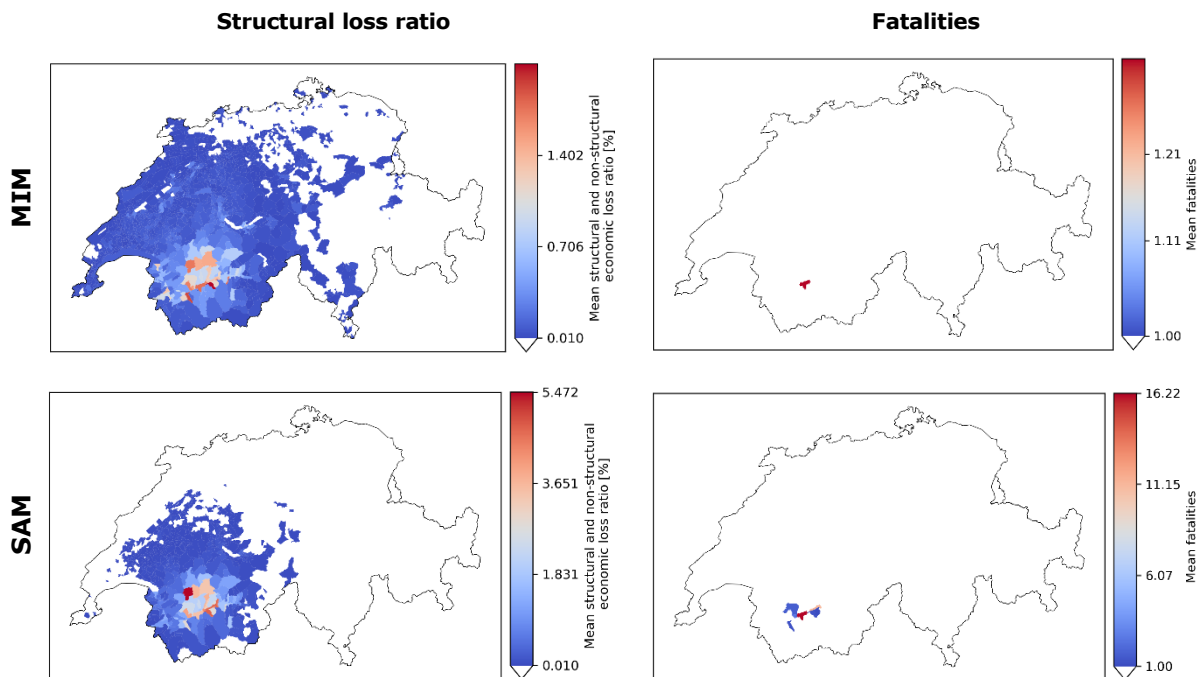
Figure 9.18. Comparison between MIM and SAM of mean structural/non-structural economic loss ratio [%] and mean number of fatalities by municipality for the Sierre Mw 5.8 earthquake scenario.
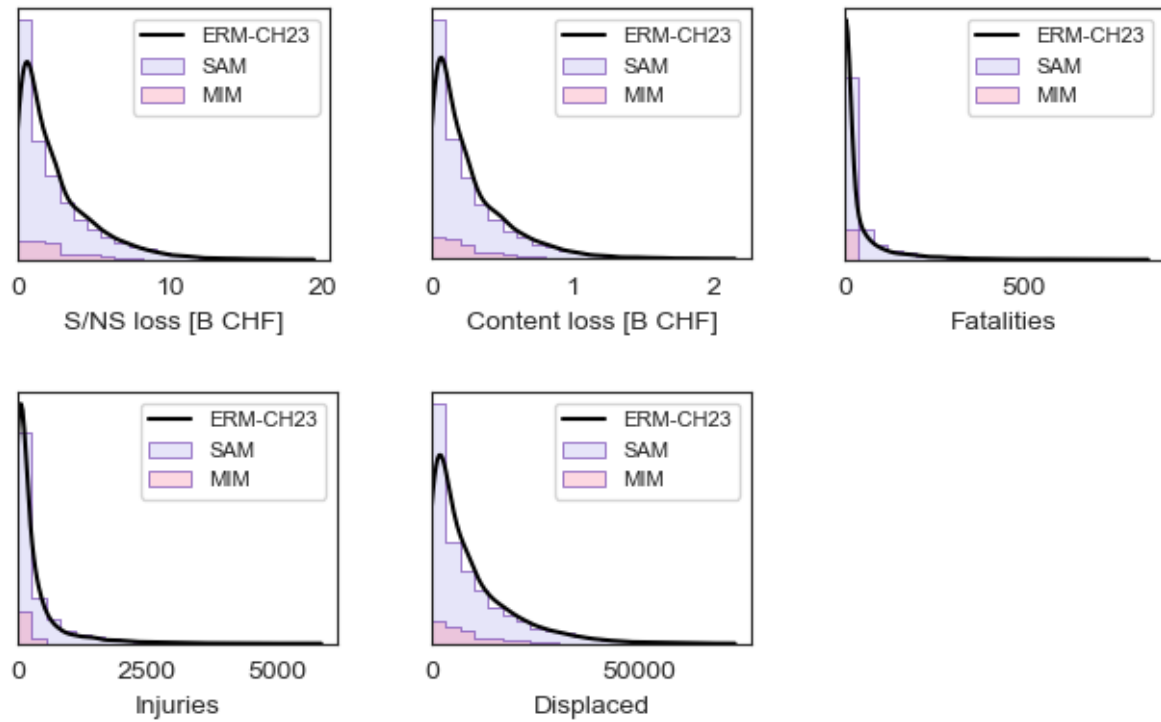
Figure 9.19. Distribution of loss estimates for the Sierre Mw 5.8 earthquake. The black outline shows the overall ERM-CH23 distribution, while the coloured histograms show the contributions of the two sub-models (MIM, SAM).

References

Faenza, L. and Michelini, A. 2011. Regression Analysis of MCS Intensity and Ground Motion Spectral Accelerations (SAs) in Italy. *Geophysical Journal International* **186**(3), 1415–1430.

10.   Sensitivity analyses and comparison with other models

10.1 Introduction

In this chapter, the results of the model are thoroughly analysed to understand the underlying mechanisms and study the effects of individual components on the final risk estimates.

10.2 Sensitivity to epistemic variables

10.2.1 Tornado plots

The sensitivity of several risk estimates on the various logic tree branches is illustrated in Figure **10.1** by means of tornado plots. The AAL values for each individual epistemic variable (e.g. exposure branch RB) were obtained as a weighted average of all branches featuring that individual epistemic variable value. The bars in the tornado plot indicate the maximum swing. For instance, in the case of IPEs in Figure 10.1, the leftmost edge of the bar refers to the weighted average of all MIM logic tree branches featuring the Bindi et al. (2011) IPE that yields the lowest risk estimates, while the rightmost edge refers to the weighted average of all logic tree branches featuring the ECOS-09 variable depth IPE that yields the highest risk estimates.
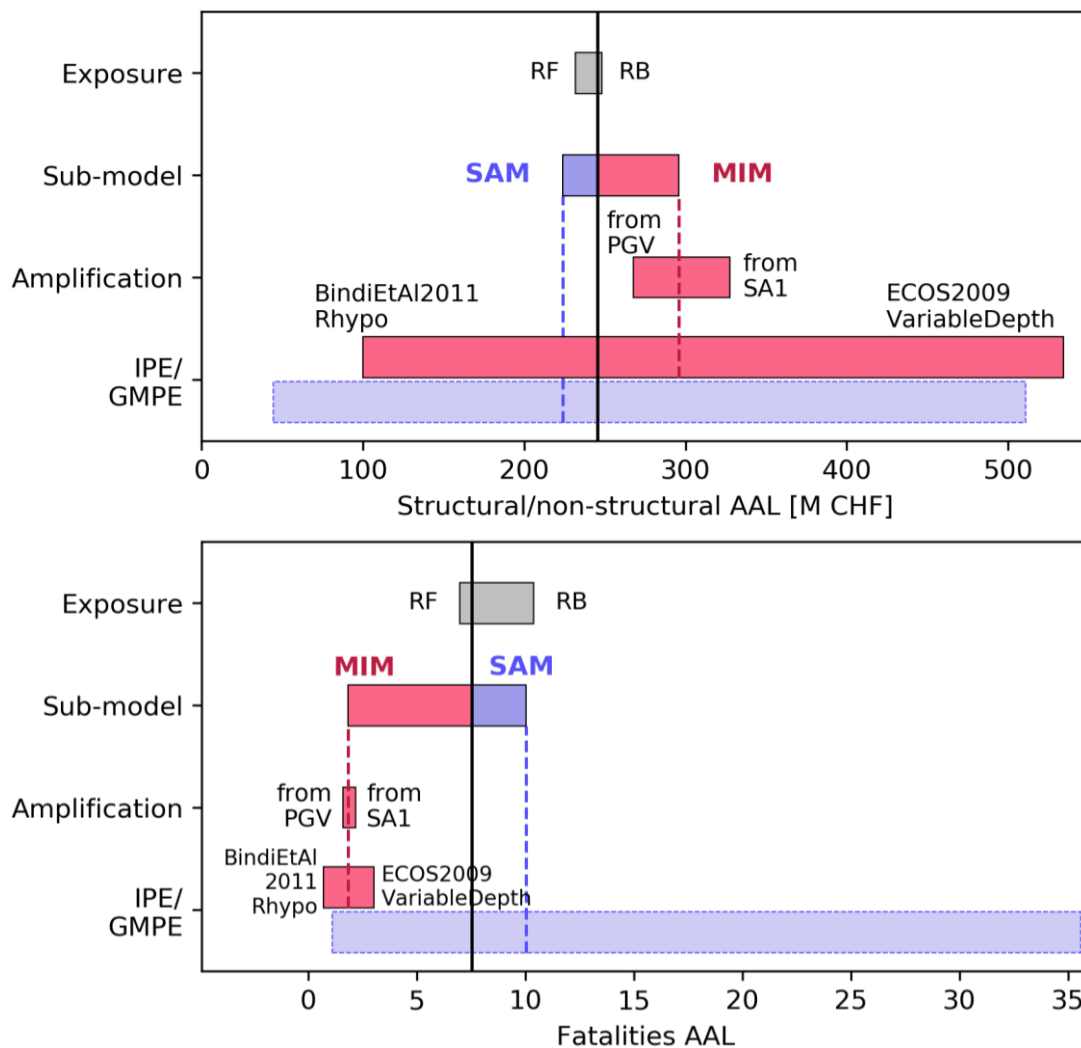
Figure 10.1. Epistemic variable tornado plots for structural/non-structural (top) and fatality (bottom) AAL. The bars show the minimum and maximum AAL estimate if only the most extreme branches were used at each level, while the remaining logic tree remained the same. The MIM and SAM specific bars refer to estimates of those submodels rather than of the entire model. Finally, in the case of GMPEs, since enumeration is not possible and 400 branches are sampled, the bars simply refer to the minimum and maximum values obtained across these 400 samples.

In the case of SAM, not all logic tree branches have been assessed, but instead 400 samples of the GMPE logic tree were taken, as reported in the implementation chapter. As a result, fully consistent tornado plots cannot be produced as in the case of MIM. Therefore, in the case of GMPEs, what is plotted is the minimum/maximum swing among all sampled branches, which is still informative. In general, we observe that in both MIM and SAM, the ground shaking component is the main driver of variability, with IPEs and GMPEs having the largest effect on the overall loss estimates. The exposure and amplification branches lead to only minor differences when it comes to country-wide loss estimates. However, local differences are present, as will be shown in the following sections.

10.2.2 Scenario result sensitivity

Figure 10.2, Figure 10.3, Figure 10.4 and Figure 10.5 below present the different aleatory distributions of structural loss and fatalities for the Basel Mw 6.6 and Sierre Mw 5.8 historical scenarios by fixing individual epistemic variables, i.e. GMPE, IPE, exposure and amplification, respectively. In line with the previous analysis, we see a significant spread when it comes to the IPE/GMPE selection, while the exposure and amplification choice has only a minimal impact on the overall epistemic uncertainty. Similar conclusions were derived for other loss types (e.g. fatalities) but are not shown here for conciseness.
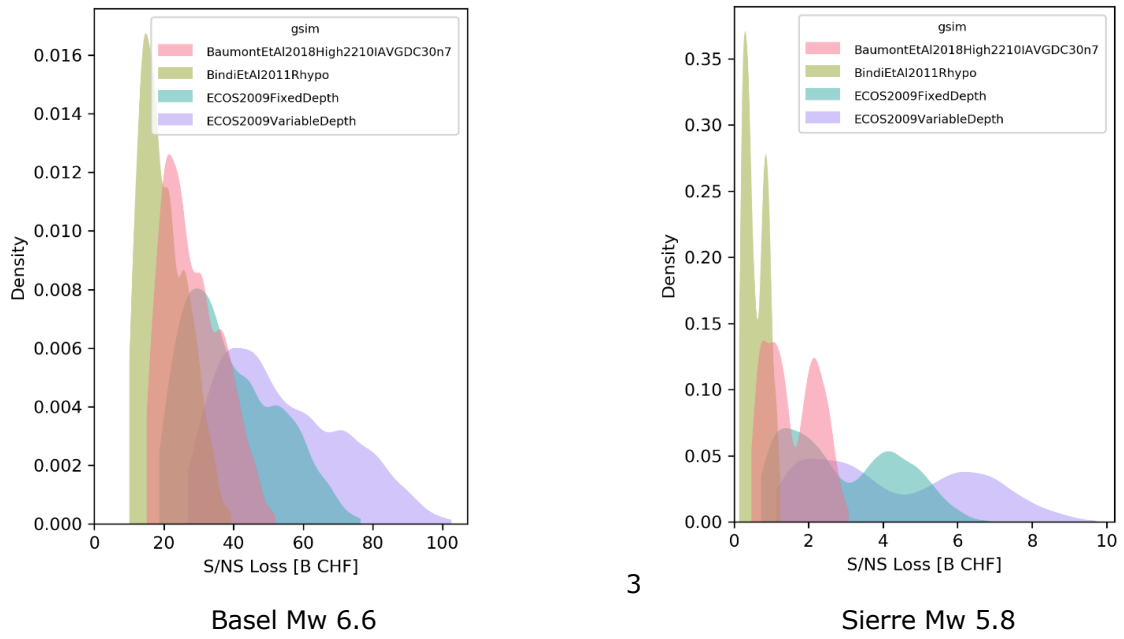

Basel Mw 6.6   Sierre Mw 5.8
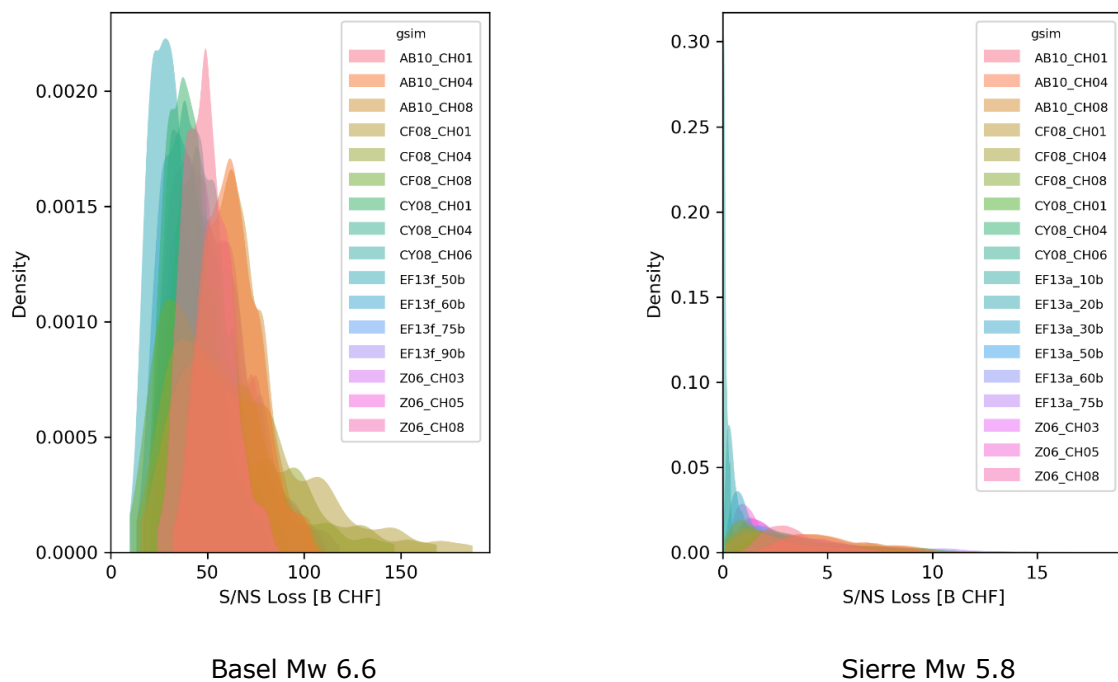
Figure 10.2. Basel Mw 6.6 (left) and Sierre Mw 5.8 (right) structural/non-structural loss aleatory distributions by GMPE.

Basel Mw 6.6

Sierre Mw 5.8

Figure 10.3. Basel Mw 6.6 (left) and Sierre Mw 5.8 (right) structural/non-structural loss aleatory distributions by IPE.
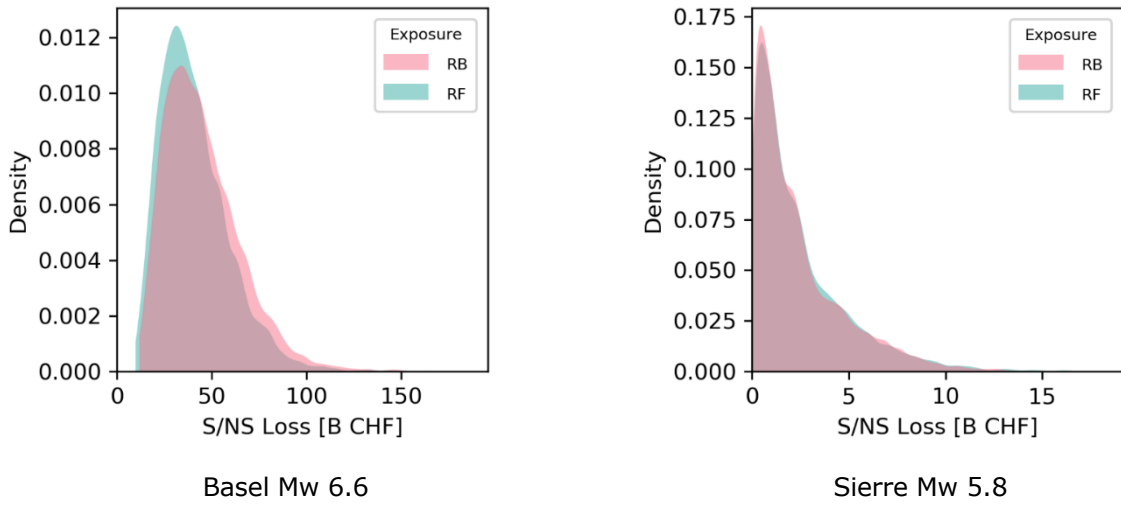

Basel Mw 6.6

Sierre Mw 5.8

Figure 10.4. Basel Mw 6.6 (left) and Sierre Mw 5.8 (right) structural/non-structural loss aleatory distributions by exposure logic tree branch.
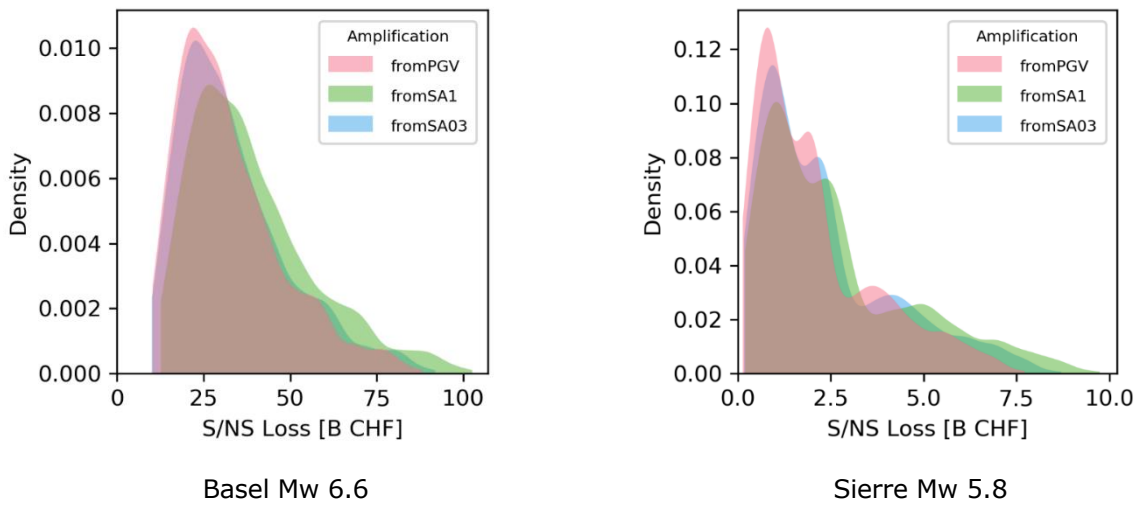

Basel Mw 6.6

Sierre Mw 5.8

Figure 10.5. Basel Mw 6.6 (left) and Sierre Mw 5.8 (right) structural/non-structural loss aleatory distributions by amplification logic tree branch.

10.2.3   RF vs RB exposure branch

The results obtained from the two different exposure branches are analysed in more detail to understand whether local differences and/or regional patterns can be identified. Figure 10.6 and Figure 10.7 show ratios of AAL obtained from the RF branches over AAL obtained from the RB branches, by canton and municipality respectively. While at the country-wide scale, the results of the two models are highly convergent, here we see notable differences, especially at the municipality level. This highlights the importance of considering both models to capture the relevant uncertainty.
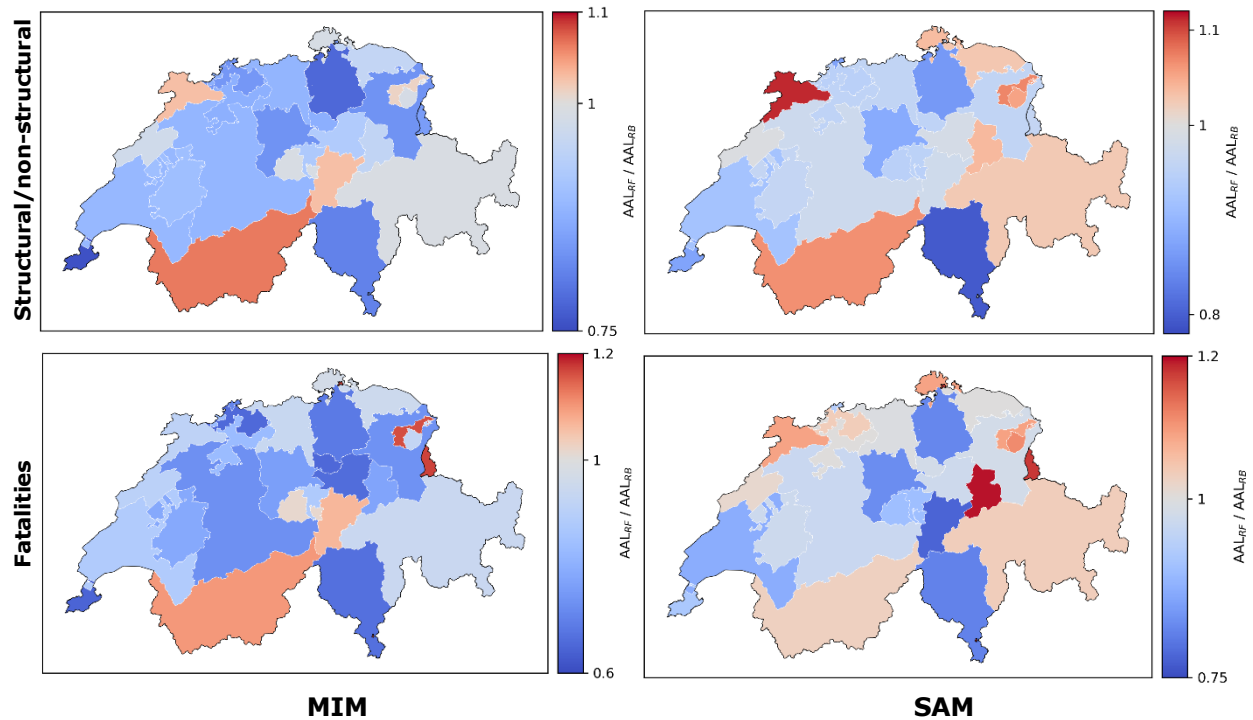
Figure 10.6. Comparison of AAL obtained from the RF versus RB exposure branches by canton. The colours refer to the ratio of AAL obtained from RF over the AAL obtained from RB.
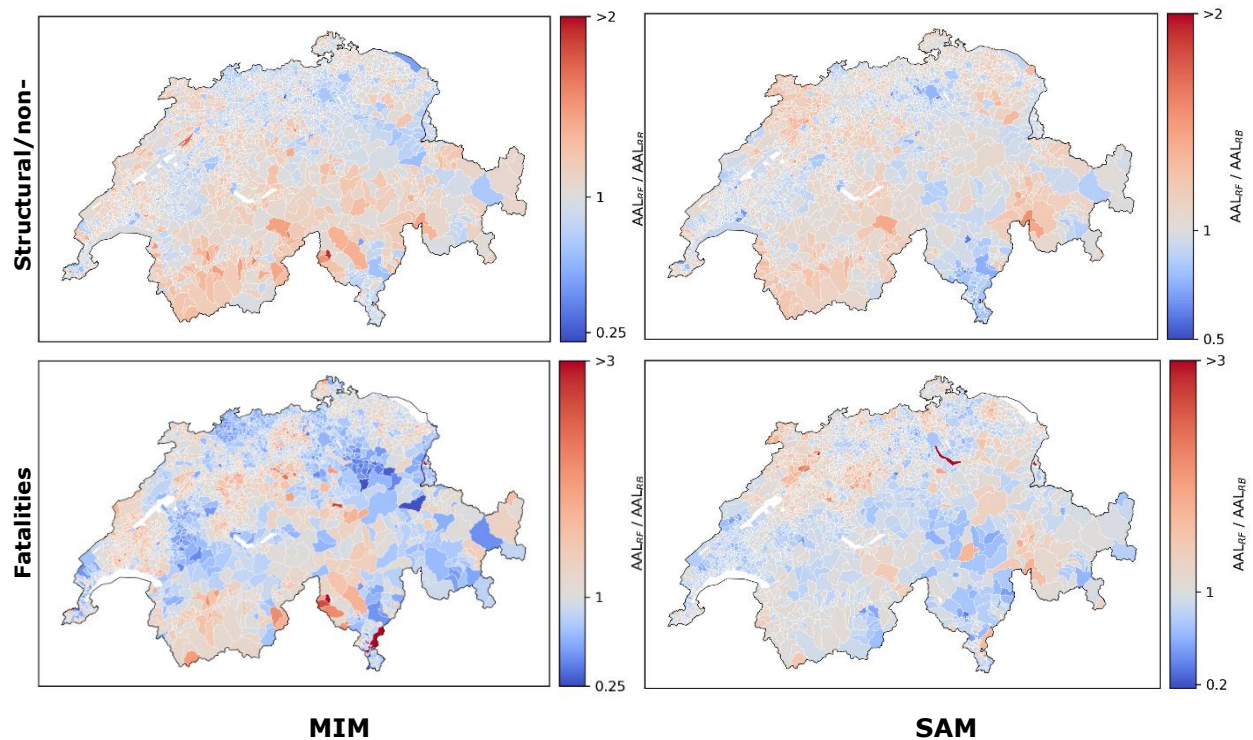
Figure 10.7. Comparison of AAL obtained from the RF versus RB exposure branches by municipality. The colours refer to the ratio of AAL obtained from RF over the AAL obtained from RB.

10.3 Model investigation

10.3.1 Effect of site amplification

ERM-CH relies upon a high-resolution amplification model, so investigating the effect of site amplification on loss estimates is of particular interest. To this end, and also for understanding the differences in the spatial pattern of loss between MIM and SAM, risk estimates were obtained for the two models, also assuming rock conditions. The left panels of Figure 10.8 show AAL estimates on rock. We can see that the pattern tracks the pattern of seismicity, with the SAM model giving a relatively smoother pattern. The latter is likely a result of the slower attenuation of intensity in MIM, which tends to result in milder differences in hazard across nearby locations. Therefore, the varying composition of the building stock in different municipalities creates this less smooth pattern in MIM. On the right panels, we can see the loss estimates on soil. As expected, areas of high site amplification, such as valleys and the shores of lakes and rivers, stand out. The 'amplified' AALR estimates are up to about an order of magnitude higher in certain locations, highlighting the importance of an adequate modelling of site amplification.

We also take a look at the difference in site condition-related loss amplification between MIM and SAM. Figure 10.9 shows the ratio of AAL on soil and rock on the left, which we will refer to as loss amplification. On the right, it shows that ratio of loss amplification in SAM over MIM. In general, we cannot discern any particular pattern, and given that the MIM and SAM amplification models are derived from the same data, the differences from municipality to municipality are likely a result of the complex relationship between ground motion intensity prediction, amplification, exposure and vulnerability.
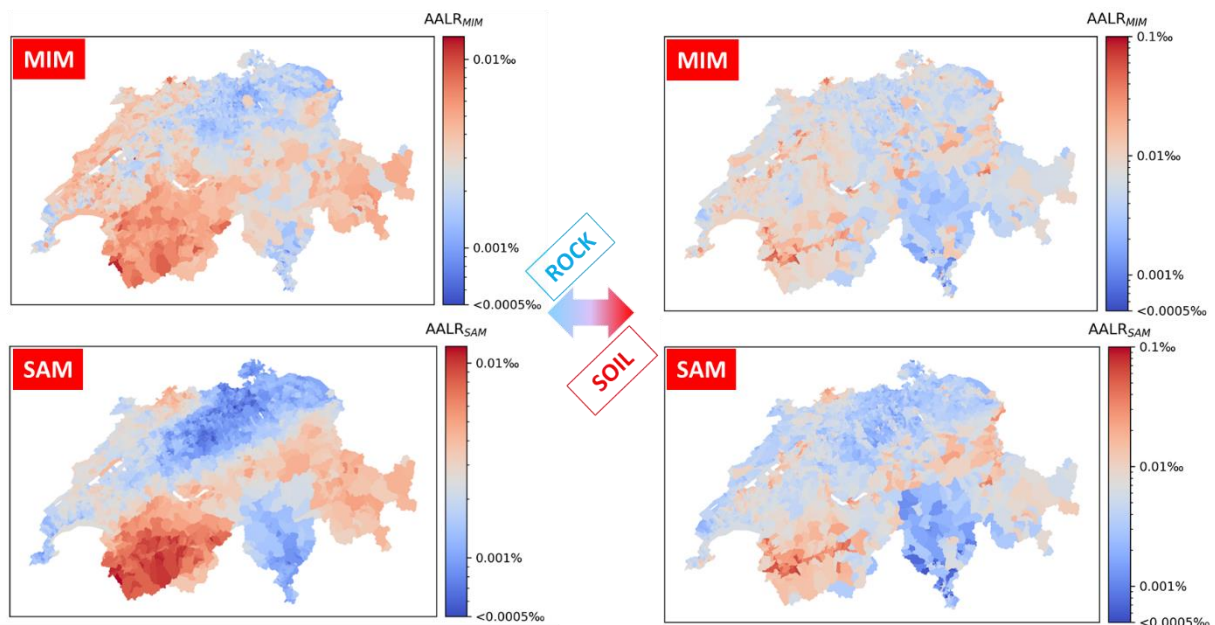
Figure 10.8. Impact of site amplification on structural/non-structural AAL for MIM and SAM.
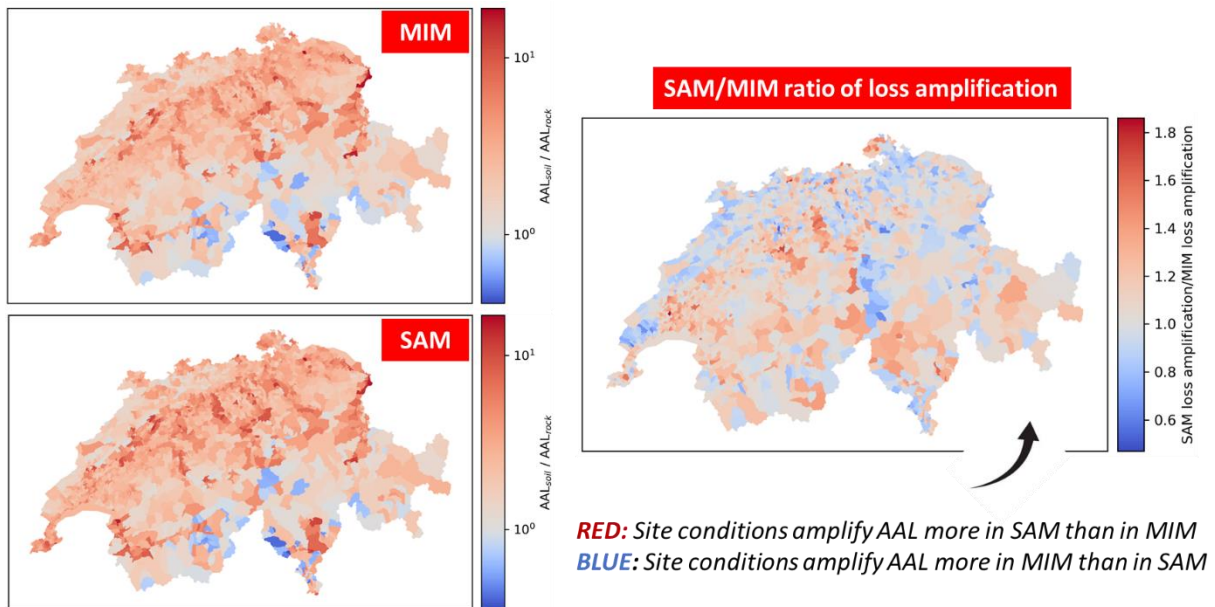
Figure 10.9. Comparison of site amplification-related increase in AAL between MIM and SAM.
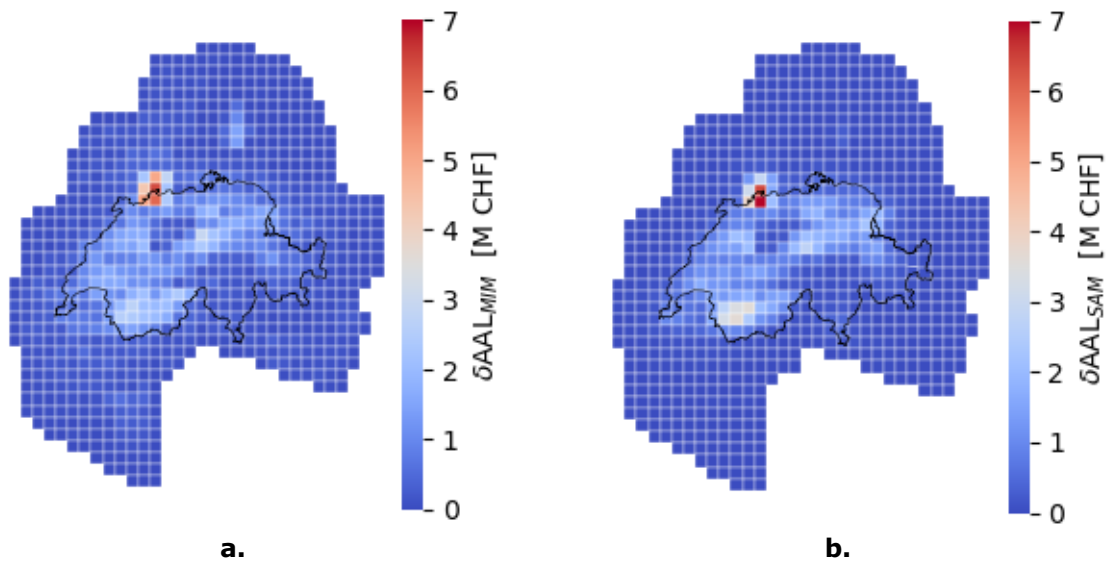
10.3.2   AAL disaggregation

Figure 10.10 presents the contribution of different magnitude bins to the overall structural/non-structural AAL estimates of MIM, SAM and the overall ERM-CH23. In general, we observe that the larger and rarer earthquakes of Mw>6.0 and even more so Mw>6.5 are the main contributors to AAL, with moderate and small earthquakes also contributing to some extent. No big differences are identified between the two submodels.

Figure 10.11 presents the disaggregation of the overall structural/non-structural AAL estimates by rupture location. In other words, the colour scale describes the contribution of ruptures occurring in each grid cell to the overall country-wide structural/non-structural AAL. We observe a some-what smoother pattern in MIM than in SAM, where the contributions are largely concentrated around areas of dense exposure. The difference between models, shown in the bottom panel of Figure **10.11**, better highlights this observation.

In general, this agrees with observations from the assessment of GMPE/IPE trellis plots and sce-nario calculations. MIM features a slower intensity attenuation with distance, which here manifests in contributions from rupture further away from exposure concentration. On the other hand, the damage/loss estimates in SAM are generally higher in the epicentral area, but attenuate faster with distance. This is shown here by the sharper contrast in adjacent grid cells. For instance, rup-tures occurring in the grid cell that contains the city of Basel (high exposure concentration) con-tribute more to the AAL in SAM compared to MIM. The opposite is true for the grid cells surround-ing Basel, where ruptures cause more losses according to MIM than according to SAM.
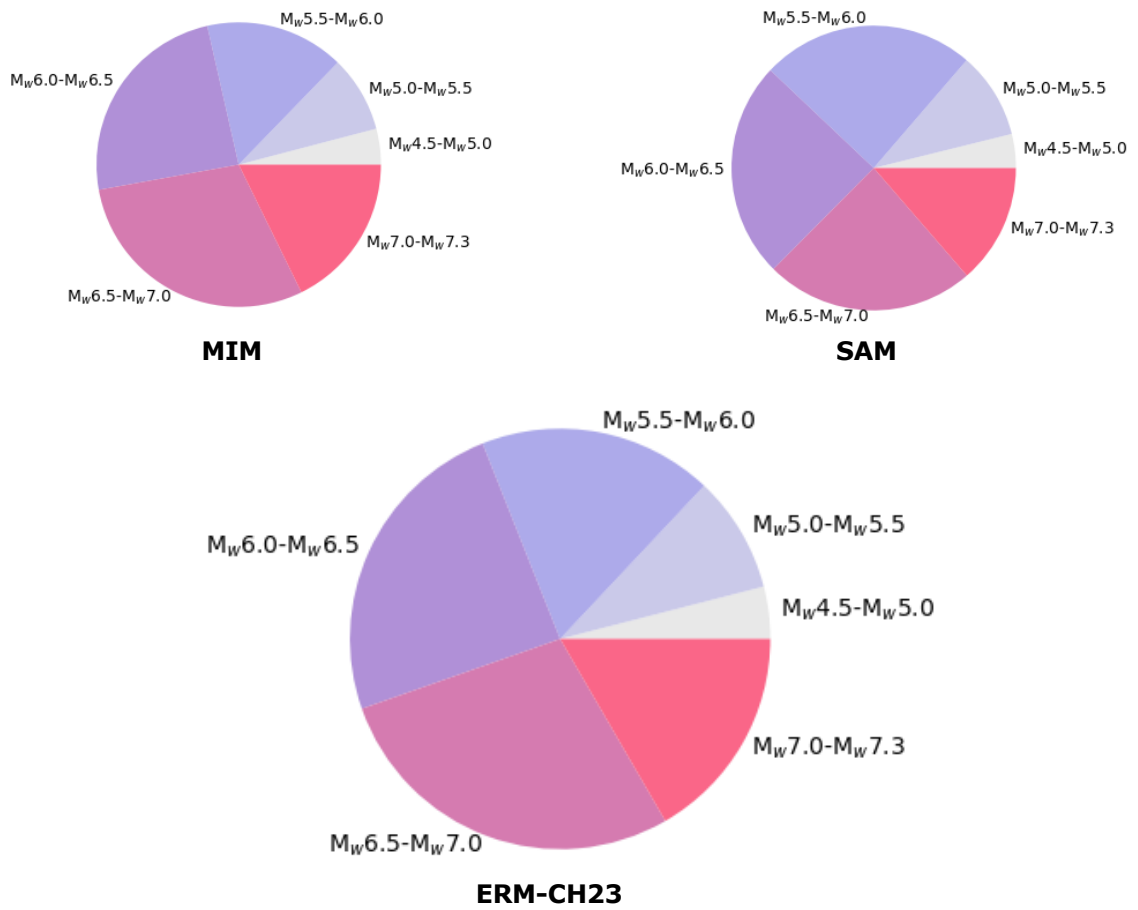
Figure 10.10. Structural/non-structural AAL disaggregation by magnitude bin for MIM, SAM and overall ERM-CH23.

c.   **d.**
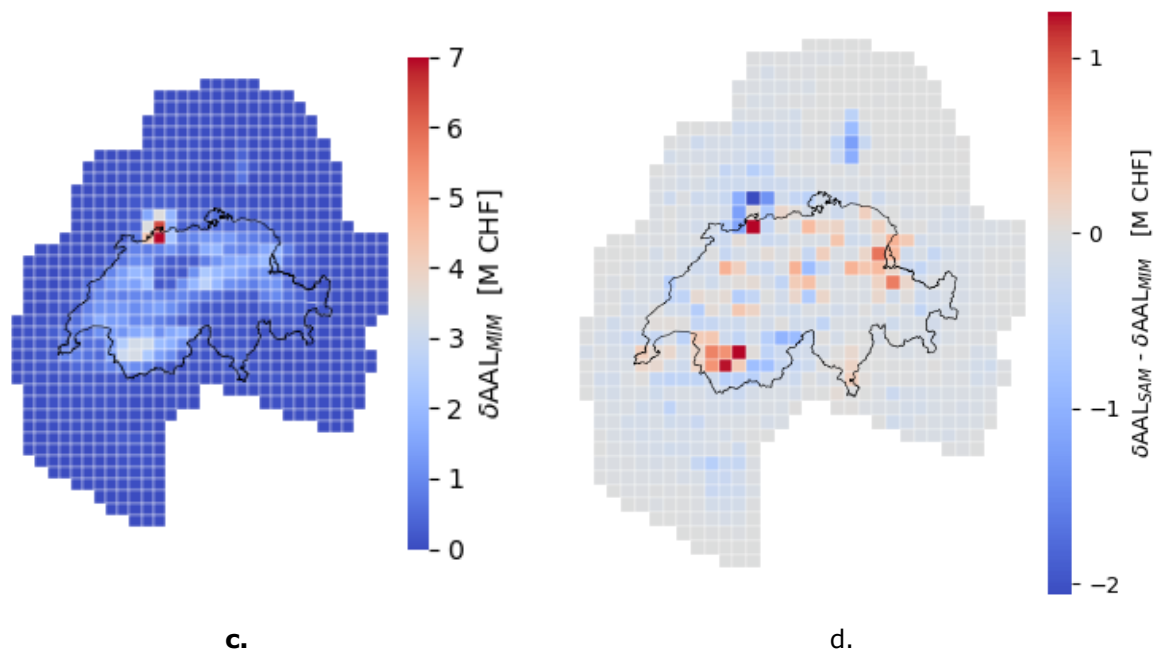
Figure 10.11. Loss disaggregation by rupture location for MIM (a), SAM (b) and overall ERM-CH2023 (c) model; difference in rupture location contributions between SAM and MIM (d).

A disaggregation was also performed for the canton of Geneva, as requested by the review committee. The top panels in Figure 10.12 below show the contribution (in CHF million) of ruptures within 15 x 15 km grid cells to the total canton of Geneva structural/non-structural AAL. The bottom panels show the disaggregation by magnitude and epicentral distance (measured to the centre of the city of Geneva); the colour refers to the contribution in percentage (normalised) towards the total AAL. As also seen in the disaggregation of country-wide AAL, likewise in Geneva we see contributions from a wider geographic area in MIM as opposed to SAM. Notably, in MIM, while (like SAM) the individual cells contributing the most to the AAL lie close to Geneva, we see a large number of cells with medium contributions in the more seismically active canton of Valais, as well as from France and Italy. This finding is in line with the previous observation of the slower attenuation of intensity/loss seen in MIM compared to SAM.

Lastly, AAL disaggregation was also indicatively performed for a few major cities. Figure 10.13 displays the disaggregation of structural/non-structural AAL for the municipalities of Basel, Bern and Thun.

MIM   **SAM**
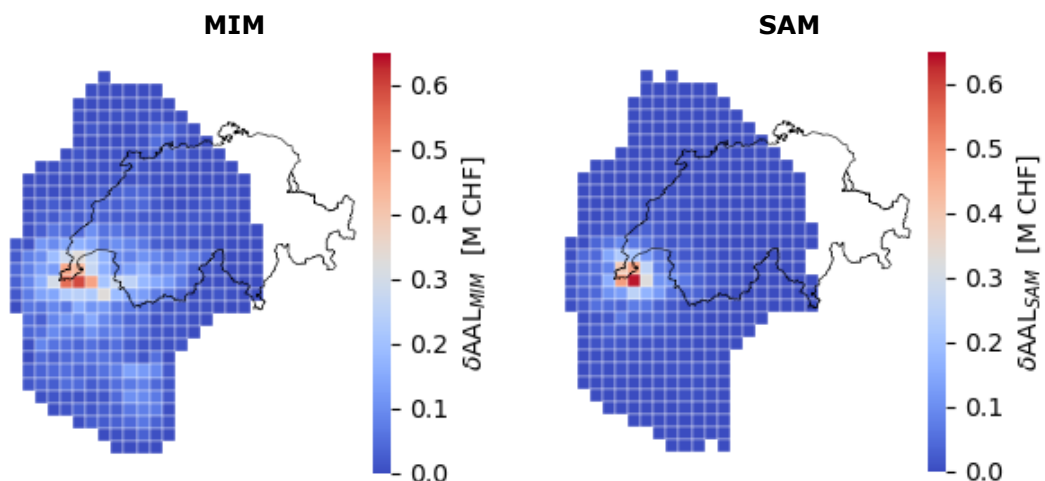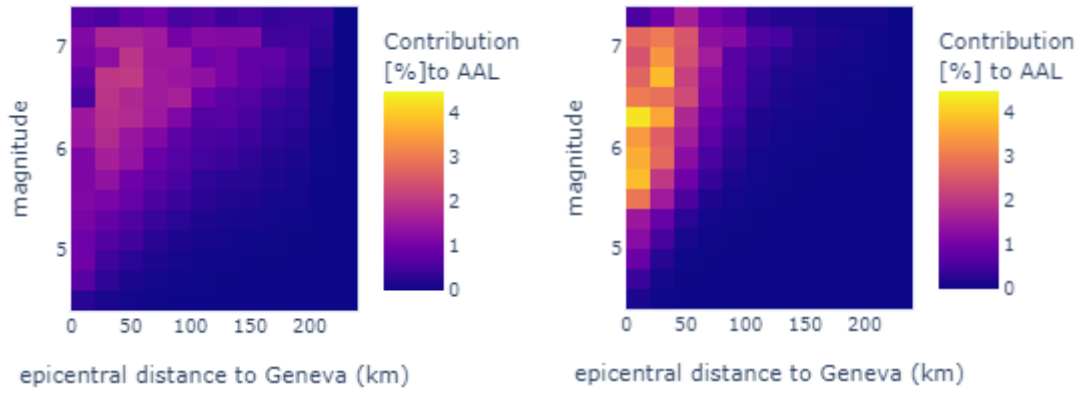
Figure 10.12. Disaggregation of canton of Geneva structural/non-structural AAL for MIM (left) and SAM (right), by location (top) and magnitude-epicentral distance to the city of Geneva (bottom).
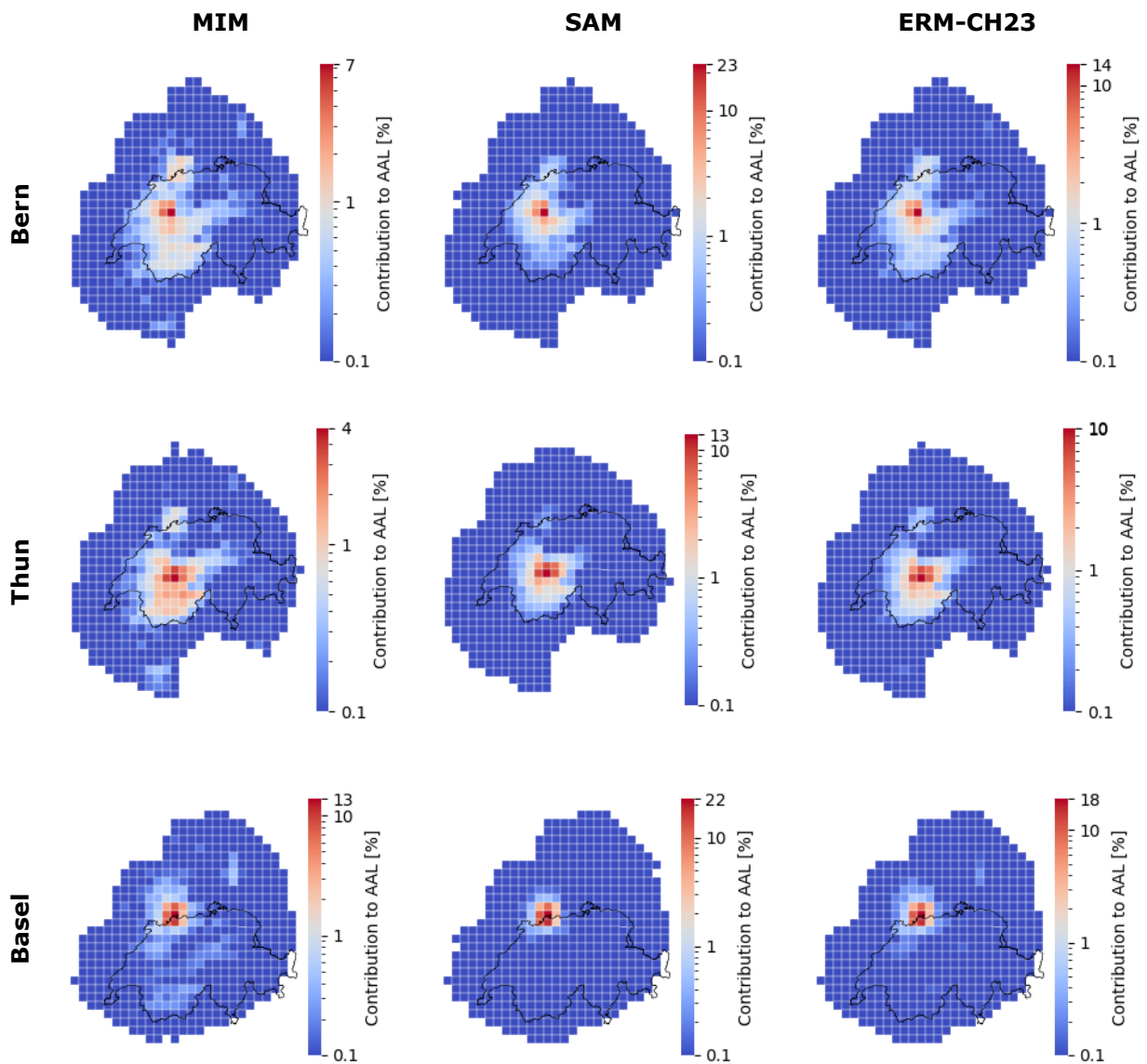
Figure 10.13. Disaggregation of municipal structural/nonstructural AAL for Basel, Bern and Thun for MIM (left), SAM (middle) and ERM-CH23 (right) by location.

10.3.3 Ground motion fields for specific loss return periods

In Figure 10.14, random ground motion fields associated with specific loss return periods are illustrated to gain insight into the kind of events that cause such loss estimates. It should be noted that these should be seen as indicative, as other earthquakes of different magnitude and location can also be retrieved from the stochastic catalogues causing only slightly lower or higher loss.
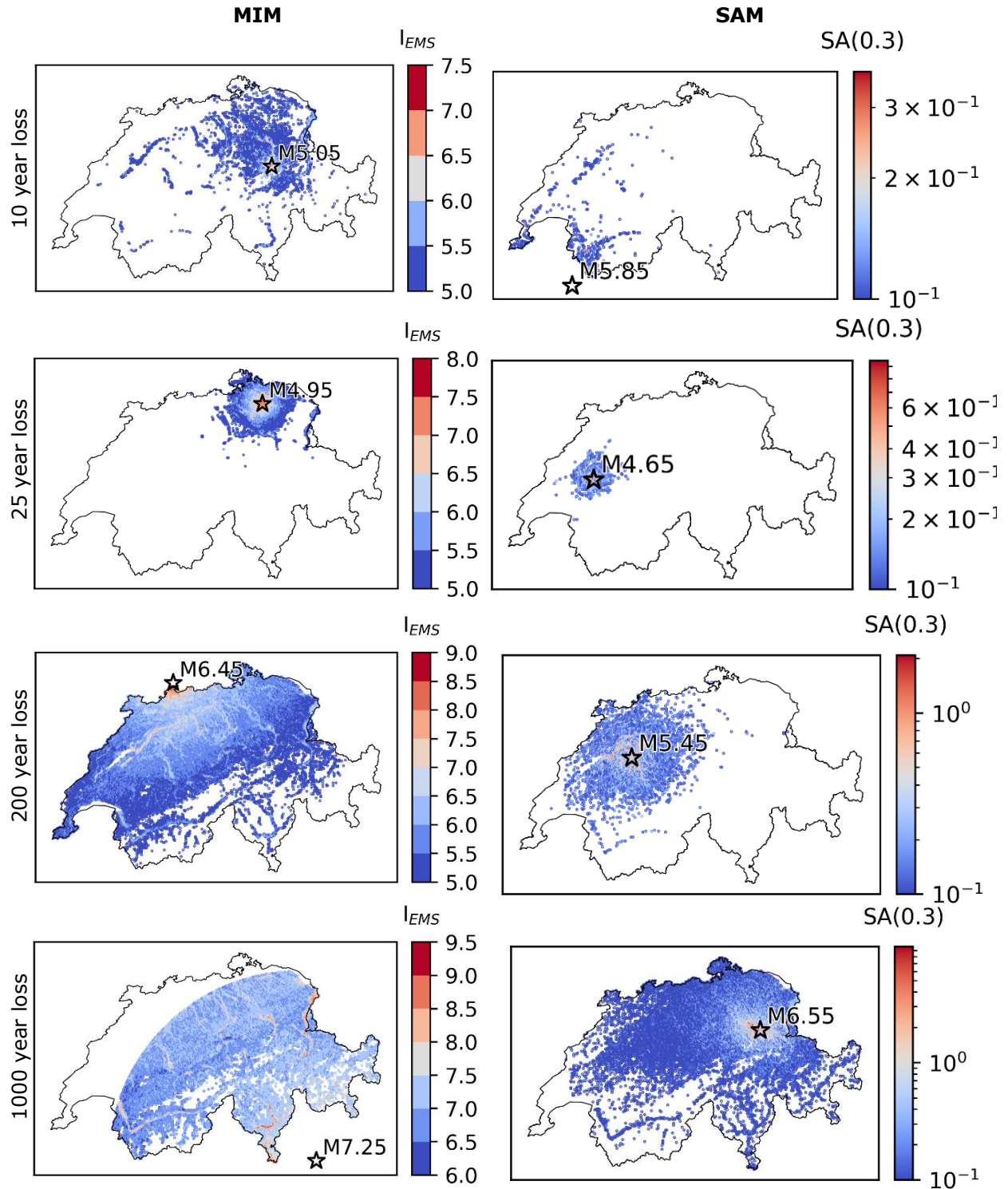

Figure 10.14. Random ground motion fields associated with events of a specific structural/non-structural loss return period for MIM and SAM.

10.4 Comparison with other risk models

It is important to place the results of ERM-CH23 in the context of other recently published models. In this section a comparison is made between the AAL and probable maximum loss curves of ERM-CH23, and those from ESRM20 (Crowley et al., 2021) model, GEM18 (Silva et al., 2020) and GAR15. Table 10.1 shows a comparison of AAL estimates. Overall, we see that ERM-CH23 predicts significantly higher losses compared to the other models. The MIM/SAM weighted average absolute S/NS loss estimates are in the order of four times higher than ESRM20 and more than double GEM18. The average annual loss ratio, on the other hand, is twice as high as ESRM20 and only slightly higher than GEM18, indicating that the total value modelled in ERM-CH23 is much higher than these other models. With respect to fatalities, the ERM-CH23 average estimate is about four times above ESRM20, although a significant discrepancy is seen between MIM and SAM, with MIM's estimate much closer to ESRM20.

Table 10.1. Comparison of ERM-CH23 AAL estimates with other models

		ERM-CH MIM	*ERM-CH SAM*	**ERM-CH**	**ESRM20**	**GEM18**	**GAR15**
Structural and nonstructural economic losses	AAL	*296 M CHF*	*224 M CHF*	245 M CHF	55 M EUR	100 M USD	786 M USD
	AALR [‰]	*0.1*	*0.077*	0.084	0.043	0.07	
Fatalities	AAL	*1.8*	*10.1*	7.6	2		
	AALR [‰]	*0.00024*	*0.0013*	0.00099	0.0002		
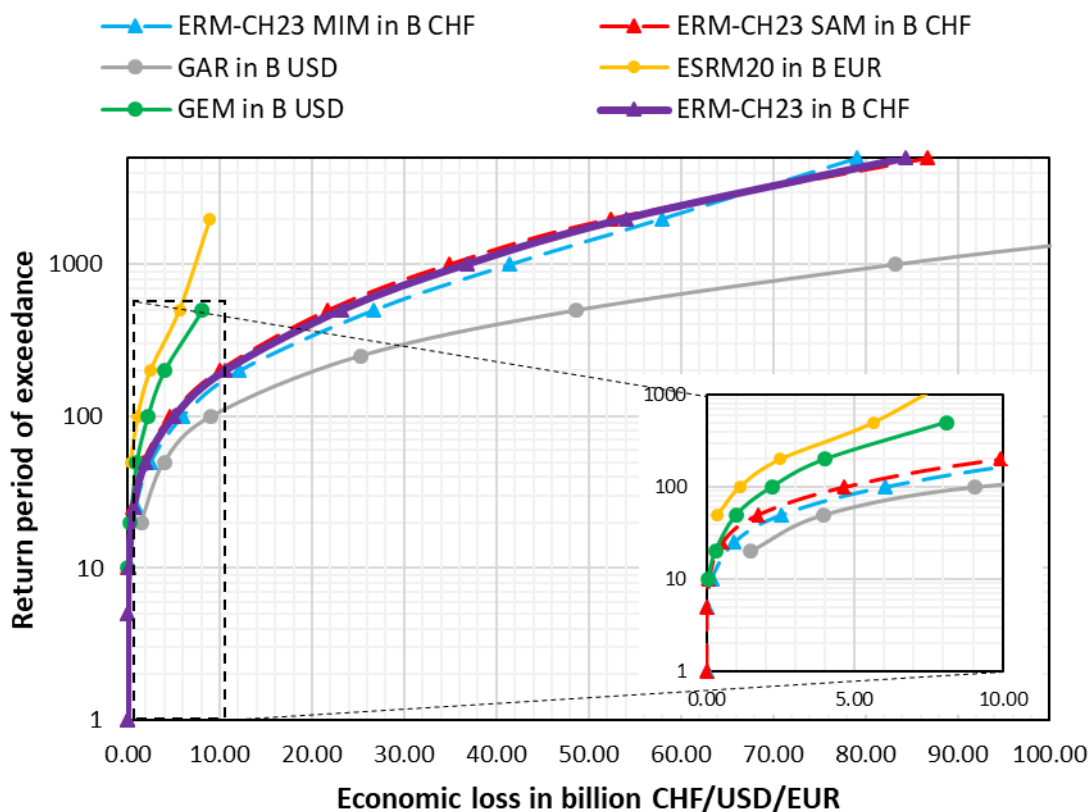
Figure 10.15. Comparison of probable maximum loss curves between different models.

Figure 10.15 provides a similar comparison in terms of probable maximum loss curves (loss versus return period). For return periods above 50 years, both models start to diverge compared to ESRM20 and GEM18, with the differences growing larger for longer return periods. That said, the normalised estimates of ERM-CH23 seem to be in the same ballpark as those of the other public models, especially taking into account the vast uncertainties involved in the development of such models.

References

Bindi, D., Parolai, S., Oth, A., Abdrakhmatov, K., Muraliev, A., Zschau, J., 2011. Intensity prediction equations for Central Asia. Geophysical Journal International **187**, 327–337. https://doi.org/10.1111/j.1365-246X.2011.05142.x

Crowley, H., Dabbeek, J., Despotaki, V., Rodrigues, D., Martins, L., Silva, V., Romão, X., Pereira, N., Weatherill, G., Danciu, L. (2021). European Seismic Risk Model (ESRM20) [EFEHR Technical Report 002 V1.0.0]. Eucentre. https://doi.org/10.7414/EUC-EFEHR-TR002-ESRM20

Silva, V., Amo-Oduro, D., Calderon, A., Costa, C., Dabbeek, J., Despotaki, N., Martins, L., Pagani, M., Rao, A., Simionato, M., Viganò, D., Yepes-Estrada, C., Acevedo, A., Crowley, H., Horspool, N., Jaiswal, K., Journeay, M., Pittore, M. 2020. Development of a Global Seismic Risk Model. Earthquake Spectra (February):875529301989995.

11.   Communicating seismic risk

Over recent decades, experience has been acquired in how best to communicate earthquake hazard and, hence, the likelihood of earthquakes occurring within a specific period in a defined region. There are already many challenges associated with earthquake hazard communication (Marti et al., 2019), so also including information about earthquake risk only adds to the complexity. One reason is that non-experts do not differentiate between hazard and risk, instead using these terms synonymously. Furthermore, general knowledge and awareness of earthquakes and their potential threats for Switzerland are very limited, demanding very instructive and explanatory information (Dallo et al., 2022a). Nevertheless, from a societal perspective and compared to seismic hazard, seismic risk is a figure that is both easier to understand and more useful when it comes to earthquake awareness, preparedness and event mitigation.

Aware of these challenges, and based on established best practices (Marti et al., 2020), we strove to test key outreach products of the Swiss earthquake risk model before their release. The aim was to design understandable communication materials that support a variety of stakeholders in taking informed decisions. All communication activities were based on a comprehensive communication concept that was developed gradually and iteratively supplemented. The communication concept defined the strategy, including target audiences, communication goals as well as key messages, and helped to ensure that all communication products were aligned with each other.

11.1 Best practices in communicating earthquake risk

Empirical evidence on how best to communicate earthquake risk to societies is limited and, thus, future research is needed to test current practices and new product versions. In the following, we summarise some relevant insights from prior studies with a focus on rapid impact assessment reports, scenarios and earthquake risk maps. Our testing results are summarised in Section 11.5.

Rapid impact assessment reports are used to inform emergency responses minutes to hours after an earthquake occurs (Erdik et al., 2011). Already-operating rapid impact assessment services include PAGER (international; see Figure 11.1), ShakeCast (national), QLARM (international) and InaSAFE (national). Whereas PAGER, QLARM and InaSAFE are publicly available to everyone, ShakeCast is only distributed to specific stakeholders since it depicts damage to specific infrastructure (Lin et al., 2020). They primarily aim at supporting first responders and emergency managers to enhance disaster management, but are also used as an information source by journalists and the public. However, Karjack et al. (2022) showed that users have difficulties in correctly interpreting the content of the PAGER leaflet – especially the histogram – and are thus hesitant to take action. This finding highlights the need for research on how to better communicate the uncertainties behind the estimates.

Scenarios bring order to complex interdependencies and, thus, support societies with translating scientific insights into, for example, management plans (Ronan and Johnston, 2005). Consequently, they can enhance societies' resilience towards earthquakes (Detweiler and Wein, 2018). Scenarios can either replicate a historical earthquake in today's context or present the estimated consequences of a possible event in the future (Fontiela et al., 2020), allowing a better understanding of what to expect and prepare for. Scenarios are relevant not only to professional stakeholders but also to the public. They may support them in taking decisions with regard to mitigation measures such as insurance contracting or the definition of emergency plans.

Earthquake risk maps are a further relevant product, especially since the public prefers this format to access risk information (Dallo et al., 2022b) and it is a common way to portray natural hazards (Fuchs et al., 2009). Risk maps make it possible to show the spatial risk distribution (Stieb et al., 2019) and so to understand where the impacts – fatalities, injuries, economic loss-

es, etc. – are the highest (Fuchs et al., 2009; Marker, 2013). An example is the European seismic risk map based on the European Seismic Risk Model (ESRM20), which was publicly released in spring 2022 (Figure 11.2). The communication team at the SED, together with the model developers, designed, among other products, the European earthquake risk map and tested it with end users, i.e. students at European universities and professional users. The main learnings from this testing are: i) white areas lead people to think that there is no earthquake risk; ii) maps with hillshading are preferred; iii) smoothing effects can be used to avoid clear borders between risk cells; iv) qualitative labels of the risk categories should be combined with numerical values, i.e. what does 'high' mean in terms of losses?; v) capitals of all countries should be displayed to facilitate geographical orientation; vi) for marking the location of cities on a map, empty circles should be used so as not to cover the colour below; and vii) an indicative legend title should be added, e.g. earthquake risk index map.
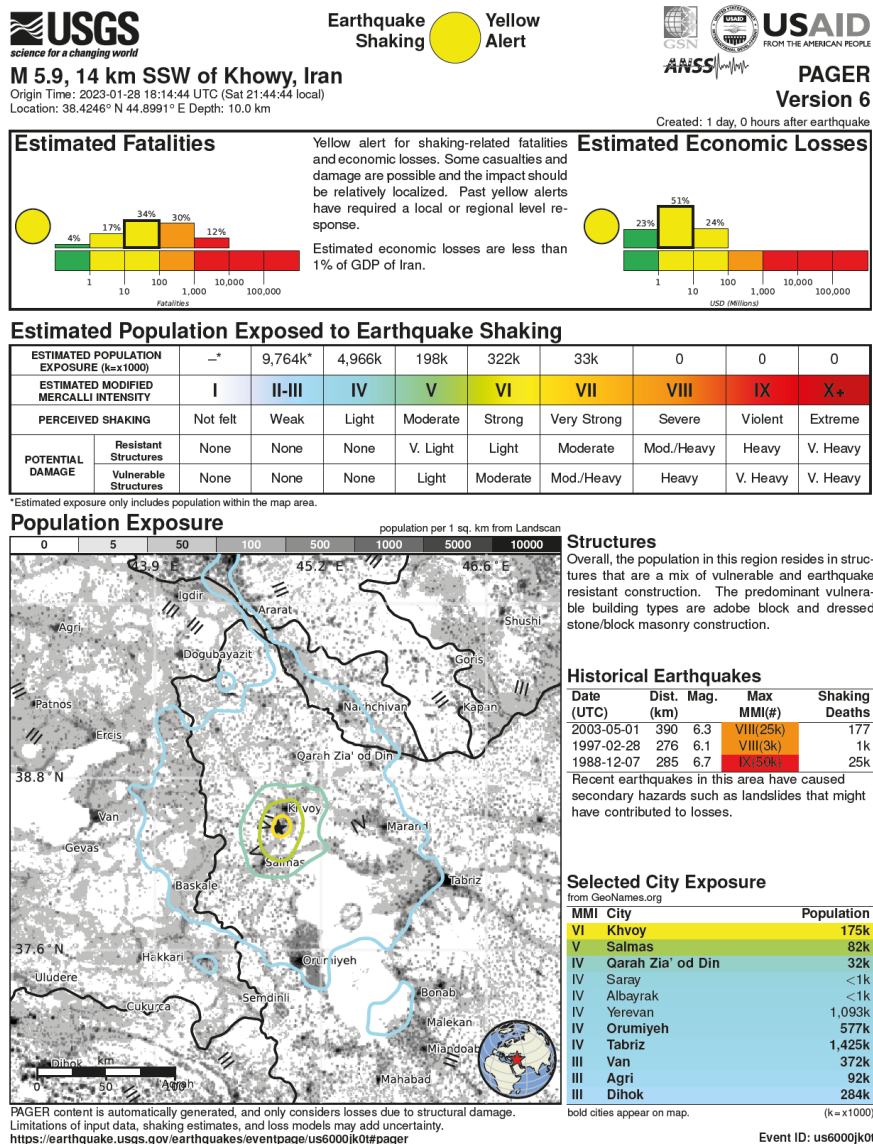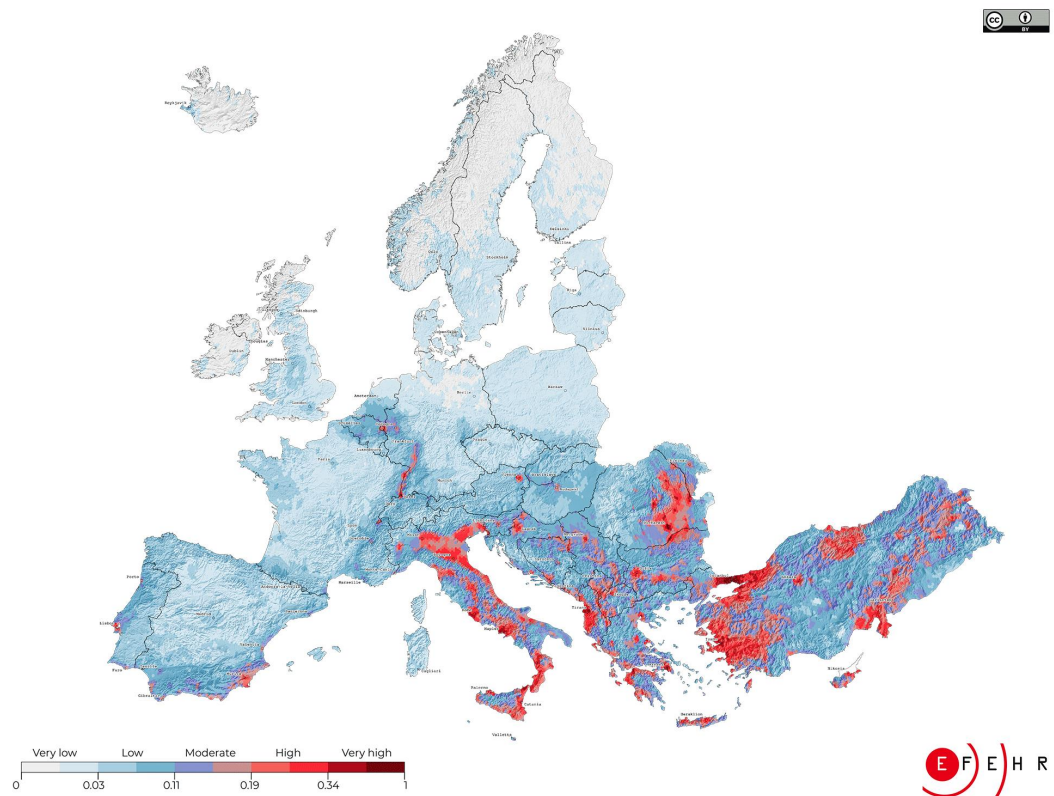

Figure 11.1. PAGER – an exemplary rapid impact assessment report

Figure 11.2. The European earthquake risk map (Crowley et al., 2021).

11.2 Insights into the communication concept

A dedicated communication concept is needed to bring the insights of Switzerland's first publicly available earthquake risk model to the different stakeholders. Communication concepts are a well-established tool in practical communication management. They serve as a systematic problem-solving approach, ranging from situation analysis through defining a strategy and implementing communication measures to evaluation efforts (Bentele and Nothhaft, 2007). There are many challenges in developing a communication concept since different aspects must be taken into consideration, including internal communication policies and external factors (Immerschitt, 2009).

The communication concept for the release of the earthquake risk model of Switzerland is based on a comprehensive analysis by the communication team, enriched by discussions at an internal workshop to consolidate the strategy and formulate key messages.

In the following, we summarise the key insights from the analysis and strategy part of the communication concept. The implemented communication activities and products are described in the next two sections.

Analysis

A SWOT analysis (Bentele and Nothhaft, 2007) was used to identify the strengths, weaknesses, opportunities and threats associated with the release of the earthquake risk model. From the SWOT analysis, we drew the following conclusions:

– Thanks to previous experiences from similar projects as well as its reputation and affiliation with ETH Zurich as a leading research institution, the SED is in a strong position to establish and apply a useful communication strategy.

– Pre-existing interest among target audiences, the established cooperation with federal authorities, and the socially relevant topic itself offer many opportunities for communication.

– The primary challenges for communication are i) the complexity of the topic and its potential for misunderstanding, ii) the high expectations of the different stakeholders with regard to the model and its results, and iii) the tone of the communication, i.e. striking a balance between raising awareness and not spreading panic.

Strategy

In the second part of the concept, we first identified the different target audiences, defined the communication goals, and formulated the key messages. All these steps had to be aligned with each other.

We defined nine **target audiences** that can all have an impact on increasing Switzerland's resilience to earthquakes in their scope of action. Based on their level of influence in this area, we consider the representatives of the cantons, the municipalities and the federal authorities as the primary target audiences. We also see the public (including homeowners), businesses, the education sector, the media, and engineers and architects to be essential for our communication activities. The latter two groups (media, engineers and architects) can be defined as 'gatekeepers' since they can help to inform the general public. Architects and engineers, for example, can improve earthquake resilience when consulting (future) homeowners regarding earthquake-resistant construction. Since the development of Switzerland's earthquake risk model is also of scientific relevance, we defined academia as an additional target audience. Another target audience comprises insurance companies, large property owners and real estate companies, which are particularly interested in specific products and applications of the model. In general, the defined target audiences are very different in terms of their prior knowledge of earthquake risk, their interests and needs. Being aware of these differences helps in the development of the communication goals and key messages as well as in the design of the products and communication activities.

The **communication goals** are divided into cognitive (attention, knowledge), affective (emotions, attitude, trust) and conative (behaviour, actions) goals which build on each other. The communication goals for this project focus particularly on knowledge transfer, information on results, and explanations of the model (development, components, purpose and uncertainties). In addition, the goals address aspects related to product information, stakeholder involvement and earthquake risk mitigation. Three examples of overarching communication goals are given here, covering the three dimensions:

1. Cognitive (goal: to increase knowledge)

The target audiences know where the earthquake risk is high in Switzerland and the reasons why.

2. Affective (goal: to build trust)

The target groups perceive the earthquake risk model of Switzerland, available information materials and services as reliable, useful and trustworthy.

3. Conative (goal: to motivate target audiences to act)

The target audiences are motivated to think about appropriate earthquake risk mitigating measures within their respective scope of action thanks to the available information materials and products.

Key messages help to highlight the essential aspects of a project and enable consistent communication with different target audiences across the various products and communication activities. The specific key messages were derived from the following core themes that we defined as essential for the release of the Swiss earthquake risk model:

– Release of the earthquake risk model

– Switzerland as an earthquake country (knowledge transfer)

– Earthquake risk model development

– Limitations and uncertainties

– Results of the earthquake risk model

– Earthquake risk mitigation measures

– Products

11.3 Products

We developed a number of products based on the assessed needs of the different target audiences. These include a range of products supporting decision-making for earthquake preparedness and response, such as rapid impact assessments and scenarios. We also designed various information materials covering the model and its results. The main products were tested beforehand and revised accordingly to ensure that they best fulfilled end users' needs (see Section 11.5).

Rapid impact assessments

The rapid impact assessments provide an overview of the expected impact shortly after the occurrence of an earthquake. Based on the earthquake risk model of Switzerland (ERM-CH23), we will publish such a report after every earthquake with a magnitude of 3 or greater. The rapid impact assessment informs the public and emergency services about the expected impacts of an event that is felt over a wide area or causes damage. Damage is possible near the epicentre with quakes of magnitude 4 and above. There will always be a national overview (Figure 11.3) and a cantonal overview. Whereas the national overview will be published on the SED website, the cantonal overview will be available for authorities only via protected access. The design and layout of the rapid impact assessment follow that of the scenarios to ensure comprehensibility since users are already used to them (see next section). Much effort went into the development and presentation of the rapid impact assessments, requiring resources from different fields such as model developers, IT specialists, graphic designers and communication specialists (see Section 11.5.3).

Scenarios

Scenarios are an essential element of earthquake preparedness. Together with the publication of ERM-CH23, 59 scenarios were made available on the SED website. They illustrate the expected impacts of historical earthquakes were they to occur again today, and of a magnitude-6 earthquake for each cantonal capital and one other locality. On average, such an event occurs every 50 to 150 years somewhere in Switzerland or its neighbouring regions.

The scenarios serve to sensitise the authorities and the public to the potential impacts of damaging earthquakes in Switzerland, and to improve the preparation for and management of earthquakes. As with the rapid impact assessments, there is also a publicly accessible national overview (Figure 11.4) and the cantonal overviews are only accessible for authorities.
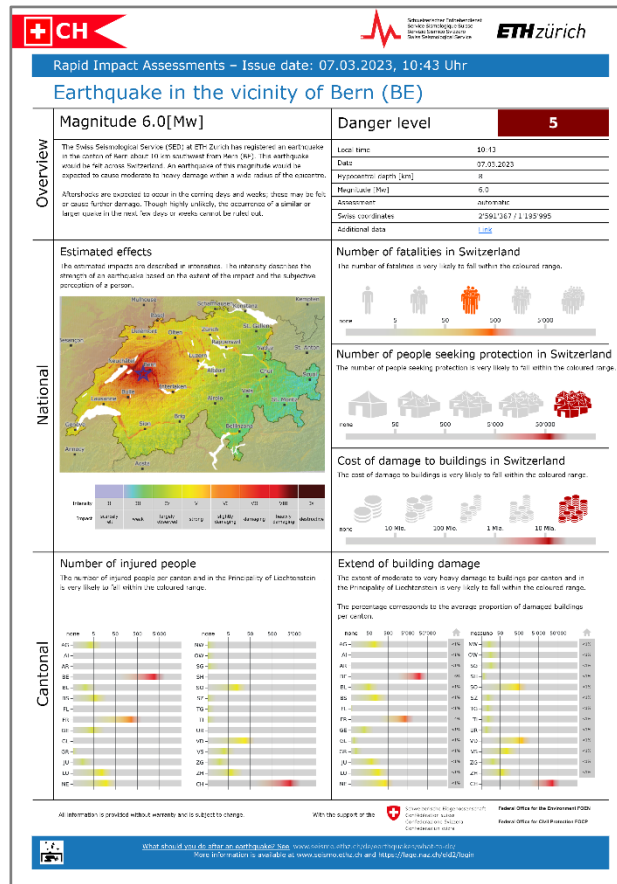
Figure 11.3. National overview of a hypothetical rapid impact assessment
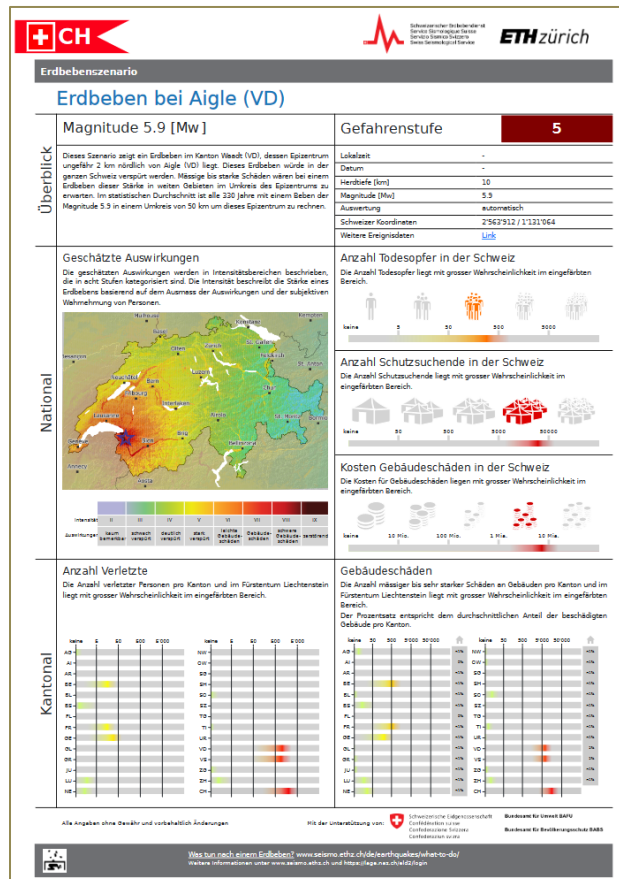

Figure 11.4. National overview of the magnitude 5.9 scenario of Aigle (VD).

Maps

Several maps help end users to explore and understand earthquake risk and its components, namely earthquake hazard, exposure, soil amplification, and vulnerability in Switzerland.

Previous experience suggests that there is interest in a single map depicting earthquake risk. The map acts as a key visual to portray the main findings of the model. It therefore has to be well aligned with the communication goals and key messages. We chose the same index used for the European Earthquake Risk Map (Crowley et al., 2021) to illustrate the earthquake risk in Switzerland. Consequently, the earthquake risk map of Switzerland is based on an index that combines the expected number of fatalities with the estimated financial losses due to building damage (Figure **11.5**). In contrast to the European map, it is not normalised by GDP per capita.

The earthquake risk is highest in the areas coloured dark red and lowest in the light blue areas. The colour scale is suitable for people with a colour vision deficiency. In a representative survey, several map and legend versions were tested to ensure that the map fulfilled its purpose (see Section 11.5).
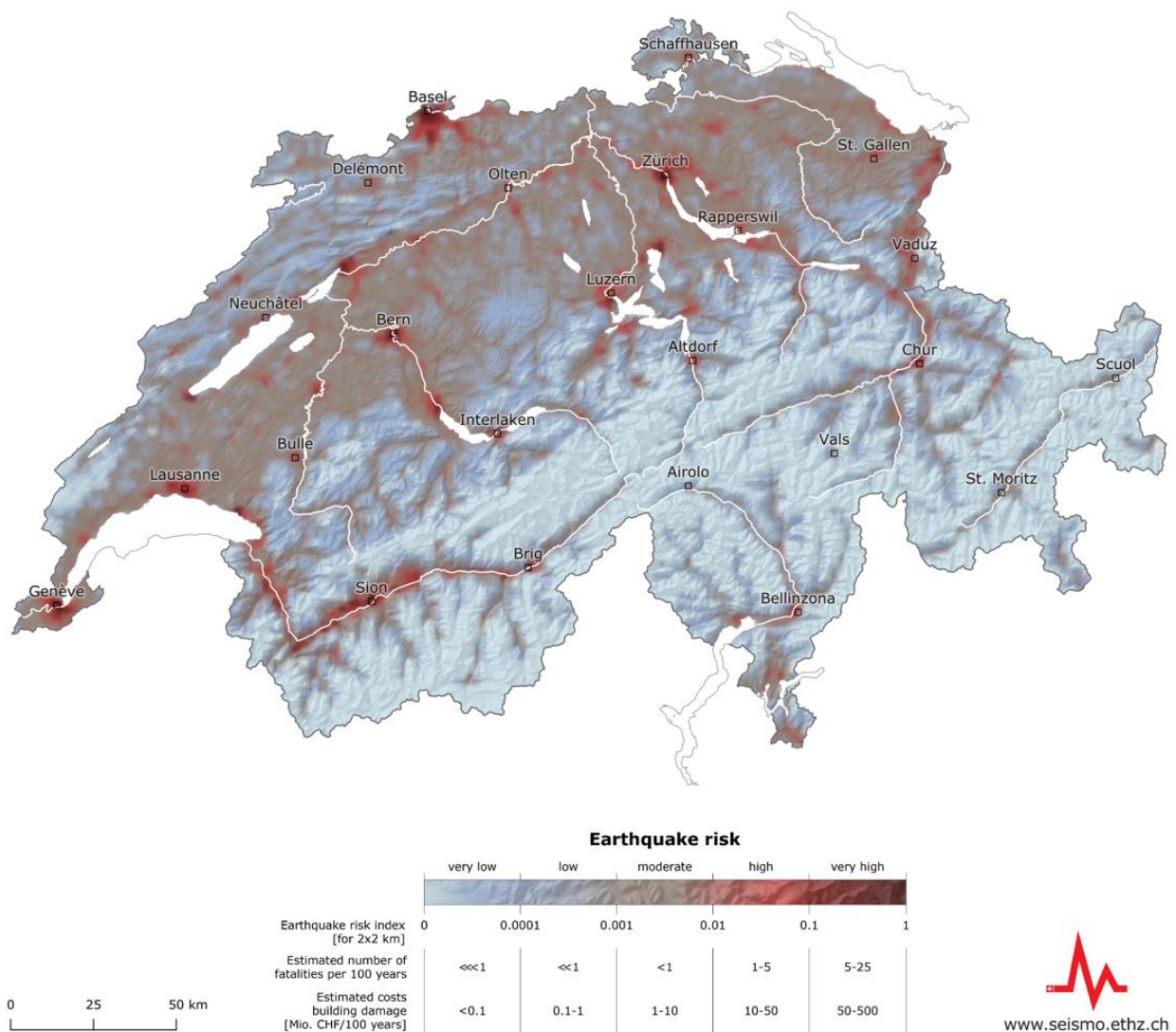
Figure 11.5: The earthquake risk map of Switzerland depicts an index that combines the number of fatalities and financial losses due to building damage expected in a 100-year period.
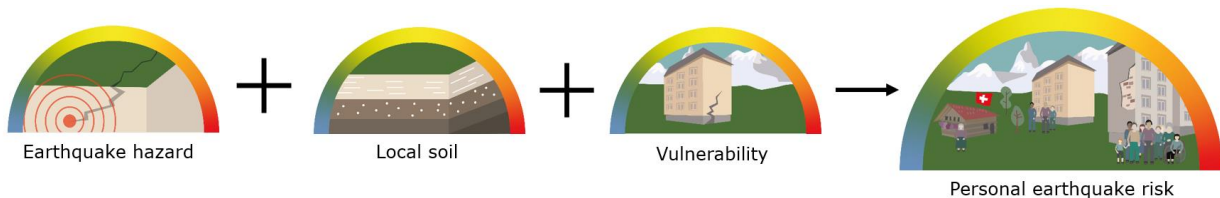
Earthquake risk tool

People are genuinely interested in learning more about their personal risk, i.e. how much they are potentially affected by earthquakes. To meet this need, the current version of an online risk tool allowing an estimation of one's personal earthquake risk was thoroughly revised. Not only was the database completely overhauled, based on the newly available results of the Swiss earthquake risk model, but the display was also redesigned.

The earthquake risk tool provides a very rough assessment of (Figure 11.6):

– the earthquake hazard at the location specified by the user;

– the local site conditions at that location;

– the vulnerability of a building, based on the specified number of floors and the construction period;

– the personal earthquake risk (risk of building damage, cost of building damage, risk of injury or death).

The earthquake risk tool is available on the SED website (www.seismo.ethz.ch).

Figure 11.6: Overview of the three components used to calculate personal earthquake risk.

Information material

A range of materials were created to inform people about the model and its results. They target different audiences and provide explanations on different levels (Figure 11.7). The SED website (www.seismo.ethz.ch) acts as a central information hub to access these materials.

– Flyer
The flyer contains the most important information about the earthquake risk in Switzerland, the model itself, and possible measures for risk mitigation. The flyer is intended as an introductory tool, offering a quick overview and potentially motivating people to seek further information.

– Poster
Posters are a popular way to present scientific findings concisely and clearly. We created a poster with the Swiss earthquake risk map as the central element.

– Explanatory video
An explanatory video was produced, allowing end users who would be unlikely to read texts to gain a brief overview of the most important aspects of the risk model and its results.

11.4 Events

A series of events was organised to publicise the release and the results of the Swiss earthquake risk model.
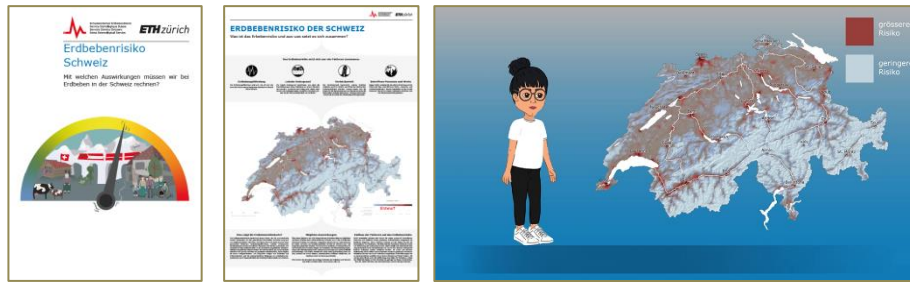
Figure 11.7. Cover page of the flyer, the poster and a snapshot of the explanatory video.

Pre-information for cantonal authorities

As already described (see Section 11.3), 59 scenarios became available with the release of the model. Since responsibility for earthquake mitigation and disaster management in Switzerland primarily lies with the cantons, their representatives were pre-informed about the scope, content, and limitations of the scenarios. To this end, an online information event including a Q&A section was held a month before the official release.

Media event

On the morning of the model release, a media event was organised to publicise the most important aspects. The media received the invitation, including a set of materials with an embargo, two weeks in advance, allowing them to prepare articles and conduct interviews, thus easing pressure on the launch day.

Event for professional stakeholders

On the afternoon of the model release, a half-day information event was conducted to inform interested professionals in more detail about the model, its development, results and applications. More than 200 people attended the event.

11.5 Testing

We involved end users from the beginning of the design process to ensure that the products met their needs (see Figure 11.8). First, we conducted interviews with international experts to learn from best practices and already-operational rapid impact assessment services. Second, we held workshops with professional stakeholders in society (e.g. cantonal authorities, civil protection) to assess their information and application needs and to further develop the prototypes based on their feedback. Third, we carried out two public surveys to evaluate which rapid impact assessment, scenario and risk map versions were correctly interpreted and best perceived. The two surveys were approved by the ETH Zurich Ethics Commission (EK 2022-N-50 and EK 2022-N-235). In Sections 11.5.1 to 11.5.4, we summarise the main insights from these efforts and provide relevant recommendations for the design of user-centred earthquake risk products. For the design, we further benefited from our previous studies on hazard maps (Marti et al., 2019), earthquake information in a multi-hazard context (Dallo, 2022), the European earthquake risk model products, and earthquake early warnings (Dallo et al., 2022a).
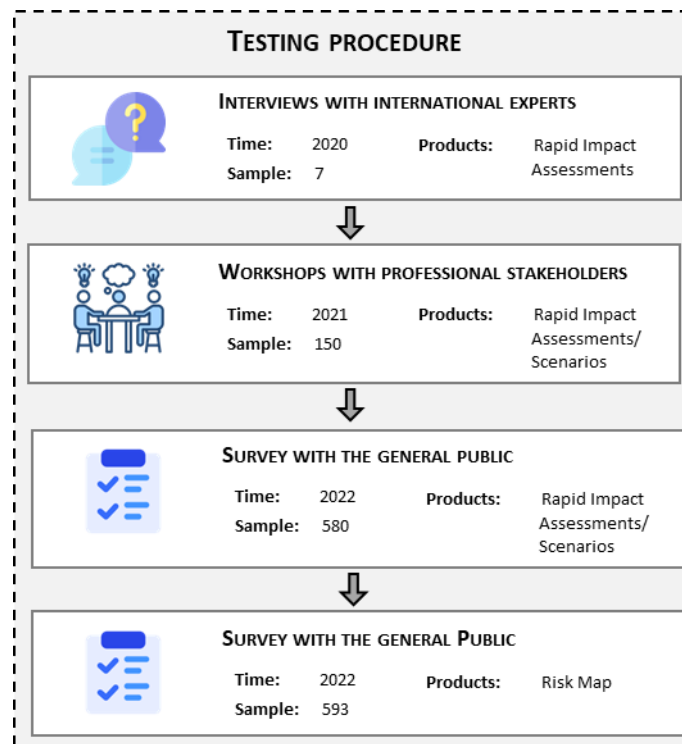
Figure 11.8. Overview of the four studies we conducted to co-design and test selected products, namely the rapid impact assessment report, scenarios and the risk map.

11.5.1 Expert interviews

In 2020, we conducted seven interviews with experts involved in the development of operational rapid impact assessments (Dryhurst et al., 2021), i.e. PAGER, ShakeCast, QLARM, InaSAFE and Global Dynamic Exposure Model (still in development). The interviews took place virtually via Zoom and lasted about one-and-a-half hours. The semi-structured interview guide consisted of five question blocks: i) products and services, i.e. short description, medium, format, update process, purposes; ii) audience, i.e. target groups, special needs, people not reached; iii) communication chain, i.e. from the production to the release and use of the information; iv) future potential, considering emerging technologies; and v) interlink to other products and services such as earthquake forecasts.

The main findings were as follows: Rapid impact assessments are key to gaining an initial estimate of the damage after an event, and scenarios are important for drawing up disaster management plans based on hypothetical and historical earthquakes. The content of the existing products around the world is similar: general event details (e.g. magnitude), intensity or mean damage map, estimate of fatalities and economic losses, histogram with alert levels, and table of affected cities. Further, the primary audiences are first responders, emergency agencies, insurance companies, critical infrastructure owners, media reporters and the general public. Current challenges are i) updating second reports after major aftershocks; ii) communicating the uncertainties of the estimates; iii) lack of time and resources for maintenance (24/7); and iv) potential misinterpretation of the estimates.

From the results we derived three main implications which should be considered when developing and operating rapid impact assessment services:

– Information from the rapid impact assessment reports is frequently picked up by the media, thus the numbers and figures are widely distributed. This means that the uncertainties behind the estimates should be communicated in a clear and understandable way.

– Multiple versions of rapid impact assessment reports with different levels of detail for different stakeholders are necessary. Communal and cantonal details, for example, can only be

communicated to professional stakeholders (e.g. authorities, civil protection) due to privacy issues.

– One should never communicate exact numbers but rather ranges since the exact numbers will always be wrong and, consequently, the public will question the credibility of the information provided.

11.5.2 Workshops with professionals

We conducted three workshops with professional stakeholders in society, namely cantonal and national authorities, first responders and civil protection (~150 participants) (Marti et al., 2022). One of the workshops took place virtually on Zoom and two were in-person, starting with the presentation of the earthquake risk model and the two preliminary products (rapid impact assessments and scenarios) and ending with the collection of feedback. For the virtual workshops, we used the online platform Mural to collect feedback on the prototypes. To this end, we created break-out rooms to ensure all participants were able to voice their opinions and needs. The break-out rooms were moderated by the developers of the earthquake risk model and products to answer participants' questions. At the in-person workshop, we collected the feedback via a short paper questionnaire.

The results indicated that the representatives of the professional target groups perceived the two products as very useful, especially to support risk and disaster management. The representatives also showed great interest in attending follow-up events to learn more. We also received some valuable feedback to improve the products. First, the products should be distributed via pre-existing communication channels. Second, the categories for the fatality and economic loss estimates should stay the same, independent of the magnitude of the event, to be able to compare the events with each other. Third, combining absolute and relative numbers in one diagram is more challenging for end users to interpret.

From the results we derived three main insights which should be considered when developing rapid impact assessment services, especially for professional stakeholders in society:

– The professional target audiences in society perceive rapid impact assessment reports and scenarios as relevant products for their work (e.g. risk and disaster management).

– The new products should be embedded in the existing communication-product provision to ensure consistency between them.

– Preferences regarding the thresholds for the categories of the number of fatalities and economic loss estimates vary across the different stakeholders.

11.5.3 Public survey I – Rapid impact assessment and scenario

We conducted a public survey, representative of the German- and French-speaking parts of Switzerland in terms of age and gender (N=580), in June 2022 (Marti et al., 2022). The participants were recruited through the ISO-accredited polling company Bilendi. The survey consisted of six question blocks (QBs). In QB1, the participants were randomly assigned to one of the five rapid impact assessment reports (only the uncertainty visualisation differed) and we assessed which one was correctly interpreted, had the highest perceived usefulness, and triggered people to take protective actions. In QB2, participants were randomly assigned to one of the five fatality uncertainty visualisations, and we assessed which version was best understood and preferred in general. In QB3, we tested the visualisation of the expected building damage, and, in QB4, we assessed participants' perceived usefulness, further information needs, and severity of the scenario. In QB5, participants were asked to indicate their general preferences for both products and, in QB6, their past earthquake experiences, risk perception, numeracy skills, trust in various actors communi-

cating hazard and risk information, availability of earthquake insurance, house/apartment type, and sociodemographic characteristics.

The detailed results are summarised in Marti et al. (2022). In general, the information on the rapid impact assessments was correctly understood, especially by people with higher numeracy skills, a higher educational level, and a lower risk perception. In addition, the perceived usefulness was high and the reports motivated people to take action. Regarding the fatality visualisation, we saw that the uncertainties were best communicated when indicating the range of possible values, without adding a precise probability that a value falls within this range (see Figure 11.9). We also showed that the current practices, i.e. histograms, were not correctly interpreted, meaning that the current use of these histograms should be reviewed. Regarding the building damage visualisation, where we combined absolute and relative numbers, participants struggled to interpret them correctly. Based on the insights, we therefore adjusted the visual to make it easier to understand (see Figure **11.10**). Regarding the scenarios, participants agreed that they helped them to better understand the possible impacts of an earthquake at their place of residence and to take preparedness measures. Most participants wished to receive risk information for earthquakes for a time horizon of ten years, followed by 50 years or one year. Information elements that were missing but would be appreciated in rapid impact assessment reports and scenarios were primarily behavioural recommendations and the probability of aftershocks.
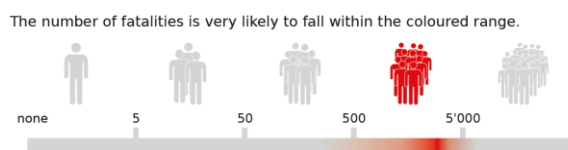
Figure 11.9. Uncertainty visualisation to indicate the estimated number of fatalities.
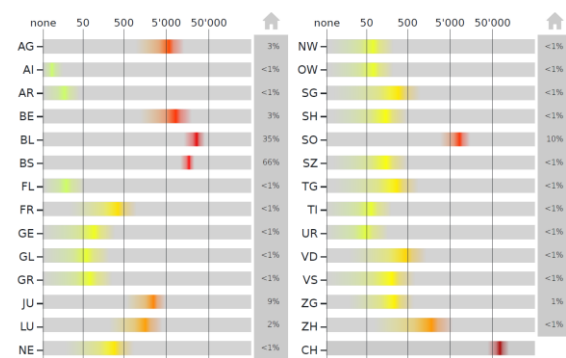
Figure 11.10. Building damage visualisation.

Aligning the rapid impact assessments and scenarios to the public's needs is key to ensure that the information provided is correctly understood, so that people can take informed decisions. Here, three recommendations were derived from our survey results:

– Taking the public's skills, needs and preferences into account when designing rapid impact assessments and scenarios increases their willingness to take preparedness or protective actions in advance or after an event.

– Good practices for communication products may work in one place but not another. Thus, testing them with the specific target audience is indispensable.

– To increase people's perceived usefulness of the products, their trust in the information source, their risk perception and their skills (e.g. numeracy skills) must be guaranteed.

11.5.4 Public survey II – Risk map

In December 2022 and January 2023, we conducted a public survey, representative of the German- and French-speaking parts of Switzerland in terms of age and gender (N=593). The participants were recruited through the ISO-accredited polling company Bilendi. The survey consisted of six question blocks. In QB1 and QB2, we assessed participants' earthquake experiences and knowledge, their risk perception for Switzerland, for their place of residence and their own personal situation, and their understanding of earthquake risk. In QB3, we randomly assigned the participants to one of the risk map versions (we varied the colour scale and legend type) and assessed their general perception, correct interpretation of the map and legend, and their map element preferences. In QB4, we again assessed participants' risk perception and, additionally, their intention to take action, their perceived usefulness for different stakeholders, and their further information wishes. In QB5, the participants saw all map and legend versions and were asked to select their preferred one. Finally, in QB6, we assessed the sociodemographic characteristics, i.e. highest educational level, house ownership, professional background and place of residence.

> *The results are still confidential for publication-related matters but are available on request.*

11.6 Conclusion

The value of an earthquake risk model is measured, among other factors, by the impact it has on making societies more resilient. To this end, it must not only comply with the scientific state of the art, but must also be presented in an understandable and adaptable manner. A primarily scientific effort, consequently, has to be translated into communication products supporting different stakeholders in making informed decisions. This is by nature a transdisciplinary effort involving seismologists, engineers, model developers, graphic designers, communication specialists, social scientists, IT specialists and members of the target audiences. The number of involved parties already implies that this is not a straightforward process but rather a comprehensive and iterative one. We conclude, however, that the effort is well worthwhile since the close collaboration between different professionals and the interaction with user groups leads to a significant improvement in the products. Even though initial drafts were already well received by the target audiences, which we attribute to the close interdisciplinary collaboration in the design process, important amendments were introduced based on user feedback. This demonstrates the importance of testing and evaluating products with relevant user groups before their release. The early implementation of a communication concept also helped to maintain an overview and coordinate the various communications activities. Such a comprehensive approach is very beneficial, but only possible if sufficient human, time and financial resources are allocated.

References

Bentele, G., Nothhaft, H. (2007). Konzeption von Kommunikationsprogrammen. In: Piwinger, M., Zerfaß, A. (eds) Handbuch Unternehmenskommunikation. Gabler Verlag, Wiesbaden. https://doi.org/10.1007/978-3-8349-9164-5_18

Bergamo, P., Panzera, F., Cauzzi, C., et al. (2022). A ground-motion amplification model for Switzerland based on site condition indicators and measured local response. Swiss Academy of Science (SCNAT), 20th Swiss Geoscience Meeting, 244–245. https://geoscience-meeting.ch/sgm2022/downloads/

Crowley, H., Dabbeek, J., Despotaki, V., Rodrigues, D., Martins, L., Silva, V., Romão, X., Pereira, N., Weatherill, G., Danciu, L. (2021). European Seismic Risk Model (ESRM20) [EFEHR Technical Report 002 V1.0.0]. Eucentre. https://doi.org/10.7414/EUC-EFEHR-TR002-ESRM20

Dallo, I. (2022). Understanding the communication of event-related earthquake information in a multi-hazard context to improve society's resilience [Doctoral dissertation]. ETH Zurich.

Dallo, I., Marti, M., Clinton, J., Böse, M., Massin, F., Zaugg, S. (2022a). Earthquake early warning in countries where damaging earthquakes only occur every 50 to 150 years – The societal perspective. International Journal of Disaster Risk Reduction **83**, 103441. https://doi.org/10.1016/j.ijdrr.2022.103441

Dallo, I., Stauffacher, M., Marti, M. (2022b). Actionable and understandable? Evidence-based recommendations for the design of (multi-)hazard warning messages. International Journal of Disaster Risk Reduction **74**, 102917.

https://doi.org/10.1016/j.ijdrr.2022.102917

Detweiler, S., Wein, A.M. (2018). The HayWired Earthquake Scenario — Earthquake Hazards Scientific Investigations Report 2017 – 5013 – A – H, Reston, Virginia. https://doi.org/https://doi.org/10.3133/sir20175013v1.

Dryhurst, S., Luoni, G., Dallo, I., Freeman, A.L.J., Marti, M. (2021). Designing & implementing the seismic portion of dynamic risk communication for long-term risks, variable short-term risks, early warnings (Society: Data Gathering and Information Sharing with the Public and Policy-Makers) [Deliverable]. European Horizon-2020 project RISE. http://static.seismo.ethz.ch/rise/deliverables/Deliverable_5.3.pdf#page=56&zoom=100,92,948

Erdik, M., Şeşetyan, K., Demircioğlu, M.B., Hancılar, U., Zülfikar, C. (2011). Rapid earthquake loss assessment after damaging earthquakes. Soil Dynamics and Earthquake Engineering, **31**(2), Article 2. https://doi.org/10.1016/j.soildyn.2010.03.009

Fontiela, J., Rosset, P., Wyss, M., Bezzeghoud, M., Borges, J., Cota Rodrigues, F. (2020). Human Losses and Damage Expected in Future Earthquakes on Faial Island–Azores. Pure and Applied Geophysics, **177**(4), Article 4. https://doi.org/10.1007/s00024-019-02329-7

Fuchs, S., Spachinger, K., Dorner, W., Rochman, J., Serrhini, K. (2009). Evaluating cartographic design in flood risk mapping. Environmental Hazards **8**(1), Article 1. https://doi.org/10.3763/ehaz.2009.0007

Immerschitt, W. (2009). Die Entwicklungsmethodik strategischer Kommunikation. In: Profil durch PR. Gabler. https://doi.org/10.1007/978-3-8349-8022-9_4

Karjack, S., Brudzinski, M.R., Shipley, T.F. (2022). Assessment of the general public's understanding of rapidly produced earthquake information products ShakeMap and PAGER. Seismological Society of America, **93**(5), 2891–2905.

Lin, K., Wald, D. J., Slosky, D. (2020). Earthquakes, ShakeCast. In H. K. Gupta (Ed.), Encyclopedia of Solid Earth Geophysics (pp. 1–5). Springer International Publishing. https://doi.org/10.1007/978-3-030-10475-7_255-1

Marker, B.R. (2013). Hazard and risk mapping. Encyclopedia of Earth Sciences Series, 426–434. https://doi.org/10.1007/978-1-4020-4399-4_165/FIGURES/83

Marti, M., Stauffacher, M., Wiemer, S. (2020). Anecdotal Evidence Is An Insufficient Basis for Designing Earthquake Preparedness Campaigns. Seismological Research Letters. https://doi.org/https://doi.org/10.1785/0220200010

Marti, M., Dallo, I., Roth, P., Papadopoulos, A.N., Zaugg, S. (2022). Illustrating the impact of earthquakes: Evidence-based and user-centered recommendations on how to design earthquake scenarios and rapid impact assessments. Submitted to International Journal of Disaster Risk Reduction.

Marti, M., Stauffacher, M., Wiemer, S. (2019). Difficulties in explaining complex issues with maps. Evaluating seismic hazard communication – the Swiss case. Natural Hazards and Earth System Sciences, **19**(12), Article 12.

Ronan, K.R., Johnston, D.M. (2005). Promoting Resilience: Readiness and Risk Reduction, in: K.R. Ronan, D.M. Johnston (Eds.), Promoting Community Resilience in Disasters: The Role for Schools, Youth, and Families, Springer, New York: pp. 1–210. https://doi.org/10.1007/b102725.

Stieb, D.M., Huang, A., Hocking, R., Crouse, D.L., Osornio-Vargas, A.R., Villeneuve, P.J. (2019). Using maps to communicate environmental exposures and health risks: Review and best-practice recommendations. Environmental Research, 176, 108518. https://doi.org/10.1016/J.ENVRES.2019.05.049

Wiemer, S., Danciu, L., Edwards, B., et al. (2016). Seismic Hazard Model 2015 for Switzerland (SUIhaz2015 – Report. Swiss Seismological Service (SED) at ETH Zurich. http://seismo.ethz.ch/export/sites/sedsite/knowledge/.galleries/pdf_knowledge/SUIhaz2015_final-report_16072016_2.pdf_2063069299.pdf

12.   Future model improvements and further developments

12.1 Introduction

During the planning of the ERM-CH23 project, a second phase of model development was explicitly provided for. This phase is intended to allow the addition of financial and human losses due to earthquake secondary effects (i.e. landslides, rock falls, liquefactions, tsunamis in lakes, ground displacement, fires after earthquakes) and damage to infrastructure.

This chapter details these and other additional developments and tries to identify still missing datasets required to reach the relevant goals. It also lists existing ERM-CH23 model elements that were internally or externally found to be good enough for a first version of a national risk model but that would require improvement or refinement for a model update, when more time and resources can be allocated to the work necessary to derive them. We start with these elements (Section 12.2). Note, however, that these improvements may turn out to be obsolete if the new developments agreed upon replace the relevant parts of the model with other approaches and methods. The boundary between the two categories is sometimes blurred.

12.2 Model improvements and refinements

12.2.1 Hazard on rock

In accordance with its federal mandate, the SED regularly updates the national hazard model for Switzerland. This happens every 10 to 15 years. These updates reflect advances in science in this area and make use of the new datasets available. While the present ERM-CH23 model is based on the latest national hazard model (Wiemer et al., 2016), the successor to ERM-CH23 – let us call it ERM-CH+ – should be based on the next release of the Swiss hazard model, currently scheduled for 2027. Precise coordination will be needed for an optimised release of these two models (hazard and risk), as consistency between the two is mandatory and any waste of resources in the form of parallel developments should be avoided.

Between these two 'official' hazard models, no specific improvements are planned for this component of the risk model.

12.2.2 Soil amplification

The soil amplification model used in ERM-CH23 already features a high level of detail for a country-wide model. By the end of 2023, the risk model for Basel (ERM-BS) will be published and it will therefore be possible to integrate it as one of the local models in ERM-CH+. This requires the replacement of the site-amplification logic tree branch of the national model with branches reflecting local site amplification methods. Of course, new stations will be deployed in the years to come and new earthquakes will be recorded that will help to improve the model in its present structure, following a 'simple' update. Improvements in the soil amplification subproject are to be envisaged as new developments (see Section 12.3 below) rather than improvements to the existing components.

The addition of non-linearity, which is likely to affect only some lithotypes, and possibly not in the same manner, is regarded as further development, also because it affects liquefaction (see Section 12.3.1 below).

12.2.3 Building database

At the federal level, efforts to improve the different datasets and databases are ongoing. For example, as for 2023, the Federal Statistical Office and Swisstopo is about to complete their Federal

Register of Buildings and Dwellings (RBD, see Chapter 4) and inventory of building footprints (AV dataset) respectively. These datasets should enable a one-to-one correspondence for all building objects in Switzerland via the unique building identification number (EGID). The completion and unification of the RBD and AV datasets will make it possible to perform checks in order to exclude objects that are not real building objects (tanks, silos, transformer housings, etc.). In the near future, the building volume above ground should also become a standard attribute of the AV dataset, which will also reduce the effort involved in preparing the building database for ERM-CH+.

As regards the cantonal insurers' databases, it is hoped that the EGID number will gradually become a standard building identifier and that buildings still without coordinates will be properly georeferenced. This should enable an easier link with the RBD and AV datasets for the importation of relevant attributes such as the building volume, including underground volume, or the category of use. It is also hoped that cantonal insurers will be willing to provide their georeferenced datasets of insured building values in order to develop improved models for the computation of the building replacement value (GEBWERT) in ERM-CH+.

When it comes to databases of private insurance companies, it is hoped that aggregated replacement values and content values at the cantonal and postcode level can be attributed to more differentiated use categories in order to refine the model for the computation of the content value INHWERT.

While the ERM-CH23 database is mostly a database of residential and commercial buildings, a small proportion of the buildings are attributed as 'industrial'. However, we know that these buildings may be headquarters or office buildings, and therefore not different in their structure from ordinary commercial buildings, or else actual production sites or factories, with their very specific structural properties. Better separation between the two categories should be a task for ERM-CH+.

These and all other pertinent improvements are obviously to be incorporated into the next risk model.

12.2.4 Building type assignment

The building typology mapping schemes could be further improved with further data collection, whether through ground surveys, expert elicitation or by leveraging digital datasets and novel technologies (remote sensing, pattern recognition, etc.). Moreover, it is considered worthwhile to alter the current assignment procedure in order to differentiate better across different areas (e.g. mountainous rural zones or business centres), as well as across occupancy types (different assignment for residential, commercial and industrial buildings).

12.2.5 Fragility model

With the advances that are being made in the mechanical approach to deriving fragility curves, ERM-CH+ will have to consider whether the inclusion of a MIM model is still appropriate or whether the uncertainty covered by the parallel consideration of an intensity-based model is not better placed in increasing and refining the epistemic uncertainty of the SAM model.

Improvements to the SAM model have been suggested by the review team experts. They include several aspects. First, multiple records from earthquakes should be considered to model multiple scenarios and thus better represent the record-to-record variability. As the record and scenario selection can be very important, special focus should be placed on this aspect of the fragility model. Making the fragility functions site-specific is a goal that ERM-CH+ will have to consider. This is a challenge given the size of the model.

Improving the building taxonomy to be in line with modern practices (e.g. GEM taxonomy) could facilitate future updates and comparison with literature. Moreover, state-of-the art procedures for

derivation of fragility models should be adopted for ERM-CH+, i.e. nonlinear time-history analyses of multi-degree-of-freedom (or well-calibrated single-degree-of-freedom) models.

Generally, a refined treatment of uncertainty in the fragility subproject should be aimed at (see Section 12.2.7) and more thorough calibration, using public building and damage inventories (e.g. for L'Aquila 2009), will be needed.

12.2.6 Consequence model

A model for **demand surge** was mentioned by the external experts as a desirable improvement. Demand surge can be defined as the increase in economic losses following large/extreme disasters due to supply and demand imbalances. Empirical evidence suggests that demand surge following large-scale disasters can lead to a general increase in costs of up to 50%[14] (Olsen and Porter, 2011a; Olsen, 2012). Input-output commercial models employ a cut-off loss amount, below which no demand surge is assumed to occur. Both commercial models and empirical evidence (albeit limited and noisy) seem to suggest that the impact of demand surge should be a function of the extent of damage and loss, not their return period (Döhrmann et al., 2013). The capping (maximum) demand surge factor and the cut-off loss are the two main variables of input-output commercial demand surge models. However, these models are proprietary – they are opaque and closed to scrutiny. Moreover, relevant literature does not shed sufficient light on building a validated input-output model largely because of a lack of understanding of its robust estimation and consistent high-quality pre/post-event data. Olsen and Porter (2011b) put demand surge modelling into perspective with the following: "*Modeling demand surge is a multivariate problem with an imprecise response variable and unknown explanatory variables.*" As such, the SPD development team believes that significant resources would need to be dedicated to the exploration and development of a prospective Swiss demand surge model separate from the consequence model.

Further investigations into Swiss construction, repair and renovation practices should help us understand whether a loss ratio *threshold* – above which repairs as opposed to reconstruction would be deemed unfeasible – should be implemented in the model. Both the existence and the value of such a threshold would likely depend on factors including but not limited to age, historical value, use (occupancy type such as residential, commercial or industrial), and ownership of the assets. The impact of a tentative threshold value of 0.60 will be assessed by the implementation team (SPC) to offer a glimpse of its impacts on modelled losses. In August 2022, SPD provided the implementation team with an updated subset of loss realisations and associated Probability Mass Functions[15] (PMFs) to facilitate this effort.

More generally, the '*helvetisation*' of the consequence model can certainly be increased, through stronger interaction with Swiss practitioners despite their limited experience with earthquake damage. The SPD development team believes that concentrated efforts towards the refinement of the model's downtime estimation module[16] would deliver the biggest improvement and aleatory uncertainty elimination per development hour (and money) invested.

12.2.7 Treatment of uncertainty

In light of new data accumulation, advancements in modelling techniques, and software development in the coming years, we should focus on reducing the model's overall uncertainty. This enhancement should be planned and targeted for all model subcomponents. Priorities might also include:

---

[14] The Northridge earthquake (20%), Hurricane Katrina (10-40%) and Cyclone Larry (50%) are examples with documented evidence. Readers are referred to Olsen and Porter (2011a) for more detailed information.

[15] These PMFs express probabilities of increasing levels of loss ratio brackets – from 0 to 1 part of the reconstruction value of an asset – for each of the five damage states as per EMS98.

[16] This refers specifically to the refinement of *delay (e.g. engineering mobilisation, financing and permitting)* function parameters leveraging local Swiss data.

- ensuring a balanced logic tree to capture a reasonable number of end branches for each subcomponent; the current logic tree is still dominated by ground motion branching levels;

- capturing the spatial and temporal variability of the uncorrelated earthquake rate prediction models;

- constructing a regional and scalable backbone logic tree to handle the epistemic uncertainties of the ground motion models; this will be coordinated with the SUIhaz2015 update, to avoid redundancy;

- reducing the aleatory uncertainties of the next generation of ground motion predictive equations;

- studying the entire issue of spatial correlation (introduced by the within-a-cell aggregation, for example) in greater depth (we may introduce underestimation or overestimation of computed losses with the present aggregation approach);

- increasing aleatory uncertainty in deriving the fragility curves to make them less steep, although the uncertainties related to material, record-to-record and building-to-building variability have been considered to some extent;

- migrating towards state-of-the-art fragility models, based on analyses of multiple degrees of freedom with full coverage of uncertainties in model development; similarly, the consequence models must be updated to capture both the epistemic and the aleatory uncertainty;

- developing a new computational framework to handle complex logic trees with uncorrelated branches, and migrating the loss/risk calculation to supercomputers; this will also require the development of a highly scalable and efficient software.

12.3 Further model developments

12.3.1 Consideration of secondary effects

ERM-CH23 allows assessment of the risk at national level arising from damage to buildings caused by individual earthquakes (scenarios) or stochastic catalogues of individual earthquakes (long-term estimates). However, earthquakes can trigger other types of hazard that put society at risk. The three main categories of such earthquake-induced secondary effects are soil liquefaction, co-seismic slope failure and tsunamis. They account for a significant proportion of the total global loss caused by earthquakes (19% for economic loss and 25% for fatalities; Nowicki Jessee et al., 2020).

Tools exist or are being developed to assess the earthquake-induced risks for scenario events (either rapid loss assessments or fictitious events): USGS provides a near-real-time risk estimation for ground failure related to earthquakes larger than magnitude 5 in the US and larger than magnitude 6 worldwide (Allstadt et al., 2021) while a similar tool is in development with customisation to New Zealand (Pradel et al., 2020). The latter was tested for application in Switzerland, both for liquefaction (Cauzzi et al., 2018a) and landslides (Cauzzi et al., 2018b).

Häusler and Fäh (2022) provide a thorough and comprehensive overview over the different methods available and the different types of datasets required for such a country-wide implementation and present an implementation strategy at three different scales: national, regional and local. They also go into the datasets that are required and still missing, like a continuous map of Vs30 or a water table depth map.

For the aforementioned secondary effects landslide, tsunami and liquefaction, risk assessment will also require the development of vulnerability models, which are different from the ground shaking models. All these developments, including the nonlinear soil response linked to liquefaction, will require substantial scientific work.

Two questions arise regarding an implementation within ERM-CH+. The first is whether 'only' a scenario assessment of earthquake-induced risk is needed, which enables efficient rescue operations and provides a tool for earthquake preparedness, or whether the secondary effects also need to be incorporated into the long-term risk assessment. The latter would mean that for that probabilistic implementation, a number of time-dependent parameters like weather, soil moisture, snow cover or river discharge situations, which are considered at the time the earthquake occurs in the scenario calculation, would have to be ignored. A second issue relates to the temporal extent of the estimate: is the risk associated with the directly induced secondary effects to be assessed or also the risk associated with the cascading effects that these earthquake-induced phenomena themselves can have (e.g. a landslide dam, its possible failure, the downstream flooding, the erratic increasing riverbed deposition, new flooding, etc., see Häusler and Fäh, 2022).

12.3.2   Consideration of infrastructure

As modern societies are increasingly dependent on their critical infrastructure to produce and distribute the essential goods and services they need, a disruption of this system following an earthquake may have a strong economic impact. Infrastructure here is understood to mean lifelines: utility systems (potable and waste water, gas, telecommunication, electric power) and transport infrastructure (road and railway system). Critical infrastructures like nuclear power plants or large dams cannot be considered in a national model and are typically the subject of site-specific studies.

Adding infrastructure to a seismic risk study presents several challenges. The use of simplified procedures requires a multitude of assumptions, which increase the uncertainty in the loss assessment, whilst detailed approaches based on in-situ data are resource-demanding and impractical for large-scale risk analyses. While today the inventory of the different lifelines is available in a digital, harmonised form in GIS, the lifelines' typology with associated intensity measure type (PGA, PGV, PGD, SA@T_0, etc.) for each of them needs to be defined. A categorisation of the strategic importance of every subcomponent of each lifeline network, the different types of interdependence between lifeline systems, a set of fragility curves, and lifeline-specific damage state definitions need to be established, and consequence models for the large spatially distributed systems are required. RISK-UE (Pitilakis et al., 2006) paved the way for all this, and was later greatly improved by the SYNER_G project (Pitilakis et al., 2014). Obviously, the correct treatment of uncertainty and spatial correlation when dealing with spatially distributed and interconnected portfolios is a major challenge too (Weatherill et al., 2014; Cavalieri and Franchin, 2020).

A feasibility study in collaboration with lifeline owners and other interested stakeholders should be carried out. Obviously, the addition of infrastructure in the model is closely related to the introduction of secondary effects.

12.3.3   Other possible additions

Based on the feedback of the stakeholders to the ERM-CH23 products and the needs they may trigger, but also depending on the founding partners involved in the next development phase, several elements may be added to ERM-CH+. Five possible additions are briefly mentioned here.

Business interruption. Loss due to business interruption as a consequence of downtime (inspection, repair, demand surge, etc.) is an important aspect of scenario risk calculation. This could be modelled in the next phase of development.

Population distribution. Time of day is roughly taken into account in ERM-CH23, including with regard to scenarios and rapid loss assessment (see Section 7.4). A more precise representation of population movement (weekend vs. weekday, holidays, seasonal variations in tourist areas, movement of border workers) could be addressed. A new project at the federal level to map population in real time may deliver an important opportunity to make progress in this area.

<u>Seismicity clustering and time-dependent building fragility.</u> ERM-CH23 only captures damage caused by mainshocks, arguably neglecting a large portion of loss-inducing events and therefore underestimating seismic risk (Papadopoulos et al., 2021; Papadopoulos and Bazzurro, 2021). Aftershock clusters could potentially be added as a future development. Furthermore, after a first, main earthquake but also as a consequence of their ageing process, structures may deteriorate. Different models exist to take this increasing fragility into account.

<u>Machine learning approaches</u>. Machine learning approaches have been gaining ground and promising applications in the field of earthquake risk assessment have already started emerging. ERM-CH+ could possibly rely on such technologies for a better modelling of different components, from ground motion to loss estimation.

<u>Time-dependent risk</u>. Earthquakes cluster in space and time and the SED is now computing on a routine basis time-dependent seismicity rates that can be useful for Operational Earthquake Forecasting (OEF). This input can then be used also to compute time-dependent seismic hazard and risk, which may serve as a decision tool, for example using cost-benefit analyses. A pilot study was published by Herrmann et al. (2016), and the SED has been extending this methodology in the RISE project (http://www.rise-eu.org), with the intermediate goal to also implement Operational Earthquake Loss Forecasting (OELF, e.g., Chioccarelli and Iervolino, 2016) for Switzerland. OEF and OELF will use the ERM-CH databases and methodologies to be internally consistent across different risk applications.

References

Allstadt, K.E., Thompson, E.M., Jibson, R.W., Wald, D.J., Hearne, M., Hunter, E.J., Fee, J., Schovanec, H., Slosky, D., Haynie, K.L. (2021). The US Geological Survey ground failure product: Near-real-time estimates of earthquake-triggered landslides and liquefaction, Earthquake Spectra, 87552930211032685, doi:10.1177/87552930211032685.

Cauzzi, C., Fäh, D., Clinton, J.F., Wiemer, S. (2018a). Calibration of global empirical models for real-time liquefaction prediction in Switzerland. Paper presented at the 16th European Conference on Earthquake Engineering, Thessaloniki.

Cauzzi, C., Fäh, D., Wald, D.J., Clinton, J.F., Losey, S., Wiemer, S. (2018b). ShakeMap-based prediction of earthquake-induced mass movements in Switzerland calibrated on historical observations, Natural Hazards, **92**(2), 1211–1235, doi:10.1007/s11069-018-3248-5.

Cavalieri, F., Franchin, P. (2020). Seismic Risk of Infrastructure Systems with Treatment of and Sensitivity to Epistemic Uncertainty. Infrastructures **5**(11), 103, doi:10.3390/infrastructures5110103

Chioccarelli, E., Iervolino, I. (2016). Operational earthquake loss forecasting: a retrospective analysis of some recent Italian seismic sequences. Bulletin of Earthquake Engineering **14**, 2607–2626 (2016). https://doi.org/10.1007/s10518-015-9837-8

Häusler, M., Fäh, D. (2022). Strategies for implementation of earthquake-induced phenomena in hazard and risk tools: current state-of-the-art, available datasets and proposals for implementation. ERM-CH, Deliverable Module E, SPE-TR-0019, 25pp.

Hermann, M., Zechar, J.D., Wiemer, S. (2016). Communicating time-varying seismic risk during an earthquake sequence. Seismological Research Letters **87**(2A), 301–312.

Nowicki Jessee, M.A., Hamburger, M.W., Ferrara, M.R., McLean, A., Fitzgerald, C. (2020), A global dataset and model of earthquake-induced landslide fatalities. Landslides **17**(6), 1363–1376, doi:10.1007/s10346-020-01356-z.

Papadopoulos, A. N., Bazzurro, P., Marzocchi, W. (2021). Exploring probabilistic seismic risk assessment accounting for seismicity clustering and damage accumulation: Part I. Hazard analysis. Earthquake Spectra **37**(2), 803–826. DOI: 10.1177/8755293020957338

Papadopoulos, A. N., Bazzurro, P. (2021). Exploring probabilistic seismic risk assessment accounting for seismicity clustering and damage accumulation: Part II. Risk analysis. Earthquake Spectra, **37**(1), 386–408. DOI: 10.1177/8755293020938816

Pitilakis K., Alexoudi, M., Argyroudis S., Monge, O., Martin, C. (2006). Earthquake risk assessment of lifelines. Bulletin of Earthquake Engineering **4**, 365–390, doi 10.1007/s10518-006-9022-1.

Pitilakis, K., Franchin, P., Khazai, B., Wenzel, H. (2014). SYNER-G: Systemic seismic vulnerability and risk assessment of complex urban, utility, lifeline systems and critical facilities. Methodology and applications. Series: Geotechnical, Geological and Earthquake Eng., 31, Springer, Netherlands.

Pradel, G.J., Lukovic, B., Dellow, S. (2020). Earthquake-Induced Landslide Forecast and Hazard Assessment, Hawke's Bay Region, GNS Science Consultancy Report, 2020, **46**.

Weatherill, G., Esposito, S., Iervolino, I., Franchin, P., Cavalieri, F. (2014): Framework for Seismic Hazard Analysis of Spatially Distributed Systems. In SYNER-G: Systemic Seismic Vulnerability and Risk Assessment of Complex Urban, Utility, Lifeline Systems and Critical Facilities: Methodology and Applications; Pitilakis, K., Franchin, P., Khazai, B., Wenzel, H., Eds.; Springer: Dordrecht, The Netherlands, **31**, 57–88.

Wiemer, S., Danciu, L., Edwards, B., Marti, M., Fäh, D., Hiemer, S., Wössner, J., Cauzzi, C., Kästli, P., Kremer, K. (2016). Seismic Hazard Model 2015 for Switzerland (SUIhaz2015). https://doi.org/10.12686/A2.

Appendix 1 – Statements by the Review Bodies

Technical Committee

Letter of opinion by the representatives of the private insurance and reinsurance companies

Technical Committee (FA) ERM-CH

As part of the technical committee for the ERM-CH, representatives from the private insurance and reinsurance industry committed to
- follow the progress of the project
- give feedback on the progress and input on the methodology
- contribute the expert knowledge from the insurance/ reinsurance side
- support the validation process, respecting all license restrictions and intellectual property rights of the private companies and their software providers.

At no point have the private insurance companies influenced the actual quantitative outcomes of the Earthquake Risk Model.

The natural catastrophe expert functions of the following companies have been involved:
- Zurich Insurance – Christoph Grass, Head Cat Perils Group Reinsurance
- Swiss Re - Michael Ewald, Earthquake Perils Lead
- Partner Re - Paul Della Marta, Head Cat Research and Robin Gee, Seismic Risk Researcher
- AXIS Re - Fortunat Kind, former Head NatCat Risk

As participants in the technical committee, we closely followed the project's progress through the annual meetings and through the project reports. Where possible, feedback and input were provided to the project as part of the technical committee review meetings.

We are happy to see that the expertise and experience we were able to share, both from a scientific as well as practitioner's point of view, has helped to guide the project team. At the same time, we note that they have retained complete independence in their scientific judgement and methodological choices.

We gladly note the use of best-practice risk modelling concepts and that the quality of data and research used to develop the model represents the best available, in some respects ground-breaking, state of knowledge.

Zürich, September 2022

F. Kind
C. Grass
M. Ewald
P. della Marta
R. Gee

External Review Team

6 October 2022

Earthquake Risk Model for Switzerland (ERM-CH)
Core team
c/o Swiss Seismological Service – ETH Zurich

Common Statement of the External Review Team

This document constitutes the final common statement of the External Review Team (ERT) for the Earthquake Risk Model for Switzerland (ERM-CH). The ERT was composed of (in alphabetic order) Alexander Allman, Pierre-Yves Bard, Helen Crowley, and Martin Koller.

Chronology

In June 2022, a draft report about the ERM-CH was delivered to the ERT. The ERT then met with the project team and the participatory Technical Committee during a review meeting held in Zurich on 6 and 7 July 2022. The ERT raised several issues and made suggestions with respect to both the model itself as well as its reporting. After the review meeting, these issues and suggestions were written down by the project team in detailed minutes of the meeting that were further commented on by all members of the ERT.

In the following summer months, the project team worked on the relevant aspects of the model. The model as well as the report were revised as far as this was possible within the time constraints of the project, i.e. within a couple of months. Issues that would have needed more time to be resolved were added in a new chapter titled "Future model improvements and further developments".

The revised report was delivered to the ERT on 21 September 2022. The members of the ERT discussed this new version and prepared the present common statement by e-mail exchange.

General approval

The ERT agrees with the three key decisions taken at the beginning of the project, namely the use of the hazard model SUIhaz'15, the use of a macroseismic intensity-based model in addition to the mechanical model based on spectral accelerations, as well as the use of the OpenQuake software, despite some limitations that were identified during implementation of the ERM-CH.

The ERT is satisfied with the changes that have been undertaken to both the model and documentation following the review meeting, given the short time that was available. In particular, the new chapters about uncertainty (Chapter 7) as well as future model improvements and further developments (Chapter 11) are well acknowledged. The ERT therefore approves the ERM-CH as presented in the September 2022 version of the corresponding report. However, the ERT recommends that a few additional aspects are addressed, as explained in the Section "Further short-term improvements" below, before final publication of the report.

Conclusions

Overall, the ERT considers the ERM-CH to be a state-of-the-art probabilistic seismic risk model, with the model for amplification even exceeding the current state-of-the-art. Among the points recommended in Chapter 11 for further developments, the aleatory variability and epistemic uncertainty of the fragility model seems to be the most important, and we underline the need to address this aspect, also with the aim of improving the current state-of-the-art.

Alexander Allmann
Munich Re, Munich

Pierre-Yves Bard
University Joseph Fourier, Grenoble
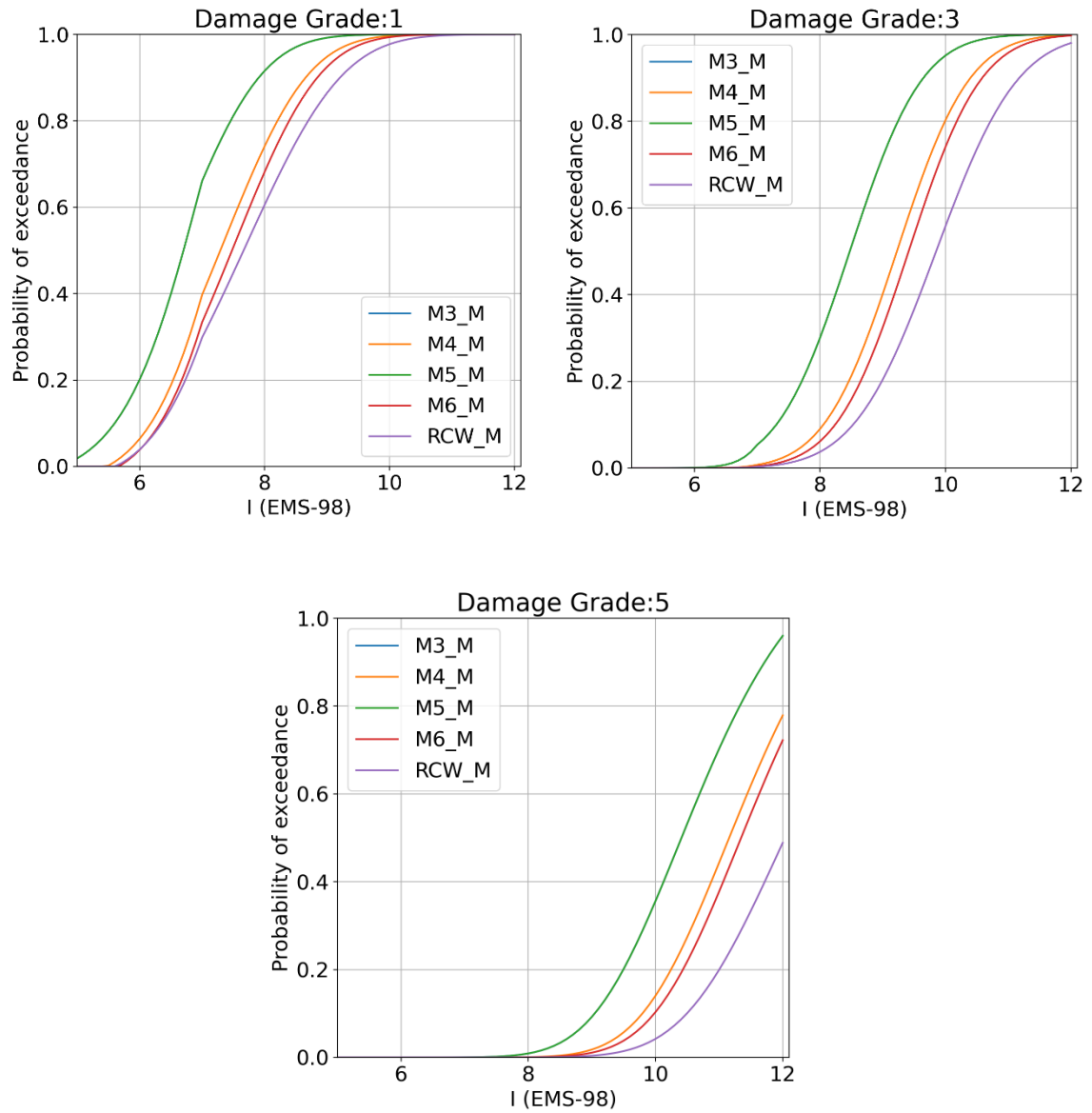
Helen Crowley
Eucentre, Pavia

Martin Koller
Résonance Ingénieurs-Conseils SA, Geneva

Appendix 2 – Additional fragility curves
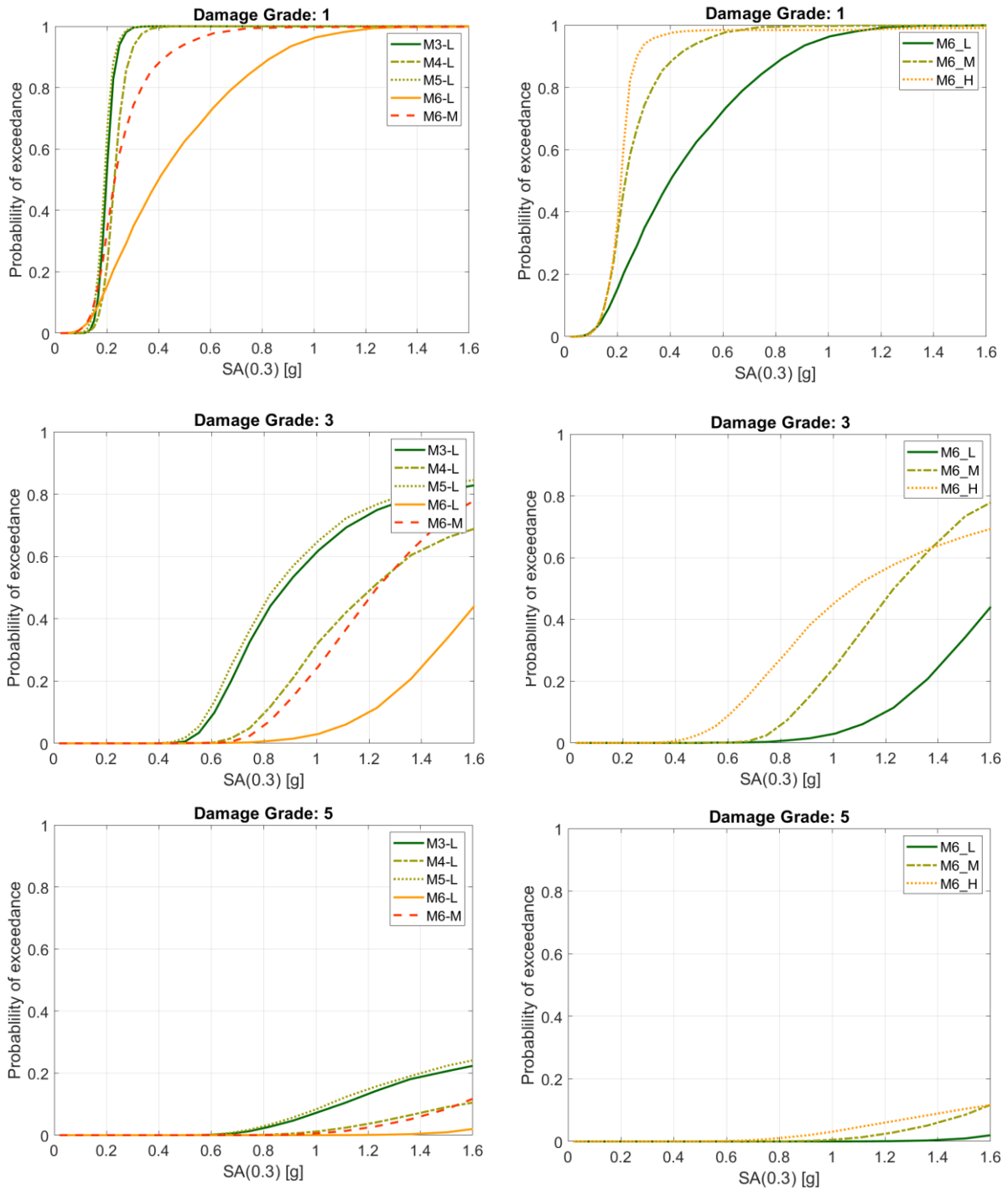
Intensity-based fragility functions
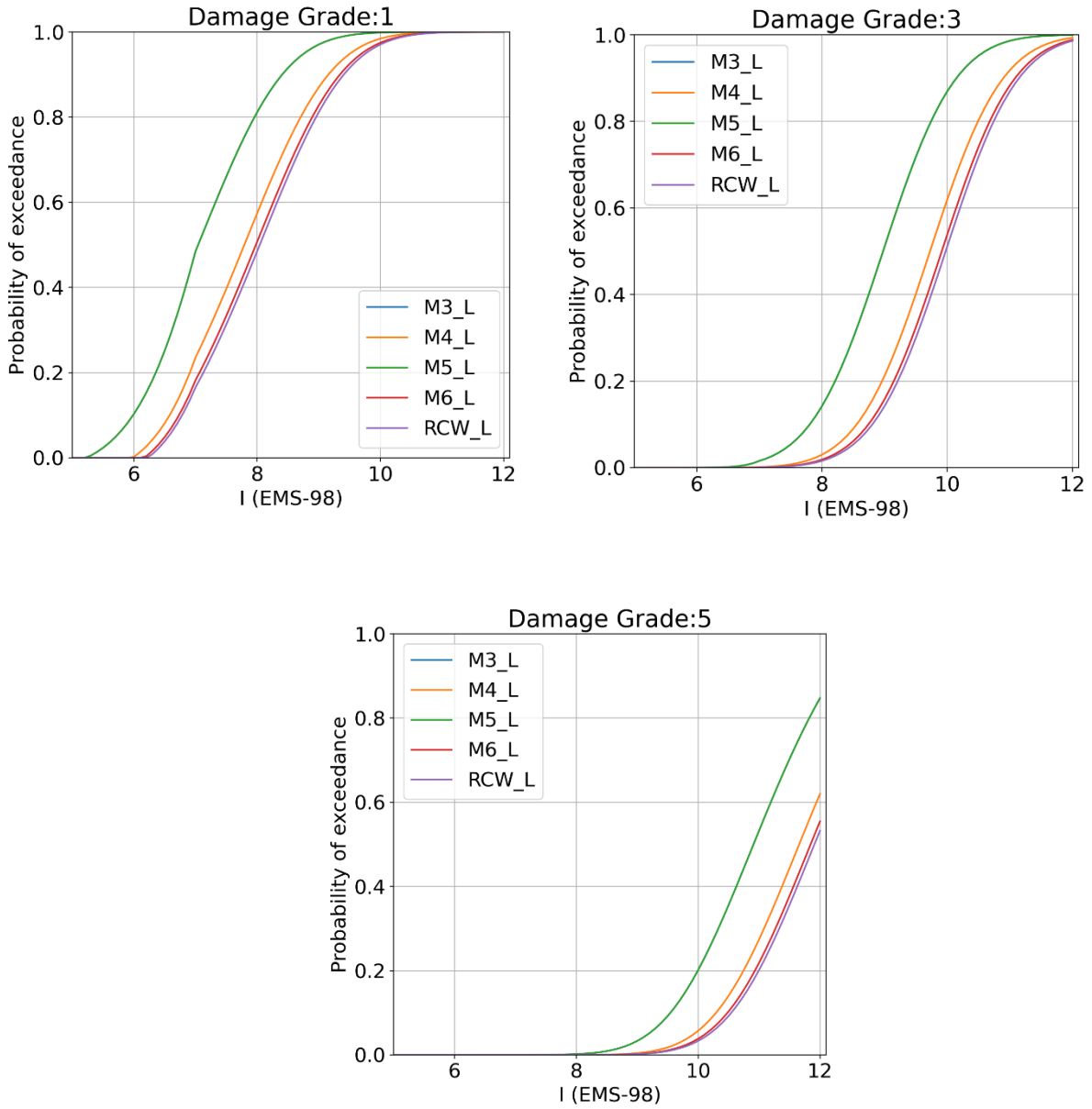
Figure A1. Intensity-based fragility functions for low-rise building types that are in the majority in the exposure model.
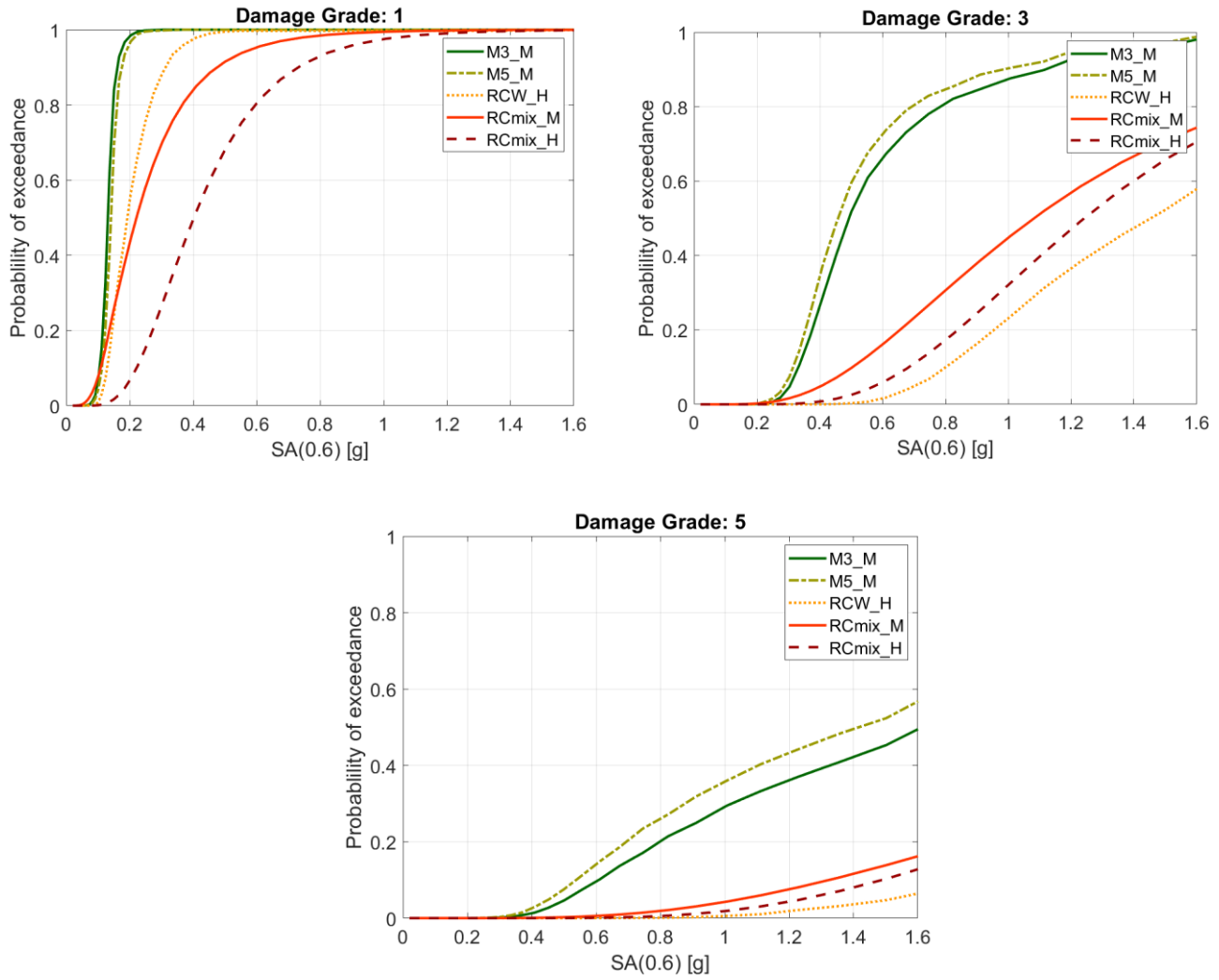
Figure A2. Intensity-based fragility functions for mid-rise building types that are in the majority in the exposure model.

Sa-based fragility functions

Figure A3. Fragility curves, derived as a function of Sa(0.3s), for (left) different masonry building types and (right) different height classes of M6.

Figure A4. Fragility curves considered as a function of Sa(0.6s).